



UNIVERSITÄT  
BAYREUTH

**Redistribution patterns of soil and  
soil nutrients: A study using process-oriented  
and machine-learning approaches, with  
applications to mountain catchments under  
monsoon climate**

Dissertation

to obtain the academic degree of Doctor of Natural Science (Dr. rer. nat.)

of the Bayreuth Graduate School for Mathematical and Natural Sciences of the University of Bayreuth

presented by

Kwanghun Choi

born in Gwangju, Republic of Korea

Bayreuth, February 2020

This doctoral thesis was prepared at the Junior Professorship of Biogeographical Modelling at the University of Bayreuth from February 2012 until January 2020 and was supervised by Prof. Dr. Björn Reineking, Prof. Dr. Bernd Huwe, and Prof. Dr. Dowon Lee.

This is a full reprint of the thesis submitted to obtain the academic degree of Doctor of Natural Sciences (Dr. rer. nat.) and approved by the Bayreuth Graduate School of Mathematical and Natural Sciences (BayNAT) of the University of Bayreuth.

Date of submission: 05. 02. 2020

Date of defense: 11. 12. 2020

Acting Director: Prof. Dr. Markus Lippitz

Doctoral Committee:

PD. Dr. Björn Reineking (1<sup>st</sup> reviewer)

Prof. Dr. Oliver Sass (2<sup>nd</sup> reviewer)

Prof. Dr. Michael Hauhs (chairman)

Prof. John Tenhunen, PhD

Prof. Dongwook Ko, PhD

---

## Summary

Soil erosion is one of the significant environmental problems worldwide, causing surface soil degradation and freshwater deterioration. As the world's population increases, the problem is worsening because erosion-resistant natural ecosystems are being converted into erosion-prone croplands to meet the increasing demands for food. South Korea is also suffering from recurrent severe soil erosion and consequent water deterioration in the monsoon season because of upland agricultural expansion driven by economic incentives. To define the optimal mitigation measures for soil erosion, we need tools that are suitable for upland agricultural areas. In this thesis, we focused on the spatial patterns of soil and soil organic matter containing nitrogen (N) and phosphorus (P), which are relevant to the soil erosion and water quality of mountainous catchments with complex terrain. Also, we aimed to propose measures to mitigate soil and soil organic matter exports to streams from mountainous catchments in the Soyang watershed by spatial reconfiguration of land use and land cover (LULC) at the landscape level.

To investigate the spatial redistribution of soils and soil organic matter from mountain catchments, we developed a soil erosion model termed the Daily based Morgan–Morgan–Finney (DMMF) soil erosion model. The DMMF model was derived from the Modified Morgan–Morgan–Finney (MMMF) model, a variant of the well-known and widely used Morgan–Morgan–Finney (MMF) model, with modifications to make it suitable for complex terrain configurations under seasonal monsoon climates. While the MMMF model improved the physical foundations of the MMF model concerning topography, physical structures of vegetation, and subsurface interflow, several additional aspects needed to be corrected for a better representation of the physical processes. As the MMMF model was originated from an area with a simple terrain configuration and comparatively regular rainfall regimes, the model needed modification for a better representation of the study area, which has a complex terrain configuration under a seasonal monsoon climate. We identified and corrected the problematic aspects of the calculation in the effective rainfall, interflow, and transport capacity of the MMMF model by analyzing its entire process (chapter 2). In chapter three, we suggest a new soil erosion model, the DMMF model, based on the MMMF model.

In chapter four, we evaluated the effect of a spatial reconfiguration of erosion hotspots on

stream sediment load from an upland agricultural catchment utilizing the DMMF model. In this study, we estimated the sediment redistribution pattern and soil erosion risk on the Haean catchment, a well-known upland agricultural catchment belonging to the Soyang watershed. According to the results, the DMMF model can be applied to catchments with complicated terrain configurations affected by a monsoon climate. Results confirmed that a spatial reconstruction of the landscape, complementarily with other best management practices emphasizing the management of dry crop field, can be an effective method to reduce sediment yield from upland agricultural catchments such as Haean.

In the final chapter five, we also investigate the environmental drivers that affect the spatial redistribution patterns of soil nutrients such as N and P in mountain forests. To achieve this goal, we used high-resolution light detection and ranging (LiDAR) to derive detailed information regarding the topography and physical structure of vegetation. Then, we predicted the spatial patterns of soil nutrients such as N and P in the organic layer and mineral topsoil. Specifically, we analyzed the relative importance of vegetation and topographical parameters extracted from LiDAR for a better understanding of the spatial patterns of N and P. In addition, we identified areas with critical P contents and tested different validation strategies for N and P.

## Zusammenfassung

Die Bodenerosion ist eines der weltweit größten Umweltprobleme und führt zu einer Verschlechterung der Bodenoberfläche und der Süßwasserqualität. Mit dem Anwachsen der Weltbevölkerung verschärft sich das Problem, da erosionsresistente natürliche Ökosysteme in erosionsgefährdete Anbauflächen umgewandelt werden, um den steigenden Bedarf an Nahrungsmitteln zu decken. Südkorea leidet auch unter der immer wieder auftretenden starken Bodenerosion und der daraus resultierenden Wasserqualitätsverschlechterung in der Monsunzeit aufgrund der landwirtschaftlichen Expansion im Hochland, die durch wirtschaftliche Anreize angetrieben wird.

Um die optimalen Maßnahmen zur Verminderung der Bodenerosion zu definieren, werden Werkzeuge benötigt, die für landwirtschaftliche Flächen im Hochland geeignet sind. In der vorliegenden Dissertation hat sich der Verfasser auf die räumlichen Verteilungsmuster von Boden sowie von Stickstoff (N) und Phosphor (P) in der organischen Bodensubstanz konzentriert, die für die Bodenerosion und die Wasserqualität von Gebirgseinzugsgebieten mit komplexem Gelände relevant sind. Ein weiteres Ziel der Arbeit besteht darin, geeignete Maßnahmen vorzuschlagen, um den Abtrag von Boden und organischer Bodensubstanz in Gewässer aus bergigen Einzugsgebieten in der Wasserscheide Soyang durch räumliche Umgestaltung von Landnutzung und Landbedeckung (LULC) auf Landschaftsebene zu verringern.

In der vorliegenden Forschungsarbeit wird das Daily based Morgan–Morgan–Finney (DMMF) Bodenerosionsmodell entwickelt, mit dem die räumliche Umverteilung von Böden und organischer Bodensubstanz aus Berggebieten untersucht werden kann. Das DMMF-Modell wurde vom MMMF-Modell (Modified Morgan–Morgan–Finney) abgeleitet, einer Variante des bekannten und weit verbreiteten MMF-Modells (Morgan–Morgan–Finney), das Modifikationen enthält, die es für komplexe Geländekonfigurationen unter saisonalen Bedingungen eines Monsunklimas geeignet machen. Während das MMMF-Modell die physikalischen Grundlagen des MMF-Modells in Bezug auf Topographie, physikalische Vegetationsstrukturen und unterirdische Strömungen verbesserte, mussten einige zusätzliche Aspekte korrigiert werden, um die physikalischen Prozesse besser darstellen zu können. Da das MMMF-Modell aus einem Gebiet mit einer einfachen Geländekonfiguration und vergleichsweise regelmäßigen Niederschlagsbedingungen stammt, musste

das Modell modifiziert werden, um das Untersuchungsgebiet, das eine komplexe Geländekonfiguration unter einem saisonalen Monsunklima aufweist, besser erfassen zu können.

In der vorliegenden Arbeit wurden die problematischen Aspekte der Berechnung in Bezug auf die effektive Niederschlags-, Interflow- und Transportkapazität des MMMF-Modells identifiziert und korrigiert, indem der Gesamtprozess analysiert wurde (Kapitel 2). In Kapitel drei schließlich wird ein neues Bodenerosionsmodell vorgeschlagen, das DMMF-Modell, das auf dem MMMF-Modell basiert.

In Kapitel 4 untersuchte der Verfasser den Effekt einer räumlichen Rekonfiguration von Erosionsherden auf die Sedimentbelastung eines landwirtschaftlichen Einzugsgebiets im Hochland mithilfe des DMMF-Modells. Dafür wurde das Sedimentumverteilungsmuster und das Bodenerosionsrisiko im Haean-Einzugsgebiet, einem bekannten landwirtschaftlichen Hochland-Einzugsgebiet der Wasserscheide Soyang, einer wissenschaftlichen Beurteilung und Einschätzung unterzogen.

Den Ergebnissen zufolge kann das DMMF-Modell auf Einzugsgebiete mit komplizierten Geländekonfigurationen angewendet werden, die von einem Monsunklima betroffen sind. Die Ergebnisse bestätigten, dass eine räumliche Rekonfiguration der Landschaft in Ergänzung zu anderen bewährten Bewirtschaftungsmethoden, bei denen die Bewirtschaftung von Trockenfeldern im Vordergrund steht, eine wirksame Methode zur Verringerung des Sedimentaustrags aus landwirtschaftlichen Einzugsgebieten im Hochland wie Haean sein kann.

Im letzten Kapitel 5 werden die Umweltfaktoren, die die räumlichen Umverteilungsmuster von Bodennährstoffen wie N und P in Bergwäldern beeinflussen, untersucht. Um dieses Ziel zu erreichen, wurde das LiDAR-Verfahren (light detection and ranging) verwendet, um detaillierte Informationen zur Topographie und physikalischen Struktur der Vegetation zu gewinnen. Daran anschließend wurde eine Einschätzung der zukünftigen räumlichen Muster von Bodennährstoffen wie N und P in der organischen Schicht und im mineralischen Oberboden vorgenommen. Im Zentrum stand dabei die Analyse der relativen Bedeutung der Vegetation und der aus LiDAR extrahierten topografischen Parameter für ein besseres Verständnis der räumlichen Muster von N und P. Zusätzlich identifizierte der Verfasser Gebiete mit kritischen P-Gehalten und testete verschiedene Validierungsstrategien für N und P.

---

## Acknowledgements

Undertaking this graduate research studies has been an invaluable experience for me, and it would not have been possible to do without the blessing of God, and the support that I received from many people.

I would like to express my wholehearted gratitude to my doctor father, Prof. Dr. Björn Reineking, for all the support, excellent guidance, and generous patience that he gave throughout my doctoral research studies. He gave me a great opportunity to study at Bayreuth University as a member of the TERRECO project and always took me in the right direction. Without his tremendous support and help, this Doctoral thesis would not have been finished. I sincerely show my thanks to Prof. Dr. Bernd Huwe for his valuable comments and discussion on the topics of soil erosion.

I gratefully acknowledge the financial support of the Deutsche Forschungsgemeinschaft (DFG). All the research studies in this thesis were carried out in the framework of the International Research Training Group TERRECO (GRK 1565/2), funded by the Deutsche Forschungsgemeinschaft (DFG) at the University of Bayreuth. I also want to thank the head of the TERRECO project, Prof. Dr. John Tenhunen, whose passion and efforts led this project successfully and has been a good model for every member of the project.

My special thanks also to all the members of the TERRECO project, especially Gwanyong Jeong, Kiyong Kim, Eun-young Jung, Saem Lee, Youngsun Kim, Ilkwon Kim, Jong Yol Park, Jintae Hwang, Mi-Hee Lee, Bumsuk Seo, Heera Lee, Ikchang Choi, Hamada Elsayed Ali, Jean-Lionel Payeur-Poirier, Ganga Ram Maharjan, Marianne Ruidisch, Cosmas Lambini, Silvia Parra, Steve Lindner, Wei Xue, and Hannes Oeverdieck, for the friendly conversations and passionate discussions that I shared with them, and the generous encouragement that I received from them. Their encouragement and support allowed me to move forward through hardship and adversity during my graduate research studies. I am also grateful to Bärbel Heindl-Tenhunen, Sandra Thomas, Margarete Wartinger and Andreas Kolb, for their outstanding help in the office work. Many thanks also go to Violaine Zigan, for her kind help in preparing documents for this thesis. Besides the other members of the TERRECO project, I would like to express my gratitude to Sebastian Arnold, my good friend and great mentor. May his soul rest in peace.

I also want to express my thanks to all members of the biogeographical modelling department, Timothy Thrippleton, Eva-Marie Obermaier, Klara Dolos, and for their sincere help from the beginning of my life in Bayreuth. I also want to show my gratitude to Jaewoo Jung, Dong-jae Lee-Otto, and Frau Mader. Thanks to them, I could enjoy happy and beautiful days in Bayreuth. I am indebted to Prof. Dongwook Ko and all the members of Landscape ecology lab in Kookmin University, for their encouragement during the final stages of my doctoral studies in Korea.

Last but not least, I would like to express my gratitude to my father, my sister, and especially to my beloved wife, Bora, for their countless sacrifices, unlimited support, and perseverance for waiting so far. And to my son, Yuchan, for being such a good little boy, and making it possible for me to complete what I started.

# Contents

|  |          |
|--|----------|
| Summary . . . . .  | i        |
| Zusammenfassung . . . . .  | iii      |
| Acknowledgements . . . . .   | v        |
| Table of contents . . . . .  | vii      |
| List of figures . . . . .  | xii      |
| List of tables . . . . .   | xiv      |
| <b>1 Synopsis . . . . .</b>  | <b>1</b> |
| 1.1 Introduction . . . . .   | 1        |
| 1.1.1 General introduction of soil erosion . . . . .   | 1        |
| 1.1.2 Soil erosion problem in the Soyang watershed . . . . .   | 2        |
| 1.1.3 State of the art of soil erosion study in the Soyang watershed . . . . .   | 3        |
| 1.1.4 Comparison of soil erosion models with the Morgan-Morgan-Finney model . . . . .  | 5        |
| 1.1.5 Spatial distribution of substances and nutrients in the mountainous forest . . . . .   | 7        |
| 1.1.6 TERRECO project . . . . .  | 8        |
| 1.1.7 Research objectives . . . . .  | 8        |
| 1.1.7.1 Development of a soil erosion model for a complex terrain region<br>under a monsoonal climate regime . . . . .                             | 9        |
| 1.1.7.2 Effect of spatial reconfiguration of landscape on stream sediment<br>load from an upland agricultural catchment . . . . .                  | 9        |
| 1.1.7.3 Investigating environmental drivers that determine spatial redi-<br>stribution patterns of soil nutrients in the mountain forest . . . . . | 10       |
| 1.2 Method and materials . . . . .   | 10       |
| 1.2.1 Study areas . . . . .  | 10       |

|              |  |           |
|--------------|--|-----------|
| 1.2.2        | Development of a soil erosion model for a complex terrain region under a monsoonal climate regime (Chapters 2 & 3) . . . . . | 12        |
| 1.2.3        | Effect of spatial reconfiguration of landscape on reducing sediment yield from the catchment (Chapter 4) . . . . .           | 14        |
| 1.2.4        | Effect of topography and vegetation structure on spatial patterns of soil nutrients (Chapter 5) . . . . .                    | 16        |
| 1.3          | Results and discussion . . . . .   | 18        |
| 1.3.1        | Development of a soil erosion model for a complex terrain region under a monsoonal climate regime (Chapters 2 & 3) . . . . . | 18        |
| 1.3.2        | Effect of spatial reconfiguration of landscape on reducing sediment yield from the catchment (Chapter 4) . . . . .           | 19        |
| 1.3.3        | Effect of topography and vegetation structure on spatial patterns of soil nutrients (Chapter 5) . . . . .                    | 20        |
| 1.4          | Outlook . . . . .  | 23        |
| 1.5          | Concluding remarks . . . . .   | 25        |
| 1.6          | List of manuscripts and specification of individual contributions . . . . .  | 26        |
| <b>2</b>     | <b>Commentary on Modified MMF model by Morgan and Duzant (2008)</b>  | <b>41</b> |
| 2.1          | Introduction . . . . .   | 42        |
| 2.2          | Problematic parts of the MMMF model . . . . .  | 43        |
| 2.2.1        | Trigonometric error in the calculation of effective rainfall . . . . .   | 43        |
| 2.2.1.1      | Consequence of the error in calculating effective rainfall . . . . .   | 44        |
| 2.2.2        | Quantity estimation error in calculating interflow . . . . .   | 46        |
| 2.2.2.1      | Incorrect formula in the interflow equation . . . . .  | 46        |
| 2.2.2.2      | Discrepancy between generated and transferred interflow . . . . .  | 48        |
| 2.2.2.3      | Consequence of the error in calculating interflow . . . . .  | 49        |
| 2.2.3        | Improperly normalized C-factor in the transport capacity equation . . . . .  | 50        |
| 2.2.3.1      | Consequence of improper normalization of the C-factor . . . . .  | 51        |
| 2.3          | Conclusions . . . . .  | 52        |
| Appendix 2.A | Derivation of the corrected interflow equation using Darcy's law . . . . .   | 53        |

---

|          |   |           |
|----------|---|-----------|
| <b>3</b> | <b>Daily Based Morgan–Morgan–Finney (DMMF) Model</b>  | <b>58</b> |
| 3.1      | Introduction . . . . .  | 59        |
| 3.2      | Model Description . . . . .   | 62        |
| 3.2.1    | The DMMF Model . . . . .  | 62        |
| 3.2.2    | Hydrological Phase . . . . .  | 63        |
| 3.2.2.1  | Surface Runoff Process . . . . .  | 63        |
| 3.2.2.2  | Interflow Process . . . . .   | 65        |
| 3.2.3    | Sediment Phase . . . . .  | 66        |
| 3.2.3.1  | Sediment Delivery to Surface Runoff . . . . .   | 67        |
| 3.2.3.2  | Gravitational Deposition of Suspended Sediments . . . . .   | 70        |
| 3.2.3.3  | Estimation of Sediment Loss from an Element . . . . .   | 72        |
| 3.2.4    | Estimation of Total Runoff and Soil Erosion for Rainfall Period . . . . .                         | 73        |
| 3.3      | Testing the DMMF Model . . . . .  | 73        |
| 3.3.1    | Sensitivity Analysis of the Model . . . . .   | 73        |
| 3.3.2    | Testing the DMMF Model in the Field . . . . .   | 75        |
| 3.4      | Summary and Conclusions . . . . .   | 79        |
| <b>4</b> | <b>Effect of spatial reconfiguration on reducing stream sediment load</b>                         | <b>90</b> |
| 4.1      | Introduction . . . . .  | 91        |
| 4.2      | Materials and Methods . . . . .   | 94        |
| 4.2.1    | Study Area . . . . .  | 94        |
| 4.2.2    | Model Description . . . . .   | 95        |
| 4.2.3    | Model Parameterization . . . . .  | 98        |
| 4.2.4    | Model Calibration and Validation . . . . .  | 101       |
| 4.2.4.1  | Sensitivity Analysis . . . . .  | 103       |
| 4.2.4.2  | Calibration . . . . .   | 104       |
| 4.2.4.3  | Validation . . . . .  | 105       |
| 4.2.5    | Identifying Annual Sediment Redistribution Patterns and Assessing Soil<br>Erosion Risk . . . . .  | 105       |
| 4.2.6    | Evaluation of the Impact of Spatial Reconfiguration of Erosion Hot Spots<br>into Forest . . . . . | 106       |

---

|          |  |            |
|----------|--|------------|
| 4.3      | Results . . . . .  | 106        |
| 4.3.1    | Model Performance . . . . .  | 106        |
| 4.3.2    | Sediment Redistribution Pattern of the Catchment . . . . .   | 110        |
| 4.3.3    | Impacts of Conversion of Erosion Hot Spots into Forest on Total Sediment<br>Yield Entering the Stream . . . . .  | 110        |
| 4.4      | Discussion . . . . .   | 112        |
| 4.4.1    | Model Performance . . . . .  | 113        |
| 4.4.2    | Assessment of Soil Erosion Risk and the Effectiveness of Spatial Reconfig-<br>uration of Erosion Hot Spots on Reducing Sediment Yield Entering the<br>Stream . . . . . | 116        |
| 4.5      | Conclusions . . . . .  | 118        |
|          | Appendix 4.A Detailed Structure of the DMMF Soil Erosion Model . . . . .   | 119        |
| 4.A.1    | Hydrological Phase . . . . .   | 120        |
| 4.A.2    | Sediment Phase . . . . .   | 121        |
| <b>5</b> | <b>Spatial patterns of topsoil nitrogen and phosphorus</b>   | <b>132</b> |
| 5.1      | Introduction . . . . .   | 133        |
| 5.2      | Materials and methods . . . . .  | 135        |
| 5.2.1    | Research area . . . . .  | 135        |
| 5.2.2    | Soil sampling and chemical analyses . . . . .  | 136        |
| 5.2.3    | Environmental predictors . . . . .   | 137        |
| 5.2.4    | Random forest . . . . .  | 138        |
| 5.3      | Results . . . . .  | 139        |
| 5.3.1    | Descriptive statistics of soil nutrients . . . . .   | 139        |
| 5.3.2    | Model validation . . . . .   | 140        |
| 5.3.3    | Environmental drivers of spatial nutrient patterns . . . . .   | 143        |
| 5.4      | Discussion . . . . .   | 145        |
| 5.4.1    | Predictors of soil N and P . . . . .   | 145        |
| 5.4.2    | Spatial patterns of N/P ratios . . . . .   | 147        |
| 5.4.3    | Model performance based on different cross validation schemes . . . . .  | 147        |
| 5.5      | Conclusions . . . . .  | 148        |

**Declaration/Erklärungen****160**

# List of Figures

|                    |  |    |
|--------------------|--|----|
| <b>Figure 1.1</b>  | Location of the Soyang watershed and two study sites . . . . .   | 11 |
| <b>Figure 1.2</b>  | Schematic hydrological phase of the model . . . . .  | 13 |
| <b>Figure 1.3</b>  | Schematic sediment phase of the model . . . . .  | 13 |
| <b>Figure 2.1</b>  | Conceptual representation of a hillslope . . . . .   | 44 |
| <b>Figure 2.2</b>  | Comparison of the effective rainfall equations from MMF model and its<br>variants with the corrected one. . . . .  | 45 |
| <b>Figure 2.3</b>  | Conceptual representation of the interflow . . . . .   | 47 |
| <b>Figure 2.4</b>  | Extent of the overestimation of $IF_{\text{MMMF}}$ compared with $IF_{\text{corrected}}$ by<br>slope and resolution . . . . .                            | 49 |
| <b>Figure 2.5</b>  | Extent of the discrepancy between the generated interflow from a con-<br>tributing element and the transferred interflow to a receiving element. . . . . | 50 |
| <b>Figure 2.A1</b> | Conceptual representation of soil water in an element . . . . .  | 53 |
| <b>Figure 3.1</b>  | Schematic hydrological processes within an element . . . . .   | 63 |
| <b>Figure 3.2</b>  | Conceptual representation of the effective rainfall ( $R_{eff}$ ) on a slope<br>element without permanent interception of rainfall . . . . .             | 65 |
| <b>Figure 3.3</b>  | Conceptual representation of interflow in an element . . . . .   | 67 |
| <b>Figure 3.4</b>  | Schematic sediment phase of an element . . . . .   | 68 |
| <b>Figure 3.5</b>  | Sobol' total indices of model input parameters for a single element . . .  | 76 |
| <b>Figure 3.6</b>  | Sobol' total indices for runoff ( $Q$ ) and sediment loss ( $SL$ ) of the two field<br>sites . . . . .   | 78 |
| <b>Figure 3.7</b>  | Comparison between simulated and observed runoff ( $Q$ ) and sediment<br>loss ( $SL$ ) for field 1 and field 2 . . . . .                                 | 80 |
| <b>Figure 4.1</b>  | General description of the study area . . . . .  | 95 |
| <b>Figure 4.2</b>  | Schematic hydrological phase of the DMMF model . . . . .   | 96 |

|                    |   |     |
|--------------------|---|-----|
| <b>Figure 4.3</b>  | Schematic sediment phase of the DMMF model . . . . .  | 97  |
| <b>Figure 4.4</b>  | Represented soil class from a 2009 catchment-wide field survey . . . . .  | 99  |
| <b>Figure 4.5</b>  | LULC classes and their spatial configurations for the Haean catchment .   | 100 |
| <b>Figure 4.6</b>  | Calibration and validation results for stream discharge and suspended<br>sediment . . . . .   | 108 |
| <b>Figure 4.7</b>  | Annual net soil erosion and soil erosion class of the Haean catchment . .   | 111 |
| <b>Figure 4.8</b>  | Total annual sediment yields and sediment yield reduction efficiency of<br>the spatial reconfiguration of erosion hot spots . . . . .                   | 113 |
| <b>Figure 5.1</b>  | Research area . . . . .   | 135 |
| <b>Figure 5.2</b>  | Model validation based on R-square with cross validation methods . . .  | 141 |
| <b>Figure 5.3</b>  | Boxplots showing standard deviations of 100 predicted values for each<br>raster cell with cross validation methods . . . . .                            | 142 |
| <b>Figure 5.4</b>  | Maps of mean and coefficient of variation (CoV) of 100 models of phos-<br>phorus in the organic layer ( $P_o$ ) with cross validation methods . . . . . | 143 |
| <b>Figure 5.5</b>  | Mean relative importance of predictors for nitrogen and phosphorus based<br>on the increased mean square error (%incMSE) from random forest . . . . .   | 145 |
| <b>Figure 5.6</b>  | Predicted mean soil N and P content and ratios . . . . .  | 146 |
| <b>Figure 5.S1</b> | Model validation based on root mean square error (RMSE) with cross<br>validation methods . . . . .  | 158 |
| <b>Figure 5.S2</b> | Predicted SD nitrogen and phosphorus content and ratios . . . . .   | 159 |

# List of Tables

|                  |  |     |
|------------------|--|-----|
| <b>Table 1.1</b> | Input parameters of the daily based Morgan–Morgan–Finney (DMMF) model . . . . .              | 15  |
| <b>Table 2.1</b> | Previous studies applying the MMF model and its variants to steep hillslopes                 | 45  |
| <b>Table 3.1</b> | Input parameters and their range for sensitivity analysis. . . . .                           | 75  |
| <b>Table 3.2</b> | Range of unmeasured parameters for sensitivity analysis. . . . .                             | 77  |
| <b>Table 3.3</b> | Optimized parameters from the DE algorithm. . . . .  | 78  |
| <b>Table 4.1</b> | Input parameters of the daily based Morgan–Morgan–Finney (DMMF) model . . . . .              | 97  |
| <b>Table 4.2</b> | Typical soil characteristics of each represented soil class of the Haean catchment . . . . . | 98  |
| <b>Table 4.3</b> | The initial parameter settings for each LULC class. . . . .                                  | 101 |
| <b>Table 4.4</b> | Soil erosion risk categories defined by OECD . . . . .                                       | 105 |
| <b>Table 4.5</b> | List of important parameters from forested site . . . . .                                    | 107 |
| <b>Table 4.6</b> | List of important parameters other than forest-related parameters . . . .                    | 109 |
| <b>Table 4.7</b> | Mean annual net soil erosion rate (t/(ha·year)) and mean slope of each LULC type. . . . .    | 112 |
| <b>Table 5.1</b> | Environmental predictors for digital soil mapping. . . . .                                   | 137 |
| <b>Table 5.2</b> | Statistical summary of N and P content (mg kg <sup>-1</sup> ) and ratios. . . . .            | 140 |
| <b>Table 5.3</b> | Statistical summary of N and P content (mg kg <sup>-1</sup> ) and ratios. . . . .            | 144 |

# Chapter 1

## Synopsis

### 1.1 Introduction

#### 1.1.1 General introduction of soil erosion

Soil erosion by water is a natural phenomenon referring to surface wear that occurs when bare soil is exposed to water (Pimentel, 2006). Soil particles are detached from the surface when the splash energy of raindrops or the shear stress of surface runoff are greater than the cohesive forces of surface soil particles. Detached particles are suspended in and transported by water when the energy of the surface runoff is strong enough to carry them (Pimentel *et al.*, 1995, Morgan, 2005). Transported sediments leave their original locations and enter aquatic ecosystems such as streams, rivers, and reservoirs. As soil nutrients adhere to surface soil, soil erosion degrades soil productivity and causes eutrophication of water, which adversely affects the sustainability of natural and human-managed ecosystems (Pimentel and Kounang, 1998, Lal, 2001).

In general, agricultural ecosystems are more vulnerable to soil erosion than natural ones because the former tend to have less surface- and canopy covers than natural ecosystems such as forests and pastures. In addition, the physical structure of the surface soil of agricultural ecosystems is weaker than those of natural ecosystems as soils in agricultural fields are exposed to frequent anthropogenic perturbations (e.g., tillage practices, and depletion of soil organic matter by intensive agricultural activity) (Pimentel and Kounang, 1998, Lal, 2001). Therefore, agricultural expansion and intensification have accelerated soil erosion and accrued environmental and economic costs such as the degradation of soil fertility, decreasing crop productivity, eutrophication, reduced reservoir storage, and increased water treatment cost (Pimentel *et al.*, 1995).

### 1.1.2 Soil erosion problem in the Soyang watershed

Soil erosion is a serious problem both environmentally and economically in the Soyang watershed, South Korea (Kim *et al.*, 2016, Maharjan *et al.*, 2016). The watershed is located upstream of the Han River basin, the largest water basin in South Korea (Chang, 2008). As the Han River basin is the main freshwater resource for over twenty million people (approximate 50% of the South Korean population), securing adequate water quantity and sustaining clean water quality are among the most important goals for the Soyang watershed (Chang, 2008, 2005, Lee *et al.*, 2017).

However, the region suffers from periodic severe soil erosion and consequent water deterioration due to the East Asian summer monsoon and its attendant concentrated rainfall (Maharjan *et al.*, 2016, Yoon and Woo, 2000). In recent decades, the soil erosion of the Soyang watershed deteriorated owing to agricultural expansion and intensification necessitated by a rapid increase in the population of the Han River basin region together with irregular and extremely heavy rainfall due to climate change (Reza *et al.*, 2016). The problem is more notable in upland agricultural areas such as the Haean catchment, where the well-preserved forest hillslopes have been converted into intensively managed dry crop fields subsequent to their being clear-cut. Owing to topography, erosion-prone hillslopes that experience massive land use and land cover (LULC) changes generate a considerable amount of sediment every summer during the monsoon season (Arnhold *et al.*, 2013, Ruidisch *et al.*, 2013, Arnhold *et al.*, 2014). To compensate for soil and soil nutrients lost from repeated soil erosion, farmers in the Haean catchment apply a large amount of fertilizer and import soils from outside of the agricultural fields as conventional practices (Maharjan *et al.*, 2016). Added soil and applied fertilizer, loosely placed on the surface, tend to be easily washed out by the seasonal concentrated rainfall, which often causes severe terrestrial soil erosion at the entrance to inland water systems, leading to eutrophication (Pimentel *et al.*, 1995, Lee, 2008).

Another source of water deterioration in the Soyang watershed is forest-originated matters, including surface soil particles and a massive amount of woody debris, both of which contain ample nutrients such as nitrogen and phosphorus (Harmon *et al.*, 1986, Choi, 2014). Inflowing forest-originated matters to the Soyang reservoir not only increase the turbidity of water but also cause eutrophication by nutrients adhering to soil particles or being released from decayed woody debris in the water (Choi, 2014).

To mitigate the problem, a variety of legislation and best management practices have been applied in the Soyang watershed. The government of South Korea established legislation on

creating crop lands, which strictly prohibits converting forests into crop lands and cultivating hillslopes with gradients of 15% or above. Soil collecting from forests and importing soils for upland agricultural areas are also regulated by legislation (Jeon and Kang, 2010). Local governments have focused on mitigation measures by adopting various best management practices (BMPs) in regions with severe soil erosion. They have encouraged farmers to plant or preserve natural vegetation on field margins around crop fields, and have instituted fallowing for the upland agricultural areas with severe soil erosion utilizing subsidies to farmers of the area. Additionally, they have built sediment capturing infrastructures such as sediment settling basins and erosion control dams, to reduce the amount of sediment flowing into streams and the Soyang reservoir (Jeon and Kang, 2010).

### 1.1.3 State of the art of soil erosion study in the Soyang watershed

Various field- and model-based studies have been conducted on the Soyang watershed and Haeon catchment to determine the main drivers of soil erosion and to help in decision-making.

Field-based studies have been performed at the plot scale, focusing on the impact of field management methods on surface water discharge and soil erosion rate in the Haeon catchment. Ruidisch *et al.* (2013), in field experiments, examined the effect of plastic mulching of the dry crop fields on surface runoff and soil erosion. They found that ridge tillage with plastic mulching caused more soil erosion than ridge tillage without plastic mulching. As the plastic-covered ridge prevents water from infiltrating into the soil, surface water is accumulated at the furrow and consequently washes out unprotected surface soil with intense energy. Arnhold *et al.* (2013) showed a result similar to those of Ruidisch *et al.* (2013), wherein the ridge tillage with plastic mulching increased soil erosion in the upland dry crop fields through a model-based study using Erosion 3D (von Werner, 1995). Arnhold *et al.* (2014) showed that organic farming was more effective in preventing soil erosion than conventional farming as organic farming had a higher vegetative surface cover ratio from leaving more weeds in the crop field. Ali and Reineking (2016) focused on the vegetation structure of field margins that were located around crop fields. They demonstrated that field margins with high vegetation density captured more sediment generated by dry crop fields and consequently reduced more off-site pollution caused by soil erosion.

Several model-based studies have attempted to identify the optimal methods to mitigate soil erosion of the Haeon catchment by simulating BMP scenarios and evaluating their effectiveness on sediment yields from the whole Haeon catchment. Utilizing the soil and water assessment

tool (SWAT) (Arnold *et al.*, 1998), Maharjan *et al.* (2016) investigated the effectiveness of split fertilization, cover crop cultivation, and a combination of the two for four major dry crops (i.e., cabbage, potato, radish, and soybean) on water discharge, nitrate loss, and soil erosion from each dry crop as well as for the whole Haean catchment. According to the simulation results, the cover crop cultivation scenario showed remarkable soil erosion reduction efficiency for cabbage, potato, and radish fields, and a slight reduction efficiency for the soybean field compared to the baseline scenario with cultivation without cover crops. When cover crop cultivation was applied to all major dry crop fields, sediment loss from the catchment decreased by 19% compared to those from the baseline scenario. Jang *et al.* (2017) also projected BMP scenarios such as vegetation buffer strip (VFS) and rice straw mulching (RSM) in the Haean catchment using the SWAT model and demonstrated that applying VFS and RMS on upland agricultural areas reduced soil erosion by 25.7% and 6.3%, respectively.

Although catchment scale studies have demonstrated the effectiveness of various kinds of BMPs in mitigating soil erosion in the Haean catchment, the BMPs suggested by these studies have several limitations for practical application in this catchment. The BMPs that were tested in the previous studies were based on the assumption that each BMP should be adopted uniformly to all dry crop fields in the Haean catchment to obtain the expected mitigation result; this would require faithful fulfillment of all stakeholders in the catchment including farmers and landowners. However, this is not easy to achieve, as each stakeholder who owns and manages dry crop fields pursues different interests (Poppenborg and Koellner, 2013). There are other types of BMPs such as constructing turbid water abatement facilities and riparian buffers at the tail water, and reforesting crop fields and barren lands considering spatial configurations in the catchment, which are frequently applied to mitigate the sediment export into the stream (Jeon and Kang, 2010). However, only a few studies have focused on the importance of spatial configurations on regulating ecosystem services (Chaplin-Kramer *et al.*, 2015, 2016). Chaplin-Kramer *et al.* (2015) and Chaplin-Kramer *et al.* (2016) showed that ecosystem services such as carbon stock and soil erosion regulation responded non-linearly to spatial relocation of forest to agriculture lands, which indicated the importance of spatial configurations in ecosystem services and functions.

Previous catchment scale studies performed in the Soyang watershed and Haean catchment have also overlooked the contribution of forests to catchment scale soil erosion and sediment yield, even though forest is the dominant land cover type in these regions (Seo *et al.*, 2014, Kim *et al.*, 2017). According to Meusburger *et al.* (2013), the annual soil erosion rate in the forested area of the Haean catchment was much higher than that reported by Pimentel (2006), as most forest in the Haean catchment is located in the steep mountainous area. Furthermore, Hou *et al.*

(2014) demonstrated the impacts of vegetation structures and compositions on soil erosion rate in forests located on hillslopes (Hou *et al.*, 2014).

#### 1.1.4 Comparison of soil erosion models with the Morgan-Morgan-Finney model

There are various types of models for projecting soil erosion, which can be categorized as empirical, process-based, and conceptual according to their model structure. Empirical models such as the universal soil loss equation (USLE) (Wischmeier and Smith, 1978), revised universal soil loss equation (RUSLE) (Renard *et al.*, 1991), and modified universal soil loss equation (MUSLE) (Williams, 1975) are simple combinations of parameters related to soil erosion. As they have a simple structure that can be easily implemented and demand a moderate amount of data and computing resources, these models have been frequently utilized for estimating soil erosion rates at every spatial scale from plot to catchment (Lal, 2001, Morgan *et al.*, 1984, Morgan, 2001, Merritt *et al.*, 2003, Lihare *et al.*, 2014). However, as the models are composed of simple empirical relationships to calculate soil erosion rate of an area, it is not easy to understand the underlying physical processes that bring out a particular result. Also, due to the empirical relationships of the models being driven mostly by their place of origin, the models are often not applicable to other regions with different environmental and LULC conditions (Merritt *et al.*, 2003, Lihare *et al.*, 2014, Hu and Flanagan, 2013).

Process-based models such as the water erosion prediction project (WEPP) (Nearing *et al.*, 1989), Limberg soil erosion model (LISEM) (De Roo *et al.*, 1996), and European soil erosion model (EUROSEM) (Morgan *et al.*, 1998), on the other hand, calculate soil erosion rate with definite and elaborated equations based on physical laws (e.g., conservation laws of mass and momentum) (Merritt *et al.*, 2003, Hu and Flanagan, 2013). Although they have theoretically firm physical foundations, these models often demand a considerable amount of data and computing resources for initialization, calibration, and simulation, as they contain various complex equations involving many parameters. Consequently, process-based models are usually limited to projecting short-term temporal soil erosion events occurring on relatively small spatial scales such as field- and plot-levels (Merritt *et al.*, 2003, Lihare *et al.*, 2014, Hu and Flanagan, 2013).

Conceptual models such as the Morgan–Morgan–Finney (MMF) (Morgan *et al.*, 1984) and the topography-based hydrological model (TOPMODEL) (Beven and Kirkby, 1979) are considered to be midway between empirical and process-based soil erosion models, taking advantages of both types. Conceptual models often simplify the soil erosion phenomenon into a few conceptual

physical processes. Although these models are basically based on rigorous laws of physics, their parameters and sub-processes are substituted with simple empirical relationships for the sake of computational convenience. As a result, conceptual models can be applied to various spatial scales for simulating surface runoff and soil erosion rates while allowing for an understanding of underlying processes of soil erosion (Morgan *et al.*, 1984, Morgan, 2001, Lilhare *et al.*, 2014, Morgan and Duzant, 2008, Devia *et al.*, 2015).

Among the conceptual soil erosion models, the MMF model and its variants (i.e., the revised Morgan–Morgan–Finney (RMMF) (Morgan, 2001) and modified Morgan–Morgan–Finney (MMMMF) (Morgan and Duzant, 2008) models) have been successfully applied for simulating surface runoff and soil erosion rates in regions with various climate and land use types (Morgan *et al.*, 1984, Morgan, 2001, Lilhare *et al.*, 2014, De Jong *et al.*, 1999, López-Vicente *et al.*, 2008, Vieira *et al.*, 2014). The MMF model and its variants calculate the annual soil erosion rate by comparing the masses of detached surface soil particles suspended in the water of a region with the sediment transport capacity of surface runoff (Morgan *et al.*, 1984, Morgan, 2001, Vigiak *et al.*, 2005). In the original MMF model, only splash erosion by raindrop impact was considered as the primary driver of sediment detachment from the surface, and there were no quantitative considerations of surface cover and vegetation structures as drivers of sediment detachment (Morgan *et al.*, 1984, Morgan, 2001). The RMMF model began to take account of sheet and rill erosion by surface runoff as well as the effect of canopy and ground cover on soil erosion to estimate the amount of sediment detachment from the surface. In addition, the model took the inter-connectivity of each area into account, which allowed for explicitly estimating the soil loss and deposition rate of each area (Morgan, 2001, Vigiak *et al.*, 2005). In the modified version, empirical parameters representing surface ground conditions and vegetation structures were substituted for the more physically explicit ones. The model also partitioned water flow into surface runoff and subsurface interflow, and calculated soil erosion according to each soil particle size class (e.g., clay, silt, and sand). These modifications allowed the model to consider the impact of land use change and crop field management practices on soil erosion more rigorously, as well as to reinforce its physical basis, which brought a more accurate projection of soil erosion rates of various regions that feature a variety of environments and management types (Lilhare *et al.*, 2014, Morgan and Duzant, 2008).

The aforementioned characteristics of the MMF model makes it suitable for application to the Haean catchment to determine the BMPs for soil erosion mitigation. The MMF model allows evaluation of the impact of the spatial configuration of the catchment on soil erosion as the model calculates a soil budget explicitly, considering inflow of soil from upslopes. The model is

also applicable to complex terrain configurations with various vegetation types, including minor crops and forests whose empirical relationships with soil erosion were not established. As there are various types of crop fields in the Haean catchment (e.g., rice, potato, cabbage, radish, bean, etc.), it is preferable to use the physical structure of crops than to parameterize the impacts of each crop field on soil erosion. Therefore, we can determine the effect of reforestation on soil redistribution patterns in the catchment.

### 1.1.5 Spatial distribution of substances and nutrients in the mountainous forest

Forests are the dominant land cover type in the Soyang watershed and are mainly located in the steep mountainous areas where agricultural development pressure is low (Kim *et al.*, 2017, Hwang *et al.*, 2008). Mountainous forests provide various ecosystem services (ES) such as supplying purified fresh water and protecting the surface soil from erosion. In addition, forests efficiently sequester atmospheric carbon dioxide through photosynthesis and store photosynthetic products as a form of biomass, an essential energy source for forest ecosystems (Kim *et al.*, 2017, Millennium Ecosystem Assessment, 2005).

Parts of forest photosynthetic products are left on the forest floor as woody debris (e.g., leaves, branch, fruit, bark, bud scale, and flower), which decompose into smaller units of organic matter and nutrients through animal activity and microbial processes (Harmon *et al.*, 1986, Choi, 2014). In the unmanaged mountain forest with little anthropogenic disturbance, the woody debris remains on the forest floor and is washed out by wind or surface runoff strong enough to carry it. Since the Soyang watershed experiences intensive heavy downpours during the summer monsoon season, concentrated surface runoff washes out a tremendous amount of soil particles as well as fresh woody debris and decayed particulate organic matter from the mountain forest, some of which enters into the aquatic system and harms the quality of the freshwater resources of the Soyang reservoirs (Choi, 2014). Spatially distributed organic matter and nutrients (e.g., nitrogen and phosphorus) from surface runoff of woody debris affect not only the biodiversity and species composition of the forest and headwater stream ecosystems but also the fresh-water resource quality of aquatic ecosystems such as rivers and reservoirs (Harmon *et al.*, 1986, Choi, 2014, Ward and Aumen, 1986, Rowland *et al.*, 2017).

Most of the soil erosion models applied to the Soyang watershed were USLE-based models such as RUSLE and SWAT. These models originally targeted agricultural fields, so they were not appropriate for steep slopes as they consider woody debris on the forest floor as the stationary

surface cover protecting against surface soil erosion (Elliot, 2004, Neitsch *et al.*, 2011). As a result, although the mountain forest is the dominant land cover of the Soyang watershed, previous studies performed in this region have often ignored the soil erosion impact of the mountain forest due to its abundant surface woody debris such as leaves (Maharjan *et al.*, 2016, Jang *et al.*, 2017).

### 1.1.6 TERRECO project

Studies for this thesis were conducted within the scope of the TERRECO (Complex **T**errain and **E**cological Heterogeneity) project. TERRECO was an international research and training group, which aimed to understand ecological processes and assess ecosystem functions and services spatially in complex terrain regions. Specifically, the project focused on evaluating those changes in ecosystem services driven by anthropogenic and environmental changes from various perspectives such as water quality and quantity, soil erosion, crop and forest production, and biodiversity. Based on this, the project aimed to provide a framework for understanding and managing such areas (Kang and Tenhunen, 2010).

In this thesis, we focused on the spatial patterns of soil and soil organic matter, which is relevant to the soil erosion and water quality of mountainous catchments with complex terrain.

### 1.1.7 Research objectives

The main objectives of this thesis were to understand the spatial patterns on the landscape scale of sediment redistribution by soil erosion in forest-dominated mountainous watersheds with complex terrain configurations and to find ways to mitigate water quality deterioration due to soil erosion of the Soyang watershed.

For these purposes, we developed a new soil erosion model that was appropriate for the climate and terrain configurations of the Soyang watershed by modifying the existing Modified Morgan–Morgan–Finney soil erosion model. We also investigated spatial patterns of soil nutrients in steep mountain forests for a better understanding of soil erosion in the mountainous forest, which is the dominant land cover of the Soyang watershed.

### **1.1.7.1 Development of a soil erosion model for a complex terrain region under a monsoonal climate regime**

The Soyang watershed is affected by an extremely irregular seasonal monsoon climate and has complex terrain configurations with various LULCs and surface cover conditions. To suggest optimal mitigation measures for soil erosion in this region, new types of soil erosion models are needed to consider extremely concentrated rainfall regimes and complex terrain configurations. For these purposes, we suggested a new soil erosion model, a daily-based Morgan–Morgan–Finney (DMMF) model, based on the Modified Morgan–Morgan–Finney (MMMMF) model with the following improvements:

- (1) conversion of the temporal scale of the model from an annual to a daily basis, which make it suitable for regions with intensive seasonal rainfall,
- (2) inclusion of the concepts of impervious surface covers for reflecting concrete ditches, pavements, and plastic mulching, and
- (3) revision of the effective rainfall equation, interflow equation, and equations relevant to the USLE C-factor in the transport capacity equation.

### **1.1.7.2 Effect of spatial reconfiguration of landscape on stream sediment load from an upland agricultural catchment**

In this section, we aimed to assess the soil erosion risk of the Haean catchment using the DMMF model and evaluate the impact of the spatial reconfiguration altering erosion hot spots into forests on reduction sediment yield into the stream. The detailed objectives were:

- (1) determining the applicability of the DMMF model for stream discharge and suspended sediment in the catchment scale,
- (2) estimating the sediment redistribution pattern of the catchment and assessing the soil erosion risk of the Haean catchment, and
- (3) evaluating the effectiveness of the spatial reconfiguration of erosion hot spots into forests on reducing sediment yield entering into the stream.

### 1.1.7.3 Investigating environmental drivers that determine spatial redistribution patterns of soil nutrients in the mountain forest

We investigated the spatial patterns of nitrogen (N) and phosphorus (P) using high-resolution light detection and ranging (LiDAR)-derived vegetation and topographical data for understanding soil erosion patterns in the steep mountainous forest. The specific goals of our research were:

- (1) to evaluate the importance of vegetation and topographic parameters derived from LiDAR on predicting spatial distribution patterns of N and P,
- (2) to identify regions with critical soil P contents, and
- (3) to test model performance based on different cross-validation strategies to suggest an optimal model for the spatial distribution pattern predictions of N and P.

## 1.2 Method and materials

### 1.2.1 Study areas

The study was performed at two catchments belonging to the Soyang watershed (127.728° to 128.588° E and 37.688° to 38.500° N), which is located in the north-eastern part of South Korea (see Fig. 1.1). The Soyang watershed is the upstream region of the Han River basin, which is the crucial freshwater resource for more than twenty million residents, including the residents of the Seoul metropolitan area. Therefore, managing its water quality and quantity to be clean and sustainable is one of the most critical environmental issues in this watershed (Chang, 2008, 2005, Lee *et al.*, 2017).

The dominant land cover type of the Soyang watershed is the forested ecosystem (83.8%) with deciduous forests (51.8%), coniferous forests (25.4%) and mixed forests (22.8%) (Kim *et al.*, 2017, Jeong, 2016). The rest of the regions are intensively managed as dry crop fields (3.8%), rice paddies (1.6%), and residential areas (1.1%) (Kim *et al.*, 2017). Dry crop fields are mostly located in the upland agricultural areas (e.g., Haeon and Jawoon-ri), which are situated at the upstream region of the watershed. Residential areas are mostly concentrated in Chuncheon, the largest city in the Soyang watershed (Kim, 2017, Maharjan *et al.*, 2013).

The second (Chapter 3) and the third (Chapter 4) parts of this study were conducted in the Haeon catchment (see Fig. 1.1c) which is located in the northern part of the Soyang watershed, bordering North Korea (128.135° E, 38.277° N). The catchment is a bowl-shaped mountainous

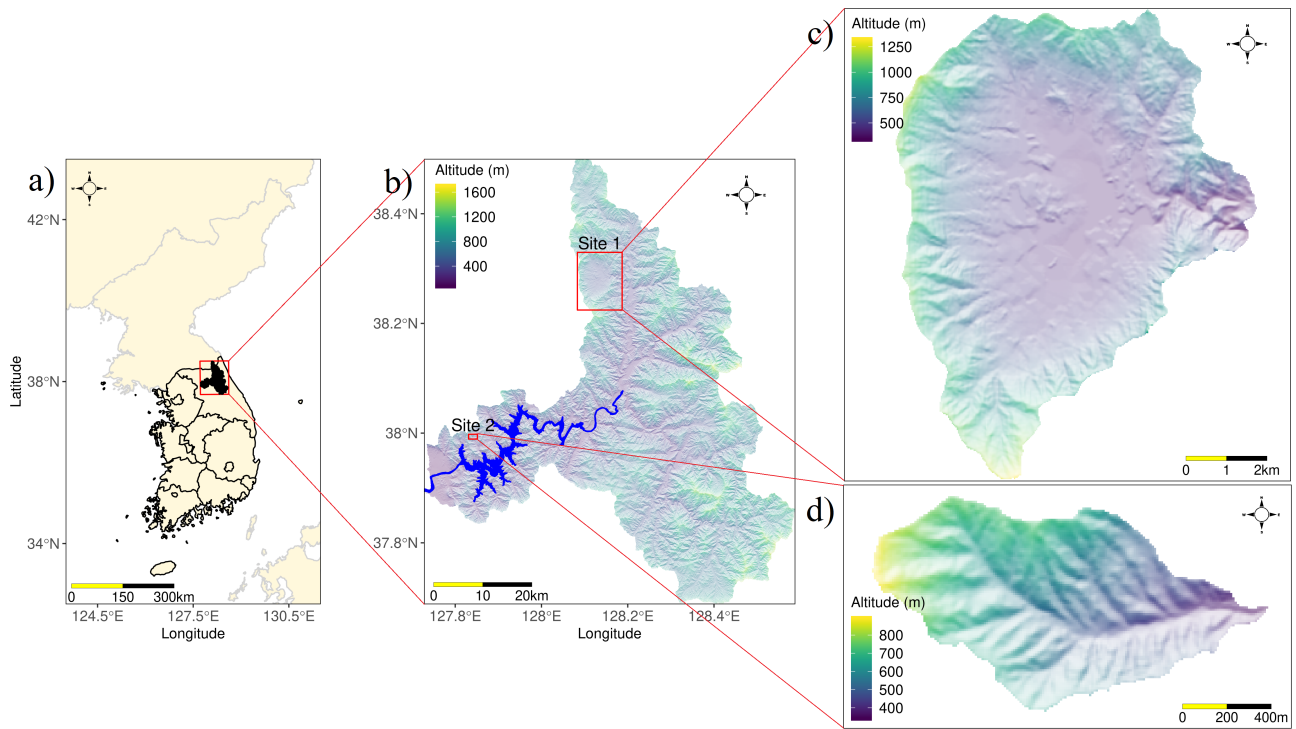


Fig. 1.1. Location of the Soyang watershed and two study sites. (a) Location of the Soyang watershed in South Korea, (b) topography of the Soyang watershed and two sub-catchments for this study, (c) topography of the Haeon catchment, mountainous catchment with complex surface configuration, and (d) topography of the forested sub-catchment in Chuncheon

erosion basin with low and flat central areas and a high, steep catchment boundary (339 to 1,321 m above sea level) (Maharjan *et al.*, 2016, Arnhold *et al.*, 2013, Lee, 2009). The unique bowl shape of the catchment was made by differential erosion of its two different bedrocks of weathering-resistant gneiss at the higher elevations close to the catchment boundary and weathering-susceptible granite in the flat central areas (Lee, 2009).

The catchment has two distinct seasonal climates: a hot and humid summer affected by the North Pacific high, and a cold and dry winter affected by the Siberian high (Shope *et al.*, 2014, Park *et al.*, 2011). The average annual temperature from 2009 to 2018 was 8.7 °C with a range of −28 to 35 °C. The average annual precipitation from 2009 and 2018 was 1,272.3 mm, and approximately 61.3% of the rainfall is concentrated in the summer monsoon season from June to August (Korea Meteorological Administration, 2019). Similar to the Soyang watershed, the dominant land cover type of the Haeon catchment is forest (58%), which ranges from the upper hillslope to the summit of the mountain surrounding the catchment. However, unlike the Soyang watershed, the catchment has an extremely high proportion of agricultural fields (30%), comprised mostly of dry crop fields (22%) cultivated in the steep upper hillslope and rice paddies (8%) cultivated in the lower flat center. The rest of the area is covered by semi-natural vegetation and shrub (9%), bare surface (5%), and residential areas (3%) (Seo *et al.*, 2014).

The fourth part of this study was performed in the small catchment of Chuncheon (see Fig. 1.1d), located in the downstream region of the Soyang watershed ( $127.841^\circ$  E,  $37.993^\circ$  N). This catchment is a small mountain forest catchment with a size of  $9.84 \text{ km}^2$ . The elevation of the catchment ranges from 320 to 868 m, including various steep slopes over  $45^\circ$  caused by Quaternary tectonic uplift (Lee, 2004). The bedrock of this area is comprised of banded and granitic gneiss formed mostly in the Paleoproterozoic period (Chough, 2013). The average annual temperature of this catchment from 2009 to 2018 was  $10.9^\circ\text{C}$  with a range of  $-24$  to  $40^\circ\text{C}$ . The average annual precipitation of this catchment between 2009 and 2018 was  $1,349.5 \text{ mm}$ , with  $62.1\%$  concentrated in the summer monsoon season from June to August (Korea Meteorological Administration, 2019). The catchment belongs to the National Forest managed by Korea Forest Service (KFS) and is dominated by Mongolian oak (*Quercus mongolica*), Korean pine (*Pinus koraiensis*), Japanese red pine (*Pinus densiflora*), and Japanese larch (*Larix kaempferi*) (Jeong *et al.*, 2017).

### 1.2.2 Development of a soil erosion model for a complex terrain region under a monsoonal climate regime (Chapters 2 & 3)

The main structure of the DMMF model can be separated into two phases: the hydrological phase and the sediment phase. The hydrological phase calculates the amount of surface runoff, which is the key factor determining the amount of soil particles detached from a region. As the model considers the interconnectivity of each region from the upslopes, the model can estimate the net water discharge and net soil budget of the region.

The schematic hydrological phase is described in Fig. 1.2. Surface runoff is generated when the amount of surface water inflow into a region exceeds the surface water infiltration capacity ( $SW_c$ , mm). The amount of surface runoff generated in a region ( $Q$ , mm) of size  $A$  ( $\text{m}^2$ ) is the sum of the effective rainfall ( $R_{eff}$ , mm) and surface water inflow from upslope areas ( $Q_{in}$ , L) minus the amount of water infiltration into the soil ( $SW_c$ ). In the soil layer, subsurface water from upslope areas ( $IF_{in}$ , L) flows into a region. The subsurface water inflows ( $IF_{out}$ ) and existing soil water in the region ( $SW_{init}$ , mm) determine water infiltration capacity ( $SW_c$ ). After water infiltration into the soil layer, soil water exceeding the soil water at field capacity ( $SW_{fc}$ , mm) flows out from a region. Some part of the surface and soil water is lost to evapotranspiration ( $ET$ , mm), while the rest flows to downslope areas as surface ( $Q_{out}$ , L) and subsurface water ( $IF_{out}$ , L).

The model estimates sediment balance in the sediment phase, as described in Fig. 1.3. In

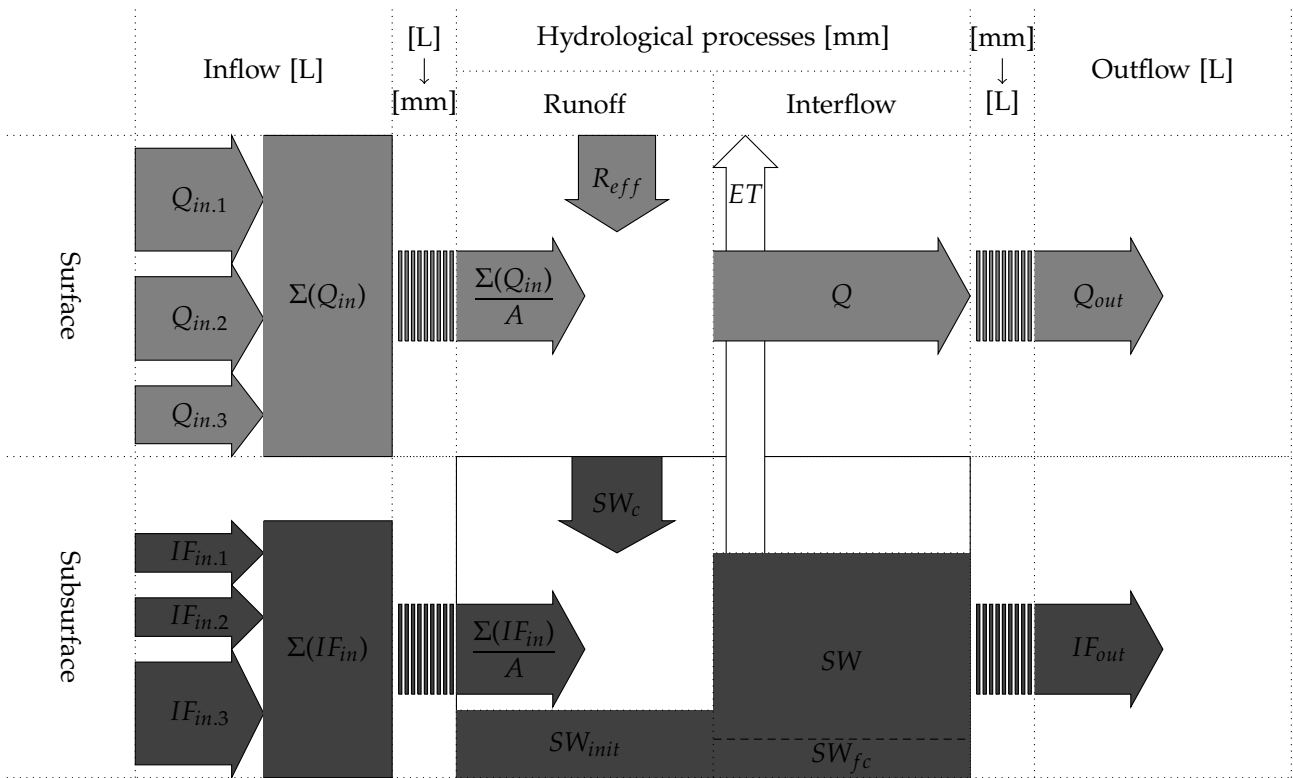


Fig. 1.2. Schematic hydrological phase of the model, adapted from Choi *et al.* (2017).

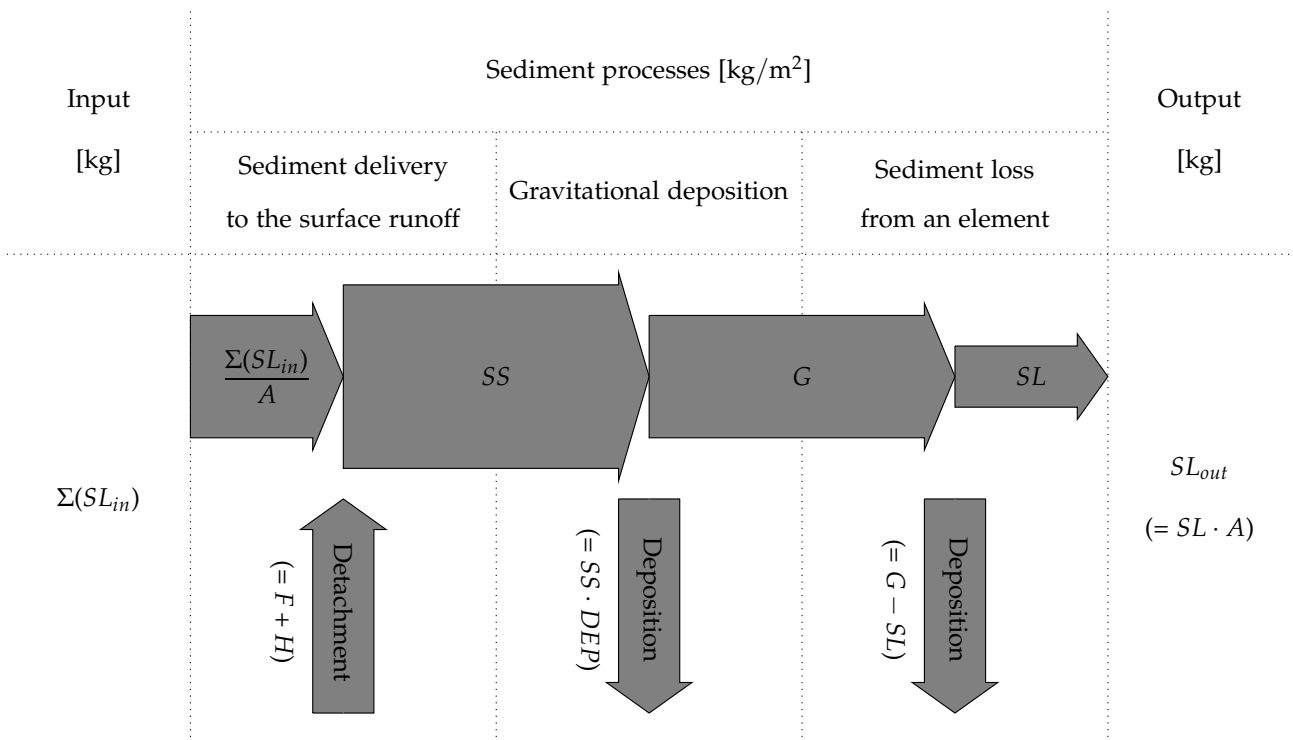


Fig. 1.3. Schematic sediment phase of the model, adapted from Choi *et al.* (2017).

the model, the amount of soil loss from a region ( $SL$ , kg/m<sup>2</sup>) is determined by comparing the transport capacity of runoff ( $TC$ , kg/m<sup>2</sup>) with available sediment for transport ( $G$ , kg/m<sup>2</sup>). The first step of the sediment phase is to calculate the amount of sediment delivered to surface

runoff. In this step, the sediment is delivered to and suspended in the surface water ( $SS$ ,  $\text{kg}/\text{m}^2$ ) of the region from two main sources: internally-originated detached soil particles from direct throughfall ( $F$ ,  $\text{kg}/\text{m}^2$ ) and surface runoff ( $H$ ,  $\text{kg}/\text{m}^2$ ), and external sediment inputs from upslope areas ( $SL_{in}$ ,  $\text{kg}$ ). A portion of suspended sediments ( $DEP$ ) in the surface runoff then settles down due to gravity, which is called gravitational deposition. The rest of the sediments ( $G$ ) are still suspended in the surface runoff, which can be transported to downslope areas. When the transport capacity of runoff ( $TC$ ) is greater than the available sediment for transport ( $G$ ), all available sediment for transport is washed out to downslope areas. Otherwise, only a portion of available sediment for transport ( $G$ ), equal to the transport capacity of runoff ( $TC$ ), can move to downslope areas. The amount of sediment lost from a region is the amount of soil loss from the region ( $SL$ ).

### 1.2.3 Effect of spatial reconfiguration of landscape on reducing sediment yield from the catchment (Chapter 4)

We performed our study in the Haean catchment to test the impact of spatial reconfiguration of a landscape on the reduction of the sediment yield entering a stream. The Haean catchment is a mountainous erosion basin with a complex surface configuration comprising forests, semi-natural areas, rice paddies, residential areas, paved roads, and dry crop fields on the hillslope (Seo *et al.*, 2014). The catchment is an intensive research area of the TERRECO project, where several weather stations and hydrological measurement facilities were installed to measure meteorological (e.g., temperature and rainfall) and hydrological data (e.g., stream discharge and suspended sediments) accurately (Kang and Tenhunen, 2010). Land use and land cover (LULC) types and soil characteristics for each representative LULC-type of the catchment were well-established (Seo *et al.*, 2014, Shope *et al.*, 2014). Having complex surface terrain configurations with various measured data for an initial model run and calibration and validation of the soil erosion model, the Haean catchment was considered suitable for the purpose of our study.

In the catchment, we selected three hydrological points for calibration, validation, and simulation of the model. The first hydrological point was in the mountainous forest site, the second covered the dry crop fields on the hillslope areas, and the last one covered larger areas that included areas that first and second hydrological points covered. Measured stream discharge and suspended sediment data from the first and the second hydrological points were used to calibrate the parameters while those from the third point were used for model validation.

We set the initial value of each parameter based on the existing data set measured from

the Haean catchment as well as literature reviews of the characteristics of crops and field management methods (see Table. 4.1). After setting the initial parameters, we selected and Table 1.1. Input parameters of the daily based Morgan–Morgan–Finney (DMMF) model and sources of initial parameter settings (adapted from Table 1 of Choi *et al.* (2017))

| Type       | Parameter  | Description  | Source                                     |                          |
|------------|--|--|--|--------------------------|
| Topography | $S$  | Slope angle [rad]  | Digital Elevation Model [30 m]             |                          |
|            | $res$  | Grid size of a raster map [m]  |  |                          |
| Climate    | $R$  | Daily rainfall [mm/d]  | Haean weather station network              |                          |
|            | $RI$   | Mean rainfall intensity of a day [mm/h]  |  |                          |
|            | $ET$   | Daily evapotranspiration [mm/d]  | MODIS Evapotranspiration (ORNL DAAC, 2008) |                          |
| Soil       | $P_c$  | Proportion of clay in the surface soil   | TERRECO field survey in 2009               |                          |
|            | $P_z$  | Proportion of silt in the surface soil   |  |                          |
|            | $P_s$  | Proportion of sand in the surface soil   |  |                          |
|            | $SD$   | Soil depth [m]   |  |                          |
|            | $\theta_{init}$  | Initial soil water content [vol/vol]   |  |                          |
|            | $\theta_{sat}$   | Saturated water content [vol/vol]  |  |                          |
|            | $\theta_{fc}$  | Soil water content at field capacity [vol/vol]   |  |                          |
|            | $K$  | Saturated soil lateral hydraulic conductivity [m/d]  |  |                          |
|            | $DK_c$   | Detachability of clay particles by rainfall [g/J]  |  | Morgan and Duzant (2008) |
|            | $DK_z$   | Detachability of silt particles by rainfall [g/J]  |  |                          |
|            | $DK_s$   | Detachability of sand particles by rainfall [g/J]  |  |                          |
|            | $DR_c$   | Detachability of clay particles by surface runoff [g/mm]   |  |                          |
|            | $DR_z$   | Detachability of silt particles by surface runoff [g/mm]   |  |                          |
|            | $DR_s$   | Detachability of sand particles by surface runoff [g/mm]   |  |                          |
| $PI$       | Area proportion of the permanent interception of rainfall                  | Literature review (Morgan, 2005, Arnhold <i>et al.</i> , 2014, Morgan and Duzant, 2008, Shope <i>et al.</i> , 2014, Rural Development Administration of South Korea, 2018) and MODIS NDVI (Didan, 2015, ORNL DAAC, 2017) |  |                          |
| $IMP$      | Area proportion of the impervious ground cover                             |  |  |                          |
| $GC$       | Area proportion of the pervious ground cover                               |  |  |                          |
| $CC$       | Area proportion of the canopy cover of the soil surface                    |  |  |                          |
| $PH$       | Average height of vegetation or crop cover [m]                             |  |  |                          |
| $D$        | Average diameter of individual plant elements at the surface [m]           |  |  |                          |
| $NV$       | Number of individual plant elements per unit area [number/m <sup>2</sup> ] |  |  |                          |
| $d_a$      | Typical flow depth of surface runoff [m]                                   |  |  |                          |
| $n$        | Manning's roughness coefficient of the soil surface [s/m <sup>1/3</sup> ]  |  |  |                          |

calculated the sensitivities of the parameters with high uncertainty: soil hydraulic ( $\theta_{sat}$ ,  $\theta_{fc}$ , and  $K$ ), soil detachability ( $DK_{c,z,s}$  and  $DR_{c,z,s}$ ), and LULC ( $PI$ ,  $IMP$ ,  $GC$ ,  $CC$ ,  $PH$ ,  $D$ ,  $NV$ ,  $d$ , and  $n$ ) parameters, none of which were measured or represented by field samples. Using the Sobol' method (Sobol', 1993), we tested the relative sensitivity of the selected parameters on model outputs for surface runoff and sediment yield into the stream. The Sobol' method is a variance-based sensitivity analysis technique that is widely used in environmental and hydrological modeling such as SWAT and TOPMODEL (Nossent *et al.*, 2011, Qi *et al.*, 2013). As the method calculates the importance of a parameter considering its combined impacts with other parameters (i.e., Sobol' total index), it was deemed suitable for non-linear and non-additive models with many parameters (Nossent *et al.*, 2011, Saltelli and Annoni, 2010).

Important parameters of the Sobol' total index higher than 0.5 were adjusted to find the optimal combination of the parameter set, which made the model outputs match well with the measured stream discharge and suspended sediments from each hydrological point. We applied the differential evolution (DE) (Storn and Price, 1997) optimization method for parameter calibration, setting the average Nash-Sutcliffe efficiency coefficient (NSE) (Nash and Sutcliffe,

1970) for both stream discharge and suspended sediments as a goal function. DE is a heuristic optimization method with an evolution strategy for finding global extreme values (Storn and Price, 1997, Price *et al.*, 2006). As the method requires few prerequisites, DE can be applied to non-differential, nonlinear, and multi-modal models, including hydrological models such as SWAT (Zheng *et al.*, 2015). As the first hydrological point was covered only by forest, we could adjust forest-related parameters such as steep forest soil characteristics and forest vegetation structure. At the second hydrological point, we could adjust the parameters of the moderate-to-steep and flat, dry field soil and vegetation structures such as semi-natural field, rice, and dry crops. Then, applying the optimal parameter set, we evaluated the model performance at the third hydrological point covering the steep mountain forest area, moderate-to-steep dry crop fields, and flat rice paddy and residential areas.

Based on the validated model outputs, we simulated the annual sediment redistribution patterns and assessed the soil erosion risk of the entire Haean catchment. To evaluate the impact of the spatial reconfiguration on the reduction of the sediment yield entering into the stream, we altered the erosion hot spots into forests and assessed the sediment yield from the catchment. We set the current sediment yield entering into the stream as the baseline conditions and then compared those from model outputs projecting spatial reconfiguration scenarios of altering one percent of erosion hot spots into forests in the order from the area with the most severe soil erosion risk to that of the least severe soil erosion risk. In addition, to investigate effective ways to reduce sediment yield entering into the stream, we repeated the above-mentioned procedure for three different types of soil erosion hot spots according to the criteria of net soil budget, sediment input, and sediment output of the area.

#### **1.2.4 Effect of topography and vegetation structure on spatial patterns of soil nutrients (Chapter 5)**

To predict spatial patterns of N and P as well as identify important environmental drivers affecting these patterns, we selected a small mountain forest catchment (9.84 km<sup>2</sup>) of Chuncheon located in the downstream area of the Soyang watershed (see Fig. 1.1c). To ascertain the effect of topography and vegetation structures on soil N and P in the organic layer and A horizon, we measured the soil N and P concentrations and analyzed the topography and vegetation structure utilizing LiDAR point data. First, we collected soil samples from the organic layer and A horizon at 91 sampling points in 2014. To efficiently obtain unbiased soil samples of at least one per a quantile of each environmental factor for predicting spatial patterns of soil nutrients,

we selected sampling points using a conditional Latin hypercube sampling method, which is a stratified random sampling that provides full coverage of the range of each variable, while preserves the distribution and multivariate correlation of the multivariate space (Minasny and McBratney, 2006). Collected organic soil samples were oven-dried, and mineral soil samples from the A horizon were air-dried and sieved under 2 mm. We preprocessed the organic soil samples and measured P and N contents utilizing an inductively-coupled plasma mass spectrometry (ICP) and elemental analyzer, respectively. After measuring the P and N contents of each soil sample, we converted nutrient contents into mass and calculated N/P ratio based on mass.

Environmental predictors were derived from detailed three-dimensional (3D) point-cloud data scanned by airborne LiDAR. We created a digital elevation model (DEM), a digital terrain model (DTM), and a digital surface model (DSM) from a 3D point-cloud generated by airborne LiDAR. In addition, we used the LiDAR-derived average first return intensity of reflected light ( $H_{\text{firavg}}$ ) of an area for forest types and physiological characteristics (Ørka *et al.*, 2009). Based on the LiDAR-driven DEM, we calculated elevation (ELEV), slope (SLO) (Zevenbergen and Thorne, 1987), catchment area (CA) (Freeman, 1991), and topographical wetness index (STWI) (Böhner *et al.*, 2002) from SAGA (Conrad *et al.*, 2015), and calculated the surface curvature of  $19 \times 19$  cells around the focusing area (CUR19) from the CURV3 program (Park *et al.*, 2001). Based on the LiDAR-driven DTM and DSM, we calculated vegetation structure metrics for maximum tree height ( $H_{\text{max}}$ ), canopy cover percentage ( $H_{\text{ccp}}$ ), and standard deviation of tree heights ( $H_{\text{std}}$ ). We created the composite values of forest canopy and height ( $H_{\text{ch}}$ ), which is the canopy cover percentage ( $H_{\text{ccp}}$ ) multiplied by maximum height ( $H_{\text{max}}$ ) as an indicator of approximate vegetation volume. In addition to the LiDAR-driven data, we also used the normalized difference vegetation index (NDVI) which is calculated from the Kompsat-2 satellite image obtained on 11th October 2014 (Jensen, 2015, Thenkabail *et al.*, 2011).

To determine the relationships between soil nutrient concentration and environmental predictors such as topography and vegetation structures, we developed a model to predict the soil concentration of each nutrient from environmental predictors utilizing the random forest (RF) method, an ensemble learning method that suggests an optimized model by constructing a multitude of regression trees and then averaging individual trees (Breiman, 2001). The method is applicable to predict a complicated non-linear relationships between responding variables and predictors, and also has better interpretability than other machine learning methods by providing the relative importance of each predictor in the result; thus, this technique is frequently used for digital soil mapping (Grimm *et al.*, 2008, Wiesmeier *et al.*, 2011, Kuhn and Johnson, 2013, Strobl *et al.*, 2009, Kampichler *et al.*, 2010).

Predictor selection can be a crucial factor in determining model performance (Miller *et al.*, 2015, Brungard *et al.*, 2015, Poggio *et al.*, 2013). Recursive feature elimination (RFE), a backward predictor selection method, can be used with RF for selecting the optimal number of important predictors essential for model construction (Miller *et al.*, 2015). Predictor selection procedures using RFE and RF consist of running RF to assess the initial importance of each predictor, and removing predictors one-by-one in increasing order of importance iteratively until the optimal predictors essential for the model obtained (Darst *et al.*, 2018).

To assess model performance, we used k-fold cross-validation (CV), which randomly partitions a given dataset into k subsets and then uses (k-1) subsets as a training dataset, leaving one subset as a validation dataset. We tried 2-, 5-, 10-, and 20-fold as well as a leave-one-out (LOO) CV to assess model performance utilizing the coefficient of determination ( $R^2$ ) and root mean square error (RMSE) as model performance criteria.

## 1.3 Results and discussion

### 1.3.1 Development of a soil erosion model for a complex terrain region under a monsoonal climate regime (Chapters 2 & 3)

We tested the performance of the DMMF model by applying it to two dry crop fields in the Haean catchment and comparing the surface runoff and soil erosion results with those from Erosion 3D (von Werner, 1995) carried out per Arnhold *et al.* (2013). The model results showed reasonable performance and similar soil redistribution patterns when compared to the results from Erosion 3D.

Based on the result, we can conclude that the corrections and modifications made on the MMMF model were appropriate with regard to improving the model for application in complex surface configurations with intensive rainfall regimes. In addition, the DMMF can be useful in establishing soil and water conservation measures in intensively used agricultural lands with complex surface configurations by estimating spatiotemporal runoff and sediment redistribution and by identifying erosion and deposition hot spots under varying conditions.

### 1.3.2 Effect of spatial reconfiguration of landscape on reducing sediment yield from the catchment (Chapter 4)

According to the result, the model showed high sensitivity to soil hydraulic parameters such as soil water content at field capacity, and saturated soil hydraulic conductivity, and vegetation and surface structures such as permanent interception of rainfall and ground cover of the surface. From the calibration and validation steps, the model showed relatively good performance in the mountain forest area; however, as more agricultural and artificial structures were included, the performance of the model decreased. The model showed relatively good performance in estimating stream discharge but relatively poor performance in estimating suspended sediments in the stream. The poor model performance in estimating suspended sediments could be analyzed from two perspectives: the discrepancy in data types between field measured data and output from the DMMF model, and the existence of manmade culvert systems and sediment reduction facilities.

Suspended sediments at each hydrological point measured sediment concentration, which is the sediment yield from the contribution area subtracted by stream deposited sediments; on the other hand, the DMMF model did not consider sediment processes in the stream. As the sediment process in the stream highly depends on the amount of stream discharge, the errors between observed and simulated data can be larger for the longer stream networks. Also, the manmade culvert system and sediment reduction facilities such as debris barriers slowed down the stream flow, which increased deposition in the stream. As the deposited sediments also floated in the stream discharge caused by concentrated rainfall, the facilities could affect model performance for sediment yield to the stream.

Based on the optimal parameters from calibration and validation, we estimated the annual sediment redistribution patterns and assessed the soil erosion risks of the entire catchment. The result showed severe soil erosion in dry crop fields on hillslope areas, and relatively tolerable soil erosion in the rice paddies and residential areas located in low, flat catchment center. Forests showed tolerable soil erosion, though they were mostly located on the very steep mountain areas.

Simulation results obtained by altering soil erosion hot spots into erosion-tolerable forests confirmed the effectiveness of spatial reconfiguration of landscapes on the reduction of the sediment yield entering into the stream. Altering only 3% of the erosion hot spots reduced the sediment yields entering the stream by approximately 10%. Furthermore, changing 10% of the erosion hot spots reduced approximately 50% of the sediment yield from the catchment.

In this study, we assessed the soil erosion risk of Hae-an catchment spatially by explicitly

projecting sediment redistribution patterns using the DMMF model. We also identified the effect of spatial reconfiguration of erosion-prone areas into erosion tolerable areas on reducing sediment yields entering the stream. Although previous studies have suggested various efficient BMPs to reduce sediment yields from the catchment, their BMPs often require compliance of stakeholders, which may not be easy and takes much time for stakeholder compliance (Maharjan *et al.*, 2016, Jang *et al.*, 2017). On the other hand, we recommend the spatial reconfiguration approach, which often reduces the number of stakeholders in mitigation measures. Therefore, we can obtain a desired sediment yield reduction from the catchment through the complementary use of two BMP approaches.

### 1.3.3 Effect of topography and vegetation structure on spatial patterns of soil nutrients (Chapter 5)

According to the soil sample analysis, the concentration of N in the organic layer (12,245 mg/kg) was approximately four times those in the A horizon (2,990 mg/kg). The concentration of P in the organic layer (624 mg/kg) was approximately one-and-a-half times those in the A horizon (389 mg/kg). From the results, it can be seen that the N concentration had a high variance between each soil layer; in contrast, the variance between soil layers was relatively low for the P concentration. We also analyzed the variance in the soil nutrients of each layer. In the organic layer, the concentration of P ( $P_o$ ) showed relatively higher variability than N ( $N_o$ ) based on the coefficient of variation (CoV). This result indicated that the N/P ratios in the organic layer could be highly dependent on the concentration of  $P_o$ . In the A horizon, the concentrations of N ( $N_a$ ) and P ( $P_a$ ) showed high variances, which were greater than those in the organic layer. In addition, the average N/P ratio in the A horizon were higher than that of the organic layers.

When we assessed model performance from various types of k-fold CV schemes, the P concentration prediction model for the organic layer and A horizon showed relatively good performance; however, the N concentration prediction model in the organic layer and A horizon showed relatively poor performances. Due to the poor performance of the N prediction model in the organic layer, the N/P prediction model showed poor performance as the N/P ratio was determined by both N and P.

From RF and RFE procedures, we identified the important environmental drivers for the spatial patterns of each nutrient and the ratio of nutrients in the soil. Concentrations of N in the soil showed a high correlation with various topographic and vegetation predictors, while concentrations of P showed significant relationships with only topographic predictors. Also, the

N/P ratio in the organic layer demonstrated a higher correlation with vegetation predictors than that in the mineral soil layer. The model for predicting spatial distribution of  $N_o$  required not only topographic predictors such as elevation (ELEV), curvature (CURV19), and topographic wetness index (STWI), but also vegetation predictors such as forest type and physiological characteristics ( $H_{firavg}$ ), standard deviation of vegetation height ( $H_{std}$ ), and maximum vegetation height of a cell ( $H_{max}$ ). However, only topographic predictors such as ELEV and CURV19 were required to predict spatial patterns of concentrations of  $P_o$ ,  $P_a$ , and  $N_a$ . For predicting N/P ratio in the organic layer, topographic predictors such as CURV19, catchment area (CA), and ELEV were selected for the model, and vegetation predictors such as standard deviation of tree heights ( $H_{std}$ ), maximum vegetation height ( $H_{max}$ ), and forest canopy and height ( $H_{ch}$ ) were selected. Topographic factors such as CURV19, CA, ELEV, and topographic wetness index (STWI), and normalized difference vegetation index (NDVI) were required for predicting N/P ratio in the A horizon.

From the predicted spatial patterns of N, P, and N/P ratio from the models, P contents were markedly higher in the lower slopes than the upper slopes and N/P ratio showed high values on the convex upper slope. Standard deviations of P and N/P ratio in the organic layer were higher at lower elevations and on the valley floor. The standard deviation of P in mineral soil layer was higher at the upper part of the catchment.

Our results showed that the soil contents of N in the organic layer had a strong relationship with various topographic and vegetation factors such as elevation, NDVI, vegetation type, curvature, topographic wetness index, and structural diversity and maximum height of vegetation. The soil contents of N in the mineral soil layer showed a strong relationship only with topographic factors such as elevation and curvature and had weak relationships with vegetation structures. The results were generally in accordance with previous studies that reported strong correlation of soil nitrogen content with topographic predictors (e.g., elevation (Bedison and Johnson, 2009, Wang *et al.*, 2013, Peng *et al.*, 2013, Kunkel *et al.*, 2011), and catchment area and topographic wetness index (Johnson *et al.*, 2000, Seibert *et al.*, 2007)) and vegetation predictors (e.g., vegetation type, structure (Bedison and Johnson, 2009, Vesterdal *et al.*, 2008, Zhang *et al.*, 2010) and NDVI (Kim *et al.*, 2016, Kunkel *et al.*, 2011, Sumfleth and Duttman, 2008)). Several studies ((Kim *et al.*, 2016, Kunkel *et al.*, 2011, Sumfleth and Duttman, 2008)) have reported on the strong correlations between  $N_a$  and NDVI, while we found significantly strong relationships between  $N_o$  and NDVI; we identified only marginal relationships between  $N_a$  and NDVI. Although previous studies found that topographic wetness index (TWI) and catchment area (CA) affects N contents in soil, we only found significant relationships between

STWI and  $N_a$  (Johnson *et al.*, 2000, Seibert *et al.*, 2007). According to our results, P contents in the soil were mainly determined by elevation (ELEV) and surface curvature (CURV19). The spatial patterns of P from the model demonstrated that P enrichment was found in the valleys near mountain-tops while low P content was found on convex slopes and valleys located in the lower areas, which were well-matched with the spatial patterns of soil P contents from other study site (Smeck, 1985). The spatial patterns of P at the study site seemed to be formed by a long-term periodic soil erosion process. Because the study site was located in the steep mountain area affected by periodic seasonal heavy rainfall, the area has suffered from severe soil erosion (Jeong *et al.*, 2012, Jung *et al.*, 2012). As P tends to adhere easily to soil particles, P content was relatively low on the mountain slope area, which was vulnerable to soil erosion. On the other hand, P content was relatively high on the mountain top, where less erosion occurred. P content was also high at the lower slope due to P inputs delivered from upslope areas along with soil particles. The vegetation in the area with high P content absorbed more P from the soil and contributed high P back to the soil through foliage and vegetation litter that can back up high P content in the organic layer. The spatial pattern of the N/P ratio from the organic layer and A horizon were similar to the reversed image of the spatial pattern of P content, which indicate that N/P ratio in both soil layers are strongly affected by soil P contents in the steep forest mountain area. According to the spatial variations of the two soil nutrient contents, the results came from the small spatial variation in soil N compared to that of soil P. As the lower N/P ratio of tree leaf in the P-enriched areas also affected the N/P ratio of the organic layer, the spatial patterns of N/P ratio in the organic layer showed a stronger correlation with those of P in the organic layer. Our results were similar to those reported by Uriarte *et al.* (2015), wherein soil N/P ratio was closely related to the N/P ratio of leaf litter and was determined by topography in a steep tropical mountainous forest with heavy rainfall. After verifying k-fold cross-validation schemes through changing k values, we found an inverse relationship between the predictive power of the model and variance of the predictive power, which was a so-called bias-variance trade-off (Hastie *et al.*, 2009). According to our test, increased k values led to the increased mean predictive power of the model from RF, but also to the decreased variance of the predictive power. The higher predictive power from the larger k was caused by the larger size of the training set as the predictive power of the learning methods were often determined by the size of the training set. This was similar to the result of Park and Vlek (2002), who reported that prediction accuracy increased with increasing numbers of soil samples the for training dataset. Although there were enough data for calibration of the model to secure reasonable predictive power, the larger size training set often led to an overfitting of the model (Remesan and Mathew,

2015). In the model test, we also found notable bias-variance trade-offs and confirmed efficiency of the 10-fold CV since the scheme had moderate levels of model error bias and variance as recommended in various studies (Remesan and Mathew, 2015, James *et al.*, 2013, Cichosz, 2015, Feigelson and Babu, 2012, Malley *et al.*, 2011, Ambroise and McLachlan, 2002).

## 1.4 Outlook

The Soyang watershed has been suffering from periodic soil erosion from upland agricultural areas and vegetative woody debris inflows from mountain forests due to its erosion-prone topography of steep slopes and occasional intensive rainfall from the seasonal monsoon climate. The problem is worsening owing to upland agricultural expansion caused by economic profit and a strong, concentrated rainfall pattern due to climate change.

Understanding the spatial redistribution of soil and soil nutrients is essential for mitigating the problems of erosion as well as managing the productivity of the terrestrial ecosystem and the quality of the aquatic ecosystem sustainably. For a better understanding of the spatial redistribution of soil and soil nutrients, we created modified soil erosion models adapted to the area and its complex surface configuration under a seasonal monsoon climate. Also, utilizing the soil erosion model, we simulated spatial redistribution of soils in Haeon, the upland agricultural mountainous catchment, and suggested soil erosion mitigation measures considering the spatial context of the landscape by converting erosion hot spots into erosion-resistant forest. Although soil erosion was not so severe in the forest, forest is the dominant land cover in the Soyang watershed, covering approximately 84% of the entire watershed, and is also the main source of natural suspended solids, such as woody debris and particulate organic matter, flowing into streams. Therefore, an understanding is needed of the spatial distribution pattern of soil nutrients and the environmental drivers that determine these patterns in the mountain forested areas for estimating the spatial redistribution process of matter in these areas. To understand the spatial redistribution process of matters in the mountain forested areas, we ascertain the spatial patterns of soil nutrients and selected the important environmental drivers that determine spatial patterns of soil nutrients and their ratios in the steep, mountainous forested area by utilizing sophisticated topographic and vegetative factors extracted from LiDAR point-cloud data. The spatial distribution of N in the organic layers could be used as indicators of the spatial redistribution of woody debris and particulate organic matter originating from vegetation, while that of P could be an indicator for soil redistribution.

We estimated soil erosion in the upland agricultural catchment and also found clues as to the

spatial redistribution patterns of soil and soil nutrients in the mountainous forested area through the spatial patterns of soil nutrients and their environmental drivers. Choi (2014) reported that a significant amount of fine and coarse woody debris (WD) and particulate organic matter (POM) exported from the mountainous forested catchment entered the streams and reservoirs when concentrated rainfall events occurred. WDs and POMs originating from forested mountains were deposited in the streams and reservoirs and often produced methane, a potent greenhouse gas, through anaerobic oxygen deprivation condition in the sediment layer under water. Also, deposited WDs and POMs in the water degraded water quality by providing dissolved organic matter (DOM) and P that caused eutrophication (Choi, 2014, Sorrell and Boon, 1994, Wood and Armitage, 1997, Baker *et al.*, 2011, Extence *et al.*, 2011, Flores *et al.*, 2013). WDs such as litter often affected the soil erosion process as they played a significant role as a surface cover that protected surface from soil erosion. However, there have only been a few studies estimating the spatial behavior of contaminants integrating vegetative WD, POM, and inorganic soil sediments from a mountainous catchment (Choi, 2014).

For the sustainable management of a water system considering contaminant inflow from terrestrial ecosystems with complex terrain configurations, an integrated model to project spatial redistribution of WDs, POMs, and soil particles is required in this area. Based on the results of the current study performed in the Soyang watershed, we plan to develop an integrated material redistribution model to simulate the spatial redistribution of materials including WDs, POMs and soil particles. We conceptualize the fine and coarse WDs and POMs as materials and take these materials to be soil particles as described in the DMMF model. The differences between WDs and other materials are that WDs are immobile until the depth of the surface runoff are deeper than the critical floating depth of the WDs (Haga *et al.*, 2002). To integrate WDs and POMs into the model, we need empirical relationships between topographic conditions and material characteristics. First, the amount of floating POMs and WDs are required to calculate the inflow of materials into the surface runoff. Second, characteristics of floating POMs and WDs in the flowing runoff such as lateral velocity of POMs and WDs and gravitational falling velocity in the water are required. To create quantitative empirical values for each material, we will perform laboratory-based and in-situ experiments to quantify the amount of floating POMs and WDs for various surface water levels and slope conditions. Third, as POMs and WDs are relatively non-static in the field as they are removable in certain locations, we should modify the model for surface POMs and WDs to be updated at daily based. Fourth, in a forest-dominated catchment having simple land cover, we will project and validate the model with the data sampled at the surface and in the stream. Fifth, after validation, we will project the model in a

catchment with complex terrain configurations that contributes large volumes of organic and inorganic matter into a stream, and devise optimal measures to mitigate contaminants entering the stream.

## 1.5 Concluding remarks

The Soyang watershed is an important freshwater resource for almost half of the South Korean population. However, every monsoon season, this area suffers from periodic water quality deterioration owing to the occurrence of soil erosion in upland agricultural soil and forest oriented organic matter such as fine and coarse woody debris. Owing to the complex surface configuration of this area, it is challenging to design optimal measures for sustainable water management.

We devised a soil erosion model that is suitable for areas with complex terrain configurations under a seasonal monsoon climate. Utilizing this model, we estimated the amount of sediment yield from Haeon catchment, one of the important sediment contributors to the Soyang watershed. Also, we evaluated the effectiveness of spatial reconfiguration of the landscape through converting erosion hot spots into forest and identified the sediment yield reduction efficiency of the spatial reconfiguration. According to the result, we demonstrated that spatial reconfiguration of the landscape could bring a synergy of sediment yield reduction with the BMP recommended for each agricultural area. We also investigated the spatial distribution of soil nutrients in the steep forested mountain area to understand the important environmental predictors affecting spatial redistribution of soil nutrients, utilizing detailed topographical and vegetation structural data. We can understand the spatial redistribution process of soil nutrients and related vegetative organic matter from the spatial patterns of soil nutrients.

Even though soil particles and organic matter from forests can degrade water quality, no studies or tools have been applied for the quantitative estimation of the transfer of materials, including both soil particles and organic matter, from terrestrial to aquatic ecosystems. Further study of woody debris and particulate organic matter transportation, and modified models integrating aforementioned organic matter transportation with soil erosion, should be helpful for the sustainable management of water in this area.

## 1.6 List of manuscripts and specification of individual contributions

This thesis contains four different manuscripts. The first manuscript (Chapter 2) was submitted to *Earth surface processes and land forms* and rejected, and is in preparation to be re-submitted to the same journal. The second manuscript (Chapter 3) was submitted to *Water* and published in 2017. The third manuscript (Chapter 4) was submitted to *Water* and published in 2019. The fourth manuscript (Chapter 5) was submitted to *Plos One* and published in 2017. The following list specifies the contributions of the individual authors to each manuscript.

### Manuscript 1 (Chapter 2)

|                       |  |
|-----------------------|--|
| <b>Authors:</b>       | Kwanghun Choi, Bernd Huwe, Björn Reineking   |
| <b>Title:</b>         | Commentary on “Modified MMF (Morgan–Morgan–Finney) model for evaluating effects of crops and vegetation cover on soil erosion” by Morgan and Duzant (2008) |
| <b>Status:</b>        | Published e-prints on arxiv and in preparation for publication   |
| <b>Contributions:</b> |  |
| K. Choi:              | 70% (concepts, analysis, interpretation, discussion, and manuscript preparation)   |
| B. Huwe:              | 10% (concepts, discussion of results, and contribution to manuscript preparation)  |
| B. Reineking:         | 20% (concepts, discussion of results, and contribution to manuscript preparation)  |

### Manuscript 2 (Chapter 3)

|                       |  |
|-----------------------|--|
| <b>Authors:</b>       | Kwanghun Choi, Sebastian Arnhold, Bernd Huwe, Björn Reineking  |
| <b>Title:</b>         | Daily Based Morgan–Morgan–Finney (DMMF) Model: A Spatially Distributed Conceptual Soil Erosion Model to Simulate Complex Soil Surface Configurations |
| <b>Status:</b>        | Published in 2017  |
| <b>Journal:</b>       | Water  |
| <b>Contributions:</b> |  |

- K. Choi: 60% (concepts, analysis, interpretation, discussion, and manuscript preparation)
- S. Arnhold: 15% (concepts, analysis, interpretation, discussion, and contribution to manuscript preparation)
- B. Huwe: 10% (concepts, discussion of results, and contribution to manuscript preparation)
- B. Reineking: 15% (concepts, discussion of results, and contribution to manuscript preparation)

### Manuscript 3 (Chapter 4)

- Authors:** Kwanghun Choi, Ganga Ram Maharjan, Björn Reineking
- Title:** Evaluating the Effectiveness of Spatially Reconfiguring Erosion Hot Spots to Reduce Stream Sediment Load in an Upland Agricultural Catchment of South Korea
- Status:** Published in 2019
- Journal:** Water
- Contributions:**
- K. Choi: 70% (concepts, analysis, interpretation, discussion, and manuscript preparation)
- G. R. Maharjan: 10% (concepts, discussion of results, and contribution to manuscript preparation)
- B. Reineking: 20% (concepts, discussion of results, and contribution to manuscript preparation)

### Manuscript 4 (Chapter 5)

- Authors:** Gwanyong Jeong, Kwanghun Choi, Marie Spohn, Soo Jin Park, Bernd Huwe, Mareike Ließ
- Title:** Environmental drivers of spatial patterns of topsoil nitrogen and phosphorus under monsoon conditions in a complex terrain of South Korea
- Status:** Published in 2017
- Journal:** PLOS ONE

**Contributions:**

- G. Jeong: 60% (concepts, field work, data analysis, interpretation, discussion, and manuscript preparation)
- K. Choi: 15% (concepts, field work, data analysis, interpretation, discussion, and contribution to manuscript preparation)
- M. Spohn: 5% (concepts, discussion of results, and contribution to manuscript preparation)
- S. Park: 5% (concepts, discussion of results, and contribution to manuscript preparation)
- B. Huwe: 5% (concepts, discussion of results, and contribution to manuscript preparation)
- M. Ließ: 10% (concepts, discussion of results, and contribution to manuscript preparation)

**References**

- Pimentel, D. Soil Erosion: A Food and Environmental Threat. *Environ. Dev. Sustain.* **2006**, 8, 119–137. doi:10.1007/s10668-005-1262-8.
- Pimentel, D.; Harvey, C.; Resosudarmo, P.; Sinclair, K.; Kurz, D.; McNair, M.; Crist, S.; Shpritz, L.; Fitton, L.; Saffouri, R.; Blair, R. Environmental and economic costs of soil erosion and conservation benefits. *Science* **1995**, 267, 1117–1122. doi:10.1126/science.267.5201.1117.
- Morgan, R.P.C. *Soil erosion and conservation*, third ed.; Blackwell Publishing: Malden, MA, 2005.
- Pimentel, D.; Kounang, N. Ecology of soil erosion in ecosystems. *Ecosystems* **1998**, 1, 416–426. doi:10.1007/s100219900035.
- Lal, R. Soil degradation by erosion. *Land Degrad. Dev.* **2001**, 12, 519–539. doi:10.1002/ldr.472.
- Kim, K.; Kim, B.; Knorr, K.H.; Eum, J.; Choi, Y.; Jung, S.; Peiffer, S. Potential effects of sediment processes on water quality of an artificial reservoir in the Asian monsoon region. *Inland Waters* **2016**, 6, 423–435. doi:10.1080/IW-6.3.852.
- Maharjan, G.R.; Ruidisch, M.; Shope, C.L.; Choi, K.; Huwe, B.; Kim, S.J.; Tenhunen, J.; Arnhold, S. Assessing the effectiveness of split fertilization and cover crop cultivation in order to

- conserve soil and water resources and improve crop productivity. *Agric. Water Manage.* **2016**, *163*, 305–318. doi:10.1016/j.agwat.2015.10.005.
- Chang, H. Spatial analysis of water quality trends in the Han River basin, South Korea. *Water Res.* **2008**, *42*, 3285–3304. doi:10.1016/j.watres.2008.04.006.
- Chang, H. Spatial and Temporal Variations of Water Quality in the Han River and Its Tributaries, Seoul, Korea, 1993–2002. *Water, Air, Soil Pollut.* **2005**, *161*, 267–284. doi:10.1007/s11270-005-4286-7.
- Lee, S.; Nguyen, T.; Kim, H.; Koellner, T.; Shin, H.J. Do Consumers of Environmentally Friendly Farming Products in Downstream Areas Have a WTP for Water Quality Protection in Upstream Areas? *Water* **2017**, *9*, 511. doi:10.3390/w9070511.
- Yoon, B.; Woo, H. Sediment problems in Korea. *J. Hydraul. Eng.* **2000**, *126*, 486–491. doi:10.1061/(ASCE)0733-9429(2000)126:7(486).
- Reza, A.; Eum, J.; Jung, S.; Choi, Y.; Owen, J.S.; Kim, B. Export of non-point source suspended sediment, nitrogen, and phosphorus from sloping highland agricultural fields in the East Asian monsoon region. *Environ. Monit. Assess.* **2016**, *188*. doi:10.1007/s10661-016-5681-9.
- Arnhold, S.; Ruidisch, M.; Bartsch, S.; Shope, C.L.; Huwe, B. Simulation of runoff patterns and soil erosion on mountainous farmland with and without plastic-covered ridge-furrow cultivation in South Korea. *Trans. ASABE* **2013**, *56*, 667–679. doi:10.13031/2013.42671.
- Ruidisch, M.; Kettering, J.; Arnhold, S.; Huwe, B. Modeling water flow in a plastic mulched ridge cultivation system on hillslopes affected by South Korean summer monsoon. *Agric. Water Manage.* **2013**, *116*, 204–217. doi:10.1016/j.agwat.2012.07.011.
- Arnhold, S.; Lindner, S.; Lee, B.; Martin, E.; Kettering, J.; Nguyen, T.T.; Koellner, T.; Ok, Y.S.; Huwe, B. Conventional and organic farming: Soil erosion and conservation potential for row crop cultivation. *Geoderma* **2014**, *219–220*, 89–105. doi:10.1016/j.geoderma.2013.12.023.
- Lee, J.Y. A Hydrological Analysis of Current Status of Turbid Water in Soyang River and Its Mitigation. *J. Soil Groundw. Environ.* **2008**, *13*, 85–92.
- Harmon, M.E.; Franklin, J.F.; Swanson, F.J.; Sollins, P.; Gregory, S.V.; Lattin, J.D.; Anderson, N.H.; Cline, S.P.; Aumen, N.G.; Sedell, J.R.; Lienkaemper, G.W.; Cromack, K.; Cummins, K.W. Ecology of Coarse Woody Debris in Temperate Ecosystems. In *Advances in Ecological Research*; Elsevier, 1986; pp. 133–302. doi:10.1016/s0065-2504(08)60121-x.

- Choi, Y. Woody Debris Runoff from Forested Watersheds and Limnological Effects in Reservoirs. PhD thesis, Department of Environmental Science, Kangwon National University, Chuncheon, South Korea, 2014.
- Jeon, M.S.; Kang, J.W. Muddy Water Management and Agricultural Development Measures in the Watershed of Soyang Dam: Focused on Haean-myeon, Yanggu-gun. Technical report, Research Institute of Gangwon, 2010.
- Ruidisch, M.; Arnhold, S.; Huwe, B.; Bogner, C. Is Ridge Cultivation Sustainable? A Case Study from the Haean Catchment, South Korea. *Appl. Environ. Soil Sci.* **2013**, *2013*, 1–11. doi:10.1155/2013/679467.
- von Werner, M. GIS-orientierte Methoden der digitalen Reliefanalyse zur Modellierung von Bodenerosion in kleinen Einzugsgebieten. PhD dissertation, Free University of Berlin, Department of Earth Sciences., Berlin, Germany, 1995.
- Ali, H.E.; Reineking, B. Extensive management of field margins enhances their potential for off-site soil erosion mitigation. *J. Environ. Manage.* **2016**, *169*, 202–209. doi:10.1016/j.jenvman.2015.12.031.
- Arnold, J.G.; Srinivasan, R.; Muttiah, R.S.; Williams, J.R. Large area hydrologic modeling and assessment part 1: model development. *J. Am. Water Resour. Assoc.* **1998**, *34*, 73–89. doi:10.1111/j.1752-1688.1998.tb05961.x.
- Jang, S.S.; Ahn, S.R.; Kim, S.J. Evaluation of executable best management practices in Haean highland agricultural catchment of South Korea using SWAT. *Agric. Water Manage.* **2017**, *180*, 224–234. Agricultural water and nonpoint source pollution management at a watershed scale Part II Overseen by: Dr. Brent Clothier, doi:10.1016/j.agwat.2016.06.008.
- Poppenborg, P.; Koellner, T. Do attitudes toward ecosystem services determine agricultural land use practices? An analysis of farmers' decision-making in a South Korean watershed. *Land Use Policy* **2013**, *31*, 422–429. Themed Issue 1-Guest Editor Romy Greiner Themed Issue 2- Guest Editor Davide Viaggi, doi:10.1016/j.landusepol.2012.08.007.
- Chaplin-Kramer, R.; Sharp, R.P.; Mandle, L.; Sim, S.; Johnson, J.; Butnar, I.; Milà i Canals, L.; Eichelberger, B.A.; Ramler, I.; Mueller, C.; McLachlan, N.; Yousefi, A.; King, H.; Kareiva, P.M. Spatial patterns of agricultural expansion determine impacts on biodiversity and carbon storage. *Proc. Natl. Acad. Sci. U.S.A* **2015**, *112*, 7402–7407. doi:10.1073/pnas.1406485112.

- Chaplin-Kramer, R.; Hamel, P.; Sharp, R.; Kowal, V.; Wolny, S.; Sim, S.; Mueller, C. Landscape configuration is the primary driver of impacts on water quality associated with agricultural expansion. *Environ. Res. Lett.* **2016**, *11*, 074012. doi:10.1088/1748-9326/11/7/074012.
- Seo, B.; Bogner, C.; Poppenborg, P.; Martin, E.; Hoffmeister, M.; Jun, M.; Koellner, T.; Reineking, B.; Shope, C.L.; Tenhunen, J. Deriving a per-field land use and land cover map in an agricultural mosaic catchment. *Earth Syst. Sci. Data* **2014**, *6*, 339–352. doi:10.5194/essd-6-339-2014.
- Kim, I.; Arnhold, S.; Ahn, S.; Le, Q.B.; Kim, S.J.; Park, S.J.; Koellner, T. Land use change and ecosystem services in mountainous watersheds: Predicting the consequences of environmental policies with cellular automata and hydrological modeling. *Environ. Modell. Software* **2017**. doi:10.1016/j.envsoft.2017.06.018.
- Meusburger, K.; Mabit, L.; Park, J.H.; Sandor, T.; Alewell, C. Combined use of stable isotopes and fallout radionuclides as soil erosion indicators in a forested mountain site, South Korea. *Biogeosciences* **2013**, *10*, 5627–5638. doi:10.5194/bg-10-5627-2013.
- Hou, J.; Fu, B.; Wang, S.; Zhu, H. Comprehensive analysis of relationship between vegetation attributes and soil erosion on hillslopes in the Loess Plateau of China. *Environ. Earth Sci.* **2014**, *72*, 1721–1731. doi:10.1007/s12665-014-3076-1.
- Wischmeier, W.H.; Smith, D.D. Predicting rainfall erosion losses—a guide to conservation planning. In *Agriculture Handbook*; Number 537, U.S. Department of Agriculture, 1978; pp. 1–58.
- Renard, K.G.; Foster, G.R.; Weesies, G.A.; Porter, J.P. RUSLE: Revised universal soil loss equation. *J. Soil Water Conserv.* **1991**, *46*, 30–33.
- Williams, J.R. Sediment-yield prediction with Universal Equation using runoff energy factor. Present and prospective technology for predicting sediment yield and sources: proceedings of the Sediment-Yield Workshop; Agricultural Research Service, U.S. Dept. of Agriculture: New Orleans, Louisiana, 1975; Vol. ARS-S-40, pp. 244–252.
- Morgan, R.P.C.; Morgan, D.D.V.; Finney, H.J. A predictive model for the assessment of soil erosion risk. *J. Agric. Eng. Res.* **1984**, *30*, 245–253. doi:10.1016/S0021-8634(84)80025-6.
- Morgan, R.P.C. A simple approach to soil loss prediction: a revised Morgan–Morgan–Finney model. *Catena* **2001**, *44*, 305–322. doi:10.1016/S0341-8162(00)00171-5.

- Merritt, W.S.; Letcher, R.A.; Jakeman, A.J. A review of erosion and sediment transport models. *Environ. Modell. Software* **2003**, *18*, 761–799. The Modelling of Hydrologic Systems, doi:10.1016/S1364-8152(03)00078-1.
- Lilhare, R.; Garg, V.; Nikam, B. Application of GIS-Coupled Modified MMF Model to Estimate Sediment Yield on a Watershed Scale. *J. Hydrol. Eng.* **2014**, *20*, C5014002. doi:10.1061/(ASCE)HE.1943-5584.0001063.
- Hu, L.J.; Flanagan, D.C. Towards new-generation soil erosion modeling: Building a unified omnivorous model. *J. Soil Water Conserv.* **2013**, *68*, 100A–103A. doi:10.2489/jswc.68.4.100A.
- Nearing, M.A.; Foster, G.R.; Lane, L.J.; Finkner, S.C. A process-based soil erosion model for USDA-Water Erosion Prediction Project technology. *Trans. ASAE* **1989**, *32*, 1587–1593.
- De Roo, A.P.J.; Wesseling, C.G.; Ritsema, C.J. LISEM: A single-event physically based hydrological and soil erosion model for drainage basins. I: Theory, Input and Output. *Hydrol. Processes* **1996**, *10*, 1107–1117. doi:10.1002/(SICI)1099-1085(199608)10:8<1107::AID-HYP415>3.0.CO;2-4.
- Morgan, R.P.C.; Quinton, J.N.; Smith, R.E.; Govers, G.; Poesen, J.W.A.; Auerswald, K.; Chisci, G.; Torri, D.; Styczen, M.E. The European Soil Erosion Model (EUROSEM): a dynamic approach for predicting sediment transport from fields and small catchments. *Earth Surf. Processes Landforms* **1998**, *23*, 527–544. doi:10.1002/(SICI)1096-9837(199806)23:6<527::AID-ESP868>3.0.CO;2-5.
- Beven, K.J.; Kirkby, M.J. A physically based, variable contributing area model of basin hydrology. *Hydrol. Sci. Bull.* **1979**, *24*, 43–69. doi:10.1080/02626667909491834.
- Morgan, R.P.C.; Duzant, J.H. Modified MMF (Morgan–Morgan–Finney) model for evaluating effects of crops and vegetation cover on soil erosion. *Earth Surf. Processes Landforms* **2008**, *32*, 90–106. doi:10.1002/esp.1530.
- Devia, G.K.; Ganasri, B.P.; Dwarakish, G.S. A Review on Hydrological Models. *Aquat. Procedia* **2015**, *4*, 1001–1007. doi:10.1016/j.aqpro.2015.02.126.
- De Jong, S.M.; Paracchini, M.L.; Bertolo, F.; Folving, S.; Megier, J.; De Roo, A.P.J. Regional assessment of soil erosion using the distributed model SEMMED and remotely sensed data. *Catena* **1999**, *37*, 291–308. doi:10.1016/S0341-8162(99)00038-7.

- López-Vicente, M.; Navas, A.; Machín, J. Modelling soil detachment rates in rainfed agrosystems in the south-central Pyrenees. *Agric. Water Manage.* **2008**, *95*, 1079–1089. doi:10.1016/j.agwat.2008.04.004.
- Vieira, D.C.S.; Prats, S.A.; Nunes, J.P.; Shakesby, R.A.; Coelho, C.O.A.; Keizer, J.J. Modelling runoff and erosion, and their mitigation, in burned Portuguese forest using the revised Morgan-Morgan-Finney model. *For. Ecol. Manage.* **2014**, *314*, 150–165. doi:10.1016/j.foreco.2013.12.006.
- Vigiak, O.; Okoba, B.O.; Sterk, G.; Groenenberg, S. Modelling catchment-scale erosion patterns in the East African Highlands. *Earth Surf. Processes Landforms* **2005**, *30*, 183–196. doi:10.1002/esp.1174.
- Hwang, T.; Kang, S.; Kim, J.; Kim, Y.; Lee, D.; Band, L. Evaluating drought effect on MODIS Gross Primary Production (GPP) with an eco-hydrological model in the mountainous forest, East Asia. *Global Change Biol.* **2008**, *14*, 1037–1056. doi:10.1111/j.1365-2486.2008.01556.x.
- Millennium Ecosystem Assessment. *Ecosystems and Human Well-being: Current State and Trends*; Island press: Washington DC, USA, 2005; chapter Mountain Systems, pp. 681–716.
- Ward, G.M.; Aumen, N.G. Woody Debris as a Source of Fine Particulate Organic Matter in Coniferous Forest Stream Ecosystems. *Can. J. Fish. Aquat. Sci.* **1986**, *43*, 1635–1642. doi:10.1139/f86-202.
- Rowland, R.; Inamdar, S.; Parr, T. Evolution of particulate organic matter (POM) along a headwater drainage: role of sources, particle size class, and storm magnitude. *Biogeochemistry* **2017**, *133*, 181–200. doi:10.1007/s10533-017-0325-x.
- Elliot, W.J. WEPP INTERNET INTERFACES FOR FOREST EROSION PREDICTION. *J. Am. Water Resour. Assoc.* **2004**, *40*, 299–309. doi:10.1111/j.1752-1688.2004.tb01030.x.
- Neitsch, S.L.; Arnold, J.G.; Kiniry, J.R.; Williams, J.R.; King, K.W. Soil and Water Assessment Tool Theoretical Documentation Version 2009. Texas Water Resources Institute Technical Report No. 406, Texas Water Resources Institute, 2011.
- Kang, S.; Tenhunen, J. Complex Terrain and Ecological Heterogeneity (TERRECO):Evaluating Ecosystem Services in Production Versus water Quantity/quality in Mountainous Landscapes. *Korean J. Agric. For. Meteorol.* **2010**, *12*, 307–316.

- Jeong, G. Digital Soil Mapping for Functional Analysis of Site Characteristics in Complex Terrain. PhD thesis, University of Bayreuth, Bayreuth, 2016.
- Kim, I. Development of integrated modeling framework of land use changes and ecosystem services in mountainous watersheds. PhD thesis, University of Bayreuth, Bayreuth, 2017.
- Maharjan, G.R.; Park, Y.S.; Kim, N.W.; Shin, D.S.; Choi, J.W.; Hyun, G.W.; Jeon, J.H.; Ok, Y.S.; Lim, K.J. Evaluation of SWAT sub-daily runoff estimation at small agricultural watershed in Korea. *Front. Environ. Sci. Eng.* **2013**, *7*, 109–119. doi:10.1007/s11783-012-0418-7.
- Lee, J.Y. Importance of hydrogeological and hydrologic studies for Hae-an basin in Yanggu. *J. Geol. Soc. Korea* **2009**, *45*, 405–414.
- Shope, C.L.; Maharjan, G.R.; Tenhunen, J.; Seo, B.; Kim, K.; Riley, J.; Arnhold, S.; Koellner, T.; Ok, Y.S.; Peiffer, S.; Kim, B.; Park, J.H.; Huwe, B. Using the SWAT model to improve process descriptions and define hydrologic partitioning in South Korea. *Hydrol. Earth Syst. Sci.* **2014**, *18*, 539–557. doi:10.5194/hess-18-539-2014.
- Park, S.; Oh, C.; Jeon, S.; Jung, H.; Choi, C. Soil erosion risk in Korean watersheds, assessed using the revised universal soil loss equation. *J. Hydrol.* **2011**, *399*, 263–273. doi:10.1016/j.jhydrol.2011.01.004.
- Korea Meteorological Administration. Open meteorological data portal, 2019. accessed on 2019.
- Lee, G.R. Characteristics of geomorphological surface and analysis of deposits in fluvial terraces at upper reach of Soyang river. *J. Korean Geogr. Soc.* **2004**, *39*, 27–44.
- Chough, S.K. Tectonic Setting. In *Geology and Sedimentology of the Korean Peninsula*; Elsevier, 2013; pp. 9–23. doi:10.1016/b978-0-12-405518-6.00002-4.
- Jeong, G.; Choi, K.; Spohn, M.; Park, S.J.; Huwe, B.; Ließ, M. Environmental drivers of spatial patterns of topsoil nitrogen and phosphorus under monsoon conditions in a complex terrain of South Korea. *PLOS ONE* **2017**, *12*, 1–19. doi:10.1371/journal.pone.0183205.
- Choi, K.; Arnhold, S.; Huwe, B.; Reineking, B. Daily Based Morgan–Morgan–Finney (DMMF) Model: A Spatially Distributed Conceptual Soil Erosion Model to Simulate Complex Soil Surface Configurations. *Water* **2017**, *9*, 278. doi:10.3390/w9040278.
- ORNL DAAC. MODIS Collection 5 Land Products Global Subsetting and Visualization Tool. ORNL DAAC, Oak Ridge, Tennessee, USA. Accessed June 09, 2017. Subset obtained for

MOD16A2 product at 38.2838N,128.1252E, time period: 2009-01-01 to 2012-01-01, and subset size: 31 x 31 km., 2008. doi:10.3334/ORNLDAAAC/1241.

Rural Development Administration of South Korea. Agricultural technology portal (Nongsaro), 2018. (accessed on 31. Jul. 2018).

Didan, K. MOD13Q1 MODIS/Terra Vegetation Indices 16-Day L3 Global 250m SIN Grid V006. NASA EOSDIS Land Processes DAAC., 2015. doi:10.5067/MODIS/MOD13Q1.006.

ORNL DAAC. MODIS Collection 6 Land Products Global Subsetting and Visualization Tool. ORNL DAAC, Oak Ridge, Tennessee, USA. Accessed November 14, 2017. Subset obtained for MOD13Q1 product at 38.2838N,128.1252E, time period: 2009-01-01 to 2012-01-01, and subset size: 20.25 x 20.25 km., 2017. doi:10.3334/ORNLDAAAC/1379.

Sobol', I.M. Sensitivity Analysis for Nonlinear Mathematical Models. *Math. Modeling Comput. Experiment* **1993**, *1*, 407–414.

Nossent, J.; Elsen, P.; Bauwens, W. Sobol' sensitivity analysis of a complex environmental model. *Environ. Modell. Software* **2011**, *26*, 1515–1525. doi:10.1016/j.envsoft.2011.08.010.

Qi, W.; Zhang, C.; Chu, J.; Zhou, H. Sobol' 's sensitivity analysis for TOPMODEL hydrological model: A case study for the Biliu River Basin, China. *J. Hydrol. Environ. Res.* **2013**, *1*, 1–10.

Saltelli, A.; Annoni, P. How to avoid a perfunctory sensitivity analysis. *Environ. Modell. Software* **2010**, *25*, 1508–1517. doi:10.1016/j.envsoft.2010.04.012.

Storn, R.; Price, K. Differential Evolution – A Simple and Efficient Heuristic for global Optimization over Continuous Spaces. *J. Global Optim.* **1997**, *11*, 341–359. doi:10.1023/A:1008202821328.

Nash, J.E.; Sutcliffe, J.V. River flow forecasting through conceptual models part I — A discussion of principles. *J. Hydrol.* **1970**, *10*, 282–290. doi:10.1016/0022-1694(70)90255-6.

Price, K.V.; Storn, R.M.; Lampinen, J.A. *Differential Evolution - A Practical Approach to Global Optimization.*; Springer-Verlag: Berlin, Heidelberg, Germany, 2006. doi:10.1007/3-540-31306-0.

Zheng, F.; Zecchin, A.C.; Simpson, A.R. Investigating the run-time searching behavior of the differential evolution algorithm applied to water distribution system optimization. *Environ. Modell. Software* **2015**, *69*, 292–307. doi:10.1016/j.envsoft.2014.09.022.

- Minasny, B.; McBratney, A.B. A conditioned Latin hypercube method for sampling in the presence of ancillary information. *Comput. Geosci.* **2006**, *32*, 1378–1388. doi:10.1016/j.cageo.2005.12.009.
- Ørka, H.O.; Næsset, E.; Bollandsås, O.M. Classifying species of individual trees by intensity and structure features derived from airborne laser scanner data. *Remote Sens. Environ.* **2009**, *113*, 1163–1174. doi:10.1016/j.rse.2009.02.002.
- Zevenbergen, L.W.; Thorne, C.R. Quantitative analysis of land surface topography. *Earth Surf. Processes Landforms* **1987**, *12*, 47–56. doi:10.1002/esp.3290120107.
- Freeman, T.G. Calculating catchment area with divergent flow based on a regular grid. *Comput. Geosci.* **1991**, *17*, 413–422. doi:10.1016/0098-3004(91)90048-i.
- Böhner, J.; Köthe, R.; Conrad, O.; Gross, J.; Ringeler, A.; Selige, T., Soil Classification 2001; The European Soil Bureau, Joint Research Centre, 2002; chapter Soil Regionalisation by Means of Terrain Analysis and Process Parameterisation, pp. 213–222.
- Conrad, O.; Bechtel, B.; Bock, M.; Dietrich, H.; Fischer, E.; Gerlitz, L.; Wehberg, J.; Wichmann, V.; Böhner, J. System for Automated Geoscientific Analyses (SAGA) v. 2.1.4. *Geosci. Model Dev.* **2015**, *8*, 1991–2007. doi:10.5194/gmd-8-1991-2015.
- Park, S.J.; McSweeney, K.; Lowery, B. Identification of the spatial distribution of soils using a process-based terrain characterization. *Geoderma* **2001**, *103*, 249–272. doi:10.1016/s0016-7061(01)00042-8.
- Jensen, J.R. *Introductory Digital Image Processing: A Remote Sensing Perspective*, 4th ed.; Prentice Hall Press: Upper Saddle River, NJ, USA, 2015.
- Thenkabail, P.; Lyon, J.; Huete, A. Advances in Hyperspectral Remote Sensing of Vegetation and Agricultural Croplands. In *Hyperspectral Remote Sensing of Vegetation*; CRC Press, 2011; pp. 3–36. doi:10.1201/b11222-3.
- Breiman, L. Random Forests. *Mach. Learn.* **2001**, *45*, 5–32. doi:10.1023/A:1010933404324.
- Grimm, R.; Behrens, T.; Märker, M.; Elsenbeer, H. Soil organic carbon concentrations and stocks on Barro Colorado Island — Digital soil mapping using Random Forests analysis. *Geoderma* **2008**, *146*, 102–113. doi:10.1016/j.geoderma.2008.05.008.

- Wiesmeier, M.; Barthold, F.; Blank, B.; Kögel-Knabner, I. Digital mapping of soil organic matter stocks using Random Forest modeling in a semi-arid steppe ecosystem. *Plant Soil* **2011**, *340*, 7–24. doi:10.1007/s11104-010-0425-z.
- Kuhn, M.; Johnson, K. *Applied predictive modeling*; Springer New York: New York, 2013. doi:10.1007/978-1-4614-6849-3.
- Strobl, C.; Malley, J.; Tutz, G. An introduction to recursive partitioning: Rationale, application, and characteristics of classification and regression trees, bagging, and random forests. *Psychol. Methods* **2009**, *14*, 323–348. doi:10.1037/a0016973.
- Kampichler, C.; Wieland, R.; Calmé, S.; Weissenberger, H.; Arriaga-Weiss, S. Classification in conservation biology: A comparison of five machine-learning methods. *Ecol. Inf.* **2010**, *5*, 441–450. doi:10.1016/j.ecoinf.2010.06.003.
- Miller, B.A.; Koszinski, S.; Wehrhan, M.; Sommer, M. Impact of multi-scale predictor selection for modeling soil properties. *Geoderma* **2015**, *239-240*, 97–106. doi:10.1016/j.geoderma.2014.09.018.
- Brungard, C.W.; Boettinger, J.L.; Duniway, M.C.; Wills, S.A.; Edwards, T.C. Machine learning for predicting soil classes in three semi-arid landscapes. *Geoderma* **2015**, *239-240*, 68–83. doi:10.1016/j.geoderma.2014.09.019.
- Poggio, L.; Gimona, A.; Brewer, M.J. Regional scale mapping of soil properties and their uncertainty with a large number of satellite-derived covariates. *Geoderma* **2013**, *209-210*, 1–14. doi:10.1016/j.geoderma.2013.05.029.
- Darst, B.F.; Malecki, K.C.; Engelman, C.D. Using recursive feature elimination in random forest to account for correlated variables in high dimensional data. *BMC Genet.* **2018**, *19*. doi:10.1186/s12863-018-0633-8.
- Bedison, J.E.; Johnson, A.H. Controls on the Spatial Patterns of Carbon and Nitrogen in Adirondack Forest Soils along a Gradient of Nitrogen Deposition. *Soil Sci. Soc. Am. J.* **2009**, *73*, 2105. doi:10.2136/sssaj2008.0336.
- Wang, K.; Zhang, C.; Li, W. Predictive mapping of soil total nitrogen at a regional scale: A comparison between geographically weighted regression and cokriging. *Appl. Geogr.* **2013**, *42*, 73–85. doi:10.1016/j.apgeog.2013.04.002.

- Peng, G.; Bing, W.; Guangpo, G.; Guangcan, Z. Spatial Distribution of Soil Organic Carbon and Total Nitrogen Based on GIS and Geostatistics in a Small Watershed in a Hilly Area of Northern China. *PLOS ONE* **2013**, *8*, e83592. doi:10.1371/journal.pone.0083592.
- Kunkel, M.L.; Flores, A.N.; Smith, T.J.; McNamara, J.P.; Benner, S.G. A simplified approach for estimating soil carbon and nitrogen stocks in semi-arid complex terrain. *Geoderma* **2011**, *165*, 1–11. doi:10.1016/j.geoderma.2011.06.011.
- Johnson, C.E.; Ruiz-Méndez, J.J.; Lawrence, G.B. Forest Soil Chemistry and Terrain Attributes in a Catskills Watershed. *Soil Sci. Soc. Am. J.* **2000**, *64*, 1804. doi:10.2136/sssaj2000.6451804x.
- Seibert, J.; Stendahl, J.; Sørensen, R. Topographical influences on soil properties in boreal forests. *Geoderma* **2007**, *141*, 139–148. doi:10.1016/j.geoderma.2007.05.013.
- Vesterdal, L.; Schmidt, I.K.; Callesen, I.; Nilsson, L.O.; Gundersen, P. Carbon and nitrogen in forest floor and mineral soil under six common European tree species. *For. Ecol. Manage.* **2008**, *255*, 35–48. doi:10.1016/j.foreco.2007.08.015.
- Zhang, Z.; Yu, X.; Qian, S.; Li, J. Spatial variability of soil nitrogen and phosphorus of a mixed forest ecosystem in Beijing, China. *Environ. Earth Sci.* **2010**, *60*, 1783–1792. doi:10.1007/s12665-009-0314-z.
- Sumfleth, K.; Duttmann, R. Prediction of soil property distribution in paddy soil landscapes using terrain data and satellite information as indicators. *Ecol. Indic.* **2008**, *8*, 485–501. doi:10.1016/j.ecolind.2007.05.005.
- Smeck, N.E. Phosphorus dynamics in soils and landscapes. *Geoderma* **1985**, *36*, 185–199. doi:10.1016/0016-7061(85)90001-1.
- Jeong, J.J.; Bartsch, S.; Fleckenstein, J.H.; Matzner, E.; Tenhunen, J.D.; Lee, S.D.; Park, S.K.; Park, J.H. Differential storm responses of dissolved and particulate organic carbon in a mountainous headwater stream, investigated by high-frequency, in situ optical measurements. *J. Geophys. Res. Biogeosci.* **2012**, *117*, n/a–n/a. doi:10.1029/2012jg001999.
- Jung, B.J.; Lee, H.J.; Jeong, J.J.; Owen, J.; Kim, B.; Meusburger, K.; Alewell, C.; Gebauer, G.; Shope, C.; Park, J.H. Storm pulses and varying sources of hydrologic carbon export from a mountainous watershed. *J. Hydrol.* **2012**, *440-441*, 90–101. doi:10.1016/j.jhydrol.2012.03.030.

- Uriarte, M.; Turner, B.L.; Thompson, J.; Zimmerman, J.K. Linking spatial patterns of leaf litterfall and soil nutrients in a tropical forest: a neighborhood approach. *Ecol. Appl.* **2015**, *25*, 2022–2034. doi:10.1890/15-0112.1.
- Hastie, T.; Tibshirani, R.; Friedman, J. *The Elements of Statistical Learning*; Springer New York, 2009. doi:10.1007/978-0-387-84858-7.
- Park, S.J.; Vlek, P.L.G. Environmental correlation of three-dimensional soil spatial variability: a comparison of three adaptive techniques. *Geoderma* **2002**, *109*, 117–140. doi:10.1016/s0016-7061(02)00146-5.
- Remesan, R.; Mathew, J. *Hydrological Data Driven Modelling: A Case Study Approach*; Springer International Publishing, 2015. doi:10.1007/978-3-319-09235-5.
- James, G.; Witten, D.; Hastie, T.; Tibshirani, R. *An Introduction to Statistical Learning with Applications in R*; Springer New York, 2013. doi:10.1007/978-1-4614-7138-7.
- Cichosz, P. *Data Mining Algorithms: Explained Using R*; John Wiley & Sons, Ltd: Chichester, West Sussex ; Malden, MA, 2015. doi:10.1002/9781118950951.
- Feigelson, E.D.; Babu, G.J. *Modern Statistical Methods for Astronomy: With R Applications*; Cambridge University Press, 2012. doi:10.1017/cbo9781139015653.
- Malley, J.D.; Malley, K.G.; Pajevic, S. *Statistical Learning for Biomedical Data*; Cambridge University Press, 2011. doi:10.1017/cbo9780511975820.
- Ambrose, C.; McLachlan, G.J. Selection bias in gene extraction on the basis of microarray gene-expression data. *Proc. Natl. Acad. Sci. U.S.A* **2002**, *99*, 6562–6566. doi:10.1073/pnas.102102699.
- Sorrell, B.K.; Boon, P.I. Convective gas flow in *Eleocharis sphacelata* R. Br.: methane transport and release from wetlands. *Aquat. Bot.* **1994**, *47*, 197–212. doi:10.1016/0304-3770(94)90053-1.
- Wood, P.J.; Armitage, P.D. Biological Effects of Fine Sediment in the Lotic Environment. *Environ. Manage.* **1997**, *21*, 203–217. doi:10.1007/s002679900019.
- Baker, D.W.; Bledsoe, B.P.; Albano, C.M.; Poff, N.L. Downstream effects of diversion dams on sediment and hydraulic conditions of Rocky Mountain streams. *River Res. Appl.* **2011**, *27*, 388–401. doi:10.1002/rra.1376.

- Extence, C.A.; Chadd, R.P.; England, J.; Dunbar, M.J.; Wood, P.J.; Taylor, E.D. The assessment of fine sediment accumulation in rivers using macro-invertebrate community response. *River Res. Appl.* **2011**, *29*, 17–55. doi:10.1002/rra.1569.
- Flores, L.; Díez, J.R.; Larrañaga, A.; Pascoal, C.; Elosegi, A. Effects of retention site on breakdown of organic matter in a mountain stream. *Freshwater Biol.* **2013**, *58*, 1267–1278. doi:10.1111/fw.12125.
- Haga, H.; Kumagai, T.; Otsuki, K.; Ogawa, S. Transport and retention of coarse woody debris in mountain streams: An in situ field experiment of log transport and a field survey of coarse woody debris distribution. *Water Resour. Res.* **2002**, *38*, 1–1–1–16. doi:10.1029/2001wr001123.

## Chapter 2

# Commentary on ‘Modified MMF (Morgan–Morgan–Finney) model for evaluating effects of crops and vegetation cover on soil erosion’ by Morgan and Duzant (2008)

Kwanghun Choi <sup>1\*</sup>, Bernd Huwe <sup>2</sup>, and Björn Reineking <sup>1,3,4</sup>

<sup>1</sup> Department of Biogeographical Modelling, Bayreuth Center of Ecology and Environmental Research (BayCEER), University of Bayreuth, Universitätsstraße 30, 95440, Bayreuth, Germany

<sup>2</sup> Department of Soil Physics, Bayreuth Center of Ecology and Environmental Research (BayCEER), University of Bayreuth, Universitätsstraße 30, 95440, Bayreuth, Germany

<sup>3</sup> Univ. Grenoble Alpes, Irstea, EMGR, F-38000 Grenoble, France

<sup>4</sup> Department of Particle Physics, Astrophysics, Geosciences, Ecology, and Environment, Université Grenoble Alpes, 38402, Grenoble, France

Correspondence: kwanghun.choi@yahoo.com; bt302546@uni-bayreuth.de

### Abstract

The Morgan–Morgan–Finney (MMF) model is a widely used semi-physically based soil erosion model that has been tested and validated in various land use types and climatic regions. The latest version of the model, the modified MMF (MMMMF) model, improved its conceptual physical representations through several modifications of the original model. However, the MMMF model has three problematic parts to be corrected: 1) the effective rainfall equation, 2) the interflow equation, and 3) the improperly normalized C-factor of the transport capacity equation. In this commentary, we identify and correct the problematic parts of the MMMF model, which should result in more accurate estimations of runoff

and soil erosion rates.

**Keywords:** effective rainfall, interflow, C-factor, MMF, soil erosion model, error correction

## 2.1 Introduction

The Morgan–Morgan–Finney (MMF) model (Morgan *et al.*, 1984) is a semi-physically based model used to estimate the amount of annual runoff and soil eroded from a field or a catchment.

Similar to physically based models such as SWAT (Neitsch *et al.*, 2011), EUROSEM (Morgan *et al.*, 1998), LISEM (De Roo *et al.*, 1996), and WEPP (Nearing *et al.*, 1989), the MMF model has the properties of both physically based and empirical models and provides an in-depth understanding of soil erosion processes by using physical concepts. Moreover, the MMF model, similarly to empirical models such as USLE (Wischmeier and Smith, 1978) and RUSLE (Renard *et al.*, 1991), maintains a conceptual simplicity by using semi-empirical relationships and does not require the excessive parameters and computing resources (Morgan *et al.*, 1984, Morgan, 2001, Morgan and Duzant, 2008, Lilhare *et al.*, 2014). For this reason, the MMF and the revised MMF (RMMF) (Morgan, 2001) models have been applied and validated in a variety of climatic regions and land use types (Morgan *et al.*, 1984, Morgan, 2001, De Jong *et al.*, 1999, Vigiak *et al.*, 2005, López-Vicente *et al.*, 2008, Pandey *et al.*, 2009, Li *et al.*, 2010, Feng *et al.*, 2014, Tesfahunegn *et al.*, 2014, Vieira *et al.*, 2014).

In the latest version of the MMF, the modified MMF (MMMMF) (Morgan and Duzant, 2008), hydrological processes were improved by considering the slope angle in the calculation of effective rainfall and introducing interflow processes. In addition, the soil erosion processes of the MMMF model were improved by introducing gravitational deposition process, generalizing the effect of ground surface on sediment deposition and transportation, and considering the characteristics of each soil particle type (Morgan and Duzant, 2008, Lilhare *et al.*, 2014). These modifications allow the MMMF model to consider physical aspects of terrain and soil surface conditions more effectively than previous versions of the MMF model.

However, we argue that errors persist in effective rainfall, interflow, and transport capacity equations, which ultimately affects the model outputs in certain conditions. Despite these errors, however, the MMMF model was implemented and used in several studies without apparent consideration of the problematical parts (i.e., Setiawan (2012) and Lilhare *et al.* (2014)). In addition, one of the problematical parts of the MMMF model, the problematic slope adjustment

factor of effective runoff, was used in the Modified-RMMF-2014 model of López-Vicente *et al.* (2015).

The objective of the present study is to identify and correct the problematic terms concerning:

1. a trigonometric error in the calculation of effective rainfall ( $Rf$ ),
2. a quantity estimation error in the calculation of interflow ( $IF$ ), and
3. an improperly normalized C-factor in the transport capacity equation ( $TC$ ).

## 2.2 Problematic parts of the MMMF model

### 2.2.1 Trigonometric error in the calculation of effective rainfall

The MMMF model represents the catchment through several interconnected elements, each of which has a uniform slope, land cover, and soil type. In the MMF model, effective rainfall is the primary source of the hydrological processes, which regulate surface runoff and the soil erosion processes. The MMMF model calculates effective rainfall ( $Rf_{\text{MMMF}}$ ; mm) while considering the slope of a given element by using the following equation (Morgan and Duzant (2008), eq. (1)):

$$Rf_{\text{MMMF}} = R \cdot (1 - PI) \cdot \frac{1}{\cos(S)}, \quad (2.1)$$

where  $R$  (mm) is the mean annual rainfall,  $PI$  is the area proportion of the permanent interception of rainfall, and  $S$  ( $^\circ$ ) is the slope of an element.

However, we argue that in order to calculate effective rainfall correctly,  $\cos(S)$  should be used as a sloping adjustment factor rather than  $\frac{1}{\cos(S)}$  as described in Sharon (1980) and Tani (1997). We demonstrate our claims through mathematical proof and in Figure 2.1. Let us consider an element on a hill slope with an angle of  $S$  ( $^\circ$ ). Assuming that the area in the horizontal plane is  $A$  ( $\text{m}^2$ ) and its projected area on the element is  $A'$  ( $\text{m}^2$ ), the trigonometric relationship between  $A$  and  $A'$  is

$$A = A' \cdot \cos(S). \quad (2.2)$$

Because the total volume of rainfall ( $P$ ; L) is the same for both  $A$  and  $A'$  (Figure 2.1), the amount of rainfall per unit area for  $A$  and  $A'$  can be calculated as

$$R = \frac{P}{A} \quad (2.3)$$

$$R' = \frac{P}{A'}. \quad (2.4)$$

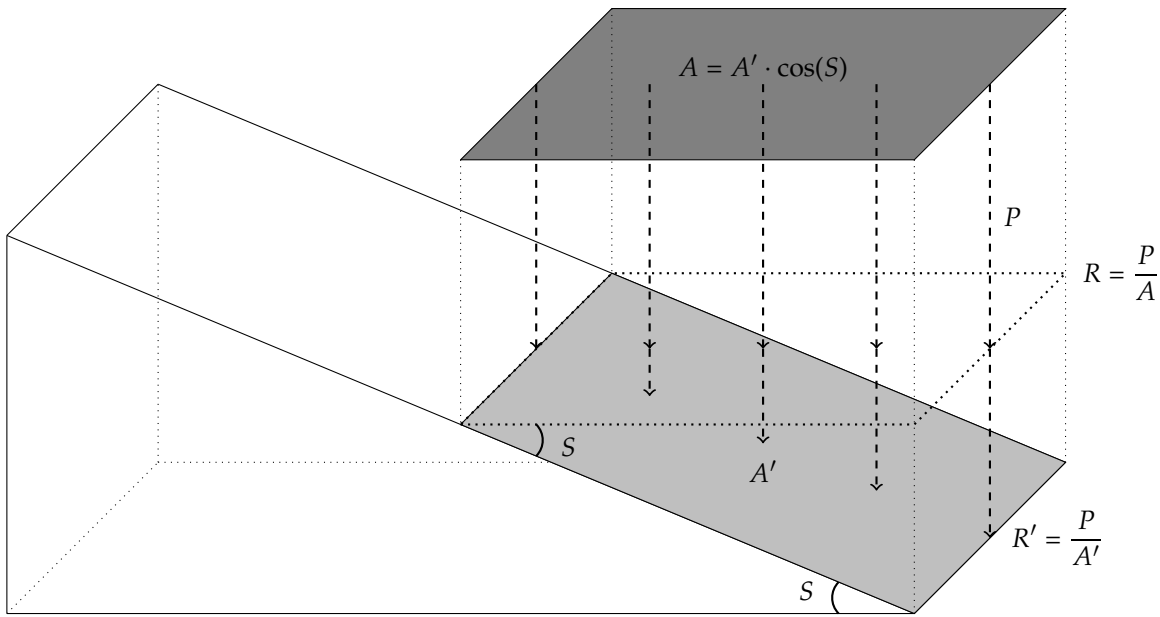


Fig. 2.1. Conceptual representation of a hillslope with a slope angle of  $S$  ( $^\circ$ ).  $A$  ( $\text{m}^2$ ) is the area of a horizontal plane, and  $A'$  ( $\text{m}^2$ ) is the projected area of  $A$  on a hillslope. Because the volume of rainfall ( $P$ ; L) is the same for both  $A$  and  $A'$ , the rainfall per unit area for both areas are  $\frac{P}{A}$  ( $= R$ ; mm) and  $\frac{P}{A'}$  ( $= R'$ ; mm). From the trigonometric rule,  $R'$  is equal to  $R \cdot \cos(S)$ .

From the equations (2.2), (2.3), and (2.4), we can estimate the rainfall per unit surface area on a hillslope ( $R'$ ; mm) with the rainfall of the area ( $R$ ; mm).

$$R' = \frac{P}{A'} = \frac{P}{A} \cdot \cos(S) = R \cdot \cos(S) \quad (2.5)$$

If the element has areas with permanent interception of rainfall ( $PI$ ), the effective rainfall per unit surface area ( $Rf_{\text{corrected}}$ ) should be calculated as

$$Rf_{\text{corrected}} = R' \cdot (1 - PI) = R \cdot (1 - PI) \cdot \cos(S). \quad (2.6)$$

Thus, the slope adjustment factor should be  $\cos(S)$  rather than  $\frac{1}{\cos(S)}$  in order to calculate effective rainfall ( $Rf$ ) considering the slope.

### 2.2.1.1 Consequence of the error in calculating effective rainfall

Owing to the problematic slope adjustment factor of the effective rainfall suggested by Morgan and Duzant (2008), the model overestimates the effective rainfall when the slope of an element increases, as shown in Figure 2.2. Considering that the MMF model and its variants have been applied in mountainous areas with steep hillslopes, as listed in Table 2.1, the MMMF model has a high risk of overestimation of effective rainfall. In the case of Setiawan (2012), the MMMF model overestimated effective rainfall by at least 136% of the corrected value at

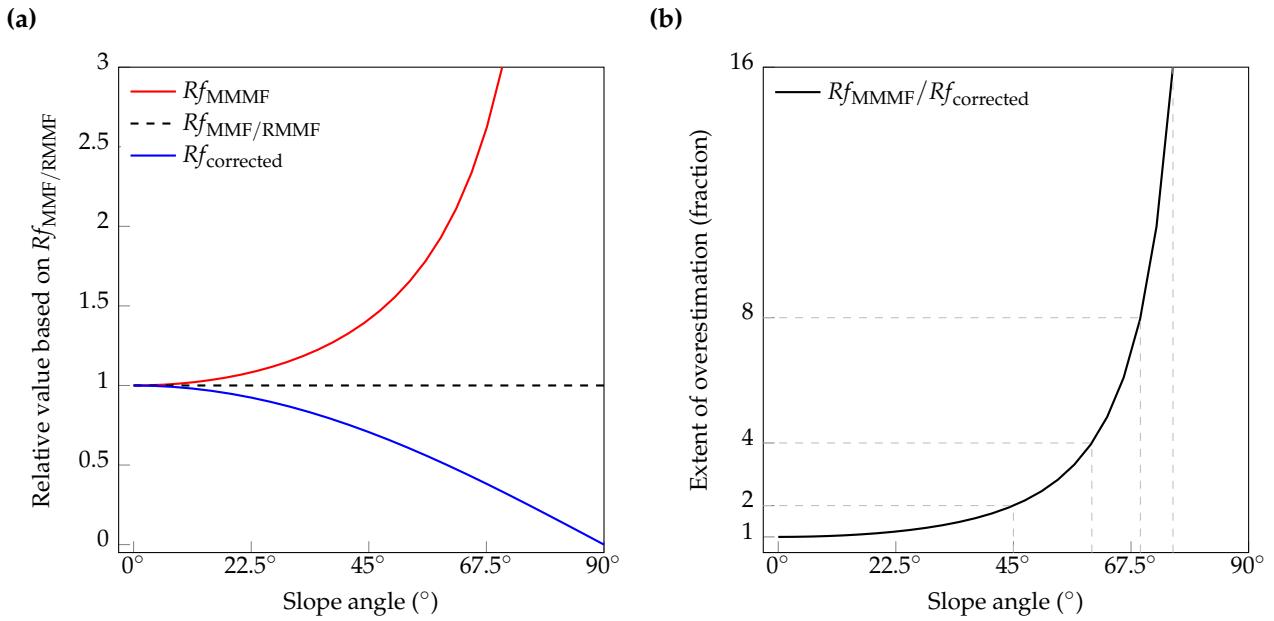


Fig. 2.2. **(a)** Relative values of effective rainfall based on the slope invariant effective rainfall of the Morgan–Morgan–Finney (MMF) and revised MMF (RMMF) models ( $Rf_{MMF/RMMF}$ ) as a function of slope angle. **(b)** Extent of overestimation of effective rainfall from the MMMF model ( $Rf_{MMMF}$ ) to the corrected value ( $Rf_{corrected}$ ) as a function of slope angle. The dashed gray lines in **(b)** indicate the extent of overestimation and the corresponding slope angles.

Table 2.1. Previous studies in which the Morgan–Morgan–Finney (MMF) model and its variants, the revised MMF (RMMF) and the modified MMF (MMMF), were applied to steep hillslopes

| Source                           | Year | Model | Site   | Slope condition   |
|----------------------------------|------|-------|--|---|
| Feng <i>et al.</i> (2014)        | 2014 | RMMF  | Guzhou catchment, China                                | > $55^{\circ}$ (15.8% of total area)<br>$35^{\circ}$ - $55^{\circ}$ (45.3% of total area)<br>$25^{\circ}$ - $35^{\circ}$ (20.7% of total area)<br>$15^{\circ}$ - $25^{\circ}$ (9.2% of total area)<br>$0^{\circ}$ - $15^{\circ}$ (9.0% of total area) |
| Lilhare <i>et al.</i> (2014)     | 2014 | MMMF  | Gamber watershed, India                                | Steep topographic gradient  |
| Tesfahunegn <i>et al.</i> (2014) | 2014 | RMMF  | Mai-Negus catchment, Ethiopia                          | Maximum slope of $73^{\circ}$   |
| Setiawan (2012)                  | 2012 | MMMF  | Kejajar Sub-district, Indonesia                        | > $31.0^{\circ}$ (42.9% of total area)<br>$16.7^{\circ}$ - $31.0^{\circ}$ (28.3% of total area)<br>$8.5^{\circ}$ - $16.7^{\circ}$ (16.1% of total area)<br>$0.0^{\circ}$ - $8.5^{\circ}$ (11.7% of total area)  |
| Li <i>et al.</i> (2010)          | 2010 | RMMF  | Zuli River Basin, China                                | Maximum slope of $45^{\circ}$   |
| Pandey <i>et al.</i> (2009)      | 2009 | RMMF  | Dikrong river basin, India                             | > $45^{\circ}$ (21.0% of total area)<br>$36^{\circ}$ - $45^{\circ}$ (1.8% of total area)<br>$16^{\circ}$ - $35^{\circ}$ (12.8% of total area)<br>$<15^{\circ}$ (64.4% of total area)  |
| Vigiak <i>et al.</i> (2005)      | 2005 | RMMF  | Kwalei catchment, Tanzania<br>Gikuuri catchment, Kenya | > $11.3^{\circ}$ (50% of total area)<br>$1.1^{\circ}$ - $28.8^{\circ}$ (mean: $10.2^{\circ}$ )  |

areas with a slope greater than  $31.0^{\circ}$ , which account for most of the research site. If the MMMF model had been applied to the site of Tesfahunegn *et al.* (2014), it would have overestimated effective rainfall 3.4 times more than that in the previous versions which do not consider the slope and 11.7 times more than the corrected value for the area with the maximum slope angle. According to the sensitivity analysis of Morgan and Duzant (2008), the model outputs of surface

runoff and soil loss are highly sensitive to effective rainfall. Moreover, the overestimation can be greater on downslope elements where the overestimated runoff from upslope accumulates. Therefore, the trigonometric error in the calculation of effective rainfall may lead to incorrect results to a significant degree if the model is applied to a large watershed with steep slopes.

## 2.2.2 Quantity estimation error in calculating interflow

### 2.2.2.1 Incorrect formula in the interflow equation

For calculating annual runoff amount, the MMMF model considers interflow ( $IF$ ; mm), which is the daily mean amount of subsurface water that flows from an element to downslope elements. The interflow from upslope elements ( $IF(CE)$ ; mm) affects runoff generation processes at an element by reducing the soil moisture storage capacity of the soil ( $R_c$ ; mm). The MMMF model uses the following equation to calculate subsurface interflow ( $IF_{\text{MMMF}}$ ; mm) from an element (Morgan and Duzant (2008), eq. (13)):

$$IF_{\text{MMMF}} = \left( \frac{R - E - Q}{365} \right) \cdot (LP \cdot \sin(S)), \quad (2.7)$$

where  $R$  (mm) is the mean annual rainfall per unit area,  $E$  (mm) is the annual evaporation per unit area,  $Q$  (mm) is the annual runoff per unit area,  $LP$  (m/d) is the saturated lateral permeability as a unit of velocity,  $S$  ( $^\circ$ ) is the slope angle of an element, and 365 is the number of days in one year. The first part of equation (2.7) corresponds to the daily mean soil water of one year ( $SW$ ; mm). The second part of the equation is the velocity (m/d) of the interflow of an element, which can be interpreted as the travel distance of interflow during one day (m) for daily time steps.

In the MMMF model, the unit of  $IF_{\text{MMMF}}$  is defined as volume per unit area ( $L/m^2 = \text{mm}$ ), which is similar to other hydrological quantities in the model (i.e.,  $R$ ,  $R_f$ ,  $R_c$ ,  $E$ , and  $Q$ ). However, the unit of interflow in equation (2.7), which is depth multiplied by velocity (or length for daily time steps), contradicts the definition of  $IF_{\text{MMMF}}$  as depth (mm) in the model.

We argue that the interflow equation is improperly formulated and that the  $IF_{\text{MMMF}}$  has the wrong unit. Let us consider the interflow generated from an element  $i$ , as shown in Figure 2.3. The daily mean soil water over one year ( $SW$ ) is

$$SW = \frac{R - E - Q}{365}. \quad (2.8)$$

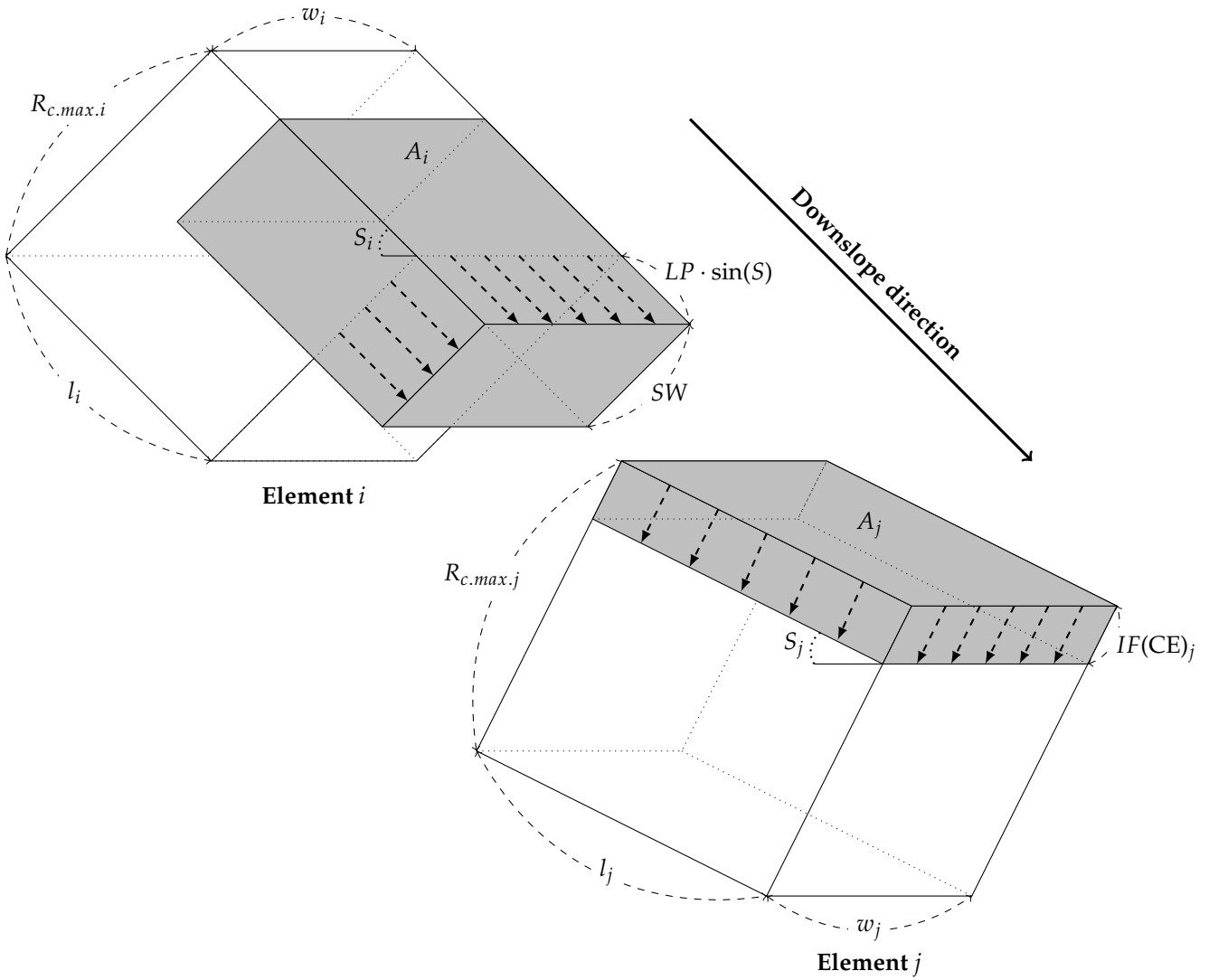


Fig. 2.3. Conceptual representation of interflow between two adjacent elements  $i$  and  $j$ . Here,  $A$ ,  $w$ ,  $l$ ,  $R_{c,max}$ , and  $S$  represent the surface area, width, length, maximum soil moisture storage capacity, and slope angle of each element, respectively. Because daily mean soil water is  $SW$  and the travel distance of soil water during one day is  $LP \cdot \sin(S_i)$ , the daily mean volume of soil water flowing from an element ( $V_{SW}$ ) is  $SW \cdot LP \cdot \sin(S_i) \cdot w_i$ . Because the interflow produced from the element  $i$  ( $IF_i$ ) is equal to  $V_{SW}$  per unit surface area of the element,  $IF_i$  should be  $\frac{SW \cdot LP \cdot \sin(S_i) \cdot w_i}{A_i}$ , and the inflows of subsurface soil water from the contributing area to the element  $j$  ( $IF(CE)_j$ ) should be  $\frac{SW \cdot LP \cdot \sin(S_i) \cdot w_i}{A_j}$ . The  $IF_i$  and the  $IF(CE)_j$  have different values when the surface areas of the elements  $i$  and  $j$  are different.

Because the travel distance of interflow during one day is equal to  $LP \cdot \sin(S)$ , the volume of interflow during one day is

$$V_{IF} = SW \cdot LP \cdot \sin(S_i) \cdot w_i. \quad (2.9)$$

$V_{IF}$  is the depth of soil water ( $SW$ ) multiplied by the travel distance of the interflow ( $LP \cdot \sin(S)$ ) and the width of the element ( $w_i$ ), as represented in Figure 2.3. Equivalent to other hydrological quantities, the quantity of interflow ( $IF_i$ ) is the total volume per surface area of an element.

Therefore,  $IF_i$  can be calculated as

$$IF_i = \frac{V_{IF}}{A_i} = \frac{SW \cdot LP \cdot \sin(S_i) \cdot w_i}{A_i} = \frac{SW \cdot LP \cdot \sin(S_i)}{l_i}. \quad (2.10)$$

According to equations (3.7) and (2.10), interflow ( $IF_{\text{corrected}}$ ) should be calculated as

$$IF_{\text{corrected}} = \left( \frac{R - E - Q}{365} \right) \cdot (LP \cdot \sin(S_i)) \cdot \frac{1}{l_i} = \frac{IF_{\text{MMMMF}}}{l_i}. \quad (2.11)$$

Therefore, the additional term of  $\frac{1}{l_i}$  is required for the interflow equation of Morgan and Duzant (2008). Furthermore, with this term,  $IF_{\text{corrected}}$  has the correct unit of depth (mm). The dependence of interflow on slope length is obvious, as shown in the lateral flow equation of the widely used SWAT model (equation 2:3.5.9 of Neitsch *et al.* (2011)), because the SWAT model also uses water volume per unit area. We derived the same formula of  $IF_{\text{corrected}}$  by using the theoretically well-established Darcy's law in the supplementary material of this article.

### 2.2.2.2 Discrepancy between generated and transferred interflow

Another problem exists in the interflow equation even if  $IF_{\text{corrected}}$  is used rather than  $IF_{\text{MMMMF}}$ . As shown in Figure 2.3, the generated interflow from the element  $i$  flows into the element  $j$ . Because the total volume of interflow ( $V_{IF}$ ) is the same for both elements, the interflow into the element  $j$  ( $IF(\text{CE})_j$ ) should be

$$IF(\text{CE})_j = \frac{V_{IF}}{A_j} \neq \frac{V_{IF}}{A_i} = IF_i. \quad (2.12)$$

The discrepancy between generated and transferred interflow is attributed to the different surface areas of the elements. If using raster maps in the MMMF models (Figure 2.3), as is performed in most MMF model studies, the extent of the discrepancy can be calculated as

$$\frac{IF_i}{IF(\text{CE})_j} = \frac{V_{IF}}{A_i} \cdot \frac{A_j}{V_{IF}} = \frac{l_j}{l_i} = \frac{\cos(S_i)}{\cos(S_j)}. \quad (2.13)$$

Therefore, the discrepancy is larger if the difference in slope between adjacent upslope and downslope elements is significant. Similar discrepancies between adjacent elements can also be found in every matter exchange processes of the MMMF model (i.e., surface runoff, interflow, and sediment). Problems of the discrepancy can be solved by using the water volume or the total sediment mass for transferring water and sediments and dividing the volume or total mass by the surface area of the receiving element.

### 2.2.2.3 Consequence of the error in calculating interflow

Owing to the incorrect formula in the interflow equation of Morgan and Duzant (2008), the MMMF model overestimates interflow when the slope length of an element increases. However, the model underestimates interflow if the slope length of an element is less than 1 m. Figure 2.4 shows the extent of the overestimation when the MMMF model is applied to raster maps such as a digital elevation model (DEM). For a DEM with a certain resolution ( $res$ ; m), the width ( $w$ ) and the length ( $l$ ) of each element are equal to  $res$  and  $\frac{res}{\cos(S)}$ . Therefore, the extent of overestimation of the interflow is dependent on the slope of an element and the resolution of the DEM. In the case of Setiawan (2012), who applied the MMMF model using a DEM with 0.05 m

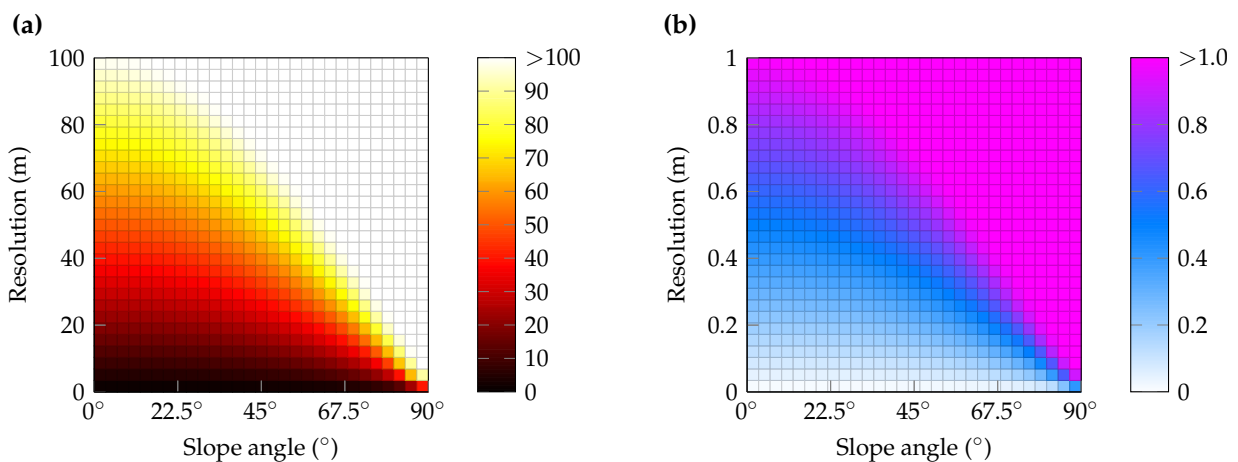


Fig. 2.4. Extent of the overestimation of  $IF_{\text{MMMF}}$  compared with  $IF_{\text{corrected}}$  as a fraction of  $\frac{IF_{\text{MMMF}}}{IF_{\text{corrected}}}$  by slope and resolution. (a) General pattern for maximum resolution of 100 m. (b) Pattern for fine-resolution section. Values larger (smaller) than one indicate overestimation (underestimation).

resolution for a maximum slope of  $41^\circ$ , the MMMF model estimated at most only 7% of the corrected interflow. In the case of Lilhare *et al.* (2014), who applied the MMMF model using a DEM with 90 m resolution, the extent of overestimation was more than 90 times compared with the corrected interflow.

Owing to the discrepancy between the generated and transferred interflow, the model overestimates the interflow from contributing elements to a receiving element when the receiving element is steeper than the contributing elements, as shown in Figure 2.5. In addition, the model underestimates the interflow from contributing elements when they are steeper than the receiving element. The extent of the discrepancy increases with the increase in slope differences between contributing and receiving elements. Because errors in the calculation of interflow are positively correlated with the size, slope, and rate of change in the slope of elements, the model is not suitable for steep mountainous terrain with complex topography. Furthermore, the interflow

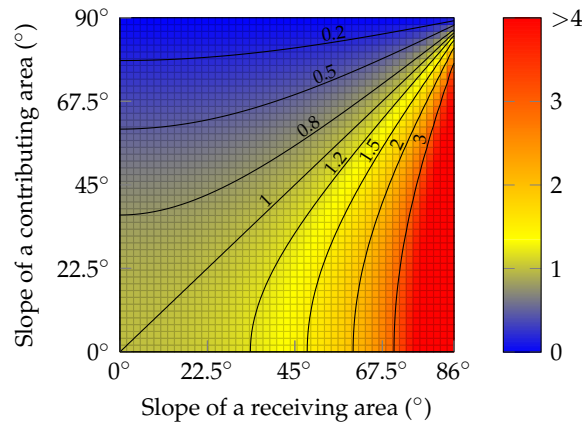


Fig. 2.5. Extent of the discrepancy between the generated interflow from a contributing element and the transferred interflow to a receiving element.

affects the quantity of surface runoff by affecting the amount of the soil moisture storage ( $R_c$ ), as shown in eq. (10) of Morgan and Duzant (2008).

### 2.2.3 Improperly normalized C-factor in the transport capacity equation

The MMF model uses a crop cover management factor (C-factor), which is the ratio of soil loss under a given surface condition (actual condition) to that from a bare ground condition (reference condition) based on the empirical values of Universal Soil Loss Equation (USLE) cropping (C) and erosion control (P) factors (Morgan *et al.*, 1984). In the MMMF model, Morgan and Duzant (2008) the C-factor is calculated by modifying the ratio of soil loss to the ratio of runoff velocity under an actual condition as that of the reference condition. This modification allows the MMMF model to generalize the empirically based C-factor by using measurable physical quantities. As a result, the model can consider the effects of surface roughness, rill depth, and vegetation structure on soil erosion in addition to the effect of crop cover management on soil erosion. However, we argue that the C-factor used in the MMMF model is not properly normalized in the course of combining multiple velocities (i.e.,  $v_a$ ,  $v_v$ , and  $v_t$ ) corresponding to different surface condition types. As a consequence, if the model considers more than one surface condition type, the unitless C-factor contains the inconsistent units of the velocity or the squared value of velocity. The MMMF model calculates the C-factor as (eqs. (39)–(41) of Morgan and Duzant (2008))

$$C_{\text{MMMF}} = \frac{v_a \cdot v_v \cdot v_t}{v_b}, \quad (2.14)$$

where  $v_a$ ,  $v_v$ , and  $v_t$  are runoff velocity considering the rill condition, vegetation cover, and surface roughness, respectively.  $v_b$  is the runoff velocity for the reference condition of unchanneled

overland flow over smooth bare ground. Moreover, adding and subtracting variables are allowed in the MMMF model, according to the surface condition. Assuming that only one of the surface condition types is considered in the model, the C-factor for each surface condition type should be calculated as

$$C_a = \frac{v_a}{v_b} \quad (2.15)$$

$$C_v = \frac{v_v}{v_b} \quad (2.16)$$

$$C_t = \frac{v_t}{v_b}. \quad (2.17)$$

As described in the MMMF model, all surface condition types are considered independently from each other, which means that a surface condition type is not affected by other surface condition types. Therefore, for the combination of the surface condition types, the C-factor should be calculated as

$$C_{\text{corrected}} = \frac{v_a}{v_b} \cdot \frac{v_v}{v_b} \cdot \frac{v_t}{v_b} = \frac{v_a \cdot v_v \cdot v_t}{v_b^3}. \quad (2.18)$$

According to equation (2.18),  $C_{\text{corrected}}$  is unitless because each velocity is normalized by the reference velocity. Even if some surface condition types are missing or added, the unit of the factor remains constant.

### 2.2.3.1 Consequence of improper normalization of the C-factor

According to Petryk and Bosmajian (1975), rill depth (hydraulic radius) acts as an accelerator of the runoff velocity, whereas vegetation and surface roughness act as resistors of the runoff velocity. Therefore, the C-factor should be increased when the model additionally considers a surface with a rill depth deeper than that of reference surface condition (0.005 m). On the contrary, the C-factor should be decreased when the model additionally considers vegetation cover and surface roughness of an element. However, for hillslopes in which  $v_a$ ,  $v_v$ , and  $v_t$  are faster than 1 m/s, the C-factor of the MMMF model sharply increases by a factor of the added runoff velocity even if the model additionally considers vegetation cover or surface roughness. For slopes with runoff velocities lower than 1 m/s, the C-factor is underestimated when the model additionally considers surface condition type. Errors occur because the C-factor of the MMMF model does not consider the relative velocity of the reference surface condition. The effect of the error is significant for elements with high runoff velocities when the soil erosion rates are high. Owing to the slope dependence of runoff velocity, increased slope of an element relates to greater overestimation.

## 2.3 Conclusions

The MMF model is a widely used semi-physically based soil erosion model because it includes rigorous physical processes, easily understood features, and moderate data requirements. The newly added features of Morgan and Duzant (2008) consider the slope angle, subsurface water processes, surface conditions, and characteristics of each soil particle type (Lilhare *et al.*, 2014), which have the potential to further strengthen the physical basis of the model. We identified three problematic formulations related to the calculations of effective rainfall, interflow, and the C-factor of transport capacity, which can produce inadequate results of runoff and soil erosion. In addition, we suggested alternative formulations to provide more accurate estimations of runoff and soil erosion.

## Acknowledgments

This study is part of the International Research Training Group “Complex Terrain and Ecological Heterogeneity” (TERRECO) (GRK 1565/1) funded by the German Research Foundation (DFG). The document was typed by  $\text{\LaTeX}$  using the modified class and bibliography style files provided by MDPI (<http://www.mdpi.com/authors/latex>). The authors would like to thank Jean-Lionel Payeur-Poirier and Anthony from Editage for English proofreading this manuscript.

## Appendix 2.A Derivation of the corrected interflow equation using Darcy's law

Let us assume that there is an amount of soil water equivalent to the daily mean soil water over one year ( $SW$ ; mm) in an element and that only soil water exerts a force on the element for the interflow process (Figure 2.A1). The volumetric flux of soil water ( $J_{SW}$ ; m<sup>3</sup>/s) in the

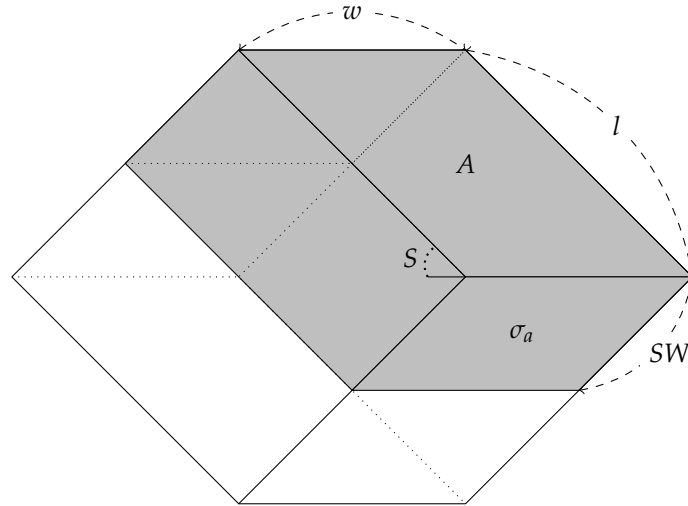


Fig. 2.A1. Conceptual representation of soil water in an element.  $A$ ,  $w$ ,  $l$ , and  $S$  are the area (m<sup>2</sup>), width (m), slope length (m), and slope angle (°) of the element, respectively;  $SW$  (mm) is the daily mean soil water over one year, and  $\sigma_a$  (m<sup>2</sup>) is the cross-sectional area of  $SW$ .

element can be derived from Darcy's law when the hydraulic conductivity ( $K$ ) of the soil is given:

$$J_{SW} = -\frac{K \cdot \sigma_a}{\rho \cdot g} \cdot \frac{\Delta P}{l}, \quad (2.A1)$$

where  $\sigma_a$  (m<sup>2</sup>) is the cross-sectional area of the soil water along the downslope direction,  $\rho$  (kg/m<sup>3</sup>) is the density of the soil water,  $g$  (m/s<sup>2</sup>) is the gravitational acceleration,  $\Delta P$  (Pa) is a pressure gradient of the soil water for both sides of the element, and  $l$  (m) is the length of the soil water along the downslope direction. Because pressure ( $P$ ) is force ( $f$ ; N) divided by the cross-sectional area,  $P$  can be calculated as

$$P = \frac{f}{\sigma_a}. \quad (2.A2)$$

The gradient of force ( $\Delta f$ ; N) acting on both ends of the element can be derived from the volume of the soil water ( $V'_{SW}$ ; m<sup>3</sup>), which is calculated as

$$V'_{SW} = 0.001 \cdot SW \cdot A = 0.001 \cdot SW \cdot w \cdot l, \quad (2.A3)$$

where  $A$  ( $\text{m}^2$ ),  $w$  (m), and  $l$  (m) are the surface area, width, and length of the element, respectively. The unit conversion factor of 0.001 is used to convert millimeters to meters. Because the gradient of force depends on the gradient of the mass of both ends of the element,  $\Delta f$  is calculated as

$$\Delta f = V'_{SW} \cdot \rho \cdot g \cdot \sin(S), \quad (2.A4)$$

where  $S$  is the slope angle ( $^\circ$ ) of the element. From equations (2.A1), (2.A2), (2.A3), and (2.A4), the volumetric flux of the soil water can be simplified as

$$J_{SW} = -0.001 \cdot K \cdot SW \cdot w \cdot \sin(S). \quad (2.A5)$$

Because the hydraulic conductivity during one day is defined as saturated lateral permeability ( $LP$ ; m/day) in the MMMF model, the volume of soil water flowing from the element ( $V_{SW.out}$ ) during one day is

$$V_{SW.out} = J_{SW} \cdot 1 \text{ (day)} = (0.001 \cdot LP \cdot SW \cdot w \cdot \sin(S)) \cdot 1 \text{ (day)}. \quad (2.A6)$$

Because the time step of one day affects only the unit of equation (2.A6), the interflow from the element ( $IF_{corrected}$ ; mm) as a quantity of volume per unit surface area can be calculated as

$$IF_{corrected} = 1000 \cdot \frac{V_{SW.out}}{A} = \frac{LP \cdot SW \cdot w \cdot \sin(S)}{l}, \quad (2.A7)$$

where 1000 is the unit converting factor from meters to millimeters. Therefore, we can use Darcy's law to obtain an identical equation as that in the main text that depends on slope length.

## References

- Morgan, R.P.C.; Morgan, D.D.V.; Finney, H.J. A predictive model for the assessment of soil erosion risk. *J. Agric. Eng. Res.* **1984**, *30*, 245–253. doi:10.1016/S0021-8634(84)80025-6.
- Neitsch, S.L.; Arnold, J.G.; Kiniry, J.R.; Williams, J.R.; King, K.W. Soil and Water Assessment Tool Theoretical Documentation Version 2009. Texas Water Resources Institute Technical Report No. 406, Texas Water Resources Institute, 2011.
- Morgan, R.P.C.; Quinton, J.N.; Smith, R.E.; Govers, G.; Poesen, J.W.A.; Auerswald, K.; Chisci, G.; Torri, D.; Styczen, M.E. The European Soil Erosion Model (EUROSEM): a dynamic

- approach for predicting sediment transport from fields and small catchments. *Earth Surf. Processes Landforms* **1998**, *23*, 527–544. doi:10.1002/(SICI)1096-9837(199806)23:6<527::AID-ESP868>3.0.CO;2-5.
- De Roo, A.P.J.; Wesseling, C.G.; Ritsema, C.J. LISEM: A single-event physically based hydrological and soil erosion model for drainage basins. I: Theory, Input and Output. *Hydrol. Processes* **1996**, *10*, 1107–1117. doi:10.1002/(SICI)1099-1085(199608)10:8<1107::AID-HYP415>3.0.CO;2-4.
- Nearing, M.A.; Foster, G.R.; Lane, L.J.; Finkner, S.C. A process-based soil erosion model for USDA-Water Erosion Prediction Project technology. *Trans. ASAE* **1989**, *32*, 1587–1593.
- Wischmeier, W.H.; Smith, D.D. Predicting rainfall erosion losses—a guide to conservation planning. In *Agriculture Handbook*; Number 537, U.S. Department of Agriculture, 1978; pp. 1–58.
- Renard, K.G.; Foster, G.R.; Weesies, G.A.; Porter, J.P. RUSLE: Revised universal soil loss equation. *J. Soil Water Conserv.* **1991**, *46*, 30–33.
- Morgan, R.P.C. A simple approach to soil loss prediction: a revised Morgan–Morgan–Finney model. *Catena* **2001**, *44*, 305–322. doi:10.1016/S0341-8162(00)00171-5.
- Morgan, R.P.C.; Duzant, J.H. Modified MMF (Morgan–Morgan–Finney) model for evaluating effects of crops and vegetation cover on soil erosion. *Earth Surf. Processes Landforms* **2008**, *32*, 90–106. doi:10.1002/esp.1530.
- Lilhare, R.; Garg, V.; Nikam, B. Application of GIS-Coupled Modified MMF Model to Estimate Sediment Yield on a Watershed Scale. *J. Hydrol. Eng.* **2014**, *20*, C5014002. doi:10.1061/(ASCE)HE.1943-5584.0001063.
- De Jong, S.M.; Paracchini, M.L.; Bertolo, F.; Folving, S.; Megier, J.; De Roo, A.P.J. Regional assessment of soil erosion using the distributed model SEMMED and remotely sensed data. *Catena* **1999**, *37*, 291–308. doi:10.1016/S0341-8162(99)00038-7.
- Vigiak, O.; Okoba, B.O.; Sterk, G.; Groenenberg, S. Modelling catchment-scale erosion patterns in the East African Highlands. *Earth Surf. Processes Landforms* **2005**, *30*, 183–196. doi:10.1002/esp.1174.

- López-Vicente, M.; Navas, A.; Machín, J. Modelling soil detachment rates in rainfed agrosystems in the south-central Pyrenees. *Agric. Water Manage.* **2008**, *95*, 1079–1089. doi:10.1016/j.agwat.2008.04.004.
- Pandey, A.; Mathur, A.; Mishra, S.K.; Mal, B.C. Soil erosion modeling of a Himalayan watershed using RS and GIS. *Environ. Earth Sci.* **2009**, *59*, 399–410. doi:10.1007/s12665-009-0038-0.
- Li, C.; Qi, J.; Feng, Z.; Yin, R.; Guo, B.; Zhang, F.; Zou, S. Quantifying the Effect of Ecological Restoration on Soil Erosion in China's Loess Plateau Region: An Application of the MMF Approach. *Environ. Manage.* **2010**, *45*, 476–487. doi:10.1007/s00267-009-9369-6.
- Feng, T.; Chen, H.; Wang, K.; Zhang, W.; Qi, X. Modeling soil erosion using a spatially distributed model in a karst catchment of northwest Guangxi, China. *Earth Surf. Processes Landforms* **2014**, *39*, 2121–2130. doi:10.1002/esp.3625.
- Tesfahunegn, G.B.; Tamene, L.; Vlek, P.L.G. Soil Erosion Prediction Using Morgan–Morgan–Finney Model in a GIS Environment in Northern Ethiopia Catchment. *Appl. Environ. Soil Sci.* **2014**, *2014*, Article ID 468751, 15. doi:10.1155/2014/468751.
- Vieira, D.C.S.; Prats, S.A.; Nunes, J.P.; Shakesby, R.A.; Coelho, C.O.A.; Keizer, J.J. Modelling runoff and erosion, and their mitigation, in burned Portuguese forest using the revised Morgan-Morgan-Finney model. *For. Ecol. Manage.* **2014**, *314*, 150–165. doi:10.1016/j.foreco.2013.12.006.
- Setiawan, M.A. Integrated Soil Erosion Management in the upper Serayu Watershed, Wonosobo District, Central Java Province, Indonesia. PhD thesis, University of Innsbruck, Austria, 2012.
- López-Vicente, M.; Quijano Gaudes, L.; Palazón Tabuenca, L.; Gaspar Ferrer, L.; Navas Izquierdo, A. Assessment of soil redistribution at catchment scale by coupling a soil erosion model and a sediment connectivity index (central spanish pre-pyrenees). *Cuad. de Investig. Geogr.* **2015**, *41*, 127–147. doi:10.18172/cig.2649.
- Sharon, D. The distribution of hydrologically effective rainfall incident on sloping ground. *J. Hydrol.* **1980**, *46*, 165–188. doi:10.1016/0022-1694(80)90041-4.
- Tani, M. Runoff generation processes estimated from hydrological observations on a steep forested hillslope with a thin soil layer. *J. Hydrol.* **1997**, *200*, 84–109. doi:10.1016/S0022-1694(97)00018-8.

Petryk, S.; Bosmajian, G. Analysis of flow through vegetation. *J. Hydraul. Eng.* **1975**, *101*, 871–884.

## Chapter 3

# Daily Based Morgan–Morgan–Finney (DMMF) Model: A Spatially Distributed Conceptual Soil Erosion Model to Simulate Complex Soil Surface Configurations

Kwanghun Choi <sup>1,\*</sup>, Sebastian Arnhold <sup>2</sup>, Bernd Huwe <sup>3</sup> and Björn Reineking <sup>1,4</sup>

<sup>1</sup> Biogeographical Modelling, Bayreuth Center of Ecology and Environmental Research (BayCEER), University of Bayreuth, Universitätsstraße 30, D-95440 Bayreuth, Germany; bt302546@uni-bayreuth.de

<sup>2</sup> Professorship of Ecological Services, Faculty of Biology, Chemistry and Earth Sciences, BayCEER, University of Bayreuth, Universitätsstraße 30, D-95440, Bayreuth, Germany; sebastian.arnhold@uni-bayreuth.de

<sup>3</sup> Soil Physics Group, University of Bayreuth, Universitätstraße 30, D-95440 Bayreuth, Germany; bernd.huwe@uni-bayreuth.de

<sup>4</sup> Univ. Grenoble Alpes, Irstea, EMGR, F-38000 Grenoble, France; bjoern.reineking@irstea.fr

Correspondence: bt302546@uni-bayreuth.de or kwanghun.choi@yahoo.com; Tel.:+49 (0)921 55 2242

## Abstract

In this paper, we present the Daily based Morgan–Morgan–Finney model. The main processes in this model are based on the Morgan–Morgan–Finney soil erosion model, and it is suitable for estimating surface runoff and sediment redistribution patterns in seasonal climate regions with complex surface configurations. We achieved temporal flexibility by utilizing daily time steps, which is suitable for regions with concentrated seasonal rainfall. We introduce the proportion of impervious surface cover as a parameter to reflect its impacts on soil erosion through blocking water infiltration and protecting

the soil from detachment. Also, several equations and sequences of sub-processes are modified from the previous model to better represent physical processes. From the sensitivity analysis using the Sobol' method, the DMMF model shows the rational response to the input parameters which is consistent with the result from the previous versions. To evaluate the model performance, we applied the model to two potato fields in South Korea that had complex surface configurations using plastic covered ridges at various temporal periods during the monsoon season. Our new model shows acceptable performance for runoff and the sediment loss estimation ( $NSE \geq 0.63$ ,  $|PBIAS| \leq 17.00$ , and  $RSR \leq 0.57$ ). Our findings demonstrate that the DMMF model is able to predict the surface runoff and sediment redistribution patterns for cropland with complex surface configurations.

**Keywords: runoff estimation; sediment redistribution; impervious area; monsoon rainfall; plastic mulching**

### 3.1 Introduction

Land degradation and freshwater deterioration by soil erosion are major environmental and economic problems faced worldwide (Pimentel and Kounang, 1998, Sidle et al., 2006). The problem is prominent in Monsoon and Mediterranean regions where intensive agricultural practices and massive land use changes are taking place on erosion-prone hilly landscapes affected by concentrated seasonal rainfall (Morgan, 2005, Onori et al., 2006, Napoli et al., 2016, Zema et al., 2016, Huon et al., 2017). In regions suffering from soil erosion, people often use simulation models to project soil erosion rates under varied environmental conditions and land use change scenarios in order to determine optimal, cost-effective soil erosion mitigation measures for vulnerable areas (Boardman, 2006, Hu and Flanagan, 2013).

Soil erosion models are classified into three categories of empirical, process-based, and conceptual models according to their characteristics; of these, empirical models such as USLE (Wischmeier and Smith, 1978), RUSLE (Renard et al., 1991), and MUSLE (Williams, 1975) have been frequently used to estimate soil erosion rate as they are easy to use and require reasonable amounts of data and computing resources (Morgan et al., 1984, Morgan, 2001, Lal, 2001, Merritt et al., 2003, Lihare et al., 2014). However, such empirical models also have fundamental limitations. The models are mostly based on empirical relationships induced by their place of origin (e.g., farmland in the American Great Plains for USLE, RUSLE, and MUSLE), and are therefore often unsuitable for regions with different land and environmental types. Additionally, the empirical models calculate soil erosion rates primarily through a few simple statistical relationships,

and are therefore unable to provide enough information on the underlying physical processes to develop a comprehensive understanding of soil erosion. (Hu and Flanagan, 2013, Merritt et al., 2003, Lilhare et al., 2014, Avwunudiogba and Hudson, 2014). In contrast, process-based models such as EUROSEM (Morgan et al., 1998), LISEM (De Roo et al., 1996), EROSION 3D (von Werner, 1995), WEPP (Nearing et al., 1989), and ANSWERS (Beasley et al., 1980) estimate soil erosion rates with well-defined and sophisticated physical equations of mass and momentum conservation laws (Hu and Flanagan, 2013, Merritt et al., 2003). However, process-based models demand a huge amount of data and computing resources for initialization, calibration, and simulation. As a result, it is often difficult to apply these types of model to large temporal and spatial scales (Hu and Flanagan, 2013, Merritt et al., 2003, Lilhare et al., 2014). Intermediately, conceptual models such as the Morgan–Morgan–Finney (MMF) (Morgan et al., 1984), TOPMODEL (Beven and Kirkby, 1979), and the Hydrologiska Byråns Vattenbalansavdelning (HBV) (Bergström and Forsman, 1973) models use semi-empirical equations with a physical basis to estimate annual runoff and soil erosion rates, and are designed to possess advantages of both empirical and process-based models (Devia et al., 2015). These features allow the model to simulate soil erosion processes on the basis of physical concepts while maintaining a simple structure and a moderate level of data demand (Morgan et al., 1984, Morgan, 2001, Lilhare et al., 2014, Morgan and Duzant, 2008).

Among the conceptual models, the MMF and the revised MMF (RMMF) (Morgan, 2001) models have been successfully tested for functionality with a variety of climate regions and land use types (Morgan et al., 1984, Morgan, 2001, De Jong et al., 1999, Vigiak et al., 2005, López-Vicente et al., 2008, Vieira et al., 2014). The modified MMF model (MMMMF) (Morgan and Duzant, 2008) exemplified the runoff processes by focusing on hillslope topography and by introducing the subsurface interflow process to the MMF model. The modified version also refined the sedimentation processes by adding the effects of vegetation structure to the soil deposition processes as well as by explicitly simulating soil redistribution processes for each soil particle size class of clay, silt, and sand (Lilhare et al., 2014, Morgan and Duzant, 2008).

Although several elements in its conceptual and physical bases are enhanced, the model still has three significant limitations in terms of general applicability. First, the temporal scale of the MMF model is fixed as an annual basis. However, this temporal scale is not suitable for regions with concentrated seasonal rainfall such as Monsoon and Mediterranean climates where a majority of soil erosion occurs by highly intensive rainfall events (Hu and Flanagan, 2013, Baartman et al., 2012). Furthermore, as computing power increases, there is a growing demand for soil erosion models that can be applied flexibly over short- and long-term scales given that the

frequency and intensity of heavy rainfall is likely to increase (Merritt et al., 2003, Stocker et al., 2013). Second, the model does not consider impervious surface covers, despite their having enormous impacts on runoff and soil redistribution patterns by reducing water infiltration, and consequently, increasing the volume of surface runoff and protecting surface soil from detachment. The area of impervious covers are expanding sharply as a result of urbanization (e.g., pavements) and advances in agricultural technology (e.g., plastic film mulching) (Espí et al., 2006, Shuster et al., 2005, Pappas et al., 2008, Arnhold et al., 2013, Ruidisch et al., 2013). Third, the three components of the effective rainfall, the interflow, and the flow velocity of the MMMF model need to be revised for a better physical representation of the model (Choi et al., 2016). The MMMF model computes the effective rainfall with the slope adjusting factor of  $1/\cos(S)$ , where  $S$  is the slope angle, which is physically incorrect and must be changed to  $\cos(S)$ . Because of the incorrect slope adjusting factor, the MMMF model overestimates the surface runoff and soil erosion under steep slope conditions (Choi et al., 2016). The Interflow equation of the MMMF model does not consider the width of a slope; a factor that should have been considered for physical consistency of the model. From this equation, the MMMF model estimates low interflow in areas wider than 1 m and higher interflow in the areas narrower than 1 m (Choi et al., 2016). Flow velocity is one of the key factors for estimating particle settling rates and transport capacity and is determined by four different equations that vary according to the surface conditions. However, the MMMF model uses only one flow velocity for particle settling but uses many for the transport capacity without proper normalization. Consequently, the MMMF model calculates transport capacity incorrectly for an element with mixed surface conditions (Choi et al., 2016).

In this study, we suggest a new soil erosion model based on the MMMF model called the Daily based Morgan–Morgan–Finney (DMMF) model. This model addresses the above mentioned limitations through the following improvements:

1. A modified temporal scale of the model from an annual basis to daily basis. This is better suited to regions with intensive seasonal rainfall
2. Inclusion of impervious surface covers (e.g., plastic mulching and artificial structures such as concrete ditches and pavements)
3. Revision of the effective rainfall equation, the interflow equation, and equations relevant to flow velocity.

## 3.2 Model Description

### 3.2.1 The DMMF Model

The DMMF model is a conceptual soil erosion model used to estimate surface runoff and sediment flux from a field scale on a daily basis. Spatially, the DMMF model represents an area as several interconnected elements of uniform topography, soil characteristics, land cover type, and vegetation structure. Through coupling the model with flow direction algorithms, each element receives water and sediments from upslope elements and delivers the generated surface runoff and eroded soils to downslope elements. Temporally, the model estimates the surface runoff and the sediment flux of each element on a daily basis and can extend its temporal scales through updating the model for a given period. The DMMF model estimates water and sediment flux of an element in two main phases; the hydrological phase and the sediment phase. The hydrological phase is based on the simple soil water storage approach where surface runoff occurs when daily surface water inputs exceed soil water storage capacity (i.e., saturation-excess overland flow) as outlined in Kirkby (1976). In the model, we redefined the soil water storage capacity as the surface water infiltration capacity after considering the blocking effect of impervious covers. The sediment phase is largely based on the sediment balance process from the MMMF model. Based on this framework, we redefined the flow velocity by adopting the modified Manning's equation from Petryk and Bosmajian (1975) and the transport capacity equation with the normalized flow velocity. Additionally, we changed to have all sediment input processes occur before the deposition process in order to apply deposition process for all the sediment inputs. The model is also adapted to consider the impact of impervious surface covers on runoff and sediment redistribution. The hydrological and the sediment phases of the model work with water volume ( $L/m^2 = mm$ ) and sediment weight ( $kg/m^2$ ) per surface area of an element, respectively. On the other hand, matter exchange between elements uses the total volume of water (L) and the total weight of sediment (kg), and considers the size difference of source areas and accepting areas. In this study, we describe the DMMF model comprehensively; although a substantial part of the model follows the MMMF model, to explain the new routines and revised processes with consistency. To distinguish the new routines and revised equations from those of the original MMMF model, we indicate unchanged MMMF equations by an asterisk next to the equation number. A detailed description of input parameters is presented in Table 4.1.

### 3.2.2 Hydrological Phase

The hydrological phase consists of two major processes: the surface runoff and the subsurface interflow processes (Figure 3.1). In the model, the subsurface process is simplified by conceptualizing a soil profile as one layer and adopting average hydraulic characteristics of an entire soil profile (i.e., soil water contents ( $\theta_{init}$ ,  $\theta_{sat}$ , and  $\theta_{fc}$ ), and saturated soil lateral hydraulic conductivity ( $K$ )).

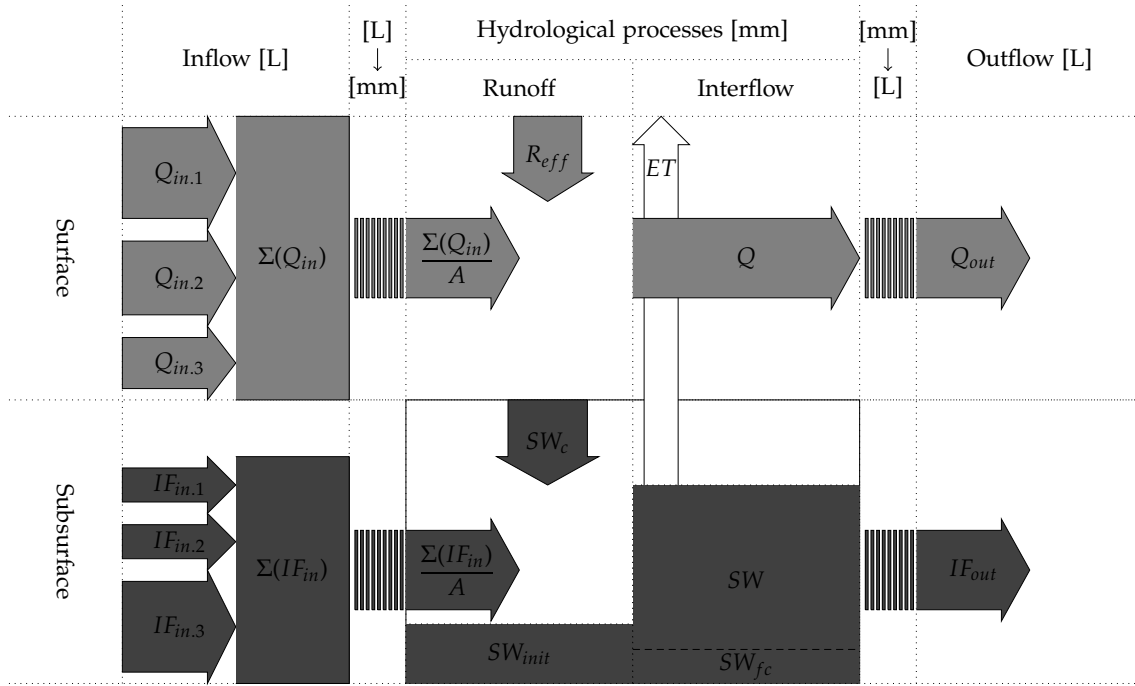


Fig. 3.1. Schematic hydrological processes within an element. The hydrological phase estimates the amount of surface runoff ( $Q$ ; mm) and subsurface interflow ( $IF_{out}$ ; L) generated from an element. Assuming that the surface area of an element is  $A$  ( $m^2$ ), surface water inputs of an element is the effective rainfall ( $R_{eff}$ ; mm) and surface water contribution from upslope elements ( $\Sigma(Q_{in})/A$ ; mm). Surface runoff occurs when surface water inputs exceed surface water infiltration capacity, ( $SW_c$ ; mm) which depends on available soil pore space left for surface water infiltration and the proportion of the impervious surface area ( $IMP$ ). The subsurface interflow occurs when the soil water budget ( $SW$ ; mm) exceeds the soil water at field capacity ( $SW_{fc}$ ; mm). In this condition, a part of the excess soil water outflows from an element as an interflow, and the surface runoff and subsurface interflow generated in an element are discharged to downslope elements.

#### 3.2.2.1 Surface Runoff Process

The fountainhead of the hydrological process is the effective rainfall ( $R_{eff}$ ; mm): the volume of rainfall reaching the unit surface area of an element. According to the corrected effective rainfall from Choi et al. (2016), with the existence of natural or artificial objects that intercept rainfall before reaching the ground, the effective rainfall on a unit surface area ( $A$ ;  $m^2$ ) of an

element can be described as,

$$R_{eff} = R \cdot (1 - PI) \cdot \cos(S), \quad (3.1)$$

where  $PI$  is the proportion of the permanent interception area and  $S$  is the slope of an element. In the MMMF model, the slope adjustment factor is  $1/\cos(S)$ , but it should be  $\cos(S)$  from the trigonometric rule as described in Choi et al. (2016) and in Figure 3.2.

The DMMF model estimates the amount of the surface runoff ( $Q$ ; mm) by considering surface water infiltration capacity, surface water input, and the proportion of the impervious surface area of an element. The surface water infiltration capacity ( $SW_c$ ; mm) is the amount of surface water that can infiltrate into the subsurface layer.  $SW_c$  is determined by potential pore space left for water infiltration and the proportion of the impervious surface area ( $IMP$ ). Because impervious surface hinders infiltration of water,  $IMP$  is assumed to decrease  $SW_c$ . Therefore,  $SW_c$  is defined as,

$$SW_c = (1 - IMP) \cdot (SW_{sat} - SW_{init} - \frac{\Sigma(IF_{in})}{A}), \quad (3.2)$$

where  $SW_{sat}$  (mm) and  $SW_{init}$  (mm) are the amount of the saturated soil water and the initial soil water that already exist in the soil before a daily event started.  $\Sigma IF_{in}$  (L) is the total volume of subsurface inflow of water from upslope elements and  $A$  (m<sup>2</sup>) is the surface area of an element. Thus  $\Sigma IF_{in}/A$  (mm) represents the inflow of subsurface water per unit surface area. The first parenthesis of Equation (3.2) indicates the blocking effect of water infiltration by impervious covers, and the second parenthesis indicates the potential pore space left for water infiltration. The saturated and initial soil water volumes are,

$$SW_{sat} = 1000 \cdot \theta_{sat} \cdot SD, \quad (3.3)$$

$$SW_{init} = 1000 \cdot \theta_{init} \cdot SD. \quad (3.4)$$

Here,  $\theta_{sat}$ , and  $\theta_{init}$  are the saturated and initial volumetric soil water contents (*vol/vol*) and  $SD$  (m) is the soil depth of an element. The factor of 1000 was used to convert meters to millimeters. The negative  $SW_c$  indicates the return flow, which contributes to additional surface water input through upwelling when soil water inputs exceed the saturation point of soil. In the model, surface runoff occurs when surface water inputs exceed the surface water infiltration capacity of an element. The surface water inputs are the sum of the effective rainfall, and surface

water contributions from upslope elements ( $\Sigma(Q_{in})/A$ ; mm). Therefore, the surface runoff of a unit surface area of an element is,

$$Q = R_{eff} + \frac{\Sigma(Q_{in})}{A} - SW_c. \quad (3.5)$$

and the total volume of surface runoff from an element ( $Q_{out}$ ; L) is,

$$Q_{out} = Q \cdot A. \quad (3.6)$$

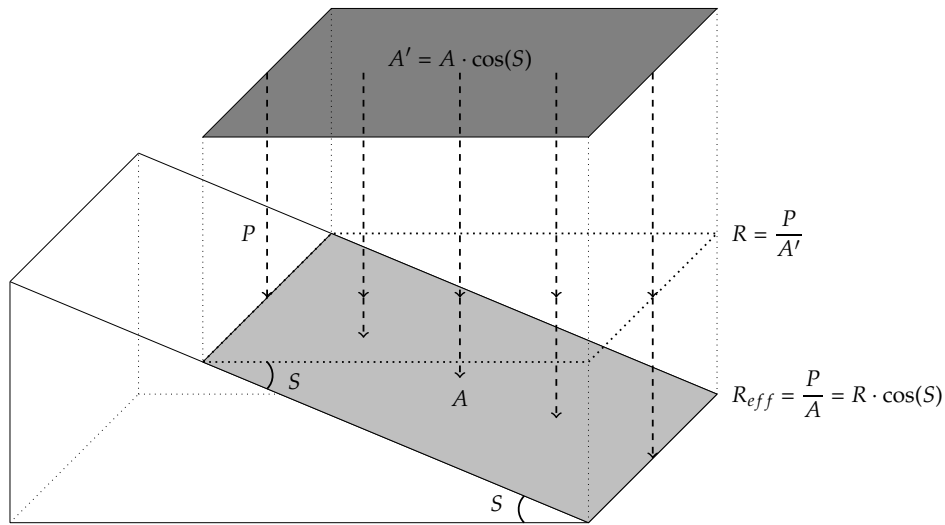


Fig. 3.2. Conceptual representation of the effective rainfall ( $R_{eff}$ ) on a slope element without permanent interception of rainfall (modified from Figure 1 of Choi et al. (2016)). Given rainfall with a total volume of  $P$ , the amount of rainfall per unit area for both  $A$  ( $\text{m}^2$ ) and  $A'$  ( $\text{m}^2$ ) is  $P/A$  and  $P/A'$  which is equal to  $R$ . From the trigonometric rule,  $A$ , the projected area of  $A'$  on the slope, is described as  $A'/\cos(S)$ . Therefore, the rainfall per unit surface area of the element (i.e., the effective rainfall) should be  $R \cdot \cos(S)$ .

### 3.2.2.2 Interflow Process

After the surface runoff process, the model estimates the subsurface interflow of an element ( $IF_{out}$ ), which is the volume of soil water being transferred to downslope elements. Interflow occurs when the amount of soil water budget ( $SW$ ; mm) exceeds soil water at field capacity ( $SW_{fc}$ ; mm). The soil water budget is calculated considering subsurface water inputs including existing soil water, surface water infiltration, and evapotranspiration, which is equal to the total water budget of an element:

$$SW = (SW_{init} + \frac{\Sigma(IF_{in})}{A}) + (R_{eff} + \frac{\Sigma(Q_{in})}{A} - Q) - ET. \quad (3.7)$$

The formula in the first parenthesis of Equation (3.7) represents subsurface water inputs

and the second formula parenthesis represents infiltrated surface water to the subsurface. Soil water at field capacity is defined as the amount of water-holding capacity of soil against the gravitational force based on Veihmeyer and Hendrickson (1931), but the value in this model covers the entire soil profile, and not a particular layer of uniform texture. In this model, soil water at field capacity is described as,

$$SW_{fc} = 1000 \cdot \theta_{fc} \cdot SD, \quad (3.8)$$

where  $\theta_{fc}$  (*vol/vol*) is the water content at field capacity of the entire soil profile. According to the corrected interflow equation suggested by Choi et al. (2016),  $IF_{out}$  of an element with a width of  $w$  is described as (see details in Figure 3.3),

$$IF_{out} = \begin{cases} K \cdot \sin(S) \cdot (SW - SW_{fc}) \cdot w, & \text{when } IF_{out} < (SW - SW_{fc}) \cdot A, \\ (SW - SW_{fc}) \cdot A, & \text{when } IF_{out} \geq (SW - SW_{fc}) \cdot A, \end{cases} \quad (3.9)$$

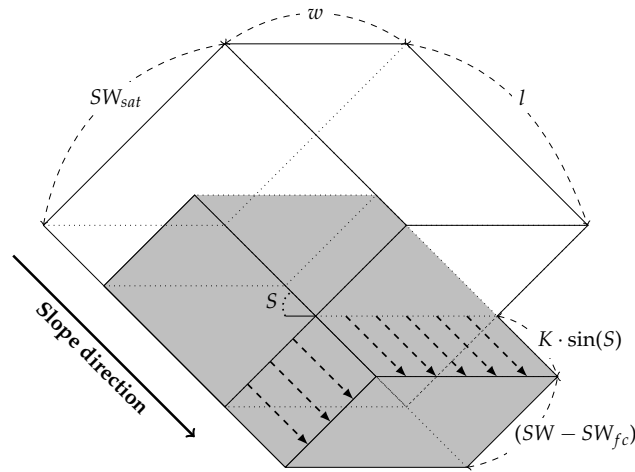
for a given saturated soil lateral hydraulic conductivity ( $K$ ; m/d). The volume of interflow cannot exceed the total volume of soil water budget over field capacity, which is the source of interflow. After the interflow process, a part of soil water remains in the soil. The remaining soil water content ( $\theta_r$ ; *vol/vol*) can then be described as,

$$\theta_r = \frac{(SW - IF_{out}/A)}{1000 \cdot SD}, \quad (3.10)$$

where 1000 is used to convert meters to millimeters. The DMMF model uses the measured initial soil water content just before the first day of a rainfall event and the remaining soil water content ( $\theta_r$ ) replaces the initial soil water content ( $\theta_{init}$ ) of the next day when the model is applied to a period longer than a day.

### 3.2.3 Sediment Phase

The sediment phase of the model inherits the basic structure of the sediment balance process of the MMMF model. Therefore the model estimates sediment budgets of each particle size class (i.e., clay, silt, and sand) separately, considering surface conditions (e.g., vegetation structures, surface roughness, and crop field management type). The model also follows step-wise processes of the sediment detachment and deposition of the MMMF model which simplify the in-element erosion process. There are three differences in the sediment phase in this model from that of the MMMF model (Figure 3.4). First, the sequence of processes was changed to have all the sediment input processes occur before deposition processes. Second, we revised the flow velocity



$$IF_{out} = K \cdot \sin(S) \cdot (SW - SW_{fc}) \cdot w$$

Fig. 3.3. Conceptual representation of interflow in an element (modified from Figure 3 of Choi et al. (2016)). Let's assume that there is an element with the width of  $w$ , the length of  $l$  and slope of  $S$ . Then, given transferable soil water for interflow ( $SW - SW_{fc}$ ) and saturated soil lateral hydraulic conductivity ( $K$ ), the volume of interflow from the element ( $IF_{out}$ ) can be represented as  $K \cdot \sin(S) \cdot (SW - SW_{fc}) \cdot w$ , and cannot exceed the volume of the transferable soil water of the element ( $(SW - SW_{fc}) \cdot A$ ).

equation from four equations of the MMMF model to two equations of reference and actual flow velocities by adopting the modified Manning's equation from Petryk and Bosmajian (1975). This modification further simplified and enhanced the conceptual clarity of the model, not only in the flow velocity equation, but also in the particle settling rates and the transport capacity calculations. Third, we changed the MMMF sediment budgeting process to that of Meyer and Wischmeier (1969) as the MMMF process is motivated by longer time steps. The sediment phase comprises of three processes: sediment delivery to the surface runoff, gravitational deposition, and soil erosion processes. A schematic description of the sediment phase is given in Figure 3.4.

### 3.2.3.1 Sediment Delivery to Surface Runoff

In the model, surface runoff and sediments that are delivered to surface runoff are the two main factors that determine sediment loss from an element. The sources of delivered sediments are in-element detached particles by the impact of rainfall and surface runoff, as well as delivered soil particles from upslope elements. Soil detachment by rainfall occurs when raindrops fall directly onto ground surface with sufficient kinetic energy to detach soil particles from the surface. Because canopy cover changes the kinetic energy of raindrops by initializing raindrop velocity and altering raindrop size (Brandt, 1990), rainfall has a different impact on areas under and without canopy cover. Grounds without canopy cover are affected by the

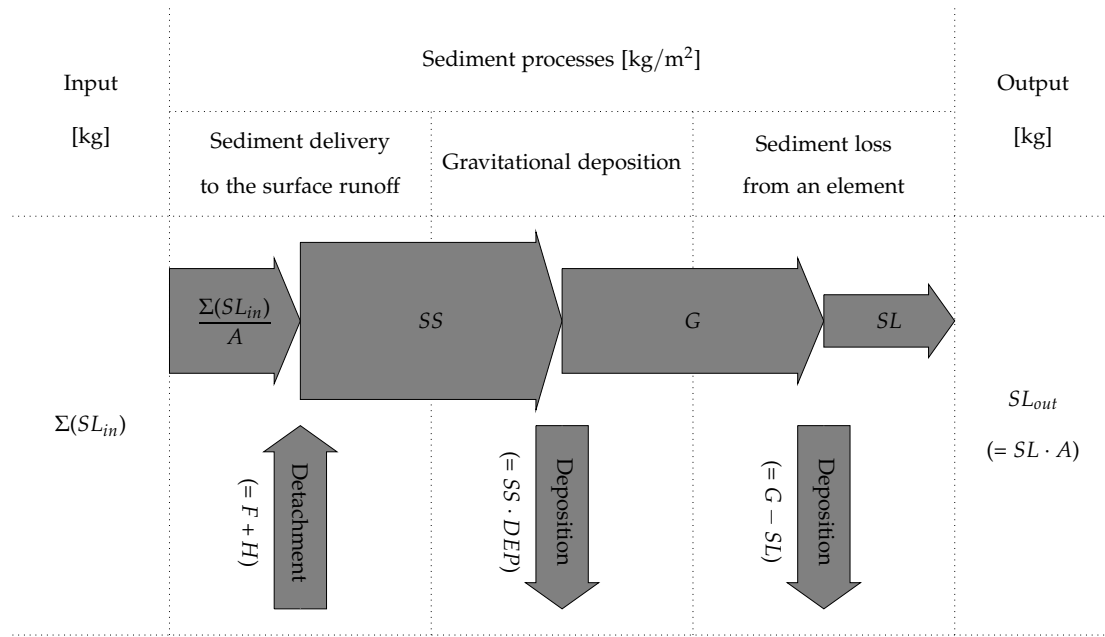


Fig. 3.4. Schematic sediment phase of an element. The model estimates the amount of sediment loss from an element through three steps. In the first step, detached soil particles from an element (by raindrop ( $F$ ) and runoff ( $H$ )) and sediment inputs from upslope elements ( $\Sigma(SL_{in})/A$ ) are delivered to the surface water of an element. Second, some of the suspended sediments ( $SS$ ) delivered in the runoff settle down due to gravity at the deposition rate of the suspended sediments in the runoff ( $DEP$ ). Third, the model estimates the amount of sediment loss from an element by comparing the transport capacity of the runoff ( $TC$ ) and sediments available for transport ( $G$ ), which are the remaining suspended sediments after gravitational deposition process. If  $TC$  is larger than  $G$ , all the remaining sediments in the water (i.e.,  $G$ ) are washed away from an element. Otherwise, the amount of sediments equal to  $TC$  is carried out by the surface runoff to downslope elements.

raindrops falling directly onto the bare soil (direct throughfall).

The kinetic energy density of direct throughfall ( $U_{DT}$ ;  $J/(m^2 mm)$ ) is estimated from the universal power law equation suggested by Shin et al. (2016) for a given rainfall intensity ( $RI$ ;  $mm/h$ ):

$$U_{DT} = 10.3 \cdot RI^{2/9}. \quad (3.11)$$

In contrast, under the canopy cover, soil surface is affected by the water-drops falling from the leaves and stems of vegetation after rainfall (leaf drainage). The kinetic energy density of leaf drainage ( $U_{LD}$ ;  $J/(m^2 mm)$ ) under a 100% canopy cover is a function of plant height ( $PH$ ;  $m$ ) (Brandt, 1990):

$$U_{LD} = \begin{cases} 15.8 \cdot \sqrt{PH} - 5.87, & \text{when } U_{LD} \geq 0, \\ 0, & \text{when } U_{LD} < 0. \end{cases} \quad (3.12^*)$$

Because  $U_{LD}$  is kinetic energy density, its value cannot be less than zero; although the empirical

equation potentially allows negative values. In an element partly covered with vegetation, the kinetic energy of the effective rainfall ( $KE$ ;  $J/m^2$ ) can be expressed as the product of the effective rainfall ( $R_{eff}$ ) and the area weighted average of kinetic energy densities of  $U_{DT}$  and  $U_{LD}$ :

$$KE = R_{eff} \cdot \{(1 - CC) \cdot U_{DT} + CC \cdot U_{LD}\}, \quad (3.13)$$

where  $CC$  is the proportion of the canopy covered area of an element. Then, the amount of soil particles detached by raindrops ( $F$ ;  $kg/m^2$ ) is calculated as a function of detachability of soil particles by raindrop impact ( $DK$ ;  $g/J$ ), proportion of each particle size class ( $P$ ), proportion of bare soil surface ( $1 - EPA$ ), and the kinetic energy of the effective rainfall ( $KE$ ):

$$F_c = DK_c \cdot P_c \cdot (1 - EPA) \cdot KE \cdot 10^{-3}, \quad (3.14)$$

$$F_z = DK_z \cdot P_z \cdot (1 - EPA) \cdot KE \cdot 10^{-3}, \quad (3.15)$$

$$F_s = DK_s \cdot P_s \cdot (1 - EPA) \cdot KE \cdot 10^{-3}. \quad (3.16)$$

Here, subscripts  $c$ ,  $z$  and  $s$  represent each particle size classes of clay, silt, and sand, respectively.  $EPA$  is the erosion protected area by ground cover ( $GC$ ) and impervious area ( $IMP$ ):

$$EPA = IMP + (1 - IMP) \cdot GC. \quad (3.17)$$

The guide values for detachability of clay, silt, and sand are 0.1, 0.5, and 0.3, respectively (Morgan and Duzant, 2008) but these values should be used carefully according to the soil characteristics of study sites as shown in Poesen (1985) and it is recommended that users employ field-measured values.

The second sediment source is detached soil particles by the surface runoff ( $H$ ;  $kg/m^2$ ). The amount of detached soil particles by runoff is calculated as a function of detachability of soil particles by runoff ( $DR$ ;  $g/mm$ ), the amount of runoff ( $Q$ ), the slope angle ( $S$ ) of the element, and the proportion of the bare surface area. Therefore,  $H$  for particle size classes are,

$$H_c = DR_c \cdot P_c \cdot Q^{1.5} \cdot (1 - EPA) \cdot (\sin(S))^{0.3} \cdot 10^{-3}, \quad (3.18)$$

$$H_z = DR_z \cdot P_z \cdot Q^{1.5} \cdot (1 - EPA) \cdot (\sin(S))^{0.3} \cdot 10^{-3}, \quad (3.19)$$

$$H_s = DR_s \cdot P_s \cdot Q^{1.5} \cdot (1 - EPA) \cdot (\sin(S))^{0.3} \cdot 10^{-3}. \quad (3.20)$$

The guide values for detachability of clay, silt, and sand are 1.0, 1.6, and 1.5, respectively (Morgan and Duzant, 2008). The values should be used carefully and can be replaced with observed site

specific data.

The third sediment source is sediment inputs from upslope elements ( $\Sigma(SL_{in})$ ) averaged by the surface area of an element. Therefore, the overall delivered sediments to the surface runoff ( $SS$ ;  $\text{kg}/\text{m}^2$ ) are represented as below,

$$SS_c = F_c + H_c + \frac{\Sigma(SL_{in.c})}{A}, \quad (3.21)$$

$$SS_z = F_z + H_z + \frac{\Sigma(SL_{in.z})}{A}, \quad (3.22)$$

$$SS_s = F_s + H_s + \frac{\Sigma(SL_{in.s})}{A}. \quad (3.23)$$

Detached sediments can be transported by surface runoff through suspension, saltation, and creeping processes. In the model, all sediments delivered to surface runoff are assumed as being in suspension.

### 3.2.3.2 Gravitational Deposition of Suspended Sediments

After sediments are delivered to the surface runoff, a part of the suspended sediments ( $SS$ ) in the runoff settle to the bottom by gravitational force. Tollner et al. (1976) estimated the settling rate of suspended sediments using the probabilistic concept of the particle fall number ( $N_f$ ), which is the ratio of falling time of soil particles to traveling time along the flow direction of an element. To calculate the particle fall number, the runoff flow velocity ( $v$ ;  $\text{m}/\text{s}$ ) and settling velocity of each particle size class ( $v_s$ ;  $\text{m}/\text{s}$ ) are required. Flow velocity depends on the flow depth ( $d$ ), the slope of an element ( $S$ ) and the modified Manning's roughness coefficient ( $n'$ ) from Petryk and Bosmajian (1975). The modified Manning's roughness coefficient is the hydraulic roughness considering the effect of the drag force by vegetation on the hydraulic roughness in addition to the Manning's roughness coefficient. The value is determined by the Manning's roughness coefficient ( $n$ ), the flow depth ( $d$ ), the diameter of plant stems ( $D$ ) and the number of stems per unit area ( $NV$ ) with the standard gravity of the Earth ( $g \approx 9.8 \text{ m}/\text{s}^2$ ):

$$v = \frac{1}{n'} \cdot d^{2/3} \cdot \sqrt{\tan(S)}, \quad (3.24)$$

$$n' = \left( n^2 + \frac{D \cdot NV \cdot d^{4/3}}{2 \cdot g} \right)^{1/2}. \quad (3.25)$$

Recommended values for  $d$  are 0.005 for unchanneled flow, 0.01 for shallow rills, and 0.25 for deeper rills, but field measured flow depth can be used. For cultivated land with tillage, the Manning's roughness coefficient can be derived empirically from the soil surface roughness

(*RFR*; cm/m) as below (Morgan and Duzant, 2008),

$$\ln(n) = -2.1132 + 0.0349 \cdot RFR. \quad (3.26^*)$$

Guide values of surface roughness (*RFR*) for different tillage implements are described in Morgan (2005) and Morgan and Duzant (2008).

The settling velocity ( $v_s$ ) is estimated from the Stokes' equation for a creeping flow when the Reynolds number is low:

$$v_s = \frac{\delta^2 \cdot (\rho_s - \rho) \cdot g}{18 \cdot \eta}. \quad (3.27^*)$$

Here,  $\delta$  and  $\rho_s$  are the diameter and density of a particle, and  $\rho$  and  $\eta$  are the density and the viscosity of a fluid. The density of each particle size class ( $\rho_s$ ) is set as 2,650 kg/m<sup>3</sup>, which is the average density of quartz. The density of overland flow ( $\rho$ ) is set as the density of water (1,000 kg/m<sup>3</sup>), and the viscosity of overland flow ( $\eta$ ) is set as 0.001,5 kg/(m·s) following Morgan and Duzant (2008). Assuming that particle diameters are  $0.2 \times 10^{-5}$  m for clay,  $0.6 \times 10^{-4}$  m for silt, and  $0.2 \times 10^{-3}$  m for sand, then the settling velocities are  $0.2 \times 10^{-5}$  m/s for clay ( $v_{s.c}$ ),  $0.2 \times 10^{-2}$  m/s for silt ( $v_{s.z}$ ), and  $0.2 \times 10^{-1}$  m/s for sand ( $v_{s.s}$ ) (Morgan and Duzant, 2008). The particle fall number ( $N_f$ ) of each particle size class is a function of the actual runoff velocity ( $v$ ), the settling velocities of each particle size class ( $v_s$ ), the depth of runoff ( $d$ ) in meters, and the length of the element ( $l$ ):

$$N_{f.c} = \frac{l}{v} \cdot \frac{v_{s.c}}{d}, \quad (3.28^*)$$

$$N_{f.z} = \frac{l}{v} \cdot \frac{v_{s.z}}{d}, \quad (3.29^*)$$

$$N_{f.s} = \frac{l}{v} \cdot \frac{v_{s.s}}{d}. \quad (3.30^*)$$

Using the particle fall number of each particle size class, the rate of deposition of the sediments suspended in runoff (*DEP*) is estimated from the equation of Tollner et al. (1976), as below,

$$DEP_c = \min(0.441 \cdot N_{f.c}, 1), \quad (3.31^*)$$

$$DEP_z = \min(0.441 \cdot N_{f.z}, 1), \quad (3.32^*)$$

$$DEP_s = \min(0.441 \cdot N_{f.s}, 1). \quad (3.33^*)$$

Because the deposited particles cannot exceed the sediments suspended in the runoff, the maximum value for the deposition rate of each particle is set to one. After a part of the suspended

sediments is deposited by gravitational force, the remaining suspended sediments become available for transport (i.e., the available sediments for transport ( $G$ ) ( $\text{kg}/\text{m}^2$ )) by the surface runoff:

$$G_c = SS_c \cdot (1 - DEP_c), \quad (3.34)$$

$$G_z = SS_z \cdot (1 - DEP_z), \quad (3.35)$$

$$G_s = SS_s \cdot (1 - DEP_s). \quad (3.36)$$

### 3.2.3.3 Estimation of Sediment Loss from an Element

The transport capacity of the runoff ( $TC$ ;  $\text{kg}/\text{m}^2$ ) of an element depends on the volume of surface runoff per unit surface area of an element ( $Q$ ), the slope steepness ( $S$ ) and the effect of surface conditions (Morgan and Duzant, 2008). The effect of surface conditions is expressed as the ratio between actual runoff velocity ( $v$ ) and the reference velocity of the element ( $v_r$ ;  $\text{m}/\text{s}$ ). The reference velocity ( $v_r$ ) is the runoff velocity of an element under a standard surface condition (i.e., unchanneled overland flow over smooth bare soil) and is described by the Manning's equation,

$$v_r = \frac{1}{n_r} \cdot d_r^{2/3} \cdot \sqrt{\tan(S)}, \quad (3.37)$$

where values of  $n_r = 0.015$  and  $d_r = 0.005$  are used for a standard surface condition. Following the corrected MMMF C-factor suggested by Choi et al. (2016), the total transport capacity of the runoff is calculated as,

$$TC = \left( \frac{v}{v_r} \right) \cdot Q^2 \cdot \sin(S) \cdot 10^{-3}. \quad (3.38)$$

The transport capacity of the runoff is partitioned into clay, silt, and sand by multiplying the mass proportion of each particle size class with  $TC$ :

$$TC_c = P_c \cdot TC, \quad (3.39)$$

$$TC_z = P_z \cdot TC, \quad (3.40)$$

$$TC_s = P_s \cdot TC. \quad (3.41)$$

The sediment loss from the element ( $SL$ ) is determined by comparing the transport capacity of the runoff ( $TC$ ) with the amount of available sediment for transport ( $G$ ) (Morgan and Duzant, 2008, Meyer and Wischmeier, 1969). Because this model calculates the output on a daily basis, it is better to follow the sedimentation process from Meyer and Wischmeier (1969), which is

appropriate for shorter time periods. When  $TC$  is greater than  $G$ , the surface runoff washes away all the sediments available for transport from an element, and in the other case, an amount of sediment ( $SL$ ) equivalent to  $TC$  is lost from an element:

$$SL_c = \min(TC_c, G_c), \quad (3.42)$$

$$SL_z = \min(TC_z, G_z), \quad (3.43)$$

$$SL_s = \min(TC_s, G_s). \quad (3.44)$$

The overall amount of sediment eroded from an element ( $SL$ ) is the sum of clay, silt, and sand discharged from an element:

$$SL = SL_c + SL_z + SL_s. \quad (3.45^*)$$

### 3.2.4 Estimation of Total Runoff and Soil Erosion for Rainfall Period

The model can estimate the total amount of surface runoff and sediment loss from an element during a rainfall period by utilizing daily input data. For long-term estimation during a rainfall period, the model requires daily values of time-variant meteorological data ( $R$ ,  $RI$ , and  $ET$ ), and vegetation structure data ( $GC$ ,  $CC$ ,  $PH$ ,  $D$ , and  $NV$ ). On the contrary, the model requires site specific data of an element for static parameters such as topography ( $S$ ,  $l$ , and  $w$ ), soil characteristics ( $SD$ ,  $\theta_{sat}$ ,  $\theta_{fc}$ ,  $DK$ ,  $DR$ , and  $K$ ), and surface conditions ( $PI$ ,  $IMP$ , and  $n$ ). It is difficult to obtain daily data for the initial soil water content ( $\theta_{init}$ ), although it is highly time-variant, similar to meteorological data. To cope with the problem, the model iteratively replaces the initial soil water content ( $\theta_{init}$ ) with the remaining soil water content ( $\theta_r$  after the interflow process. Through daily updates, the model estimates the surface runoff and the sediment loss from an element during a period by accumulating daily results of  $Q$  and  $SL$  for the period.

## 3.3 Testing the DMMF Model

### 3.3.1 Sensitivity Analysis of the Model

A sensitivity analysis of the DMMF model was conducted to investigate the relative importance of input parameters on the amount of surface runoff and sediment loss from an element. We analyzed the sensitivity of the model to each parameter with the Sobol' method. The Sobol' method is a variance-based sensitivity analysis through variance decomposition and has the

advantage to estimate the total effect of a parameter including its effects in combination with other parameters (Sobol', 1993, Saltelli, 2002, Saltelli et al., 2010, Qi et al., 2013). Therefore, unlike the local and the one factor at a time (OAT) sensitivity analysis, the Sobol' method can be applied to non-linear and non-additive models with many parameters (Saltelli and Annoni, 2010, Nossent et al., 2011). Because of its advantages, the Sobol' method has become popular in environmental and hydrological modeling that employ models such as SWAT and TOPMODEL (Qi et al., 2013, Nossent et al., 2011). The total effect of a parameter by the Sobol' total index (SI) is the amount of total variance caused by a parameter normalized by the amount of variance induced from all parameters (unconditional variance of the model). Parameters with large SI have relatively high impacts and those with small SI have low impacts on the model output. To estimate SIs for the input parameters of the DMMF model, we set the range of the parameters based on the values recommended by Morgan and Duzant (2008). For meteorological parameters, we took extreme values to consider various weather events from a variety of regions. We set the range of the element size (*res*) considering various DEM resolutions, and set the complete range of the slope (*S*), from a flat surface to a vertical cliff. The detailed range of parameters is listed in Table 4.1. Sobol' total indices for input parameters are estimated through the “sobolmartinez” function of the “sensitivity” package (Pujol et al., 2016) using R version 3.2.3 (R Core Team, 2015). We used the default bootstrapping option of the function employing a sample size of  $10^5$ .

According to Sobol' total indices (Figure 3.5), runoff of an element is highly sensitive to the factors determining surface water infiltration capacity (i.e.,  $\theta_{init}$ ,  $\theta_{sat}$ , *SD*, and *IMP*) and water input from the effective rainfall (i.e., *R*, *S*, and *PI*). The amount of sediment loss from an element is also highly sensitive to the factors that show high sensitivity to surface runoff, because the amount of surface runoff is the main driver of soil redistribution. Furthermore, sediment loss of an element shows sensitivities to surface conditions (*IMP*, and *GC*) and vegetation structures (*D*, *NV*, and *CC*). For a single element sensitivity analysis, the soil water content at field capacity ( $\theta_{fc}$ ) and the lateral hydraulic conductivity (*K*) show no effects on the model because they are involved in subsurface water exchange among elements that are not considered in the sensitivity analysis for one element. These sensitivity analysis results are agree well with the model assumptions as well as conform to parameter sensitivity analysis of the MMMF model described by Morgan and Duzant (2008).

Table 3.1. Input parameters and their range for sensitivity analysis.

| Parameter       | Description  | Unit                     | Range                               |
|-----------------|--|--------------------------|-------------------------------------|
| $R$             | Daily rainfall   | [mm]                     | 1–1825 <sup>(a)</sup>               |
| $RI$            | Mean rainfall intensity of a day   | [mm/h]                   | 15.0–305.0 <sup>(a)</sup>           |
| $ET$            | Daily evapotranspiration   | [mm]                     | 0.0–15.0 <sup>(b)</sup>             |
| $S$             | Slope angle  | [rad]                    | 0.0–1.5 <sup>(c)</sup>              |
| $res$           | Grid size of a raster map for the width ( $w$ ) and the length ( $l$ ) of an element that are equal to $res$ and $res/\cos(S)$ | [m]                      | 0.25–100 <sup>(d)</sup>             |
| $P_c$           | Proportion of clay of the surface soil   | [proportion]             | 0–1                                 |
| $P_z$           | Proportion of silt of the surface soil   | [proportion]             | 0–1                                 |
| $P_s$           | Proportion of sand of the surface soil   | [proportion]             | 0–1                                 |
| $SD$            | Soil depth   | [m]                      | 0.3–68.0 <sup>(e)</sup>             |
| $\theta_{init}$ | Initial soil water content of entire soil profile  | [vol/vol]                | 0.00– $\theta_{sat}$ <sup>(f)</sup> |
| $\theta_{sat}$  | Saturated water content of entire soil profile   | [vol/vol]                | 0.31–0.56 <sup>(f)</sup>            |
| $\theta_{fc}$   | Soil water content at field capacity of entire soil profiles   | [vol/vol]                | 0.10– $\theta_{sat}$ <sup>(f)</sup> |
| $K$             | Saturated soil lateral hydraulic conductivity  | [m/d]                    | 1–230 <sup>(g)</sup>                |
| $DK_c$          | Detachability of clay particles by rainfall  | [g/J]                    | 0.10–1.50 <sup>(h)</sup>            |
| $DK_z$          | Detachability of silt particles by rainfall  | [g/J]                    | 0.50–5.15 <sup>(h)</sup>            |
| $DK_s$          | Detachability of sand particles by rainfall  | [g/J]                    | 0.15–4.15 <sup>(h)</sup>            |
| $DR_c$          | Detachability of clay particles by surface runoff  | [g/mm]                   | 0.020–2.0 <sup>(h)</sup>            |
| $DR_z$          | Detachability of silt particles by surface runoff  | [g/mm]                   | 0.016–1.6 <sup>(h)</sup>            |
| $DR_s$          | Detachability of sand particles by surface runoff  | [g/mm]                   | 0.015–1.5 <sup>(h)</sup>            |
| $PI$            | Area proportion of the permanent interception of rainfall  | [proportion]             | 0–1                                 |
| $IMP$           | Area proportion of the impervious ground cover   | [proportion]             | 0–1                                 |
| $GC$            | Area proportion of the ground cover of the soil surface protected by vegetation or crop cover on the ground                    | [proportion]             | 0–1                                 |
| $CC$            | Area proportion of the canopy cover of the soil surface protected by vegetation or crop canopy                                 | [proportion]             | 0–1                                 |
| $PH$            | Average height of vegetation or crop cover of an element where leaf drainage starts to fall                                    | [m]                      | 0–30 <sup>(h)</sup>                 |
| $D$             | Average diameter of individual plant elements at the surface   | [m]                      | 0.00001–3.0 <sup>(h)</sup>          |
| $NV$            | Number of individual plant elements per unit area  | [number/m <sup>2</sup> ] | 0.00001–2000 <sup>(h)</sup>         |
| $d$             | Typical flow depth of surface runoff in an element   | [m]                      | 0.005–3 <sup>(h)</sup>              |
| $n$             | Manning’s roughness coefficient of the soil surface  | [s/m <sup>1/3</sup> ]    | 0.01–0.05 <sup>(i)</sup>            |

Notes: <sup>(a)</sup> is based on WMO; <sup>(b)</sup> is based on Senay et al. (2008), Jia et al. (2009); <sup>(c)</sup> represents the range of slope from a flat surface to a vertical cliff; <sup>(d)</sup> is based on Lilhare et al. (2014), Arnhold et al. (2013), Pandey et al. (2009); <sup>(e)</sup> is based on the range of rooting depth from Canadell et al. (1996); <sup>(f)</sup> is based on Saxton et al. (1986); <sup>(g)</sup> is based on the hydraulic conductivity of semi-pervious soils from Irmay (1968); <sup>(h)</sup> is based on Morgan and Duzant (2008); <sup>(i)</sup> is based on Manning’s  $n$  of bare soil in Table 3.6 from Morgan (2005).

### 3.3.2 Testing the DMMF Model in the Field

We applied the DMMF model to two potato fields (field 1 and field 2) in the Haeon-Myeon catchment, South Korea, previously described by Arnhold et al. (2013) to test the validity of the model. The fields are located on erosion-prone hillslopes with complex surface configurations of plastic-covered ridges with potatoes and bare soil furrows. Mean annual precipitation in the study area in 2009 and 2010 was about 1,514 mm, with 50 to 60% of the annual rainfall concentrated during the summer monsoon season from June to August (Arnhold et al., 2013). Soils of the fields range from sandy to silty loams, with higher proportions of clay and silt in field 2. Field 1 is located on a concave hillslope with a topographical depression along the center line of

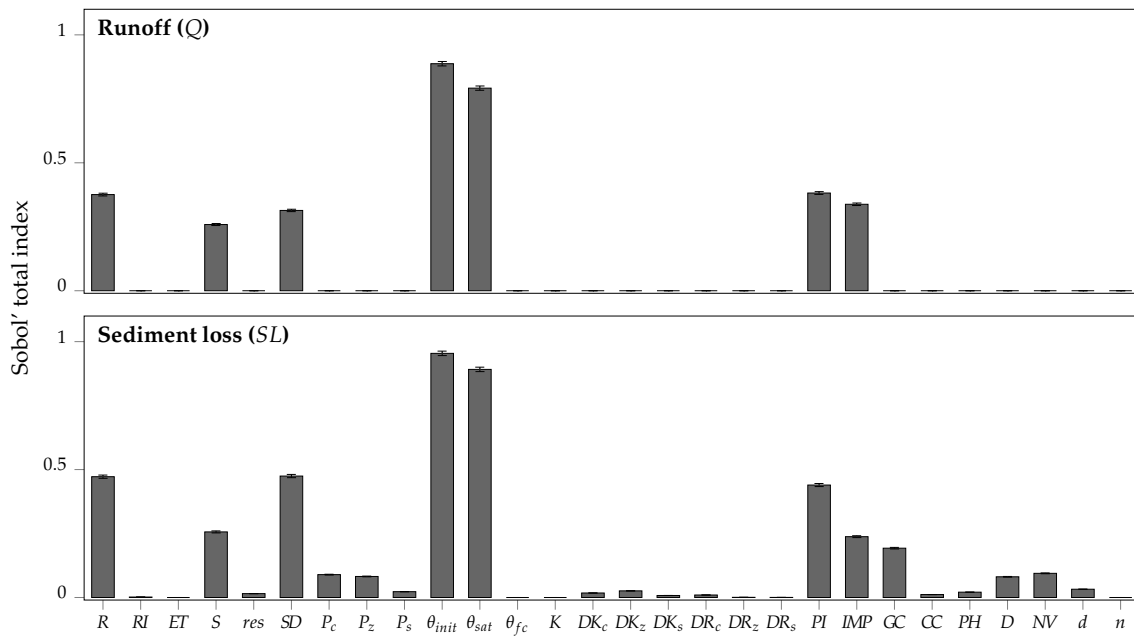


Fig. 3.5. Sobol' total indices of model input parameters for a single element. The bars indicate the Sobol' total indices and the error bars indicate the 95% confidence intervals of the indices from bootstrapping.

the field, and the field 2 is on a concave slope without any topographical depressions. Both fields have an average slope angle of about  $9^\circ$  and a slope length of about 25 m. On each field, runoff and sediment loss were measured by three 5 m wide runoff samplers for seven rainfall periods with a variety of rainfall characteristics and time intervals in the monsoon season from 5 July to 10 August 2010 (Arnhold et al., 2013). These conditions in both fields are suitable for testing the model at a variety of temporal rainfall periods including the new concept of impervious areas. We used available measured and estimated input parameters to test the model. Digital elevation models (for  $S$ ,  $w$  and  $l$ ),  $R$ ,  $RI$ ,  $SD$ ,  $n$ ,  $P_c$ ,  $P_z$ ,  $P_s$ ,  $\theta_{init}$ ,  $CC$ , and  $PH$  were obtained from Arnhold et al. (2013). For  $ET$ , we utilized the MODIS/Terra Evapotranspiration (ORNL DAAC, 2014), because it provides an 8-day sum of ET data based on the modified Penman-Monteith equation (Mu et al., 2011). For unmeasured input parameters ( $\theta_{sat}$ ,  $\theta_{fc}$ ,  $K$ ,  $PI$ ,  $GC$ ,  $NV$ ,  $D$ ,  $DK_c$ ,  $DK_z$ ,  $DK_s$ ,  $DR_c$ ,  $DR_z$ ,  $DR_s$ , and  $d$ ), site-specific sensitivity analyses were performed to determine the required parameters to be adjusted, which is recommended under the situation of limited data availability. We selected parameters for calibration when one of their Sobol' total index values from field 1 or field 2 was larger than 0.05 (i.e., contribute 5% of the total variance of the model output). For parameters related to soil detachability (i.e.,  $DK_c$ ,  $DK_z$ ,  $DK_s$ ,  $DR_c$ ,  $DR_z$ , and  $DR_s$ ), we used a wide range of parameters from zero to maximum values as given in Table 4.1. We set the range of  $K$  according to ranges of the optimized vertical hydraulic conductivities from Ruidisch et al. (2013), who conducted hydrological studies on the same fields. The up-

per boundary was defined by multiplying  $K$  by 18 to consider the average ratio of lateral to vertical hydraulic conductivities of the hillslope (Brooks et al., 2004). The range of  $d$  was set from 0.005 (unchanneled flow) to 0.01 (shallow rill) from Morgan and Duzant (2008), considering surface conditions of both fields. Ranges of  $\theta_{sat}$  were estimated from Saxton et al. (1986) using soil texture of each field. Ranges of  $\theta_{fc}$  were derived from ranges of initial soil water content before rainfall, because excess soil water usually drained away two or three days after the soil was fully saturated by rainfall. Initial soil water contents from Arnold et al. (2013) were measured between one and three days after previous rainfall events ended. We adjusted the other parameters using a range of  $\pm 20\%$  of guide values given in Morgan and Duzant (2008). The detailed range of parameters for sensitivity analysis is listed in Table 3.2. According to the result,  $K$ ,  $\theta_{sat}$ , and  $\theta_{fc}$  showed relatively high impacts on the

Table 3.2. Range of unmeasured parameters for sensitivity analysis.

| Field   |      | $\theta_{sat}$ | $\theta_{fc}$ | $K$  | $PI$  | $GC$ | $NV$ | $D$  | $DK_c$ | $DK_z$ | $DK_s$ | $DR_c$ | $DR_z$ | $DR_s$ | $d$   |
|---------|------|----------------|---------------|------|-------|------|------|------|--------|--------|--------|--------|--------|--------|-------|
| Field 1 | Sup. | 0.454          | 0.351         | 17.9 | 0.144 | 0.48 | 5.4  | 0.12 | 1.50   | 5.15   | 4.15   | 2.0    | 1.6    | 1.5    | 0.010 |
|         | Inf. | 0.351          | 0.345         | 0.29 | 0.096 | 0.32 | 3.6  | 0.08 | 0      | 0      | 0      | 0      | 0      | 0      | 0.005 |
| Field 2 | Sup. | 0.494          | 0.435         | 5.22 | 0.144 | 0.48 | 5.4  | 0.12 | 1.50   | 5.15   | 4.15   | 2.0    | 1.6    | 1.5    | 0.010 |
|         | Inf. | 0.435          | 0.407         | 0.15 | 0.096 | 0.32 | 3.6  | 0.08 | 0      | 0      | 0      | 0      | 0      | 0      | 0.005 |

\* Sup. indicates upper bound of a range (Supremum) and Inf. indicates lower bound of a range (Infimum).

amount of surface runoff and sediment loss from an element.  $DR_c$ ,  $DR_z$ ,  $DR_s$  and  $d$  show relatively high impacts (over 0.1) on sediment loss result (see Figure 3.6). These seven parameters have high in-situ variations as well (Morgan and Duzant, 2008, Brooks et al., 2004, Boll et al., 1998). We calibrated the model by adapting  $K$ ,  $\theta_{sat}$ ,  $\theta_{fc}$ ,  $DR_c$ ,  $DR_z$ ,  $DR_s$  and  $d$  with the same range of parameters used in the sensitivity analysis. For parameters with relatively low impacts on the model results, we used reference values for potato fields from Morgan and Duzant (2008). We used the differential evolution (DE) optimization method (Storn and Price, 1997) for model calibration through the “DEoptim” package (Ardia et al., 2015) using R version 3.2.3 (R Core Team, 2015). The DE algorithm is a heuristic optimization method with an evolution strategy to find the global minimum of a real-valued model of real-valued parameters. It is suitable for non-differentiable, nonlinear and multimodal models. Therefore, the DE algorithm and its variants have been successfully applied to a variety of fields (Storn and Price, 1997, Ardia et al., 2015, Mullen et al., 2011) and have been used for hydrological model calibration (Joseph and Guillaume, 2013, Zheng et al., 2015). To find the best parameter set for the model output, we used the root mean square error (RMSE) between model outputs and the field measured data as the objective function for the DE algorithm. Because the sur-

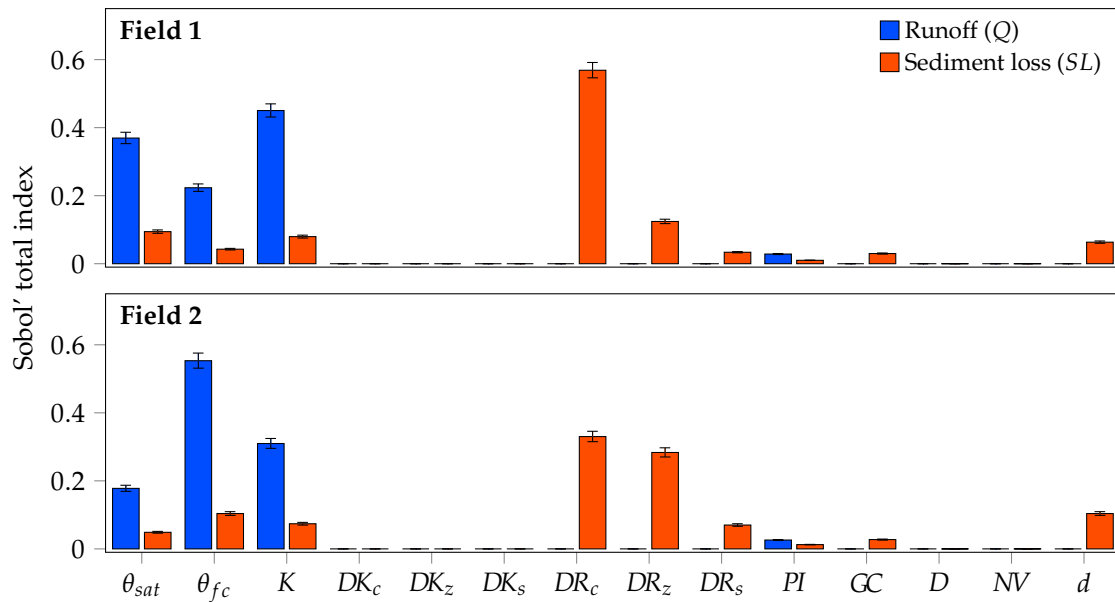


Fig. 3.6. Sobol' total indices for runoff ( $Q$ ) and sediment loss ( $SL$ ) of the two field sites. Bars indicate the Sobol' total indices and the error bars indicate the 95% confidence intervals of the indices from bootstrapping. We checked the sensitivity of the model to the parameters with high uncertainty due to absence of field data, such as parameters related to soil detachability (i.e.,  $DK_c$ ,  $DK_z$ ,  $DK_s$ ,  $DR_c$ ,  $DR_z$ , and  $DR_s$ ), soil hydraulic parameters (i.e.,  $K$ ,  $\theta_{sat}$ , and  $\theta_{fc}$ ), vegetation structural parameters (i.e.,  $GC$ ,  $D$ ,  $NV$ ), the permanent interception ( $PI$ ), and the rill depth ( $d$ ).  $K$ ,  $\theta_{sat}$  and  $\theta_{fc}$  showed relatively high impacts on the runoff ( $Q$ ) and the sediment loss ( $SL$ ). The sediment loss ( $SL$ ) also showed high sensitivity to  $DR_c$ ,  $DR_z$ ,  $DR_s$  and  $d$ .

face runoff is one of the main drivers of sediment processes, we optimized  $K$ ,  $\theta_{sat}$ , and  $\theta_{fc}$  for the surface runoff ( $Q$ ) and then, with these optimized parameters, we optimized  $DR$ , and  $d$  for sediment loss ( $SL$ ). Values of optimized parameters from the DE algorithm are listed in Table 3.3. The optimized  $K$  for each field is in the range of optimized (for field 1) and esti-

Table 3.3. Optimized parameters from the DE algorithm.

|         | $K$   | $\theta_{sat}$ | $\theta_{fc}$ | $DR_c$ | $DR_z$ | $DR_s$ | $d$   |
|---------|-------|----------------|---------------|--------|--------|--------|-------|
| Field 1 | 0.500 | 0.362          | 0.345         | 0.015  | 0.012  | 0.011  | 0.010 |
| Field 2 | 0.284 | 0.453          | 0.435         | 0.007  | 0.005  | 0.005  | 0.005 |

imated (for field 2) vertical hydraulic conductivity from Ruidisch et al. (2013). It means that the lateral hydraulic conductivity of the entire soil profile is affected not only by the top soil layer but also by other deeper layers with low hydraulic conductivities. The optimized  $\theta_{sat}$  for each field has a relatively higher value than the corresponding optimized values from Ruidisch et al. (2013). The higher values are possible because the model considers the entire soil profile, including deeper soil layers with higher saturated soil water contents. The optimized  $\theta_{fc}$  values for both fields are consistent with the values for silt loam (0.35) for field 1 and silt clay loam (0.42) for field 2 from Morgan and Duzant (2008). The optimized  $DR$  values are lower than

those in the ranges of  $DR$  for sensitivity analysis from Morgan and Duzant (2008). However, the optimized values are possible because the values were induced from laboratory data from Quansah (1982) and possess a significant amount of uncertainty according to Morgan and Duzant (2008). Finally, the optimized  $d$  indicates that field 1 has shallow rills and field 2 has a comparatively smooth surface, which are consistent with actual field surface conditions. With the optimized parameters, we tested the model with three other statistical criteria for evaluating the model performance: the Nash-Sutcliffe efficiency (NSE), the percent bias (PBIAS), and the ratio of RMSE to the standard deviation of the observation (RSR). A model is considered to be acceptable when it has an NSE value larger than 0.5, a PBIAS value in the range  $\pm 25\%$ , and a RSR value less than or equal to 0.7 (Moriasi et al., 2007). The testing results of the model are acceptable for both runoff and sediment loss (Figure 3.7).

The test results from field 2 show better performance than those from field 1. The putative causes of the differing model performance for two fields are data gaps due to damages of a runoff collector in field 1. This collector covered a large proportion of the field area and, thus, might have strongly affected outputs of the entire field (Arnhold et al., 2013). Although data gaps were also present in field 2, contributing areas of each runoff collector were rather similar, which decreased the influence of an individual collector on the average output of the entire field (see Figure 2 and Table 2 in Arnhold et al. (2013)). Further, model performance for runoff is better than that for sediment loss for both fields. The poorer performance for sediment loss than for runoff is assumed to be caused by error propagation of runoff as the main driver of sediment loss. Although more evenly distributed observed data are desirable for better model performance testing, observation data were clustered into low and high extremes due to the highly irregular rainfall pattern of the Monsoon climate and the limited period of observation.

### 3.4 Summary and Conclusions

In this study, we present a new soil erosion model, the Daily based Morgan–Morgan–Finney (DMMF) model, which is suitable for estimating surface runoff and soil erosion of a complex surface terrain within an intensive seasonal rainfall region. The DMMF model is based on the simple conceptual soil erosion model, the Modified Morgan–Morgan–Finney model, with several modifications. First, the temporal scale of the model changed from an annual to a continuous daily scale. Second, we added a new surface cover type of impervious area that highly affects runoff generation and soil redistribution patterns. Third, we revised the main equations and rearranged the sequence of the subprocesses for a better physical representation of the model.

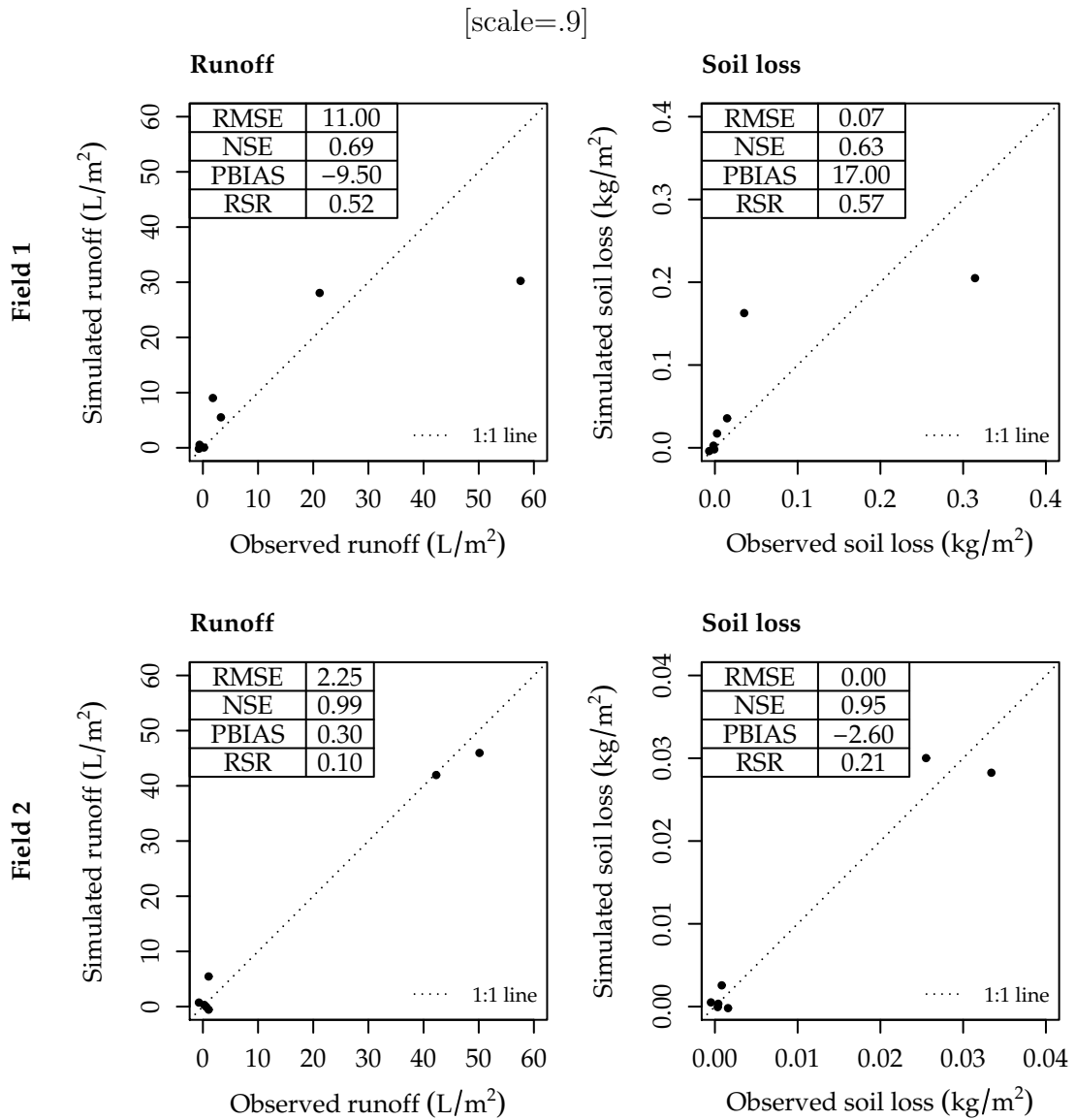


Fig. 3.7. Comparison between simulated and observed runoff ( $Q$ ) and sediment loss ( $SL$ ) for field 1 and field 2. We tested the model performance for both fields with optimized parameters (Table 3.3). Model performance was evaluated using the Nash-Sutcliffe efficiency coefficient (NSE), percent bias (PBIAS), and RMSE-observation standard deviation ratio (RSR) with the observed data from Arnhold et al. (2013). To make all overlapping points with values close to zero visible, we slightly jittered the points.

In the hydrological phase, we revised the effective rainfall and the interflow equations. In the sediment phase, we modified the flow velocity equations, the transport capacity equations, and the sediment input sequence.

Owing to these modifications, the DMMF model offers expanded temporal and spatial applicability while retaining the advantages of the MMMF model. Temporally, the model can estimate short- and long-term soil erosion flexible in regions with concentrated seasonal rainfall for which the annual-based MMMF model is not suitable. Spatially, the model can estimate

runoff and soil erosion for complex surface configurations with plastic mulching, pavements and so on by introducing the proportion of the impervious area. Furthermore, the model represents the effect of vegetation on soil erosion by utilizing easy-to-measure vegetation structure information, in contrast to other soil erosion models that require either detailed vegetation information or empirical relationships between vegetation and erosion. This feature enables the model to estimate spatiotemporal patterns of runoff and soil loss from non-conventional crop fields (e.g., ginseng fields in South Korea) for which only little is known about the role of the vegetation and practices such as impervious covers on soil conservation potentials. According to the sensitivity analysis and field application results, the DMMF model showed reasonable responses to parameters, which agrees with the model assumptions. The model also showed acceptable performances for both runoff and sediment loss predictions when it was tested on two potato fields with different topographic and soil characteristics in seven different rainfall periods of the monsoon season. Those results demonstrate that the new model is capable of simulating surface runoff and soil redistribution patterns at various temporal scales of monsoonal rainfall in crop fields with impervious cover.

As more national- and continental-wide topographic, soil and land use data (e.g., European Soil Data Centre (Panagos et al., 2012)) are becoming available, increasing attempts have been made to apply soil erosion models at larger scales (Panagos et al., 2015). Because the DMMF model is designed for field and catchment scales, and has not yet been tested at larger scales, it is challenging at this time to directly estimate runoff and soil erosion at national and continental scales. However, the model may contribute to large scale modeling by providing appropriate parameters on non-conventional cultivation fields where insufficient information is available, to be used in large scale model approaches such as USLE and RUSLE.

We conclude that DMMF can be useful to establish soil and water conservation measures in intensively used agricultural lands with complex surface configurations composed of multiple crop types, artificial structures, and plastic mulching by estimating spatiotemporal runoff and sediment redistributions and by identifying erosion and deposition hotspots under varying conditions. Since model performance to date was tested for a single land use type and with a limited amount of observation data with data gaps, further studies are required to validate the model's utility at extended temporal and spatial scales under various rainfall patterns and land use types as well as to provide appropriate parameterizations of non-conventional crop fields for large scale modeling.

## Acknowledgments

This study is part of the International Research Training Group “Complex Terrain and Ecological Heterogeneity” (TERRECO) (GRK 1565/1) funded by the German Research Foundation (DFG). This publication was funded by the German Research Foundation (DFG) and the University of Bayreuth in the funding programme Open Access Publishing. We would like to thank Editage ([www.editage.co.kr](http://www.editage.co.kr)) for English language editing.

## Author contributions

Björn Reineking and Bernd Huwe designed and supervised the model algorithm and edited the manuscript. Sebastian Arnhold provided the field data for model testing, supervised the field application analysis of the model, and edited the manuscript. Kwanghun Choi designed and developed the model, analyzed the field application of the model, and wrote the paper.

## Conflicts of interest

The authors declare no conflict of interest. The founding sponsors had no role in the design of the study; in the collection, analyses, or interpretation of data; in the writing of the manuscript, and in the decision to publish the results.

## References

- Pimentel, D.; Kounang, N. Ecology of soil erosion in ecosystems. *Ecosystems* **1998**, *1*, 416–426.
- Sidle, R.C.; Ziegler, A.D.; Negishi, J.N.; Nik, A.R.; Siew, R.; Turkelboom, F. Erosion processes in steep terrain—Truths, myths, and uncertainties related to forest management in Southeast Asia. *For. Ecol. Manage.* **2006**, *224*, 199–225.
- Morgan, R.P.C. *Soil Erosion and Conservation*, 3rd ed.; Blackwell Publishing: Malden, MA, USA, 2005.
- Onori, F.; De Bonis, P.; Grauso, S. Soil erosion prediction at the basin scale using the revised universal soil loss equation (RUSLE) in a catchment of Sicily (southern Italy). *Environ. Geol.* **2006**, *50*, 1129–1140.
- Napoli, M.; Cecchi, S.; Orlandini, S.; Mugnai, G.; Zanchi, C.A. Simulation of field-measured soil loss in Mediterranean hilly areas (Chianti, Italy) with RUSLE. *Catena* **2016**, *145*, 246–256.

- Zema, D.A.; Denisi, P.; Taguas Ruiz, E.V.; Gómez, J.A.; Bombino, G.; Fortugno, D. Evaluation of Surface Runoff Prediction by AnnAGNPS Model in a Large Mediterranean Watershed Covered by Olive Groves. *Land Degrad. Dev.* **2016**, *27*, 811–822.
- Huon, S.; Evrard, O.; Gourdin, E.; Lefèvre, I.; Bariac, T.; Reyss, J.L.; des Tureaux, T.H.; Sengtaheuanghoung, O.; Ayrault, S.; Ribolzi, O. Suspended sediment source and propagation during monsoon events across nested sub-catchments with contrasted land uses in Laos. *J. Hydrol. Reg. Stud.* **2017**, *9*, 69–84.
- Boardman, J. Soil erosion science: Reflections on the limitations of current approaches. *Catena* **2006**, *68*, 73–86.
- Hu, L.J.; Flanagan, D.C. Towards new-generation soil erosion modeling: Building a unified omnivorous model. *J. Soil Water Conserv.* **2013**, *68*, 100A–103A.
- Wischmeier, W.H.; Smith, D.D. Predicting rainfall erosion losses—a guide to conservation planning. In *Agriculture Handbook*, Number 537; United States Department of Agriculture (USDA): Washington, DC, USA, 1978; pp. 1–58.
- Renard, K.G.; Foster, G.R.; Weesies, G.A.; Porter, J.P. RUSLE: Revised universal soil loss equation. *J. Soil Water Conserv.* **1991**, *46*, 30–33.
- Williams, J.R. Sediment-yield prediction with Universal Equation using runoff energy factor. Present and prospective technology for predicting sediment yield and sources: Proceedings of the Sediment-Yield Workshop; United States Department of Agriculture (USDA): New Orleans, LA, USA, 1975; Volume ARS-S-40, pp. 244–252.
- Morgan, R.P.C.; Morgan, D.D.V.; Finney, H.J. A predictive model for the assessment of soil erosion risk. *J. Agric. Eng. Res.* **1984**, *30*, 245–253.
- Morgan, R.P.C. A simple approach to soil loss prediction: A revised Morgan–Morgan–Finney model. *Catena* **2001**, *44*, 305–322.
- Lal, R. Soil degradation by erosion. *Land Degrad. Dev.* **2001**, *12*, 519–539.
- Merritt, W.; Letcher, R.; Jakeman, A. A review of erosion and sediment transport models. *Environ. Modell. Softw.* **2003**, *18*, 761–799.
- Lilhare, R.; Garg, V.; Nikam, B. Application of GIS-Coupled Modified MMF Model to Estimate Sediment Yield on a Watershed Scale. *J. Hydrol. Eng.* **2014**, *20*, C5014002.

- Avwunudiogba, A.; Hudson, P.F. A Review of Soil Erosion Models with Special Reference to the needs of Humid Tropical Mountainous Environments. *Eur. J. Sustain. Dev.* **2014**, *3*, 299–310.
- Morgan, R.P.C.; Quinton, J.N.; Smith, R.E.; Govers, G.; Poesen, J.W.A.; Auerswald, K.; Chisci, G.; Torri, D.; Styczen, M.E. The European Soil Erosion Model (EUROSEM): A dynamic approach for predicting sediment transport from fields and small catchments. *Earth Surf. Processes Landforms* **1998**, *23*, 527–544.
- De Roo, A.P.J.; Wesseling, C.G.; Ritsema, C.J. LISEM: A single-event physically based hydrological and soil erosion model for drainage basins. I: Theory, Input and Output. *Hydrol. Processes* **1996**, *10*, 1107–1117.
- von Werner, M. GIS-orientierte Methoden der digitalen Reliefanalyse zur Modellierung von Bodenerosion in kleinen Einzugsgebieten. Ph.D. Thesis, Department of Earth Sciences, Free University of Berlin, Berlin, Germany, 1995.
- Nearing, M.A.; Foster, G.R.; Lane, L.J.; Finkner, S.C. A process-based soil erosion model for USDA-Water Erosion Prediction Project technology. *Trans. ASAE* **1989**, *32*, 1587–1593.
- Beasley, D.B.; Huggins, L.F.; Monke, E.J. ANSWERS: A Model for Watershed Planning. *Trans. ASAE* **1980**, *23*, 938–944.
- Beven, K.J.; Kirkby, M.J. A physically based, variable contributing area model of basin hydrology. *Hydrol. Sci. Bull.* **1979**, *24*, 43–69.
- Bergström, S.; Forsman, A. Development of a conceptual deterministic rainfall-runoff model. *Nord. Hydrol.* **1973**, *4*, 147–170.
- Devia, G.K.; Ganasri, B.; Dwarakish, G. A Review on Hydrological Models. *Aquat. Procedia* **2015**, *4*, 1001–1007.
- Morgan, R.P.C.; Duzant, J.H. Modified MMF (Morgan–Morgan–Finney) model for evaluating effects of crops and vegetation cover on soil erosion. *Earth Surf. Processes Landforms* **2008**, *32*, 90–106.
- De Jong, S.M.; Paracchini, M.L.; Bertolo, F.; Folving, S.; Megier, J.; De Roo, A.P.J. Regional assessment of soil erosion using the distributed model SEMMED and remotely sensed data. *Catena* **1999**, *37*, 291–308.

- Vigiak, O.; Okoba, B.O.; Sterk, G.; Groenenberg, S. Modelling catchment-scale erosion patterns in the East African Highlands. *Earth Surf. Processes Landforms* **2005**, *30*, 183–196.
- López-Vicente, M.; Navas, A.; Machín, J. Modelling soil detachment rates in rainfed agrosystems in the south-central Pyrenees. *Agric. Water Manage.* **2008**, *95*, 1079–1089.
- Vieira, D.C.S.; Prats, S.A.; Nunes, J.P.; Shakesby, R.A.; Coelho, C.O.A.; Keizer, J.J. Modelling runoff and erosion, and their mitigation, in burned Portuguese forest using the revised Morgan–Morgan–Finney model. *For. Ecol. Manage.* **2014**, *314*, 150–165.
- Baartman, J.E.; Jetten, V.G.; Ritsema, C.J.; de Vente, J. Exploring effects of rainfall intensity and duration on soil erosion at the catchment scale using openLISEM: Prado catchment, SE Spain. *Hydrol. Processes* **2012**, *26*, 1034–1049.
- Stocker, T.F.; Qin, D.; Plattner, G.K.; Alexander, L.V.; Allen, S.K.; Bindoff, N.L.; Bréon, F.M.; Church, J.A.; Cubasch, U.; Emori, S.; et al. *Climate Change 2013: The Physical Science Basis. Contribution of Working Group I to the Fifth Assessment Report of the Intergovernmental Panel on Climate Change*; Cambridge University Press: Cambridge, United Kingdom; New York, NY, USA, 2013; chapter Technical Summary, pp. 33–115.
- Espí, E.; Salmerón, A.; Fontecha, A.; García, Y.; Real, A.I. Plastic Films for Agricultural Applications. *J. Plast. Film Sheeting* **2006**, *22*, 85–102.
- Shuster, W.D.; Bonta, J.; Thurston, H.; Warnemuende, E.; Smith, D.R. Impacts of impervious surface on watershed hydrology: A review. *Urban Water J.* **2005**, *2*, 263–275.
- Pappas, E.A.; Smith, D.R.; Huang, C.; Shuster, W.D.; Bonta, J.V. Impervious surface impacts to runoff and sediment discharge under laboratory rainfall simulation. *Catena* **2008**, *72*, 146–152.
- Arnhold, S.; Ruidisch, M.; Bartsch, S.; Shope, C.; Huwe, B. Simulation of runoff patterns and soil erosion on mountainous farmland with and without plastic-covered ridge-furrow cultivation in South Korea. *Trans. ASABE* **2013**, *56*, 667–679.
- Ruidisch, M.; Kettering, J.; Arnhold, S.; Huwe, B. Modeling water flow in a plastic mulched ridge cultivation system on hillslopes affected by South Korean summer monsoon. *Agric. Water Manage.* **2013**, *116*, 204–217.
- Choi, K.; Huwe, B.; Reineking, B. Commentary on ‘Modified MMF (Morgan–Morgan–Finney) model for evaluating effects of crops and vegetation cover on soil erosion’ by Morgan and

- Duzant (2008). Available online: <https://arxiv.org/abs/1612.08899> (accessed on 13 April 2017).
- Kirkby, M.J., Hydrological Slope Models: The Influence of Climate. In *Geomorphology and Climate*; Derbyshire, E., Ed.; Wiley: London, UK, 1976; pp. 247–267.
- Petryk, S.; Bosmajian, G. Analysis of flow through vegetation. *ASCE J. Hydraul. Div.* **1975**, *101*, 871–884.
- Veihmeyer, F.J.; Hendrickson, A.H. The moisture equivalent as a measure of the field capacity of soils. *Soil Sci.* **1931**, *32*, 181–194.
- Meyer, L.D.; Wischmeier, W.H. Mathematical simulation of the process of soil erosion by water. *Trans. ASAE* **1969**, *12*, 754–758.
- Brandt, C.J. Simulation of the size distribution and erosivity of raindrops and throughfall drops. *Earth Surf. Processes Landforms* **1990**, *15*, 687–698.
- Shin, S.S.; Park, S.D.; Choi, B.K. Universal Power Law for Relationship between Rainfall Kinetic Energy and Rainfall Intensity. *Adv. Meteorol.* **2016**, *2016*, Article ID 2494681.
- Poesen, J. An improved splash transport model. *Z. Geomorphol.* **1985**, *29*, 193–211.
- Tollner, E.W.; Barfield, B.J.; Haan, C.T.; Kao, T.Y. Suspended Sediment Filtration Capacity of Simulated Vegetation. *Trans. ASAE* **1976**, *19*, 678–682.
- Sobol', I. Sensitivity Analysis for Nonlinear Mathematical Models. *Math. Model. Comput. Exp.* **1993**, *1*, 407–414.
- Saltelli, A. Making best use of model evaluations to compute sensitivity indices. *Comput. Phys. Commun.* **2002**, *145*, 280–297.
- Saltelli, A.; Annoni, P.; Azzini, I.; Campolongo, F.; Ratto, M.; Tarantola, S. Variance based sensitivity analysis of model output. Design and estimator for the total sensitivity index. *Comput. Phys. Commun.* **2010**, *181*, 259–270.
- Qi, W.; Zhang, C.; Chu, J.; Zhou, H. Sobol' 's sensitivity analysis for TOPMODEL hydrological model: A case study for the Biliu River Basin, China. *J. Hydrol. Environ. Res.* **2013**, *1*, 1–10.
- Saltelli, A.; Annoni, P. How to avoid a perfunctory sensitivity analysis. *Environ. Modell. Softw.* **2010**, *25*, 1508–1517.

- Nossent, J.; Elsen, P.; Bauwens, W. Sobol' sensitivity analysis of a complex environmental model. *Environ. Modell. Softw.* **2011**, *26*, 1515–1525.
- Pujol, G.; Iooss, B.; Janon, A.; with contributions from Boumhaout, K.; Da Veiga, S.; Fruth, J.; Gilquin, L.; Guillaume, J.; Le Gratiet, L.; Lemaitre, P.; Ramos, B.; Touati, T.; Weber, F. *Sensitivity: Global Sensitivity Analysis of Model Outputs*, R package version 1.12.1; Available online: <https://CRAN.R-project.org/package=sensitivity> (accessed on 15 May 2016).
- R Development Core Team. *R: A Language and Environment for Statistical Computing*; R Foundation for Statistical Computing: Vienna, Austria, 2015.
- World Meteorological Organization's World Weather & Climate Extremes Archive. Available online: [wmo.asu.edu/content/world-meteorological-organization-global-weather-climate-extremes-archive](http://wmo.asu.edu/content/world-meteorological-organization-global-weather-climate-extremes-archive) (accessed on 16 November 2016).
- Senay, G.; Verdin, J.; Lietzow, R.; Melesse, A. Global Daily Reference Evapotranspiration Modeling and Evaluation. *J. Am. Water Resour. Assoc.* **2008**, *44*, 969–979.
- Jia, L.; Xi, G.; Liu, S.; Huang, C.; Yan, Y.; Liu, G. Regional estimation of daily to annual regional evapotranspiration with MODIS data in the Yellow River Delta wetland. *Hydrol. Earth Syst. Sci.* **2009**, *13*, 1775–1787.
- Pandey, A.; Mathur, A.; Mishra, S.K.; Mal, B.C. Soil erosion modeling of a Himalayan watershed using RS and GIS. *Environ. Earth Sci.* **2009**, *59*, 399–410.
- Canadell, J.; Jackson, R.B.; Ehleringer, J.B.; Mooney, H.A.; Sala, O.E.; Schulze, E.D. Maximum rooting depth of vegetation types at the global scale. *Oecologia* **1996**, *108*, 583–595.
- Saxton, K.E.; Rawls, W.J.; Romberger, J.S.; Papendick, R.I. Estimating generalized soil-water characteristics from texture. *Soil Sci. Soc. Am. J.* **1986**, *50*, 1031–1036.
- Irmay, S., Hydrodynamics in soils. In *Physical Principles of Water Percolation and Seepage*; Bear, J., Zaslavsky, D., Irmay, S., Eds.; UNESCO: Paris, France, 1968; Volume 29, pp. 60.
- MODIS Collection 5 Land Products Global Subsetting and Visualization Tool*; ORNL DAAC: Oak Ridge, TN, USA, 2009; Available online: <http://dx.doi.org/10.3334/ORNLDAAC/1241> (accessed on 22 September 2015).

- Mu, Q.; Zhao, M.; Running, S.W. Improvements to a MODIS global terrestrial evapotranspiration algorithm. *Remote Sens. Environ.* **2011**, *115*, 1781–1800.
- Brooks, E.S.; Boll, J.; McDaniel, P.A. A hillslope-scale experiment to measure lateral saturated hydraulic conductivity. *Water Resour. Res.* **2004**, *40*, W04208.
- Boll, J.; Brooks, E.S.; Campbell, C.R.; Stockle, C.O.; Young, S.K.; Hammel, J.E.; McDaniel, P.A. Progress toward development of a GIS based water quality management tool for small rural watersheds: Modification and application of a distributed model. In Proceedings of the ASAE Annual International Meeting in Orlando, FL, USA, 12–16 July 1998.
- Storn, R.; Price, K. Differential Evolution—A Simple and Efficient Heuristic for global Optimization over Continuous Spaces. *J. Global Optim.* **1997**, *11*, 341–359.
- Ardia, D.; Mullen, K.M.; Peterson, B.G.; Ulrich, J. *DEoptim: Differential Evolution in R*, R package version 2.2-3; Available online: <http://CRAN.R-project.org/package=DEoptim> (accessed on 11 November 2016)
- Mullen, K.; Ardia, D.; Gil, D.; Windover, D.; Cline, J. DEoptim: An R Package for Global Optimization by Differential Evolution. *J. Stat. Softw.* **2011**, *40*, 1–26.
- Joseph, J.; Guillaume, J. Using a parallelized MCMC algorithm in R to identify appropriate likelihood functions for SWAT. *Environ. Modell. Softw.* **2013**, *46*, 292–298.
- Zheng, F.; Zecchin, A.C.; Simpson, A.R. Investigating the run-time searching behavior of the differential evolution algorithm applied to water distribution system optimization. *Environ. Modell. Softw.* **2015**, *69*, 292–307.
- Quansah, C. Laboratory Experimentation for the Statistical Derivation of Equations for Soil Erosion Modelling and Soil Conservation Design. Ph.D. Thesis, Cranfield Institute of Technology, England, United Kingdom, April 1982.
- Moriasi, D.N.; Arnold, J.G.; Van Liew, M.W.; Bingner, R.L.; Harmel, R.D.; Veith, T.L. Model evaluation guidelines for systematic quantification of accuracy in watershed simulations. *Trans. ASABE* **2007**, *50*, 885–900.
- Panagos, P.; Liedekerke, M.V.; Jones, A.; Montanarella, L. European Soil Data Centre: Response to European policy support and public data requirements. *Land Use Policy* **2012**, *29*, 329–338.

Panagos, P.; Borrelli, P.; Poesen, J.; Ballabio, C.; Lugato, E.; Meusbürger, K.; Montanarella, L.; Alewell, C. The new assessment of soil loss by water erosion in Europe. *Environ. Sci. Policy* **2015**, *54*, 438–447.

## Chapter 4

# Evaluating the Effectiveness of Spatially Reconfiguring Erosion Hot Spots to Reduce Stream Sediment Load in an Upland Agricultural Catchment of South Korea

Kwanghun Choi <sup>1,2,\*</sup>, Ganga Ram Maharjan <sup>3,4</sup> and Björn Reineking <sup>1,5</sup>

<sup>1</sup> Biogeographical Modelling, Bayreuth Center of Ecology and Environmental Research (BayCEER), University of Bayreuth, Universitätsstraße 30, 95440 Bayreuth, Germany; bjoern.reineking@irstea.fr

<sup>2</sup> Department of Forestry, Environment, and Systems, Kookmin University, Seoul 02707, Republic of Korea

<sup>3</sup> Department of Soil Physics, University of Bayreuth, Universitätsstraße 30, 95440 Bayreuth, Germany; mhjgangaram@gmail.com

<sup>4</sup> YARA- Crop Nutrition Research and Development, Hanninghof 35, 48249 Dülmen, Germany

<sup>5</sup> Univ. Grenoble Alpes, Irstea, LESSEM, 38000 Grenoble, France

Correspondence: kchoi@kookmin.ac.kr or kwanghun.choi@yahoo.com

## Abstract

Upland agricultural expansion and intensification cause soil erosion, which has a negative impact on the environment and socioeconomic factors by degrading the quality of both nutrient-rich surface soil and water. The Haean catchment is a well-known upland agricultural area in South Korea, which generates a large amount of sediment from its cropland. The transportation of nutrient-rich sediment to the stream adversely affects the water quality of the Han River watershed, which supports over twenty million people. In this paper, we suggest a spatially explicit mitigation method to reduce the amount

of sediment yield to the stream of the catchment by converting soil erosion hot spots into forest. To evaluate the effectiveness of this reconfiguration, we estimated the sediment redistribution rate and assessed the soil erosion risk in the Haean catchment using the daily based Morgan–Morgan–Finney (DMMF) model. We found that dry crop fields located in the steep hill-slope suffer from severe soil erosion, and the rice paddy, orchard, and urban area, which are located in a comparatively lower and flatter area, suffer less from erosion. Although located in the steep hill-slope, the forest exhibits high sediment trapping capabilities in this model. When the erosion-prone crop lands were managed by sequentially reconfiguring their land use and land cover (LULC) to the forest from the area with the most severe erosion to the area with the least severe erosion, the result showed a strong reduction in sediment yield flowing to the stream. A change of 3% of the catchment’s crop lands of the catchment into forest reduced the sediment yield entering into the stream by approximately 10% and a change of 10% of crop lands potentially resulted in a sediment yield reduction by approximately 50%. According to these results, identifying erosion hot spots and managing them by reconfiguring their LULC is effective in reducing terrestrial sediment yield entering into the stream.

**Keywords:** DMMF; landscape configuration; landscape ecology; hydrology

## 4.1 Introduction

Agriculture expansion and intensification often lead to severe soil erosion in the course of altering naturally dominated surface configurations (Hu et al., 2000, Lee, 2009, Maharjan et al., 2016). The problem is prominent in upland agriculture areas under monsoonal climate because of the disturbed erosion-prone hill-slopes receiving intermittent concentrated heavy rainfall (Lee et al., 2003, Ali and Reineking, 2016). A large amount of surface runoff from heavy rainfall washes out nutrient-rich surface soil from deforested upland agriculture areas and degrades the soil quality of the agricultural area (Jeon et al., 2017). Eroded nutrient-rich soil particles cause not only soil quality degradation of the agricultural area but also on- and off-site water deterioration when these particles enter the stream of a catchment (Pimentel et al., 1995, Pimentel and Kounang, 1998, Lal, 2001).

The Han River watershed in South Korea experiences extreme downpours that cause severe soil erosion and subsequent water deterioration every summer monsoon season (Maharjan et al., 2016, Yoon and Hyoseop, 2000, Arnhold et al., 2013). These problems are worsening, as upland agricultural areas expand and the intensity of monsoonal rainfall increase due to ongoing climate change (Park et al., 2010, Stocker et al., 2013). The Han River is the primary freshwater

source for the Seoul Metropolitan area where over 25 million inhabitants (ca. 50% of the South Korean population) reside. Therefore, soil erosion control in this region is highly relevant to provide clean and usable freshwater resources to the residents (Chang, 2008, Choi et al., 2017). With increasing demand for food crops, intensive upland agriculture is expanding in the mountainous upstream regions of the Han River watershed where few agricultural activities had been performed previously (Lee, 2009). The Haeon catchment is one of the largest contributors to sediment in the watershed, where abrupt land use and land cover (LULC) changes have taken place on forested hill-slope areas (Arnhold et al., 2013, Ruidisch et al., 2013, Arnhold et al., 2014). The LULC changes on the erosion-prone hill-slopes of this catchment generate a massive amount of sediment flowing into the river system and eventually deteriorate the water quality of the Han River (Maharjan et al., 2016). Various studies have been conducted in this catchment to understand the sediment redistribution patterns and determine optimal measures to mitigate this problem. Field-level studies have focused on the effect of surface configurations of the dry croplands and their field margins on sediment yields. Arnhold et al. (2013) and Ruidisch et al. (2013) investigated the effect of plastic mulch applied to dry croplands on surface runoff and sediment yield. Ali and Reineking (2016) showed the effectiveness of natural field margin (i.e., vegetated filter strip next to the dry cropland) for preventing off-site sediment yield. They reported that the natural field margin captured sediments more efficiently under the increased rainfall and slope conditions than intensively managed field margins with less dense vegetation cover. Arnhold et al. (2014) found that organic farming yielded less sediment than conventional farming because organic farming tends to protect the soil surface by preserving more vegetations that are not cultivated crops.

At the catchment level, the soil and water analysis tool (SWAT) (Arnold et al., 1998) has been widely used to test the effectiveness of various best management practices (BMPs) to reduce the sediment yield under complex terrain and landscape configurations (Maharjan et al., 2016, Jang et al., 2017). Maharjan et al. (2016) showed the effectiveness of catchment-wide cover crop cultivation in the dry croplands to reduce suspended sediment yields entering the stream. Jang et al. (2017) projected vegetation filter strip, rice straw mulching, and fertilizer control scenarios to dry croplands of the catchment and found that the application of vegetation filter strips and rice straw mulching was efficient in reducing sediment yields from the catchment. The BMPs suggested in the aforementioned studies are often premised on the compliance of each stakeholder, which is not easily accomplished (Fujisaka, 1994, Pannell, 1999, Poppenborg and Koellner, 2013). Different from the BMP approaches relying on stakeholders participation, several studies are paying attention to the importance of the landscape and its spatial configuration, which has a

significant impact on ecosystem services and functions, including soil erosion and water quality control (Chaplin-Kramer et al., 2015, 2016, Lee, 2017). Furthermore, these studies showed that ecosystem services and functions often responded non-linearly to the spatial relocation of the agricultural landscape, implying the effectiveness of spatial configuration on enhancing ecosystem services (Chaplin-Kramer et al., 2015, 2016, Polasky et al., 2008). Therefore, identifying soil erosion hot spots and assessing the sediment reduction rate by altering the surface configuration of hot spots promise to help establishing cost-effective soil erosion control methods in the catchment.

To consider the spatial context of soil erosion, a spatially explicit and distributed soil erosion model that can simulate the sediment budget of each element, considering the sediment inputs from the upslope areas is needed. Among the various soil erosion models, the daily based Morgan–Morgan–Finney (DMMF) model (Choi et al., 2017) is one of the most appropriate tools because the model can project soil erosion and deposition explicitly, considering the spatial connectivity, which facilitates the assessment of the impact of the spatial context of landscape on sediment redistribution patterns. Furthermore, the DMMF is suitable for projecting under a monsoon climate, accompanying concentrated rainfall during a short period (Choi et al., 2017). Vegetative filter strips (VFSs) are known as an effective tool for reducing sediment yield from the field or catchment because of their cost-effective surface protecting and sediment trapping capabilities (Ali and Reineking, 2016, Jang et al., 2017, Lee, 2017, Dillaha et al., 1989, Delgado et al., 1995, Muñoz-Carpena et al., 1999). We adopt the forest, which is a type of VFS, as an alternative LULC for soil erosion hot spots to reduce the total sediment yield into the stream of the catchment. In this study, we assessed the importance of the spatial conversion of erosion hot spots into forest on soil erosion control using the spatially explicit daily based Morgan–Morgan–Finney (DMMF) soil erosion model. The detailed objectives are to:

1. determine the applicability of the DMMF model for stream discharge and suspended sediment in the Haean catchment,
2. estimate the sediment redistribution pattern and assess the soil erosion risk of the Haean catchment, and
3. evaluate the impact of the spatial reconfiguration of erosion hot spots into forest on soil erosion control.

## 4.2 Materials and Methods

### 4.2.1 Study Area

The study was conducted in the Haeon catchment (Figure 4.1). The Haeon catchment is a bowl-shaped small mountainous erosion basin (64.4 km<sup>2</sup>) located in the northeastern part of South Korea (38.277° N, 128.135° E). As an erosion basin, the central area is low and flat, and it becomes higher and steeper toward the boundary. The lowest altitude of the catchment is 339 m, and the highest one is 1,321 m (Lee, 2009, Maharjan et al., 2016, Arnhold et al., 2013, Shope et al., 2014). Geologically, the catchment consists primarily of two bedrocks. One is gneiss at the higher elevation near the catchment boundary, and the other is highly weathered granite at the flat central area (Lee, 2009, Shope et al., 2014). Differential erosion between the two bedrocks formed the unique bowl-shaped catchment (Lee, 2009). The major soil type of the catchment is cambisol from weathered granite. The dominant soil texture of the catchment is loamy sand (59.4%) followed by sandy loam (27.5%), and sand (10.5%), which has a high infiltration capacity (Maharjan et al., 2016, Shope et al., 2014).

The climate of the catchment is characterized by cold and dry winter, affected by the continental Siberian high, and hot and humid summer affected by the subtropical North Pacific high (Shope et al., 2014, Park et al., 2011, Bartsch et al., 2013). The average annual precipitation from 2009 to 2011 is 1,599 mm, and almost 70% of the rainfall is concentrated in the three months from June to August (Maharjan et al., 2016, Arnhold et al., 2013, Jang et al., 2017, Shope et al., 2014). Due to climate change, the period of rain spell, as well as the frequency and intensity of heavy rainfall, has increased in this region (Ha et al., 2005, Jung et al., 2011).

The dominant land cover type of the catchment is forest. Forest mainly covers the summit and upper hill-slope areas around the boundary of the catchment, occupying 58% of the entire catchment area. Dry croplands (22%), including bean, cabbage, potato, radish, and ginseng, dominate the lower hill-slope areas adjacent to the forest edge. Rice paddies (8%) and residential areas (3%) (e.g., roads and artificial structures) occupy the flat central area of the catchment. Semi-natural vegetation field (8%), shrublands (1%), and bare surface (5%), including fallow and barren field, cover the remaining areas (Seo et al., 2014).

The dry croplands have been expanded into the forest that is located in the hill-slope area. Due to the upland agriculture expansion after deforestation, the catchment yields a massive amount of sediment into the stream during the summer monsoon season. The sediment is transported to the Soyang reservoir. This reservoir is the largest reservoir in South Korea as well

as the crucial freshwater source for citizens living in the Seoul metropolitan area (Maharjan et al., 2016, Arnhold et al., 2013, Shope et al., 2014). Weather stations and hydrological measurement facilities are installed in the catchment to monitor the climate and stream conditions, and erosion control dams and the reservoir have been constructed to reduce the sediment yield from the catchment (Shope et al., 2014, Jeon and Kang, 2010).

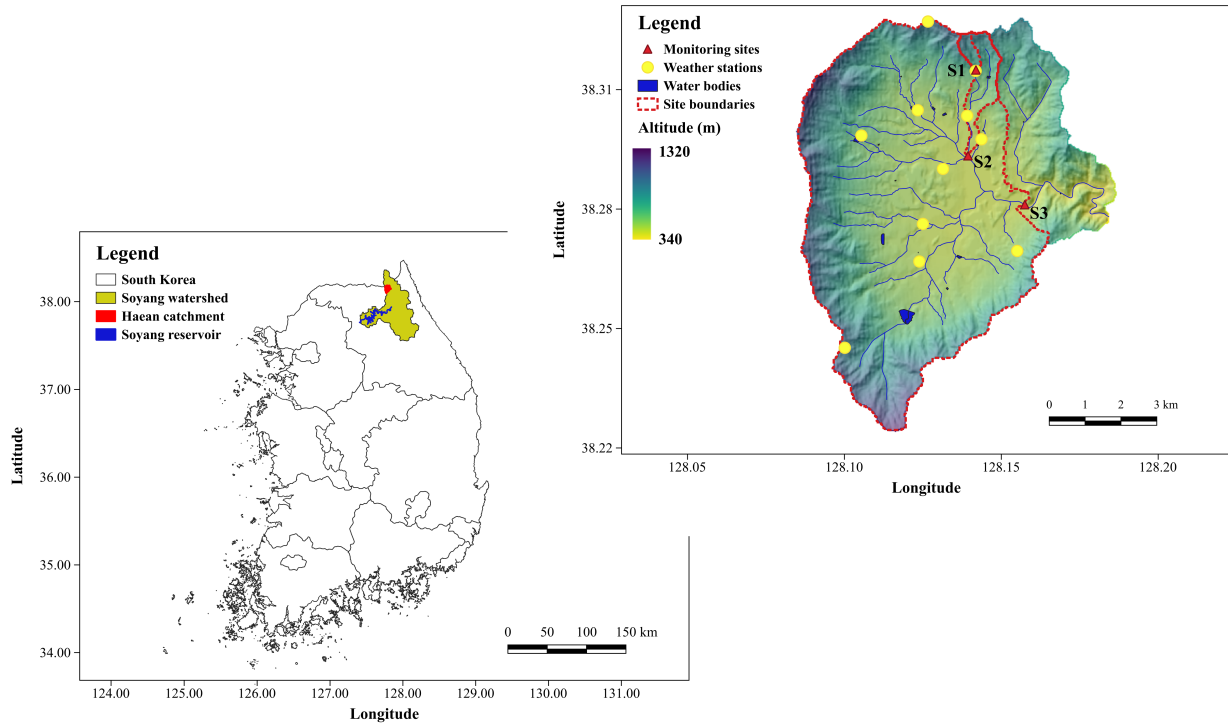


Fig. 4.1. General description of the study area. Locations of the Soyang lake watershed and Haeon catchment in South Korea are described in the lower left figure. In the upper right figure, the topography and stream networks of the study area, with the monitoring sites (red triangles) and weather stations (yellow circles) used for the DMMF model are presented.

## 4.2.2 Model Description

We used the DMMF model (Choi et al., 2017) to assess the soil erosion risk and simulate the impact of the spatial reconfiguration of erosion hot spots into forest on sediment yield within the Haeon catchment. The DMMF model was modified from the widely used Morgan–Morgan–Finney (MMF) soil erosion model (Morgan et al., 1984), which has a simple structure while maintaining physical foundations (Choi et al., 2017, Morgan, 2001, Vigiak et al., 2005, Morgan and Duzant, 2008, Lilhare et al., 2014).

The DMMF model has three significant modifications relative to the MMF model: the adoption of a daily time step, the consideration of the effect of impervious ground cover on soil erosion, and the revision of the equations and sequence of the subprocesses for a better physical representation of physical processes, such as surface runoff and sediment redistribution

(Choi et al., 2017, Choi et al., 2016). These modifications enable the model to be more suitable for estimating surface runoff and soil erosion on a complex surface terrain under an intensive seasonal rainfall regime than the previous version.

The DMMF model can estimate the amount of surface and subsurface water input from the upslope area and output to the downslope area after hydrological processes for each element (e.g., each grid cell in a raster map). The model also estimates the sediment budget of each element by calculating the amount of sediments flowing into and out of the element. The hydrological processes of the model are determined by rainfall, evapotranspiration, surface/subsurface water inflows, and initial soil water content (Figure 4.2). After calculating the water budget for the element, the model calculates sediment budgets, considering the amount of sediment input from the upslope areas, rainfall intensity, topography, soil characteristics, surface configurations, and vegetation structures (Figure 4.3). The detailed input parameters are presented in Table 4.1 and detailed structure and equations are described in the Appendix 4.A.

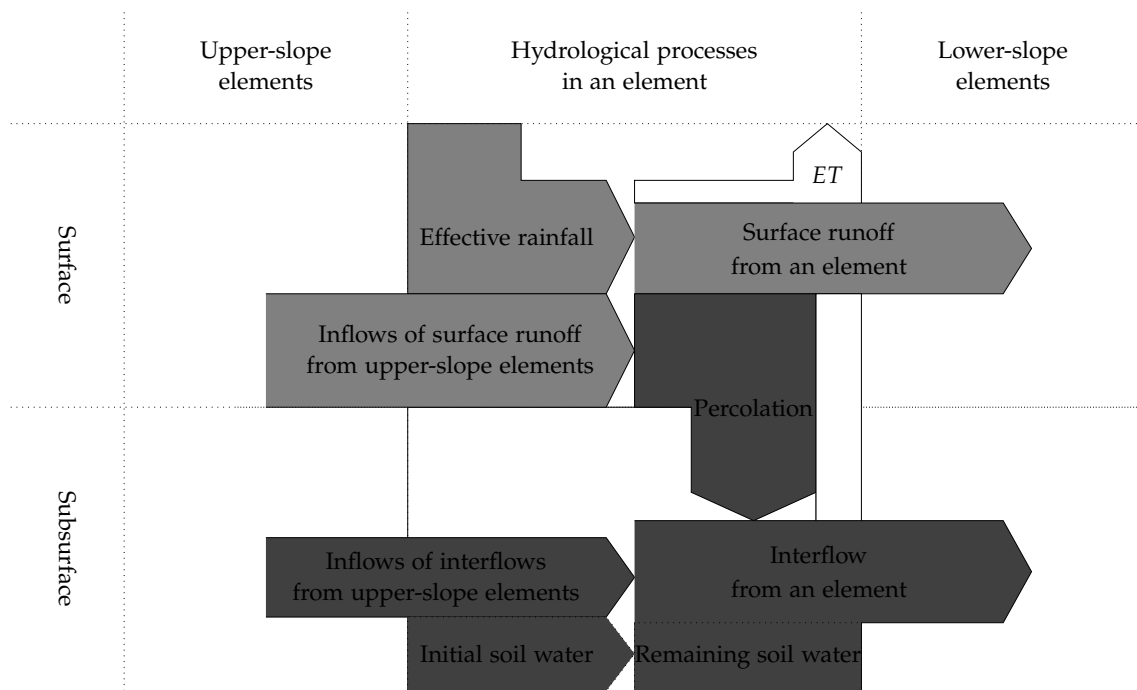


Fig. 4.2. Schematic hydrological phase of the DMMF model (modified from Figure 3 of Choi et al. (2017)).

In contrast with the SWAT model, which has been frequently applied to this catchment, the DMMF model can estimate the erosion and deposition of an element, considering the interconnectivity with adjacent elements. Therefore, the model can be used to estimate the impact of the spatial reconfiguration of erosion hot spots into forest on sediment yields more explicitly for each element and the entire catchment.

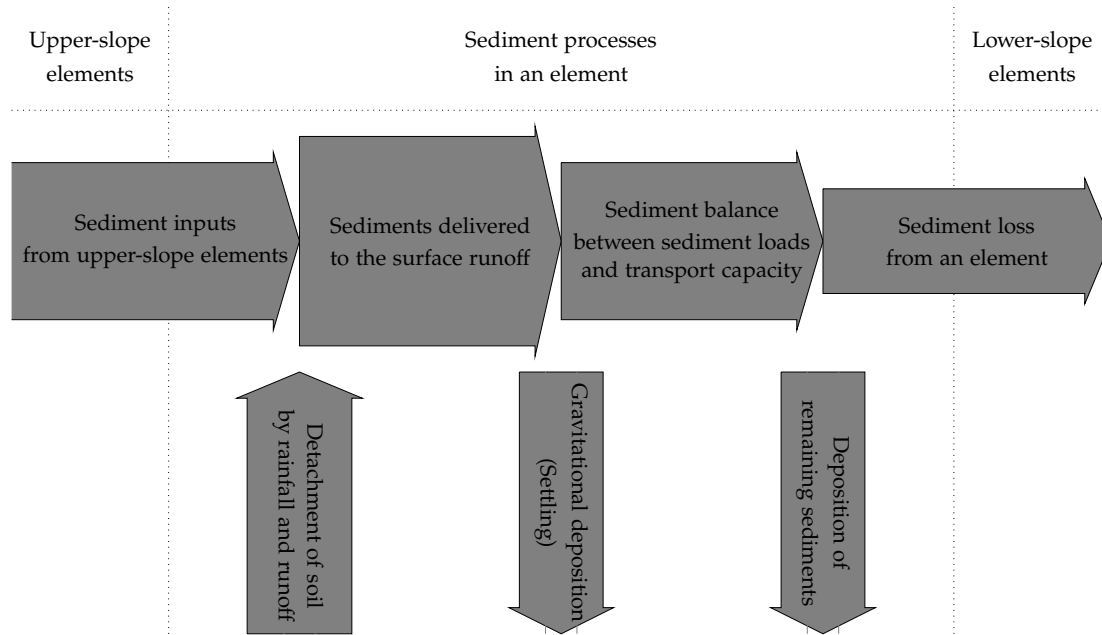


Fig. 4.3. Schematic sediment phase of the DMMF model (modified from Figure 4 of Choi et al. (2017)).

Table 4.1. Input parameters of the daily based Morgan–Morgan–Finney (DMMF) model (modified from Table 1 of Choi et al. (2017))

| Type       | Parameter   | Description  | Unit                     |
|------------|---|--|--------------------------|
| Topography | $S$   | Slope angle  | (rad)                    |
|            | $res$   | Grid size of a raster map  | (m)                      |
| Climate    | $R$   | Daily rainfall   | (mm/d)                   |
|            | $RI$  | Mean rainfall intensity of a day   | (mm/h)                   |
|            | $ET$  | Daily evapotranspiration   | (mm/d)                   |
| Soil       | $P_c$   | Proportion of clay in the surface soil                                   | (proportion)             |
|            | $P_z$   | Proportion of silt in the surface soil                                   | (proportion)             |
|            | $P_s$   | Proportion of sand in the surface soil                                   | (proportion)             |
|            | $SD$  | Soil depth   | (m)                      |
|            | $\theta_{init}$                                   | Initial soil water content of the entire soil profile                    | (vol/vol)                |
|            | $\theta_{sat}$                                    | Saturated water content of the entire soil profile                       | (vol/vol)                |
|            | $\theta_{fc}$                                     | Soil water content at field capacity of the entire soil profile          | (vol/vol)                |
|            | $K$   | Saturated soil lateral hydraulic conductivity of the entire soil profile | (m/d)                    |
|            | $DK_c$  | Detachability of clay particles by rainfall                              | (g/J)                    |
|            | $DK_z$  | Detachability of silt particles by rainfall                              | (g/J)                    |
|            | $DK_s$  | Detachability of sand particles by rainfall                              | (g/J)                    |
|            | $DR_c$  | Detachability of clay particles by surface runoff                        | (g/mm)                   |
|            | $DR_z$  | Detachability of silt particles by surface runoff                        | (g/mm)                   |
| $DR_s$     | Detachability of sand particles by surface runoff | (g/mm)   |                          |
| LULC       | $PI$  | Area proportion of the permanent interception of rainfall                | (proportion)             |
|            | $IMP$   | Area proportion of the impervious ground cover                           | (proportion)             |
|            | $GC$  | Area proportion of the pervious ground cover of the soil surface         | (proportion)             |
|            | $CC$  | Area proportion of the canopy cover of the soil surface                  | (proportion)             |
|            | $PH$  | Average height of vegetation or crop cover                               | (m)                      |
|            | $D$   | Average diameter of individual plant elements at the surface             | (m)                      |
|            | $NV$  | Number of individual plant elements per unit area                        | (number/m <sup>2</sup> ) |
|            | $d_a$   | Typical flow depth of surface runoff                                     | (m)                      |
|            | $n$   | Manning’s roughness coefficient of the soil surface                      | (s/m <sup>1/3</sup> )    |

### 4.2.3 Model Parameterization

As shown in Table 4.1, the DMMF model requires the topography, climate, soil, and LULC datasets to project surface runoff and sediment redistribution patterns of the catchment.

Topography data (i.e., the slope angle ( $S$ ) and grid size of a raster map ( $res$ )) were derived from the digital elevation model (DEM) with 30 m resolution. The parameter  $res$  is used to calculate the width ( $w$ ) and length ( $l$ ) of an element that are equivalent to  $res$  and  $res/\cos(S)$ , respectively (Choi et al., 2017).

Climate data were obtained from two sources. The daily rainfall ( $R$ ) and mean rainfall intensity of a day ( $RI$ ) were obtained from weather stations installed in the catchment, and the evapotranspiration ( $ET$ ) was obtained from remote sensing data provided by the Moderate Resolution Imaging Spectroradiometer (MODIS) (ORNL DAAC, 2008). We estimated  $R$  and  $RI$  from each weather station and spatially interpolated them using inverse distance weighted (IDW) method, which showed the optimal result on this catchment among four methods such as inverse distance weighted, spline, nearest neighbor, and kriging, according to Shope et al. (2014). For the  $ET$ , we resampled the 8-day average MODIS/Terra Evapotranspiration data to fit to the DEM of this catchment.

The soil data set covers the texture, depth, hydraulic properties, and detachabilities. The soil texture (i.e., the proportion of clay ( $P_c$ ), silt ( $P_z$ ), and sand ( $P_s$ ) in the surface soil), soil depth ( $SD$ ), and soil hydraulic properties (i.e., saturated soil water content ( $\theta_{sat}$ ), soil water content at field capacity ( $\theta_{fc}$ ), and saturated lateral hydraulic conductivity ( $K$ ) of the entire soil profile) were derived from a 2009 catchment-wide field survey from the TERRECO project (see Table 4.2 and Figure 4.4) (Shope et al., 2014).

Table 4.2. Typical soil characteristics of each represented soil class of the Haean catchment from a 2009 catchment-wide field survey from TERRECO project.

| Classification              | $SD$ | $P_c$ | $P_z$ | $P_s$ | $\theta_{sat}^*$ | $\theta_{fc}^*$  | $K^*$            |
|-----------------------------|------|-------|-------|-------|------------------|------------------|------------------|
| Very steep forest           | 2.55 | 0.17  | 0.33  | 0.50  | 0.47 (0.41–0.53) | 0.21 (0.06–0.31) | 1.97 (0.63–4.55) |
| Forest                      | 4.38 | 0.22  | 0.35  | 0.43  | 0.45 (0.41–0.54) | 0.17 (0.06–0.33) | 2.18 (0.63–4.55) |
| Moderate to steep dry field | 2.18 | 0.08  | 0.29  | 0.64  | 0.36 (0.34–0.39) | 0.18 (0.17–0.20) | 0.33 (0.18–0.66) |
| Flat dry field              | 4.85 | 0.03  | 0.15  | 0.82  | 0.36 (0.34–0.41) | 0.18 (0.08–0.25) | 0.49 (0.09–2.25) |
| Rice paddy                  | 1.60 | 0.07  | 0.32  | 0.62  | 0.37 (0.36–0.39) | 0.16 (0.14–0.18) | 0.50 (0.41–0.72) |
| Sealed ground               | 2.00 | 1.00  | 0.00  | 0.00  | -                | -                | -                |

\*  $\theta_{sat}$ ,  $\theta_{fc}$ , and  $K$  were estimated with the model ROSETTA Lite v.1.1 (Schaap et al., 2001). The numbers in parentheses indicate the range of values of soil layers that constitute each represented soil class.

Reference values for soil detachability from Morgan and Duzant (2008) were used as the initial values of soil detachability by rainfall (i.e., for clay ( $DK_c$ ), silt ( $DK_z$ ), and sand ( $DK_s$ ))

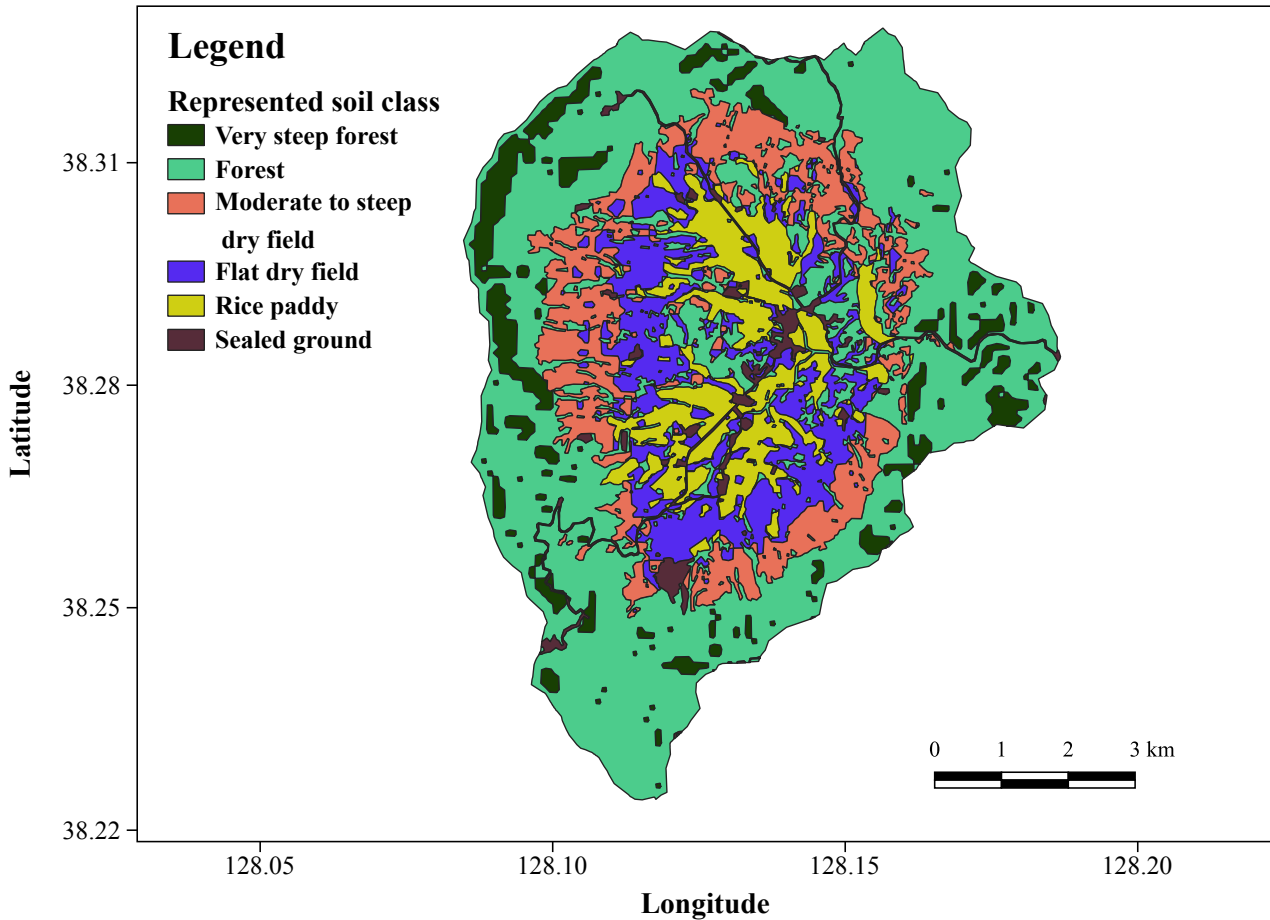


Fig. 4.4. Represented soil class from a 2009 catchment-wide field survey from the TERRECO project.

and by runoff (i.e., for clay ( $DR_c$ ), silt ( $DR_z$ ), and sand ( $DR_s$ )). We assumed that the initial soil water content of the entire soil profile ( $\theta_{init}$ ) is equal to the soil water content at field capacity ( $\theta_{fc}$ ) by starting the simulation at three days after the first heavy rainfall of the year, because the excess soil water was usually drained away two or three days after the soil was fully saturated by rainfall.

The LULC types characterize the physical structures of surface and vegetation, which regulate the quantity of surface runoff and runoff velocity. Surface structures incorporate a portion of the impervious cover area ( $IMP$ ), such as plastic mulching and paved facilities, flow depth of surface runoff ( $d_a$ ), and Manning's roughness coefficient of the soil surface ( $n$ ). Vegetation structures contain the permanent interception of rainfall ( $PI$ ), pervious ground cover ( $GC$ ), canopy cover ( $CC$ ), average vegetation height ( $PH$ ), average diameter of individual plant elements at the surface ( $D$ ), and number of individual plant elements per unit area ( $NV$ ). LULC parameters were derived based on the LULC map of the Haeon catchment in the year 2010 from Seo et al. (2014) (see Figure 4.5).

We classified the original LULCs into 14 categories (i.e., forest, rice paddy, semi-natural,

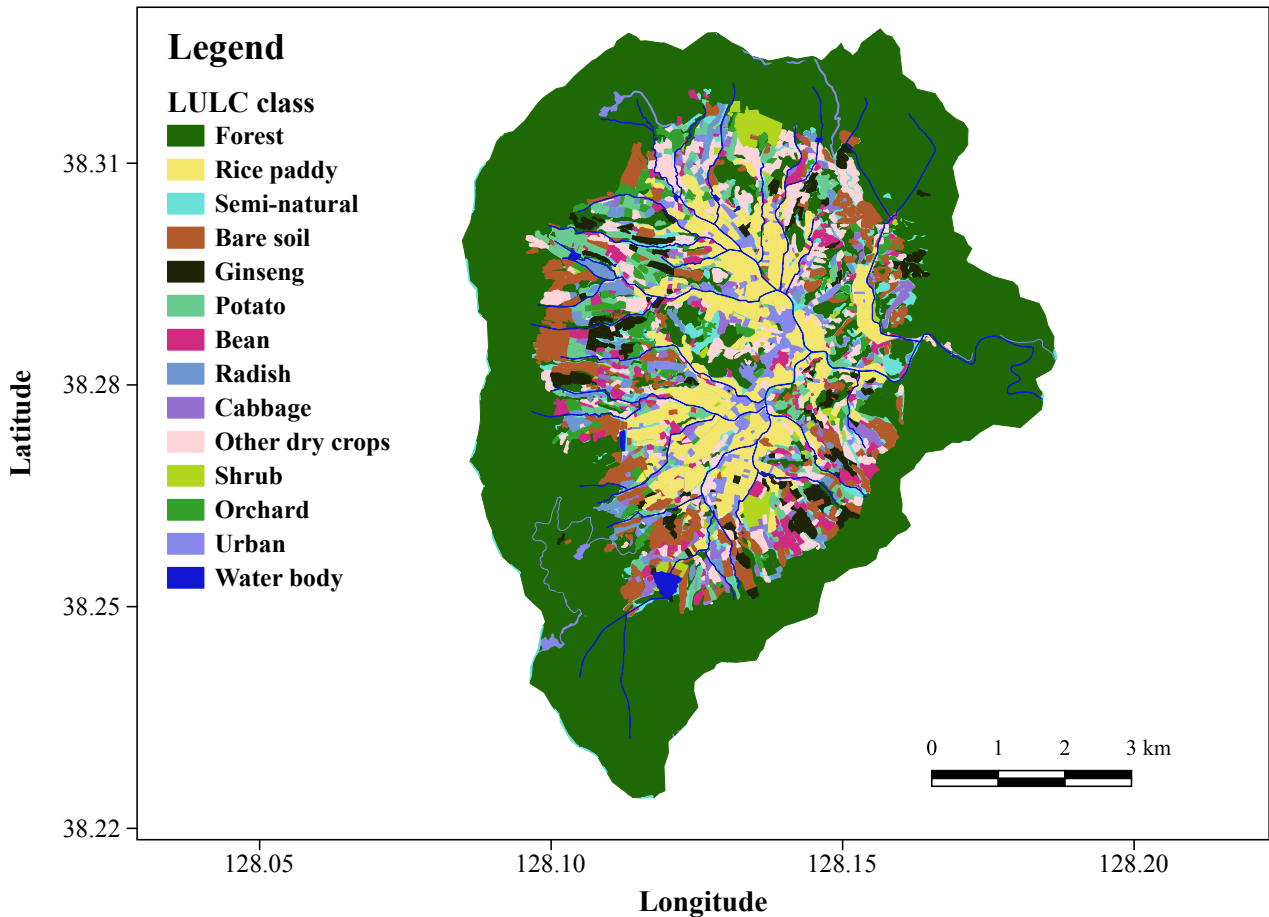


Fig. 4.5. LULC classes and their spatial configurations for the Haeon catchment in the year 2010 (Seo et al., 2014).

bare soil, ginseng, potato, bean, radish, cabbage, other dry crops, shrub, orchard, urban, and water bodies). Forest, rice paddy, semi-natural, bare soil, ginseng, potato, bean radish, and cabbage are major LULCs that covered more than 1% of the catchment area. Minor LULCs were aggregated into groups of other dry crops, shrub, orchard, urban, and water bodies according to their physical characteristics. We used field measurement data of  $CC$ ,  $PH$ ,  $NV$ ,  $IMP$ ,  $d_a$ , and  $n$  for major dry crops such as bean, cabbage, potato, and radish, whose data were obtained from the field campaign of the TERRECO project, which was also used in Arnhold et al. (2014). The daily forest  $CC$  was estimated using the average values of 8-day normalized difference vegetation index (NDVI) for forest in the catchment from MODIS (ORNL DAAC, 2017, Didan, 2015). The average NDVI values were converted to canopy cover ( $CC$ ), using the equation suggested by Gutman and Ignatov (1998). LULC parameters for rice and ginseng, and the average diameter of individual plant elements ( $D$ ) for major dry crops were obtained from agricultural technology portal provided by Rural Development Administration of South Korea (RDA) (Rural Development Administration of South Korea, 2018). The average LULC parameters of major dry crops were used for the LULC parameters of other dry crops, while the guide values from Morgan and

Duzant (2008) were adopted for other LULC parameters. Detailed initial parameter settings are presented in Table 4.3.

Table 4.3. The initial parameter settings for each LULC class.

| LULC            | Leaf-out <sup>(a)</sup><br>(Planting) | Leaf-fall <sup>(a)</sup><br>(Harvest) | $PI$ <sup>(b)</sup> | $IMP$ <sup>(c)</sup> | $GC$ <sup>(d)</sup> | $CC_{max}$ <sup>(e)</sup> | $PH$ <sup>(f)</sup> | $D$ <sup>(g)</sup> | $NV$ <sup>(h)</sup> | $d_a$ <sup>(i)</sup> | $n$ <sup>(j)</sup> |
|-----------------|---------------------------------------|---------------------------------------|---------------------|----------------------|---------------------|---------------------------|---------------------|--------------------|---------------------|----------------------|--------------------|
| Forest          | 112                                   | 307                                   | 0.20                | 0.00                 | 1.00                | 0.95                      | 30.0                | 2.00               | 0.60                | 0.100                | 0.20               |
| Semi-natural    | 112                                   | 307                                   | 0.30                | 0.00                 | 1.00                | 0.95                      | 0.50                | 0.01               | 500                 | 0.100                | 0.20               |
| Shrub           | 112                                   | 307                                   | 0.20                | 0.00                 | 0.30                | 0.95                      | 0.50                | 0.12               | 20                  | 0.100                | 0.20               |
| Rice paddy      | 136                                   | 283                                   | 0.30                | 0.00                 | 1.00 (0.00)         | 0.80                      | 1.00                | 0.04               | 200                 | 0.050                | 0.10               |
| Potato          | 120                                   | 243                                   | 0.12                | 0.50 (0.00)          | 0.00 (0.26)         | 0.71                      | 0.45                | 0.10               | 6.00                | 0.150                | 0.10               |
| Bean            | 147                                   | 304                                   | 0.20                | 0.50 (0.50)          | 0.00 (0.58)         | 0.89                      | 0.70                | 0.02               | 6.00                | 0.150                | 0.10               |
| Radish          | 153                                   | 235                                   | 0.15                | 0.50 (0.25)          | 0.00 (0.14)         | 0.64                      | 0.48                | 0.06               | 6.00                | 0.150                | 0.10               |
| Cabbage         | 140                                   | 201                                   | 0.25                | 0.50 (0.50)          | 0.00 (0.31)         | 0.85                      | 0.55                | 0.20               | 3.64                | 0.150                | 0.10               |
| Other dry crops | 120                                   | 304                                   | 0.18                | 0.50 (0.31)          | 0.00 (0.32)         | 0.77                      | 0.57                | 0.10               | 5.32                | 0.150                | 0.10               |
| Orchard         | 120                                   | 303                                   | 0.25                | 0.00                 | 0.40                | 0.95                      | 4.00                | 1.50               | 0.16                | 0.050                | 0.10               |
| Ginseng *       | 123                                   | 298                                   | 0.20                | 0.00                 | 0.50                | 1.00                      | 1.30                | 0.01               | 37.5                | 0.400                | 0.20               |
| Bare soil       | -                                     | -                                     | 0.00                | 0.00                 | 0.00                | 0.00                      | 0.00                | 0.00               | 0.00                | 0.050                | 0.01               |
| Urban           | -                                     | -                                     | 0.00                | 1.00                 | 0.00                | 0.00                      | 0.00                | 0.00               | 0.00                | 0.005                | 0.01               |

<sup>(a)</sup> Typical leaf-out and leaf-fall dates of each LULC were presented as day of the year (DOY). For annual crops, the dates represented the typical planting and harvest date of each crop (Shope et al., 2014); <sup>(b)</sup> The reference values from Morgan and Duzant (2008) were used for the area proportion of the permanent interception of rainfall ( $PI$ ) for each LULC type; <sup>(c)</sup>  $IMP$  for dry fields are different between cultivation and non-cultivation periods. Values in parentheses represent  $IMP$  for non-cultivation periods; <sup>(d)</sup>  $GC$  for dry fields is different before and after harvest. After harvest, crop residues and weeds remained as the ground cover of dry fields, according to dry crop data, from the field campaign of the TERRECO project in 2009.  $GC$  for rice paddy in cultivation season was set to one reflecting water-filled condition that protected the surface from erosion; <sup>(e)</sup> Because  $CC$  values varied with time, we made a list of maximum  $CC$  ( $CC_{max}$ ). Semi-natural, shrub, and ginseng utilize fixed reference values from Morgan and Duzant (2008); <sup>(f)</sup> We used fixed reference  $PH$  values from Morgan and Duzant (2008) for LULCs of other than dry crops. Maximum  $PH$  values for dry crops were listed from the field measurement data varying with time; <sup>(g)</sup> We used fixed reference  $D$  values from Morgan and Duzant (2008) for LULCs of other than dry crops.  $D$  values for dry crops utilized typical crop characteristics from Rural Development Administration of South Korea (2018); <sup>(h)</sup> We used reference  $NV$  values from Morgan and Duzant (2008) for LULCs of other than dry crops and ginseng.  $NV$  values which were estimated from the field measurement data and Rural Development Administration of South Korea (2018) were used for dry crops and ginseng, respectively; <sup>(i)</sup> We assumed shallow rill condition for forest, semi-natural and shrub, and assumed unchannelled flow condition for bare soil, rice paddy, and orchard using values presented in Morgan and Duzant (2008).  $d_a$  values for other LULCs derived from furrow heights of the fields, using field measurement data for dry crops and data from the Rural Development Administration of South Korea (2018) for ginseng; <sup>(j)</sup> According to the guide values for Manning's  $n$  from Morgan (2005), the values of  $n$  for natural land covers (i.e., forest, semi-natural, and shrub), crop fields, ginseng, and smooth surfaces (bare soil and urban) are 0.2, 0.1, 0.2, and 0.01, referring to natural range land, average tillage conditions, wheat mulching, and smooth bare soil or asphalt conditions, respectively; \* The permeable black awning screen is generally installed 1.3m above the ginseng field (Rural Development Administration of South Korea, 2018), and it acts as a plant canopy. Therefore, the cover ratio of the screen in the field and height of the screen is utilized for canopy cover ( $CC$ ) and plant height ( $PH$ ) values for ginseng.

#### 4.2.4 Model Calibration and Validation

The DMMF model was calibrated and validated for stream discharge and suspended sediment to test its performance in the Haeon catchment. The testing was performed utilizing data from the year 2010 when the LULC map, as well as the field-measured stream discharge and suspended sediment data, were well established (Shope et al., 2014, Seo et al., 2014). We confined the testing

period from the 67th day of the year (DOY), which is three days after first heavy rainfall of the year, to reduce the uncertainty of initial soil water content by equating it with the soil water content at field capacity. We equalized the two parameters based on the field measurement guidelines for soil water content at field capacity, which recommend soil sampling two or three days after rainfall that is heavy enough to saturate the soil. The three sub-catchments of S1, S2, and S3 (see Figure 4.1) were selected for model calibration and validation. The data from the S1 and S2 were utilized for two-step calibration, and those from the S3 were used for model validation. Two-step calibration was performed on the forest-related parameters utilizing the data from the S1 site, and the other parameters were calibrated utilizing the data from S2. This calibration method enables us to prevent the significance of forest-related parameters of dominant LULC type in the entire catchment, from overtaking the importance of other parameters, resulting in those parameters being ignored. The DMMF model can estimate the outputs of the surface and subsurface runoff, and the sediment from the elements. However, the measured data are stream discharge and suspended sediments at the outlet of each sub-catchment. Because the model does not consider in-stream processes and the impact of groundwater on the base flow of the stream, it is not appropriate to directly compare the result from the model with the measured data. To match different comparative objects, we compared the total daily discharge of each site to total daily surface runoff and subsurface interflow flowing into the stream from the model, while adding a constant corresponding to base flow from groundwater. To match the sediment yield from the terrestrial part with the suspended sediments measured at the outlet of each sub-catchment, we should consider the in-stream sediment processes and impact of erosion control facilities. Reflecting sediment deposition on the stream bed load, we assumed that only a part of the terrestrial sediment yield entering the stream was sampled at each measuring point for each sub-catchment. Therefore, we compared the suspended sediments measured from the outlet of each measuring point to the sediment flowing into the stream from the model, multiplied by a constant, reflecting the in-stream sediment process. Our assumptions can be described as below,

$$Q_m = Q_s + IF_s + \alpha, \quad (4.1)$$

$$SL_m = \beta \times SL_s. \quad (4.2)$$

Here,  $Q_m$  represents the measured daily total discharge, and  $Q_s$ ,  $IF_s$ , and  $\alpha$  represent the daily surface runoff, daily subsurface interflow simulated from the DMMF model, and a constant reflecting the base flow from groundwater (unit:  $\text{m}^3/\text{s}$ ).  $SL_m$  represents the total daily suspended

sediments measured at the outlet of each sub-catchment, and  $SL_s$  and  $\beta$  represent the terrestrial sediment yield entering the stream from the model simulation and constant representing the in-stream sediment deposition rate, respectively.

#### 4.2.4.1 Sensitivity Analysis

To select important parameters to be calibrated among unmeasured or highly uncertain parameters, we performed site-specific sensitivity analyses, using the Sobol' method (Sobol', 1993, Saltelli, 2002, Saltelli et al., 2010). The Sobol' method is a variance based sensitivity analysis that is widely used in environmental and hydrological modeling, such as SWAT and TOPMODEL (Nossent et al., 2011, Qi et al., 2013). This method can estimate the total effect of each parameter on the model output, considering the combined effects among parameters. Therefore, the Sobol' method is more suitable for analyzing the sensitivity of non-linear and non-additive models containing many parameters, as opposed to the local or one-at-a-time (OAT) methods (Nossent et al., 2011, Saltelli and Annoni, 2010). The relative sensitivity of parameters is expressed as the Sobol' total index ( $SI$ )—the ratio of the amount of total variance caused by a parameter to the amount of variance induced from all parameters (i.e., the unconditional variance of the model) (Saltelli et al., 2010). If we have  $p$ -dimensional parameter set, the first-order sensitivity of the  $i$ -th parameter can be described as,

$$S_i = \frac{V_{X_i}(E_{X_{-i}}(Y|X_i))}{V(Y)}, \quad (4.3)$$

where  $V_{X_{-i}}(E_{X_i}(Y|X_{-i}))$  is the variance of the model solely by  $i$ -th parameter ( $X_i$ ). Then the total sensitivity of the  $i$ -th parameter ( $SI_i$ ) can be calculated as below,

$$SI_i = 1 - \frac{V_{X_{-i}}(E_{X_i}(Y|X_{-i}))}{V(Y)}, \quad (4.4)$$

where  $\frac{V_{X_{-i}}(E_{X_i}(Y|X_{-i}))}{V(Y)}$  indicates that the sum of first-order sensitivities of all parameters except  $i$ -th parameter. Parameters with large  $SI$  indicate a relatively high impact on the model output, while those with small  $SI$  indicate a relatively low impact on the model output.

Because the soil hydraulic parameters (i.e.,  $\theta_{sat}$ ,  $\theta_{fc}$ , and  $K$ ), soil detachabilities (i.e.,  $DK_c$ ,  $DK_z$ ,  $DK_s$ ,  $DR_c$ ,  $DR_z$ , and  $DR_s$ ) and LULC parameters (i.e.,  $PI$ ,  $IMP$ ,  $GC$ ,  $CC$ ,  $PH$ ,  $D$ ,  $NV$ ,  $d$ , and  $n$ ) were not measured or had high uncertainties, their importance was tested on model outputs. Before performing sensitivity analysis, we set the range of the parameters to be tested. The ranges of soil hydraulic parameters (i.e.,  $\theta_{sat}$ ,  $\theta_{fc}$ , and  $K$ ) were set based on the

range of estimated values for each represented soil class (see Table 4.2). The upper bound of  $\theta_{fc}$  was set as the minimum  $\theta_{sat}$ , and the upper bound of  $K$  was set to 18 times of the maximum  $K$  to reflect high uncertainty of the parameter (Brooks et al., 2004). The ranges of the un-measured LULC parameters were set based on the initial parameter settings for each LULC type (see Table 4.3). We adjusted the parameters using a range of  $\pm 100\%$  for the initial parameter settings for each LULC type. If the upper or lower limits of the proportional parameters is out of the range between zero to one, we set the lower limits to zero and the upper limits to one. In this study, SIs for the input parameters were estimated using the “sobolmartinez” function of the “sensitivity” package (Iooss et al., 2018) on R version 3.5.1 (R Core Team, 2018), a well-established open-source program for statistical computing, providing many analysis packages. We used the default bootstrapping option of the function, employing a sample size of  $10^3$ .

#### 4.2.4.2 Calibration

To find the optimal combination of the parameter set, which allows model outputs to explain the measured stream discharge and suspended sediments from each site, we performed two-step calibration. For each step, we adjusted the important parameters with  $SI$  greater than 0.05 (i.e., contributing 5% of the total variance), and we adjusted the constants for the in-stream processes ( $\alpha$  and  $\beta$ ) additionally for sub-catchment S2, where data were measured in the stream outlet. We searched for the optimal combination of the parameter set, using the differential evolution (DE) optimization method (Storn and Price, 1997, Price et al., 2006). The DE algorithm is a heuristic optimization method with an evolution strategy for finding the global optimum value. Requiring few prerequisites for its execution, the algorithm is applicable to non-differential, nonlinear, and multimodal models. As a result, the DE algorithm has been applied to a variety of fields including hydrological model calibration (Choi et al., 2017, Storn and Price, 1997, Price et al., 2006, Ardia et al., 2016, Joseph and Guillaume, 2013, Zheng et al., 2015). We applied the DE algorithm for model calibration using the “DEoptim” package (Ardia et al., 2016, Mullen et al., 2011) on R version 3.5.1 (R Core Team, 2018). We used the Nash-Sutcliffe efficiency coefficient (NSE) (Nash and Sutcliffe, 1970) between model outputs and field-measured data as an objective function for the DE algorithm. To treat NSE values from stream discharge and suspended sediments fairly, we evaluated the NSE values for each measurement and used the average NSE value as the final objective function:

$$F_{obj} = 1 - \frac{\text{NSE}(Q_m) + \text{NSE}(SL_m)}{2}, \quad (4.5)$$

where  $F_{obj}$  is the objective function to evaluate the model performance. We ran the function for  $10^3$  iterations, and ran for three different initial states to try to find the global minimum as an optimum value.

#### 4.2.4.3 Validation

Using adjusted parameters from calibration steps, model performance was tested for the S3 site, which is located near the catchment outlet. Considering site-specific base flow from groundwater and in-stream sediment processes for the S3 site, we adjusted the constants for the in-stream processes ( $\alpha$  and  $\beta$ ). We utilized the NSE, the percent bias (PBIAS), and the coefficient of determination ( $R^2$ ) as statistical criteria for model performance evaluation (Moriassi et al., 2007, 2015). The function “gof” from the “hydroGOF” package (Mauricio Zambrano-Bigiarini, 2017) in R version 3.5.1 (R Core Team, 2018) was used to evaluate statistical criteria.

#### 4.2.5 Identifying Annual Sediment Redistribution Patterns and Assessing Soil Erosion Risk

Projecting validated parameters on the DMMF model, we simulated and calculated the annual sediment redistribution patterns of the catchment. Based on the simulated result, we assessed the net soil erosion rate ( $SL_{net}$ : t/(ha year)) for each element of the catchment.  $SL_{net}$  is the net soil erosion for each element, which is the amount of sediment input to each element from upslope elements ( $SL_{in}$ ) subtracted from the amount of sediment output from the element ( $SL_{out}$ ). Soil erosion risk was assessed by using  $SL_{net}$  of each element. We classified  $SL_{net}$  into five categories, namely tolerable, low, moderate, high, and severe, as shown in Table 4.4 according to the soil erosion risk categories defined by OECD (OECD, 2001, 2008) which is one of the internationally used criteria. Based on the net soil erosion rate of the entire catchment, we

Table 4.4. Soil erosion risk categories defined by OECD (OECD, 2001, 2008).

| Erosion Class                   | Tolerable | Low    | Moderate | High    | Severe |
|---------------------------------|-----------|--------|----------|---------|--------|
| Soil erosion rate (t/(ha year)) | <6        | 6–10.9 | 11–21.9  | 22–32.9 | >33    |

assessed the soil erosion characteristics for each LULC class. For the assessment, we calculated the mean  $SL_{net}$  for each LULC class.

## 4.2.6 Evaluation of the Impact of Spatial Reconfiguration of Erosion Hot Spots into Forest

We assessed the impact of the spatial reconfiguration of erosion hot spots into forest, based on the annual sediment redistribution patterns of the catchment. Erosion hot spots represent elements in which much annual net soil erosion ( $SL_{net}$ ) occurs. To compare the impact of spatial reconfiguration, we calculated the annual sediment yields being generated from the terrestrial area and entering to the water bodies of the entire catchment ( $SY_{base}$ ) as a base line condition.  $SY_{base}$  is the total amount of sediment yields entering the water bodies of the entire catchment, which is equal to the total amount of  $SL_{in}$  flowing into water bodies. To increase the robustness of our analysis, we only used the values between the 2.5th percentile and the 97.5th percentile for all the elements in the catchment to exclude the impact of extreme values that can occur from model outputs. The lower extreme values were set to the value of the 2.5th percentile and the upper extreme values were set to the value of the 97.5th percentile. The impact of the spatial reconfiguration of erosion hot spots into forest was evaluated by calculating the total annual sediment yields entering the stream ( $SY_{tot}$ ), using the DMMF model as bare soil and croplands (i.e., bean, cabbage, ginseng, orchard, potato, radish and rice field) being sequentially changed into the forest. We selected forest, the original LULC type before anthropogenic land cover changes, as the alternative LULC to mitigate erosion-prone areas. Similar to the methods Chaplin-Kramer et al. (2015) and Chaplin-Kramer et al. (2016) which compute ecosystem services by marginally changing forest into agricultural areas, we computed  $SY_{tot}$  by gradually converting 1% of the bare soil and croplands in the catchment into forest until all bare soil and croplands elements are converted into forest. Based on this result, we presented the total sediment yields ( $SY_{tot}$ ), reduction rate of the sediment yields entering the stream compared to base line condition ( $SY_{base}$ ), and sediment yield reduction efficiency per conversion area ( $t/m^2$ ).

## 4.3 Results

### 4.3.1 Model Performance

According to the calibration and validation results, the DMMF model showed competitive performance, predicting stream discharge, but showed poorer performance in evaluating the amount of suspended sediments at the outlet of each sub-catchment. We performed two-step calibration by comparing the model outputs to the measured data collected from sub-catchment

S1 and S2. The LULC and soil types of sub-catchment S1 are classified as forest and forest soil, according to Tables 4.2 and 4.3. The calculated Sobol' index for important parameters, both for stream discharge ( $SI_Q$ ) and suspended sediments to the stream ( $SI_{SL}$ ), are presented in Table 4.5.

Table 4.5. List of important parameters from forested site with Sobol' index greater than 0.05 for stream discharge ( $SI_Q$ ) and suspended sediment to the stream ( $SI_{SL}$ ), and their optimized values from the DE algorithm.

| Parameters    | Soil Class / LULC | $SI_Q$ | $SI_{SL}$ | Optimized Values      |
|---------------|-------------------|--------|-----------|-----------------------|
| $\theta_{fc}$ | Forest soil       | 0.035  | 0.118     | $2.24 \times 10^{-1}$ |
| $K$           | Forest soil       | 0.202  | 0.082     | $6.17 \times 10^1$    |
| $DR_c$        | Forest soil       | 0      | 0.213     | $2.25 \times 10^{-1}$ |
| $PI$          | Forest            | 0.781  | 0.180     | $6.66 \times 10^{-5}$ |
| $GC$          | Forest            | 0      | 0.775     | $9.92 \times 10^{-1}$ |
| $d_a$         | Forest            | 0      | 0.144     | $7.77 \times 10^{-3}$ |

According to the Sobol' index, the amount of stream discharge was highly influenced by the permanent interception of rainfall ( $PI$ ) and lateral soil hydraulic conductivity ( $K$ ), which regulate the amount of rainfall and flow rate of subsurface interflow of the sub-catchment, respectively. Vegetation and surface cover structures ( $GC$ ,  $PI$ , and  $d_a$ ), detachability of clay particles ( $DR_c$ ), soil water content at field capacity ( $\theta_{fc}$ ), and lateral soil hydraulic conductivity ( $K$ ) exhibited a relatively large impact on suspended sediments generated from the sub-catchment. This result indicates that the suspended sediments generated from the sub-catchment are determined by the amount of surface runoff and the erosivity of surface, because  $PI$ ,  $K$ , and  $\theta_{fc}$  determine the amount of surface runoff by regulating the amount of rainfall and partitioning the rate of surface and subsurface water. Parameters  $GC$ ,  $d_a$ , and  $DR_c$  determine the erosivity by surface runoff.

We determined an optimized parameter set by adjusting selected important parameters from sensitivity analysis using the DE algorithm (see Table 4.5). With the optimized parameter set, the stream discharge and suspended sediment from the model outputs were compared with those from field measurements (see Figure 4.6).

After calibrating the forest-related parameters, we calibrated the other parameters, based on the measurement data collected from sub-catchment S2. We calculated the relative importance of parameters for both the stream discharge ( $SI_Q$ ) and suspended sediments to the stream ( $SI_{SL}$ ), using the Sobol' index, and presented them in Table 4.6.

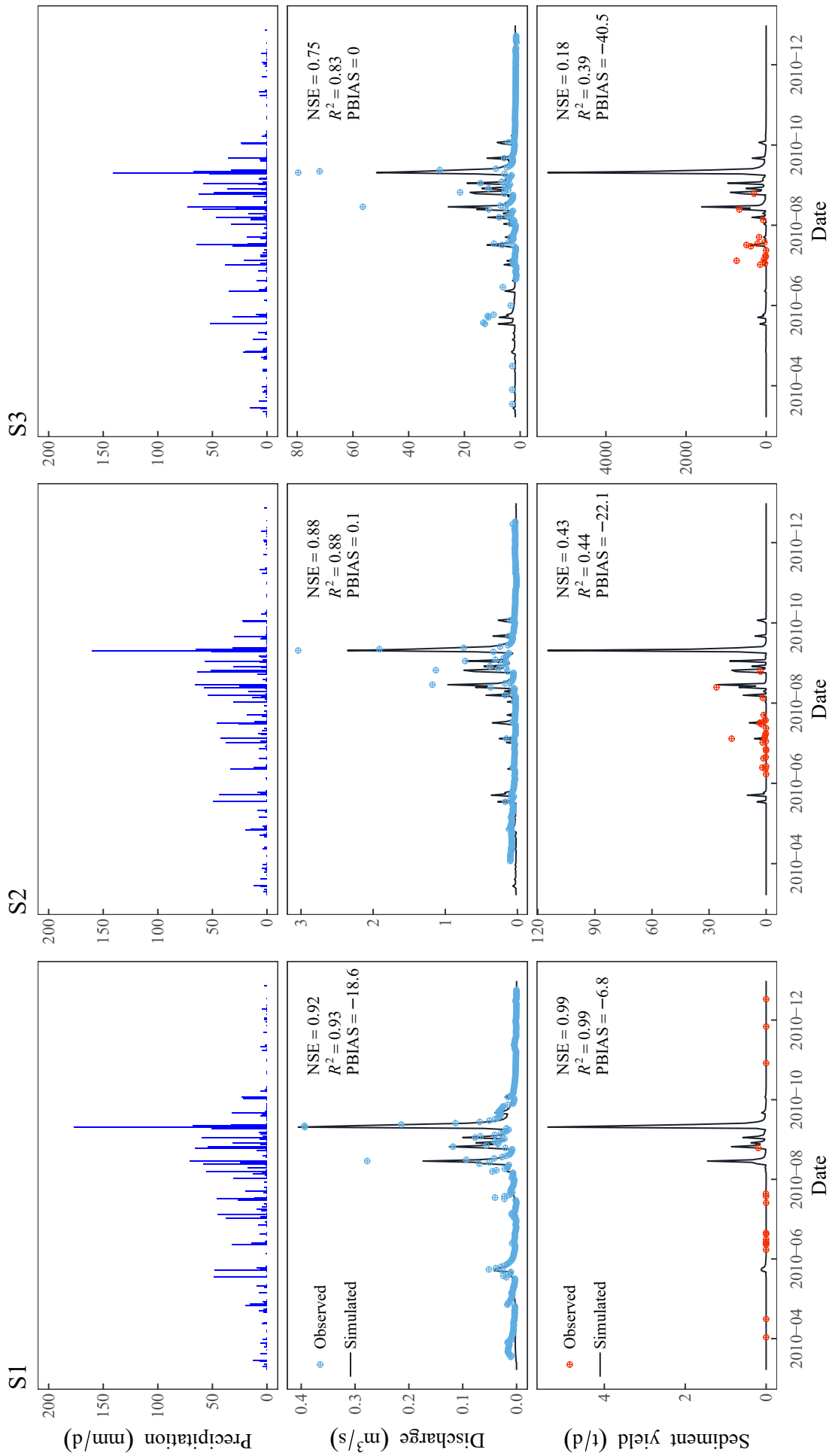


Fig. 4.6. Calibration (S1 and S2) and validation (S3) result for stream discharge, and suspended sediment measured at the outlet of each sub-catchment.

Table 4.6. List of important parameters ( $SI > 0.05$ ) for stream discharge ( $SI_Q$ ) and suspended sediment ( $SI_{SL}$ ), and their optimized values from DE algorithm.

| Parameters    | Soil Class / LULC                | $SI_Q$ | $SI_{SL}$ | Optimized Values      |
|---------------|----------------------------------|--------|-----------|-----------------------|
| $\theta_{fc}$ | Moderate to steep dry field soil | 0.115  | 0.112     | $3.18 \times 10^{-1}$ |
| $K$           | Moderate to steep dry field soil | 0.223  | 0.020     | $6.06 \times 10^{-1}$ |
| $K$           | Flat dry field soil              | 0.062  | 0.001     | $1.59 \times 10^{-1}$ |
| $DR_c$        | Moderate to steep dry field soil | 0      | 0.217     | 1.39                  |
| $DR_z$        | Moderate to steep dry field soil | 0      | 0.119     | $9.59 \times 10^{-1}$ |
| $PI$          | Semi-natural                     | 0.252  | 0.048     | $4.16 \times 10^{-4}$ |
| $PI$          | Rice paddy                       | 0.101  | 0.000     | $2.91 \times 10^{-1}$ |
| $PI$          | Other dry crops                  | 0.178  | 0.011     | $1.28 \times 10^{-4}$ |
| $GC$          | Semi-natural                     | 0      | 0.080     | $3.60 \times 10^{-2}$ |
| $d_a$         | Semi-natural                     | 0      | 0.158     | $1.74 \times 10^{-1}$ |
| $d_a$         | Bean                             | 0      | 0.105     | $2.93 \times 10^{-1}$ |
| $\alpha$      | -                                | -      | -         | $1.75 \times 10^{-2}$ |
| $\beta$       | -                                | -      | -         | $4.57 \times 10^{-2}$ |

According to sensitivity analysis, model outputs were highly sensitive to soil hydraulic characteristics of moderate to steep dry field soil and land cover structures of the semi-natural field. In details, the stream discharge of the sub-catchment was highly sensitive to the permanent interception of rainfall ( $PI$ ) of the semi-natural, rice paddy, and other dry crops; the lateral hydraulic conductivity ( $K$ ) of the moderate to steep dry field and flat dry field soils; and the soil water content at field capacity ( $\theta_{fc}$ ) of the moderate to steep dry field. This result indicates that stream discharge is highly influenced by the amount of rainfall reaching the ground ( $PI$ s) and the flow rate of subsurface interflow ( $K$ s and  $\theta_{fc}$ ) of this region. The sediment yield to the stream is sensitive to the soil detachability by runoff ( $DR_c$  and  $DR_z$ ) of the moderate to steep dry field soil, soil water content at field capacity ( $\theta_{fc}$ ) of the moderate to steep dry field soil, flow depth ( $d_a$ ) of the semi-natural field and bean field, and ground cover ratio ( $GC$ ) of the semi-natural field. This result emphasizes the role of the moderate to steep dry field soil, which is the second largest soil type, following forest soil, and demonstrates the crucial role of the semi-natural field on determining suspended sediment output from the model.

The performance statistics for the calibration and its time series plots of observed versus simulated stream discharge and suspended sediment were presented in Figure 4.6. For the calibration steps, the NSE values for stream discharge were 0.92 and 0.88 for sub-catchment S1 and S2, respectively. The  $R^2$  values for stream discharge were 0.93 and 0.88, respectively, and the PBIAS values for stream discharge were  $-18.6$  and  $0.1$ , respectively. The NSE values for suspended sediment were 0.99 and 0.43 for sub-catchments S1 and S2, respectively. The  $R^2$  values for suspended sediment were 0.99 and 0.44, and the PBIAS values for suspended sediment were

−6.8 and −22.1 for the sub-catchments, respectively. The site-specific constants reflecting the baseflow from groundwater ( $\alpha$ ) and in-stream sediment deposition rate ( $\beta$ ) for sub-catchment S2 are  $1.75 \times 10^{-2} \text{ m}^3/\text{s}$  and  $4.57 \times 10^{-2}$ . In validation steps, the NSE values for stream discharge and suspended sediment were 0.75 and 0.18, respectively, with the site-specific  $\alpha$  and  $\beta$  being  $1.711 \text{ m}^3/\text{s}$  and  $6.76 \times 10^{-2}$ , respectively. The  $R^2$  for discharge and sediment were 0.83 and 0.39, respectively, and the PBIAS for discharge and sediment were 0 and −40.5, respectively. According to the model performance evaluation criteria suggested by Moriasi et al. (2015), the DMMF model showed good performance for discharge in both calibration and validation steps. Though there is no clear model performance evaluation criteria suggested for daily time scale sediment result for watershed model due to limited reported data (Moriasi et al., 2015), When we apply the performance evaluation criteria for monthly time scale sediment result for watershed scale model, the model might be considered to have a slightly poor performance for sediment during the calibration and validation steps, as the NSE and  $R^2$  values were less than 0.45 and 0.40, respectively.

### 4.3.2 Sediment Redistribution Pattern of the Catchment

Simulating the model with optimized parameters, we calculated the annual net soil erosion rate ( $SL_{net}$ ) for each element and classified them into five classes—tolerate, low, moderate, high, and severe—as in Figure 4.7.

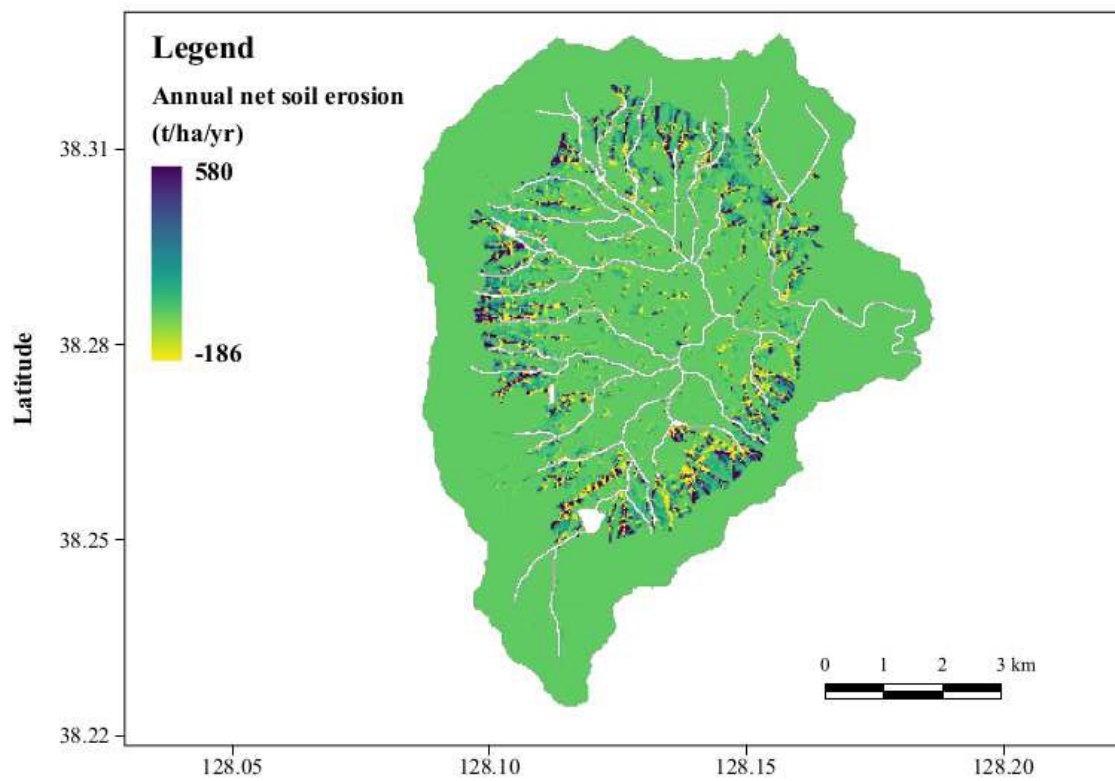
According to Figure 4.7, elements with severe soil erosion ( $>33 \text{ t}/(\text{ha year})$ ) were concentrated on the dry crop field with moderate to steep slope conditions on the interface with the forest. The estimate of the mean annual net soil erosion rate by each LULC type (Table 4.7) shows that bare soil and dry crop field suffered from severe soil erosion. On the other hand, forest, rice paddy, orchard, and urban areas showed good sediment capturing capabilities.

### 4.3.3 Impacts of Conversion of Erosion Hot Spots into Forest on Total Sediment Yield Entering the Stream

The LULC conversion of erosion hot spots into forest showed a dramatic impact in the reduction of sediment yields entering the stream, as shown in Figure 4.8.

When each bare soil and crop field element in the catchment was converted into the forest sequentially from the area with the highest soil erosion rate to the area with the lowest soil erosion rate, the amount of total annual sediment yield of the catchment to the stream sharply decreased having a shape similar to an inverted sigmoid function. Changing the 3% of erosion

(a)



(b)

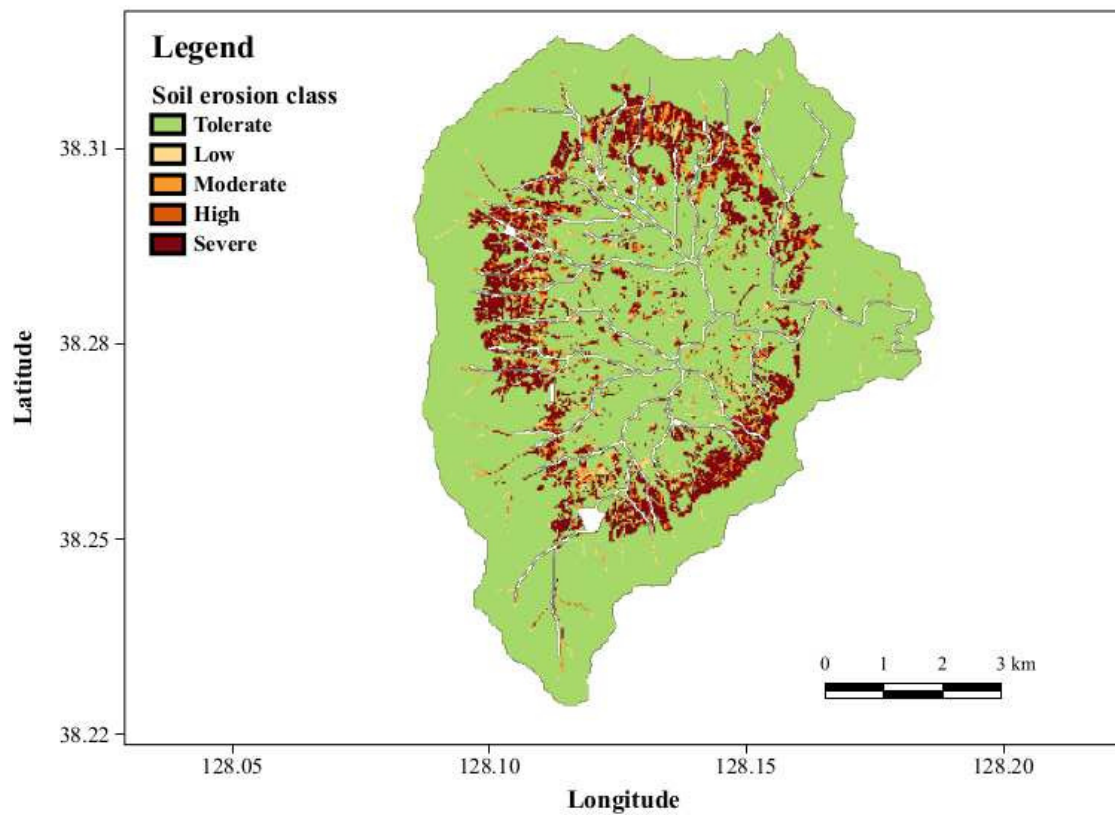


Fig. 4.7. (a) Annual net soil erosion (t/(ha/year)) of the entire Haeon catchment and (b) soil erosion class according to the soil erosion risk categories from OECD (OECD, 2001, 2008).

Table 4.7. Mean annual net soil erosion rate (t/(ha year)) and mean slope of each LULC type.

| LULC              | Mean Annual Net Soil Erosion Rate (t/ha/year) | Mean Slope (°) |
|-------------------|---|----------------|
| Bare soil         | 997.80  | 9.8            |
| Bean              | 763.82  | 7.6            |
| Ginseng           | 388.83  | 8.5            |
| Potato            | 357.60  | 7.9            |
| Radish            | 310.06  | 8.4            |
| Other dry crops   | 294.23  | 8.4            |
| Semi-natural      | 126.34  | 9.0            |
| Shrub             | 105.54  | 11.1           |
| Cabbage           | 79.30   | 7.6            |
| Catchment average | 52.68   | 16.0           |
| Forest            | -75.25  | 22.0           |
| Rice paddy        | -171.83                                       | 3.0            |
| Orchard           | -227.14                                       | 8.1            |
| Urban             | -284.71                                       | 6.0            |

hot spots that have suffered the most from severe soil erosion caused a reduction in sediment yield entering the stream of ca. 10% from the baseline condition ( $SY_{base}$ ), and a change in 10% of most severe hot spots is expected to reduce sediment yields by ca. 50%. Among the elements  $SL_{net}$ ,  $SL_{in}$ , and  $SL_{out}$ , the altered areas revealed that outputs from the element ( $SL_{out}$ ) proved to be the most effective in reducing the total sediment yield into the stream. A simulation of the sediment yields entering the stream showed that the reducing rate in sediment yield for  $SL_{net}$  was less effective than those for  $SL_{out}$  and  $SL_{in}$ . Due to total annual sediment yields sigmoidally decreases as bare soil and crop fields begin changed into forest, sediment yield reduction efficiency per unit conversion area increased until ca. 10% of total crop land area converted to forest and then gradually decreased. A simulation of the sediment yield reduction efficiency showed that the element ( $SL_{out}$ ) was most efficient for all conversion intervals.

## 4.4 Discussion

Our findings emphasize the importance of landscape configuration on regulating ecosystem services by showing the effectiveness of spatial reconfiguration of soil erosion hot spots into forest on reducing the amount of sediment yield entering the stream. We simulated the annual sediment redistribution pattern in the Haean catchment, utilizing the daily based Morgan–Morgan–Finney (DMMF) soil erosion model. According to the result, the soil erosion rate varied greatly depending on the topography and LULC type, and the area located on the steep hill-slope, which is adjacent to the forest severely suffered from soil erosion. When reconfiguring

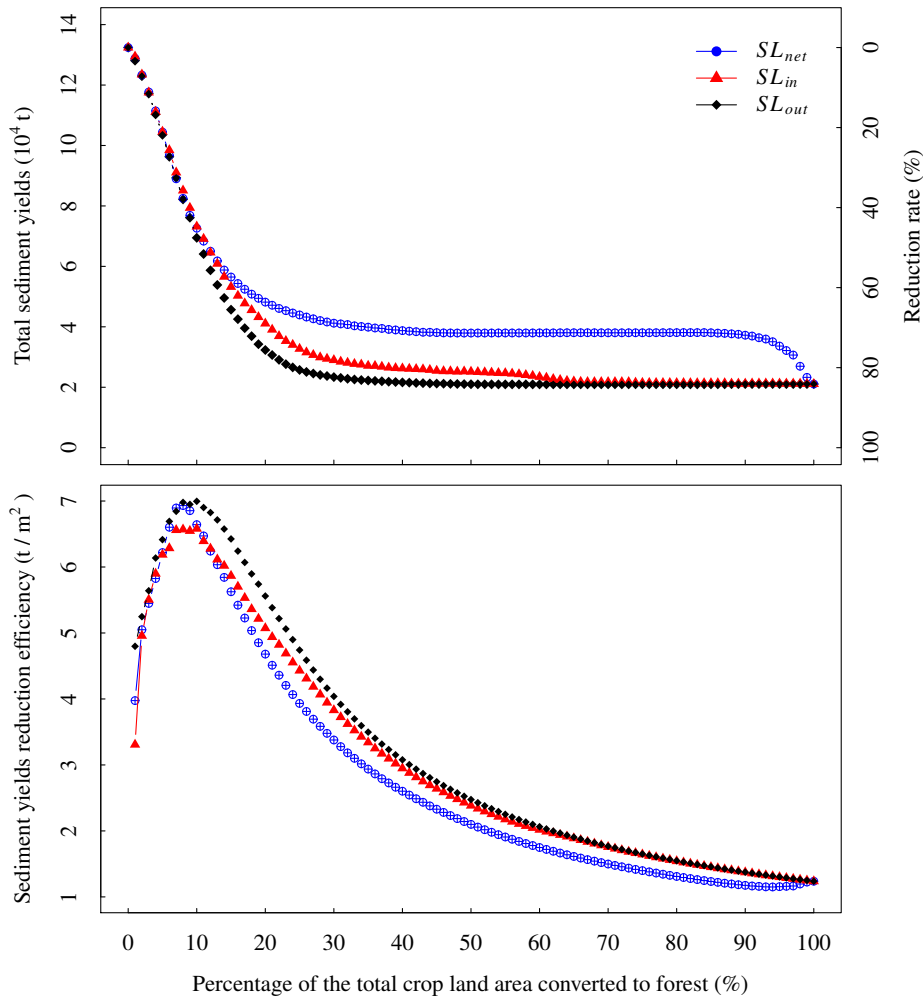


Fig. 4.8. Total annual sediment yields entering the stream (**upper panel**) and sediment yield reduction efficiency per unit conversion area (**lower panel**) through changing bare soil and crop fields into forest sequentially from the area with the highest to the area with the lowest amount of net soil erosion ( $SL_{net}$ ), sediment inflow to the element ( $SL_{in}$ ), and sediment output from the element ( $SL_{out}$ ).

the landscape patterns of croplands by sequentially altering erosion hot spots from the most severe to the least severe areas into forest, we found dramatic effects in the reduction of sediment yields entering the stream in this catchment. The reduction rate may reach ca. 50% when the 10% most severe erosion hot spots were altered, and we can expect a reduction rate of over 80% when the ca. 20% most severe erosion hot spots are altered. In the following, we first discuss model performance and limitation, and then potential management implications.

#### 4.4.1 Model Performance

The assessment of soil erosion risk and measurement of the effectiveness of the spatial reconfiguration of erosion hot spots in reducing sediment yields entering the stream were based on the calibrated and validated simulations of the DMMF soil erosion model. According to the

model performance criteria from Moriasi et al. (2015), the DMMF model showed satisfactory performance for predicting stream discharge during the calibration and validation processes, with mean NSE values of 0.90 and 0.75, mean  $R^2$  of 0.91 and 0.83, and maximum PBIAS of  $-18.6$  and  $0$  during calibration and validation steps, respectively. The model showed comparatively poor performance for predicting suspended sediment at the outlet of each sub-catchment, except the small forested site (S1) where the stream does not exist. The mean NSE values were 0.66 and 0.18, mean  $R^2$  were 0.67 and 0.39, and maximum PBIAS were  $-22.1$  and  $-40.5$ , respectively. When we compared the model performance statistics of the DMMF model to those from previous studies using soil and water analysis tool (SWAT), the model showed competitive performance in predicting stream discharge but poorer performance in terms of predicting suspended sediments in the stream (Maharjan et al., 2016, Jang et al., 2017). Maharjan et al. (2016) reported that mean NSE values for stream discharge were 0.82 during calibration and 0.45 during validation. In addition, they showed that mean NSE values for suspended sediment were 0.78 and 0.60 during calibration and validation, respectively. Jang et al. (2017) also reported mean NSE values for stream discharge of 0.78 and 0.66 during calibration and validation, respectively. They reported mean  $R^2$  for suspended sediment were 0.80 and 0.76 during calibration and validation, respectively. In terms of soil erosion rate for each crop field, the DMMF model estimated that the average annual soil loss of major dry crops ranged between  $79.3 \text{ t}/(\text{ha year})$  and  $763.8 \text{ t}/(\text{ha year})$  for bean, radish, potato, and cabbage, and the average annual soil loss from whole dry crop fields was  $379.7 \text{ t}/(\text{ha year})$ . Arnhold et al. (2014) reported that  $30\text{--}54 \text{ t}/(\text{ha year})$  of soil loss occurred in the dry crop fields, including bean, radish, potato, and cabbage, from the plot-level field measurement. Furthermore, Maharjan et al. (2016) estimated that  $35.5\text{--}53.0 \text{ t}/(\text{ha year})$  of soil loss occurred in the dry crop fields from the SWAT model. When we compared the results from the DMMF model with those from other studies, the amount of soil loss from this study is far greater. The reasons that the DMMF model showed poor performance for predicting suspended sediment in the stream can be analyzed from two perspectives. The first reason involves the discrepancy of data types between the DMMF model and observed data. The observed data were stream discharge and suspended sediment at the outlet of each sub-catchment. On the other hand, the DMMF model can estimate the total sediment yields entering the stream that belongs to each sub-catchment. The DMMF model is efficient for estimating sheet and rill erosion, but it has limitations in estimating in-stream sediment processes such as stream bed deposition, channel erosion, and sediment transport in the stream. Considering the limitations of the model, we use site-specific coefficients, which assume that suspended sediments measured at the outlet are proportional to the sediment yields inflowing into the

stream. However, incorporating the quantity and the velocity of stream water discharge, sediment flux, and physical characteristics of channel structures such as gradient, width, depth, and length, into the in-stream sediment process, is complicated (Tucker and Whipple, 2002, Neitsch et al., 2011). The reasons above may lead to a high sediment deposition rate in the stream (i.e., low measured sediment ratio ( $\beta$ )), which in turn, causes a high soil erosion rate in the terrestrial area. Because the study sites are affected by monsoon climate, such that its rainfall pattern is not uniform but rather with a lot of extremes, a large amount of sediment is deposited during low rainfall events, and the deposited sediments are washed out by a huge amount of fast stream discharge accompanying heavy rainfall. Temporal lags between the rainfall event and stream discharge are negligible for the Haean catchment, but for suspended sediments, the lags are significant and highly depend on the stream length because of the difference in travel velocities between water and soil particles (Lee, 2008, Kim et al., 2015, Gellis, 2013, Vercruyssen et al., 2017). Therefore, the model performance for predicting stream discharge may be better than that for predicting suspended sediments. The stream widens and deepens as it descends to the lower area, according to Lee (2009), and the length of the stream also increases as the size of sub-catchment grows. The uncertainty caused by in-stream processes increases as the size of the sub-catchment grows, which reduces the model performance in predicting suspended sediments in this study. SWAT and USLE-based models are usually calibrated and validated at the fixed spatial area with a different temporal period. Therefore, in-stream sediment processes can be included in the parameters, which may lead to better model performance. However, the DMMF model is a spatially distributed semi-processed model and used the same temporal period with a different spatial area for calibration and validation in this research, so that the in-stream processes cannot be included in the model.

Secondly, many sediment reduction facilities, such as dams for freshwater, debris barrier and culvert systems around crop fields, and road infrastructures, which can affect sediment transport processes, have been installed in the Haean catchment (Shope et al., 2014, Jeon and Kang, 2010). The dam and debris barriers create reservoirs that impede the stream flow and filter out sediments in the facilities. This disrupts the correct evaluation of the model performance for this catchment. Shope et al. (2014) showed complex stream networks, including the culvert systems around crop fields and the road infrastructure. The culvert systems extend the travel time of suspended sediments and reduce the runoff and transport velocities of sediments by altering the flow direction abruptly. Increased travel time and decreased transport velocity tend to increase the deposition rate of sediments compared to the condition without the culvert system. The deposited sediments in the culvert flow into the stream by runoff, with sufficient

power to wash out. The culvert system is also responsible for the temporal lag between the rainfall event and the presence of suspended sediments in the catchment. Sediment reduction facilities trap a huge amount of sediments, which make the measured sediment ratio ( $\beta$ ) in this study have very low values. Because of the small  $\beta$ , the stream bed deposition rate became too large, and consequently, the overall erosion rate from terrestrial area increased. To cope with this problem, the in-stream processes will need to be considered more precisely through model improvements.

#### 4.4.2 Assessment of Soil Erosion Risk and the Effectiveness of Spatial Reconfiguration of Erosion Hot Spots on Reducing Sediment Yield Entering the Stream

We estimated the annual net soil erosion rate of the entire catchment and assessed the soil erosion risk class according to the OECD criteria. According to this study, soil erosion is concentrated on the hill-slope of the catchment, and the problem is more significant for the bare soil and dry crop fields, such as bean, radish, and potato, in this area. In addition, forest in the valley showed a considerable amount of soil loss, also suffering from erosion due to the concentrated surface runoff and steep slope. Compared with other studies, the soil erosion risk pattern and the average annual soil loss from the DMMF model is qualitatively consistent with the soil erosion risk map from Lee et al. (2014), with average climate conditions for the 2010s using the USLE-based SATEEC (Lim et al., 2005) model. According to this study, urban area, orchard, and rice field showed better performance for sediment capturing capabilities than forest. However, the urban area and rice field are located in the lower and flatter area than forest, so that the sediment inputs from the upslope area tend to be deposited in this area. Furthermore, because the urban area is usually paved with impervious covers, such as concrete and asphalt, and the rice field is filled with water, which acts as a pervious cover that prevents surface erosion, these areas have little soil loss but receive huge input from the upslope area. Though the forest is in a region where the slope is very steep, the average amount of soil loss is smaller compared with other land types, and it also shows excellent sediment capturing capability, in general. Like the other studies, we can conclude that the main cause of severe erosion in the catchment is cropland extension after deforestation at the hill-slope area of the catchment (Lee, 2009, Maharjan et al., 2016, Arnhold et al., 2013, 2014, Jang et al., 2017, Lee et al., 2014). We also assessed the effect of spatial reconfiguration of LULCs on reducing sediment yields entering the stream. In this study, the spatial reconfiguration of erosion hot spots into forest

showed excellent reduction efficiency in sediment yields entering the stream. We identified that the sediment yields entering the stream were reduced sharply, as crop lands were sequentially changed into forest from the area with the most severe soil loss to the area with the least soil loss. An sigmoidal sediment reduction rate from altering LULCs to forest indicates that forest is not only effective in preventing surface erosion but also effective in capturing sediment input from the upslope area. In addition, the result suggested that altering LULCs based on the amount of sediment output from the element is the most effective way of reducing sediment yields entering the stream. This result is consistent with previous studies that emphasize the effectiveness of vegetative filter strips located at sediment sources such as crop fields (Maharjan et al., 2016, Ali and Reineking, 2016, Jang et al., 2017, Dillaha et al., 1989, Delgado et al., 1995, Muñoz-Carpena et al., 1999). The result can also be generalized to consider the effect of riparian vegetation buffer strip on reducing sediment yields entering the stream, located at the interface between crop fields or natural sediment sources and the stream channel (Lee et al., 2003, Cooper et al., 1987, Osborne and Kovacic, 1993). This study also demonstrated that the sediment yield reduction efficiency initially increased as the first few bare soil area and crop lands with the most severe soil loss were converted into forest. The sediment yield reduction efficiency were maximized when ca. 10% of the area converted, and then the efficiency decreased gradually. These patterns can be explained by two aspects of the forest's sediment yield reduction capability; protecting surface from soil erosion, and capturing sediment inputs. The areas with the most severe soil loss are located at the steep hillslope where surface runoff is concentrated. These areas have a large transport capacity of the runoff, beyond the sediment capturing capability of forest because transport capacity is greater than the available sediment for transport (Choi et al., 2017). In these areas, conversion of crop lands into forest can reduce soil loss from the surface but cannot capture sediment inputs from upslope which is larger than surface soil loss. As slope becomes milder and the amount of surface runoff decreases due to gradual conversion of crop lands into forest, transport capacity gradually decreases. Decreased transport capacity caused by decreased slope gradient and surface runoff lets forest capture more sediments, maintaining the surface protecting capability from soil loss. Therefore, the sediment yield reduction capabilities of forest become small and the sediment yield reduction efficiency by changing crop lands into forest decreases gradually. According to these results, one can reduce sediment yields entering stream efficiently by identifying an optimal percentage of crop land conversion into forest which brings out the best efficiency of sediment yield reduction per unit conversion area.

## 4.5 Conclusions

In this study, we identified the soil erosion risk of Haean catchment spatially explicitly by projecting sediment redistribution patterns using the DMMF model. In addition, we measured the sediment yield reduction efficiency entering the stream by sequentially altering erosion hot spots into forest from that which has the highest soil loss to that which has the lowest soil loss. The DMMF model showed competitive performance estimating stream discharge but exhibited lower performance estimating suspended sediments at each sub-catchment outlet. When we applied the DMMF model to the Haean catchment, the bare soil surface and dry crop fields located on the steep hill-slope of the catchment suffered mostly from severe soil erosion. On the other hand, forest, rice paddy, orchard, and urban areas suffer less from soil erosion. By changing the erosion hot spots from cropland to forest, the overall amount of sediments exporting to the stream of the catchment was effectively reduced. The sediment yield reduction efficiency was maximized when ca. 10% of crop lands were converted to forest. This study implies that one can achieve the goal of reducing sediment yields entering the stream by identifying the location of erosion hot spots and managing the area intensively. Although previous studies showed good mitigation effects of BMPs that require compliance of stakeholders, this may not be easy and takes much time for stakeholders to follow the BMPs, because the degree of acceptance of the policy depends on the situation and tendency of each stakeholder (Jang et al., 2017). On the other hand, the spatial reconfiguration approach proposed in this study can reduce the number of stakeholders relevant to soil erosion mitigation measures. However, this approach reduces crop yields because crop lands are converted to non-crop lands to reduce sediment yields from the catchment. In addition, the sediment yield reduction efficiency decreases after a certain point of spatial reconfiguration. Therefore, the two approaches—BMP measures such as cultivating cover crops, mulching surface with straw, and managing field margin naturally, and conversion of crop lands with the more severe soil loss—are complementary measures to reduce sediment yields into the stream.

### Author contributions

Conceptualization, K.C. and B.R.; Data curation, K.C. and G.R.M.; Formal analysis, K.C.; Investigation, K.C.; Methodology, K.C.; Resources, G.R.M.; Software, K.C.; Supervision, B.R.;

Validation, K.C.; Visualization, K.C.; Writing original draft, K.C.; Writing review & editing, G.R.M. and B.R.

## Funding

This study is part of the International Research Training Group “Complex Terrain and Ecological Heterogeneity” (TERRECO) funded by the German Research Foundation (DFG) with the grant number [GRK 1565/1]. This study was also supported by the National Research Foundation of Korea (NRF) with the grant number [NRF-2017R1A2B4010460].

## Acknowledgments

This paper is dedicated to the memory of our wonderful colleague, Sebastian Arnhold, who passed away last year. This publication was funded by the German Research Foundation (DFG), the National Research Foundation of Korea (NRF). This publication was also funded by the German Research Foundation (DFG) and the University of Bayreuth in the funding programme Open Access Publishing. We would like to thank Editage ([www.editage.co.kr](http://www.editage.co.kr)) for English language editing.

## Conflicts of interest

The authors declare no conflict of interest. The founding sponsors had no role in the design of the study; in the collection, analyses, or interpretation of data; in the writing of the manuscript, and in the decision to publish the results.

## Appendix 4.A Detailed Structure of the DMMF Soil Erosion Model

Morgan–Morgan–Finney (MMF) model (Morgan et al., 1984) is a conceptual soil erosion model, which estimates the annual soil erosion rate from an area by comparing the amount soil particles detached from the surface ( $SS$ ) and transport capacity of surface runoff ( $TC$ ) (Morgan et al., 1984, Morgan, 2001, Morgan and Duzant, 2008). The first version of MMF model (Morgan et al., 1984) estimated soil erosion rate of an area by comparing the amount of soil particles detached by raindrop impact ( $F$ ) and transport capacity of surface runoff ( $TC$ ). The second

version of model, the revised Morgan–Morgan–Finney (RMMF) model (Morgan, 2001) started to consider the amount of soil particles generated by surface runoff ( $H$ ). In the third version, the modified Morgan–Morgan–Finney (MMMF) model (Morgan and Duzant, 2008), the interconnectivity of surface runoff, various sub-processes such as the subsurface interflow and gravitational deposition processes, and parameters such as the physical structure of vegetation and surface ground conditions were introduced to calculate transport capacity of surface runoff ( $TC$ ) and the amount of soil particles available for transport ( $G$ ) more physically rigorously (Lilhare et al., 2014). The daily based Morgan–Morgan–Finney (DMMF) soil erosion model (Choi et al., 2017) is also estimates daily soil loss from an element by comparing transport capacity of surface runoff ( $TC$ ) and the available sediment for transport ( $G$ ). The DMMF model is mainly comprised of hydrological and sediment phases. The hydrological phase determines the amount of surface runoff and subsurface interflow, and the sediment phase determines the amount of sediment budgets of the element.

#### 4.A.1 Hydrological Phase

The effective rainfall ( $R_{eff}$ ; mm) which is the volume of rainfall reaching the unit surface area of an element is the main driver of hydrological phase. Following the corrected version of the effective rainfall ( $R_{eff}$ ) from Choi et al. (2016),  $R_{eff}$  is calculated as,

$$R_{eff} = R \times (1 - PI) \times \cos(S), \quad (A1)$$

where  $PI$  is the proportion of the permanent interception area and  $S$  is the slope of an element. Similar to MMF model, surface runoff can be generated when the total input of water to the element exceeds the surface water infiltration capacity ( $SW_c$ ; mm), which is the soil moisture storage capacity considering the proportion of the impervious area ( $IMP$ ).  $SW_c$  is defined as,

$$SW_c = (1 - IMP) \times (SW_{sat} - SW_{init} - \frac{\Sigma IF_{in}}{A}), \quad (A2)$$

where  $SW_{sat}$  (mm) is the volume of water per unit area when soil is fully saturated, and  $SW_{init}$  (mm) is the volume of initial water per unit area that is already existed in the soil.  $\Sigma IF_{in}$  (L) is the volume of subsurface water inputs from upslope and  $A$  (m<sup>2</sup>) is the area of an element. The amount of the surface runoff ( $Q$ ; mm) is calculated as,

$$Q = R_{eff} + \frac{\Sigma Q_{in}}{A} - SW_c, \quad (A3)$$

where  $Q_{in}$  (L) is the volume of surface runoff inflow from upslope areas. The amount of water in the soil also flows out from the element as a subsurface interflow ( $IF_{out}$ ; L) when the volume of soil water budget per unit area ( $SW$ ; mm) of the element exceeds the volume of soil water at field capacity per unit area ( $SW_{fc}$ ; mm). The soil water budget ( $SW$ ) is estimated as,

$$SW = (SW_{init} + \frac{\Sigma IF_{in}}{A}) + (R_{eff} + \frac{\Sigma Q_{in}}{A} - Q) - ET, \quad (A4)$$

where  $ET$  (mm) is the volume of water evapotranspires per unit area from the element. Then the volume of subsurface water flowing out from the element ( $IF_{out}$ ) can be described as,

$$IF_{out} = K \times \sin(S) \times (SW - SW_{fc}) \times w, \quad (A5)$$

where  $K$  (m/d) is the saturated soil lateral hydraulic conductivity and  $w$  (m) is the width of the element. A part of soil water remains with remaining water content ( $\theta_r$ ; vol/vol) which can be described as,

$$\theta_r = \frac{(SW - IF_{out}/A)}{1000 \times SD}, \quad (A6)$$

where  $SD$  is the soil depth of the element, and 1000 is the constant to convert meters to millimeters. The  $\theta_r$  can be changed into  $\theta_{init}$  for the next day.

#### 4.A.2 Sediment Phase

Sediment phase determines the total mass of soil particles which is taken out of the element through three steps: delivery of detached soil particles into the surface runoff, gravitational deposition, and estimation of the sediment loss from the element ( $SL$ ) by comparing transport capacity of the runoff ( $TC$ ; kg/m<sup>2</sup>) and sediment available for transport ( $G$ ; kg/m<sup>2</sup>). In the model, soil particles are detached from the surface by raindrop impact and surface runoff. The mass of soil particles detached by raindrops per unit area ( $F$ ; kg/m<sup>2</sup>) is described as,

$$F = 0.001 \times DK \times P \times (1 - EPA) \times KE, \quad (A7)$$

where  $DK$  (g/J) is the detachability of soil particles by raindrop impact,  $P$  (%) is the proportion of each soil particle size class (i.e., clay, silt, and sand),  $KE$  (J/m<sup>2</sup>) is the kinetic energy of the effective rainfall considering direct throughfall and leaf drainage from the plant, and 0.001 is

the unit conversion factor from g to kg. Also,  $EPA$  is the erosion protected area:

$$EPA = IMP + (1 - IMP) \times GC, \quad (A8)$$

where  $GC$  is the proportion of ground cover and  $IMP$  is the proportion of the impervious area ( $IMP$ ) of the element. The mass of detached soil particles by the surface runoff ( $H$ ; kg/m<sup>2</sup>) is described as,

$$H = 0.001 \times DR \times P \times Q^{1.5} \times (1 - EPA) \times (\sin(S))^{0.3}, \quad (A9)$$

where  $DR$  (g/mm) is the detachability of soil particles by runoff per unit volume of surface runoff and  $Q$  is the volume of runoff per unit area,  $S$  is the slope of the element, and 0.001 is the unit conversion factor from g to kg. Sediment inputs from upslope elements ( $\Sigma SL_{in}$ ) also flows into surface runoff. The mass of delivered sediments to the surface runoff per unit area ( $SS$ ; kg/m<sup>2</sup>) is,

$$SS = F + H + \frac{\Sigma SL_{in}}{A}. \quad (A10)$$

A part of sediments delivered to the surface runoff ( $SS$ ) in the runoff settle down to the ground by gravity. The gravitational deposition rate of the suspended sediments ( $SS$ ) in runoff ( $DEP$ ) is,

$$DEP = 0.441 \times N_f, \quad (A11)$$

where  $N_f$  is the particle fall number which is the probabilistic ratio of falling particles (Tollner et al., 1976), The  $N_f$  can be estimated as,

$$N_f = \frac{l}{v} \times \frac{v_s}{d}, \quad (A12)$$

where  $v$  (m/s) is the velocity of the surface runoff,  $v_s$  is the settling velocity of each particle size class, and  $d$  (m) is the depth of the surface runoff.

The remaining suspended sediments become available for transport per unit volume of surface runoff per unit area ( $G$ ; kg/m<sup>2</sup>) and be estimated as,

$$G = SS \times (1 - DEP). \quad (A13)$$

The part of the available sediments for transport ( $G$ ) can flow out from the element according to the transport capacity of the runoff ( $TC$ ; kg/m<sup>2</sup>) of an element which is determined by the volume of runoff per unit area of an element ( $Q$ ), the slope angle ( $S$ ) and the surface conditions

(Morgan and Duzant, 2008). Due to the physical condition of surface affect runoff velocity, the transport capacity of runoff can be described using the ratio between actual runoff velocity ( $v$ ) and the reference velocity of the element ( $v_r$ ; m/s) (Choi et al., 2016).

$$TC = 0.001 \times \left(\frac{v}{v_r}\right) \times Q^2 \times \sin(S). \quad (\text{A14})$$

The reference velocity ( $v_r$ ) is,

$$v_r = \frac{1}{n_r} \times d_r^{2/3} \times \sqrt{\tan(S)}, \quad (\text{A15})$$

with 0.015 for Manning's coefficient ( $n_r$ ) and 0.005 for runoff depth ( $d_r$ ) representing for a standard surface condition. The transport capacity of the runoff ( $TC$ ) and the available sediment for transport ( $G$ ) determines the amount of sediment loss from the element ( $SL$ ) (Morgan and Duzant, 2008, Meyer and Wischmeier, 1969). When  $TC$  is greater than  $G$ , the surface runoff washes out all the sediments available for transport, otherwise, the amount of sediment ( $SL$ ) which is equal to  $TC$  can be transported from the element.

## References

- Hu, Q.; Gantzer, C.J.; Jung, P.K.; Lee, B.L. Rainfall erosivity in the Republic of Korea. *J. Soil Water Conserv.* **2000**, *55*, 115–120.
- Lee, J.Y. Importance of hydrogeological and hydrologic studies for Haeon basin in Yanggu. *J. Geol. Soc. Korea* **2009**, *45*, 405–414.
- Maharjan, G.R.; Ruidisch, M.; Shope, C.L.; Choi, K.; Huwe, B.; Kim, S.J.; Tenhunen, J.; Arnhold, S. Assessing the effectiveness of split fertilization and cover crop cultivation in order to conserve soil and water resources and improve crop productivity. *Agric. Water Manag.* **2016**, *163*, 305–318, doi:10.1016/j.agwat.2015.10.005.
- Lee, K.H.; Isenhardt, T.M.; Schultz, R.C. Sediment and nutrient removal in an established multi-species riparian buffer. *J. Soil Water Conserv.* **2003**, *58*, 1–8.
- Ali, H.E.; Reineking, B. Extensive management of field margins enhances their potential for off-site soil erosion mitigation. *J. Environ. Manag.* **2016**, *169*, 202–209, doi:10.1016/j.jenvman.2015.12.031.

- Jeon, J.H.; Park, C.G.; Choi, D.; Kim, T. Characteristics of Suspended Sediment Loadings under Asian Summer Monsoon Climate Using the Hydrological Simulation Program-FORTRAN. *Sustainability* **2017**, *9*, 44, doi:10.3390/su9010044.
- Pimentel, D.; Harvey, C.; Resosudarmo, P.; Sinclair, K.; Kurz, D.; McNair, M.; Crist, S.; Shpritz, L.; Fitton, L.; Saffouri, R.; et al. Environmental and economic costs of soil erosion and conservation benefits. *Science* **1995**, *267*, 1117–1122.
- Pimentel, D.; Kounang, N. Ecology of soil erosion in ecosystems. *Ecosystems* **1998**, *1*, 416–426.
- Lal, R. Soil degradation by erosion. *Land Degrad. Dev.* **2001**, *12*, 519–539, doi:10.1002/ldr.472.
- Yoon, B.; Hyoseop, W. Sediment problems in Korea. *J. Hydraul. Eng.* **2000**, *126*, 486–491.
- Arnhold, S.; Ruidisch, M.; Bartsch, S.; Shope, C.L.; Huwe, B. Simulation of runoff patterns and soil erosion on mountainous farmland with and without plastic-covered ridge-furrow cultivation in South Korea. *Trans. ASABE* **2013**, *56*, 667–679, doi:10.13031/2013.42671.
- Park, J.H.; Duan, L.; Kim, B.; Mitchell, M.J.; Shibata, H. Potential effects of climate change and variability on watershed biogeochemical processes and water quality in Northeast Asia. *Environ. Int.* **2010**, *36*, 212–225, doi:10.1016/j.envint.2009.10.008.
- Stocker, T.F.; Qin, D.; Plattner, G.K.; Alexander, L.V.; Allen, S.K.; Bindoff, N.L.; Bréon, F.M.; Church, J.A.; Cubasch, U.; Emori, S.; et al. *Climate Change 2013: The Physical Science Basis. Contribution of Working Group I to the Fifth Assessment Report of the Intergovernmental Panel on Climate Change*; Cambridge University Press: Cambridge, UK; New York, NY, USA, 2013; pp. 33–115.
- Chang, H. Spatial analysis of water quality trends in the Han River basin, South Korea. *Water Res.* **2008**, *42*, 3285–3304, doi:10.1016/j.watres.2008.04.006.
- Choi, K.; Arnhold, S.; Huwe, B.; Reineking, B. Daily Based Morgan–Morgan–Finney (DMMF) Model: A Spatially Distributed Conceptual Soil Erosion Model to Simulate Complex Soil Surface Configurations. *Water* **2017**, *9*, 278, doi:10.3390/w9040278.
- Ruidisch, M.; Kettering, J.; Arnhold, S.; Huwe, B. Modeling water flow in a plastic mulched ridge cultivation system on hillslopes affected by South Korean summer monsoon. *Agric. Water Manag.* **2013**, *116*, 204–217, doi:10.1016/j.agwat.2012.07.011.

- Arnhold, S.; Lindner, S.; Lee, B.; Martin, E.; Kettering, J.; Nguyen, T.T.; Koellner, T.; Ok, Y.S.; Huwe, B. Conventional and organic farming: Soil erosion and conservation potential for row crop cultivation. *Geoderma* **2014**, *219–220*, 89–105, doi:10.1016/j.geoderma.2013.12.023.
- Arnold, J.G.; Srinivasan, R.; Muttiah, R.S.; Williams, J.R. Large area hydrologic modeling and assessment part I: Model development. *J. Am. Water Resour. Assoc.* **1998**, *34*, 73–89, doi:10.1111/j.1752-1688.1998.tb05961.x.
- Jang, S.S.; Ahn, S.R.; Kim, S.J. Evaluation of executable best management practices in Haean highland agricultural catchment of South Korea using SWAT. *Agric. Water Manag.* **2017**, *180*, 224–234.
- Fujisaka, S. Learning from six reasons why farmers do not adopt innovations intended to improve sustainability of upland agriculture. *Agric. Syst.* **1994**, *46*, 409–425, doi:10.1016/0308-521X(94)90104-N.
- Pannell, D.J. Social and economic challenges in the development of complex farming systems. *Agrofor. Syst.* **1999**, *45*, 395–411, doi:10.1023/A:1006282614791.
- Poppenborg, P.; Koellner, T. Do attitudes toward ecosystem services determine agricultural land use practices? An analysis of farmers' decision-making in a South Korean watershed. *Land Use Policy* **2013**, *31*, 422–429, doi:10.1016/j.landusepol.2012.08.007.
- Chaplin-Kramer, R.; Sharp, R.P.; Mandle, L.; Sim, S.; Johnson, J.; Butnar, I.; Milà i Canals, L.; Eichelberger, B.A.; Ramler, I.; Mueller, C.; et al. Spatial patterns of agricultural expansion determine impacts on biodiversity and carbon storage. *Proc. Natl. Acad. Sci. USA* **2015**, *112*, 7402–7407, doi:10.1073/pnas.1406485112.
- Chaplin-Kramer, R.; Hamel, P.; Sharp, R.; Kowal, V.; Wolny, S.; Sim, S.; Mueller, C. Landscape configuration is the primary driver of impacts on water quality associated with agricultural expansion. *Environ. Res. Lett.* **2016**, *11*, 074012, doi:10.1088/1748-9326/11/7/074012.
- Lee, T. Analyzing the Effectiveness of a Best Management Practice on Sediment Yields Using a Spatially Distributed Model. *J. Korean Geogr. Soc.* **2017**, *52*, 15–24.
- Polasky, S.; Nelson, E.; Camm, J.; Csuti, B.; Fackler, P.; Lonsdorf, E.; Montgomery, C.; White, D.; Arthur, J.; Garber-Yonts, B.; et al. Where to put things? Spatial land management to sustain biodiversity and economic returns. *Biol. Conserv.* **2008**, *141*, 1505–1524, doi:10.1016/j.biocon.2008.03.022.

- Dillaha, T.A.; Reneau, R.B.; Mostaghimi, S.; Lee, D. Vegetative Filter Strips for Agricultural Nonpoint Source Pollution Control. *Trans. ASAE* **1989**, *32*, 513–519, doi:10.13031/2013.31033.
- Delgado, A.N.; Periago, E.L.; Viqueira, F.D.F. Vegetated filter strips for wastewater purification: A review. *Bioresour. Technol.* **1995**, *51*, 13–22, doi:10.1016/0960-8524(94)00113-F.
- Muñoz-Carpena, R.; Parsons, J.E.; Gilliam, J.W. Modeling hydrology and sediment transport in vegetative filter strips. *J. Hydrol.* **1999**, *214*, 111–129, doi:10.1016/S0022-1694(98)00272-8.
- Shope, C.L.; Maharjan, G.R.; Tenhunen, J.; Seo, B.; Kim, K.; Riley, J.; Arnhold, S.; Koellner, T.; Ok, Y.S.; Peiffer, S.; et al. Using the SWAT model to improve process descriptions and define hydrologic partitioning in South Korea. *Hydrol. Earth Syst. Sci.* **2014**, *18*, 539–557, doi:10.5194/hess-18-539-2014.
- Park, S.; Oh, C.; Jeon, S.; Jung, H.; Choi, C. Soil erosion risk in Korean watersheds, assessed using the revised universal soil loss equation. *J. Hydrol.* **2011**, *399*, 263–273, doi:10.1016/j.jhydrol.2011.01.004.
- Bartsch, S.; Peiffer, S.; Shope, C.L.; Arnhold, S.; Jeong, J.J.; Park, J.H.; Eum, J.; Kim, B.; Fleckenstein, J.H. Monsoonal-type climate or land-use management: Understanding their role in the mobilization of nitrate and DOC in a mountainous catchment. *J. Hydrol.* **2013**, *507*, 149–162, doi:10.1016/j.jhydrol.2013.10.012.
- Ha, K.J.; Park, S.K.; Kim, K.Y. On interannual characteristics of Climate Prediction Center merged analysis precipitation over the Korean peninsula during the summer monsoon season. *Int. J. Climatol.* **2005**, *25*, 99–116, doi:10.1002/joc.1116.
- Jung, I.W.; Bae, D.H.; Kim, G. Recent trends of mean and extreme precipitation in Korea. *Int. J. Climatol.* **2011**, *31*, 359–370, doi:10.1002/joc.2068.
- Seo, B.; Bogner, C.; Poppenborg, P.; Martin, E.; Hoffmeister, M.; Jun, M.; Koellner, T.; Reineking, B.; Shope, C.L.; Tenhunen, J. Deriving a per-field land use and land cover map in an agricultural mosaic catchment. *Earth Syst. Sci. Data* **2014**, *6*, 339–352, doi:10.5194/essd-6-339-2014.
- Jeon, M.S.; Kang, J.W. *Muddy Water Management and Agricultural Development Measures in the Watershed of Soyang Dam: Focused on Haean-myeon, Yanggu-gun*; Technical Report; Research Institute of Gangwon: Chuncheon, Republic of Korea, 2010.

- Morgan, R.P.C.; Morgan, D.D.V.; Finney, H.J. A predictive model for the assessment of soil erosion risk. *J. Agric. Eng. Res.* **1984**, *30*, 245–253, doi:10.1016/S0021-8634(84)80025-6.
- Morgan, R.P.C. A simple approach to soil loss prediction: A revised Morgan–Morgan–Finney model. *CATENA* **2001**, *44*, 305–322, doi:10.1016/S0341-8162(00)00171-5.
- Vigiak, O.; Okoba, B.O.; Sterk, G.; Groenenberg, S. Modelling catchment-scale erosion patterns in the East African Highlands. *Earth Surf. Process. Landf.* **2005**, *30*, 183–196, doi:10.1002/esp.1174.
- Morgan, R.P.C.; Duzant, J.H. Modified MMF (Morgan–Morgan–Finney) model for evaluating effects of crops and vegetation cover on soil erosion. *Earth Surf. Process. Landf.* **2008**, *32*, 90–106, doi:10.1002/esp.1530.
- Lilhare, R.; Garg, V.; Nikam, B. Application of GIS-Coupled Modified MMF Model to Estimate Sediment Yield on a Watershed Scale. *J. Hydrol. Eng.* **2014**, *20*, C5014002, doi:10.1061/(ASCE)HE.1943-5584.0001063.
- Choi, K.; Huwe, B.; Reineking, B. Commentary on “Modified MMF (Morgan–Morgan–Finney) model for evaluating effects of crops and vegetation cover on soil erosion” by Morgan and Duzant (2008). *arXiv* **2016**, arXiv:physics.geo-ph/1612.08899 (accessed on 5 May 2019).
- ORNL DAAC. *MODIS Collection 5 Land Products Global Subsetting and Visualization Tool*; ORNL DAAC: Oak Ridge, TN, USA. Available online: <https://doi.org/10.3334/ORNLDAAC/1379> (accessed on 9 June 2017).
- Schaap, M.G.; Leij, F.J.; van Genuchten, M.T. ROSETTA: A computer program for estimating soil hydraulic parameters with hierarchical pedotransfer functions. *J. Hydrol.* **2001**, *251*, 163–176, doi:10.1016/S0022-1694(01)00466-8.
- ORNL DAAC. *MODIS Collection 6 Land Products Global Subsetting and Visualization Tool*; ORNL DAAC: Oak Ridge, TN, USA. Available online: <https://doi.org/10.3334/ORNLDAAC/1557> (accessed on 14 November 2017).
- Didan, K. *MOD13Q1 MODIS/Terra Vegetation Indices 16-Day L3 Global 250m SIN Grid V006*; NASA EOSDIS Land Processes DAAC: Oak Ridge, TN, USA, 2015.
- Gutman, G.; Ignatov, A. The derivation of the green vegetation fraction from NOAA/AVHRR data for use in numerical weather prediction models. *Int. J. Remote Sens.* **1998**, *19*, 1533–1543, doi:10.1080/014311698215333.

- Rural Development Administration of South Korea. Agric. Technol. Portal (Nongsaro). 2018. Available online: <http://nongsaro.go.kr/portal/farmTechMain.ps?menuId=PS00002> (accessed on 31 July 2018).
- Morgan, R.P.C. *Soil Erosion and Conservation*; Blackwell Publishing: Malden, MA, USA, 2005; pp. 45–66.
- Sobol', I.M. Sensitivity Analysis for Nonlinear Mathematical Models. *Math. Model. Comput. Exp.* **1993**, *1*, 407–414.
- Saltelli, A. Making best use of model evaluations to compute sensitivity indices. *Comput. Phys. Commun.* **2002**, *145*, 280–297, doi:10.1016/S0010-4655(02)00280-1.
- Saltelli, A.; Annoni, P.; Azzini, I.; Campolongo, F.; Ratto, M.; Tarantola, S. Variance based sensitivity analysis of model output. Design and estimator for the total sensitivity index. *Comput. Phys. Commun.* **2010**, *181*, 259–270, doi:10.1016/j.cpc.2009.09.018.
- Nossent, J.; Elsen, P.; Bauwens, W. Sobol' sensitivity analysis of a complex environmental model. *Environ. Model. Softw.* **2011**, *26*, 1515–1525, doi:10.1016/j.envsoft.2011.08.010.
- Qi, W.; Zhang, C.; Chu, J.; Zhou, H. Sobol's sensitivity analysis for TOPMODEL hydrological model: A case study for the Biliu River Basin, China. *J. Hydrol. Environ. Res.* **2013**, *1*, 1–10.
- Saltelli, A.; Annoni, P. How to avoid a perfunctory sensitivity analysis. *Environ. Model. Softw.* **2010**, *25*, 1508–1517, doi:10.1016/j.envsoft.2010.04.012.
- Brooks, E.S.; Boll, J.; McDaniel, P.A. A hillslope-scale experiment to measure lateral saturated hydraulic conductivity. *Water Resour. Res.* **2004**, *40*, W04208, doi:10.1029/2003WR002858.
- Iooss, B.; Janon, A.; Pujol, G.; Boumhaout, K.; Veiga, S.D.; Delage, T.; Fruth, J.; Gilquin, L.; Guillaume, J.; Le Gratiet, L.; et al. *Sensitivity: Global Sensitivity Analysis of Model Outputs*; R package version 1.15.1; 2018. Available online: <https://CRAN.R-project.org/package=sensitivity> (accessed on 8 August 2018).
- R Core Team. *R: A Language and Environment for Statistical Computing*; R Foundation for Statistical Computing: Vienna, Austria, 2018.
- Storn, R.; Price, K. Differential Evolution—A Simple and Efficient Heuristic for global Optimization over Continuous Spaces. *J. Glob. Optim.* **1997**, *11*, 341–359, doi:10.1023/A:1008202821328.

- Price, K.V.; Storn, R.M.; Lampinen, J.A. *Differential Evolution—A Practical Approach to Global Optimization*; Springer: Berlin/Heidelberg, Germany, 2006.
- Ardia, D.; Mullen, K.M.; Peterson, B.G.; Ulrich, J. ‘DEoptim’: *Differential Evolution in ‘R’*, version 2.2-4; 2016. Available online: <https://cran.r-project.org/web/packages/DEoptim> (accessed on 5 May 2019).
- Joseph, J.F.; Guillaume, J.H.A. Using a parallelized MCMC algorithm in R to identify appropriate likelihood functions for SWAT. *Environ. Model. Softw.* **2013**, *46*, 292–298, doi:10.1016/j.envsoft.2013.03.012.
- Zheng, F.; Zecchin, A.C.; Simpson, A.R. Investigating the run-time searching behavior of the differential evolution algorithm applied to water distribution system optimization. *Environ. Model. Softw.* **2015**, *69*, 292–307, doi:10.1016/j.envsoft.2014.09.022.
- Mullen, K.; Ardia, D.; Gil, D.; Windover, D.; Cline, J. DEoptim: An R Package for Global Optimization by Differential Evolution. *J. Stat. Softw.* **2011**, *40*, 1–26, doi:10.18637/jss.v040.i06.
- Nash, J.E.; Sutcliffe, J.V. River flow forecasting through conceptual models part I—A discussion of principles. *J. Hydrol.* **1970**, *10*, 282–290, doi:10.1016/0022-1694(70)90255-6.
- Moriasi, D.N.; Arnold, J.G.; Van Liew, M.W.; Bingner, R.L.; Harmel, R.D.; Veith, T.L. Model evaluation guidelines for systematic quantification of accuracy in watershed simulations. *Trans. ASABE* **2007**, *50*, 885–900, doi:10.13031/2013.23153.
- Moriasi, D.N.; Gitau, M.W.; Pai, N.; Daggupati, P. Hydrologic and Water Quality Models: Performance Measures and Evaluation Criteria. *Trans. ASABE* **2015**, *58*, 1763–1785, doi:10.13031/trans.58.10715.
- Mauricio Zambrano-Bigiarini. *hydroGOF: Goodness-of-Fit Functions for Comparison of Simulated and Observed Hydrological Time Series*; R Package Version 0.3-10; 2017. Available online: <https://cran.r-project.org/web/packages/hydroGOF> (accessed on 5 May 2019).
- OECD. *Environmental Indicators for Agriculture: Methods and Results*, volume 3; OECD Publishing: Paris, France, 2001.
- OECD. *Environmental Performance of Agriculture in OECD Countries Since 1990*; OECD Publishing: Paris, France, 2008.

- Tucker, G.E.; Whipple, K.X. Topographic outcomes predicted by stream erosion models: Sensitivity analysis and intermodel comparison. *J. Geophys. Res. Solid Earth* **2002**, *107*, 1–16, doi:10.1029/2001JB000162.
- Neitsch, S.L.; Arnold, J.G.; Kiniry, J.R.; Williams, J.R. *Soil and Water Assessment Tool Theoretical Documentation Version 2009*; Technical Report; Texas Water Resources Institute: College station, TX, USA. 2011.
- Lee, J.Y. A Hydrological Analysis of Current Status of Turbid Water in Soyang River and Its Mitigation. *J. Soil Groundw. Environ.* **2008**, *13*, 85–92.
- Kim, J.H.; Choi, H.T.; Lim, H.G. Analysis of Suspended Solid Generation with Rainfall-Runoff Events in a Small Forest Watershed. *J. Environ. Sci. Int.* **2015**, *24*, 1617–1627, doi:10.5322/JESI.2015.24.12.1617.
- Gellis, A.C. Factors influencing storm-generated suspended-sediment concentrations and loads in four basins of contrasting land use, humid-tropical Puerto Rico. *CATENA* **2013**, *104*, 39–57, doi:10.1016/j.catena.2012.10.018.
- Vercruyssen, K.; Grabowski, R.C.; Rickson, R.J. Suspended sediment transport dynamics in rivers: Multi-scale drivers of temporal variation. *Earth Sci. Rev.* **2017**, *166*, 38–52, doi:10.1016/j.earscirev.2016.12.016.
- Lee, J.M.; Park, Y.S.; Kum, D.; Jung, Y.; Kim, B.; Hwang, S.J.; Kim, H.B.; Kim, C.; Lim, K.J. Assessing the effect of watershed slopes on recharge/baseflow and soil erosion. *Paddy Water Environ.* **2014**, *12*, 169–183, doi:10.1007/s10333-014-0448-9.
- Lim, K.J.; Sagong, M.; Engel, B.A.; Tang, Z.; Choi, J.; Kim, K.S. GIS-based sediment assessment tool. *CATENA* **2005**, *64*, 61–80, doi:10.1016/j.catena.2005.06.013.
- Cooper, J.R.; Gilliam, J.W.; Daniels, R.B.; Robarge, W.P. Riparian Areas as Filters for Agricultural Sediment. *Soil Sci. Soc. Am. J.* **1987**, *51*, 416–420, doi:10.2136/sssaj1987.03615995005100020029x.
- Osborne, L.L.; Kovacic, D.A. Riparian vegetated buffer strips in water-quality restoration and stream management. *Freshwater Biol.* **1993**, *29*, 243–258, doi:10.1111/j.1365-2427.1993.tb00761.x.
- Tollner, E.W.; Barfield, B.J.; Haan, C.T.; Kao, T.Y. Suspended Sediment Filtration Capacity of Simulated Vegetation. *Trans. ASAE* **1976**, *19*, 678–682, doi:10.13031/2013.36095.

Meyer, L.D.; Wischmeier, W.H. Mathematical simulation of the process of soil erosion by water.  
*Trans. ASAE* **1969**, *12*, 754–758, doi:10.13031/2013.38945.

## Chapter 5

# Environmental drivers of spatial patterns of topsoil nitrogen and phosphorus under monsoon conditions in a complex terrain of South Korea

Gwanyong Jeong <sup>1,#,\*</sup>, Kwanghun Choi <sup>2</sup>, Marie Spohn <sup>3</sup>, Soo Jin Park <sup>4</sup>, Bernd Huwe <sup>1</sup>, Mareike Ließ <sup>5</sup>

<sup>1</sup> Department of Geosciences/ Soil Physics Division, Bayreuth Center of Ecology and Environmental Research (BayCEER), University of Bayreuth, Bayreuth, Germany

<sup>2</sup> Biogeographical Modelling, Bayreuth Center of Ecology and Environmental Research (BayCEER), University of Bayreuth, Bayreuth, Germany

<sup>3</sup> Department of Soil Ecology, Bayreuth Center of Ecology and Environmental Research (BayCEER), University of Bayreuth, Bayreuth, Germany

<sup>4</sup> Department of Geography, Seoul National University, Shilim-dong, Kwanak-gu, Seoul, South Korea

<sup>5</sup> Department of Soil Physics, Helmholtz Centre for Environmental Research UFZ, Halle, Germany

# Current Address: Department of Geography, Chonnam National University, Yongbong-ro, Buk-gu, Gwangju, South Korea

Correspondence: gyjeong@jnu.ac.kr

### Abstract

Nitrogen (N) and phosphorus (P) in topsoils are critical for plant nutrition. Relatively little is known about the spatial patterns of N and P in the organic layer of mountainous landscapes. Therefore, the spatial distributions of N and P in both the organic layer and the A horizon were analyzed using a light detection and ranging (LiDAR) digital elevation model and vegetation metrics. The objective of the study was to analyze the effect of vegetation and topography on the spatial patterns of N

and P in a small watershed covered by forest in South Korea. Soil samples were collected using the conditioned Latin hypercube method. LiDAR vegetation metrics, the normalized difference vegetation index (NDVI), and terrain parameters were derived as predictors. Spatial explicit predictions of N/P ratios were obtained using a random forest with uncertainty analysis. We tested different strategies of model validation (repeated 2-fold to 20-fold and leave-one-out cross validation).

Repeated 10-fold cross validation was selected for model validation due to the comparatively high accuracy and low variance of prediction. Surface curvature was the best predictor of P contents in the organic layer and in the A horizon, while LiDAR vegetation metrics and NDVI were important predictors of N in the organic layer. N/P ratios increased with surface curvature and were higher on the convex upper slope than on the concave lower slope. This was due to P enrichment of the soil on the lower slope and a more even spatial distribution of N. Our digital soil maps showed that the topsoils on the upper slopes contained relatively little P. These findings are critical for understanding N and P dynamics in mountainous ecosystems.

## 5.1 Introduction

Nitrogen (N) and phosphorus (P) are the most important nutrients for primary productivity in terrestrial ecosystems (Vitousek *et al.*, 2002, 2010). Soil nutrient content varies during long-term soil development, such that N increases while P declines during the course of pedogenesis. This is because N enters the ecosystem via N-fixing microorganisms, whereas P is derived from the weathering of minerals. As a result, primary productivity is initially N-limited in lightly weathered soils but becomes increasingly P-limited in highly weathered soils over millions of years (Laliberté *et al.*, 2013).

P limitation is enhanced by atmospheric N deposition (Vitousek *et al.*, 2010, Braun *et al.*, 2010). In East Asia, where the population and economy are growing rapidly, atmospheric N deposition is currently very high (Manning, 2012). In South Korea, atmospheric N inputs have rapidly increased due to large industrial operations and agricultural intensification (Jang *et al.*, 2011, Kim *et al.*, 2014, 2011). The annual average wet input of N ranged from 12.9 to 24.9 kg ha<sup>-1</sup> year<sup>-1</sup> from 2005 to 2010 (Jang *et al.*, 2011), and is markedly higher than that during pre-industrial times. This might have effects on the productivity, biodiversity, and community composition of plants (Turner, 2008).

An understanding of nutrient contents in the organic layer is critical for mountainous ecosystem management. Organic layers are made up of freshly fallen organic matter, including whole leaves, twigs, and fruits. Following mineralization of organic matter, the organic layer slowly

supplies nutrients, which are absorbed by plant roots (Osman, 2013). Therefore, nutrients that are returned to soil by litterfall are important for plant nutrition (Huang and Spohn, 2015). In particular, the N/P ratio in topsoil is used as an indicator of potential growth limitation (Cleveland and Liptzin, 2007), and the spatial patterns of nutrients in the organic layer and in the A horizon can provide insight into soil-vegetation relationships.

Many studies have assessed spatial patterns of soil N (Peng *et al.*, 2013, Liu *et al.*, 2013, Kunkel *et al.*, 2011) and P (Kim *et al.*, 2014, Roger *et al.*, 2014, McKenzie and Ryan, 1999). Previous studies on mountain ecosystems have found environmental correlations between the N contents in the organic layer and topographic parameters in a temperate forested watershed (Johnson *et al.*, 2000) and in boreal forests (Seibert *et al.*, 2007). Wilcke *et al.* (2008) reported an elevation gradient of decreasing N and P content in organic layers, and Soethe *et al.* (2008) found that the N stocks of the organic layer differ significantly between different elevations in tropical mountain forests. However, our understanding of quantitative relationships between the content of nutrients (especially P) in the organic layer, topography, and vegetation is limited. In this regard, recent advances in digital soil mapping (DSM) have allowed us to improve our knowledge on spatial patterns of N and P and their environmental controls.

DSM often uses topographical predictors derived from digital elevation models (DEM), such as elevation, slope angle, curvature, and wetness index (McBratney *et al.*, 2003, Grunwald, 2005). According to Ballabio (2009), maps of soil properties can be produced with good accuracy using only terrain parameters as predictors in mountainous areas. In addition, vegetation data might improve DSM results, especially for the organic layer since it strongly depends on the vegetation (Dan Binkley, 2012). Various vegetation parameters derived from satellite images have helped to explain the spatial variability of soil nutrients when used as DSM predictors (Grunwald *et al.*, 2015, Mulder *et al.*, 2011). However, to our knowledge, no attempt has been made to use Light detection and ranging (LiDAR) derived vegetation metrics for the spatial predictions of soil properties.

LiDAR-derived vegetation metrics could extend our understanding of spatial soil data by providing insight into the relationship between soils and vegetation as they are related to the vegetation's vertical variability, which reflects forest structure metrics (Jones and Vaughan, 2010). Canopy cover percentage and maximum height can indicate the above ground biomass and forest productivity (Zellweger *et al.*, 2015). LiDAR predictors may also act as ecological indicators, such as light condition on the forest floor (Zellweger *et al.*, 2015). LiDAR intensity varies with land cover and forest types (Ørka *et al.*, 2009). Additionally, LiDAR predictors are high-resolution data, which provide more detailed spatial information than can be obtained

from other types of remote sensing data (e.g., Aster [15 m] or Landsat [30 m] images). The normalized difference vegetation index (NDVI) and LiDAR data are expected to be important for N predictions related to forest biomass, but most probably not for P since it is assumed to mainly originate from bedrock.

LiDAR DEM could also be useful for predicting the spatial distributions of soil nutrients, especially P. P in soils tends to be fixed into stable forms as iron, aluminium, and calcium combinations (Walker and Syers, 1976). Most P in soils is lost by soil erosion and is moved along surface configuration (Smeck, 1985). The LiDAR DEM can provide high resolution information on topography which might benefit the investigation of spatial P patterns.

To better understand the spatial patterns of N and P in the organic layer and mineral topsoil, the aim of this study was to use high-resolution LiDAR data and the derived DEM and vegetation metrics to predict topsoil N and P content by a DSM regression approach. The specific objectives of our research were: (1) to test the importance of LiDAR-derived vegetation and topographical parameters to understand the spatial patterns of N and P; (2) to identify subareas with critical P contents; and (3) to test different validation strategies for N and P.

## 5.2 Materials and methods

### 5.2.1 Research area

The study area has a size of 9.84 km<sup>2</sup> and is located in the downstream area of the Soyang lake watershed, Gangwon province, South Korea (Fig 5.1). The mean annual air temperature

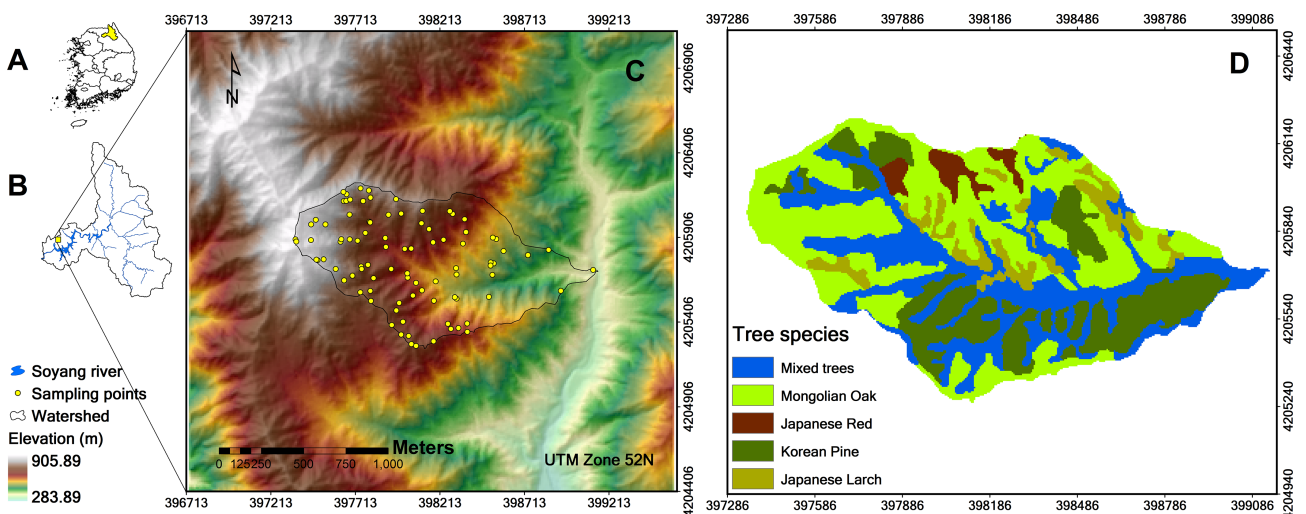


Fig. 5.1. **Research area.** (A) The Soyang watershed within South Korea. (B) The research area within the Soyang watershed. (C) The research area with the sampling points. (D) The tree species map (fgis.forest.go.kr).

of the study area is 11.1 °C and it receives a mean annual rainfall of 1,347 mm with about 70% of the annual rain (824.4 mm) falling in the summer monsoon season (June, July, and August) (Korea meteorological administration, 2015). The area's bedrock is part of the Gyeonggi gneiss complex, which consists of granitic gneiss and banded gneiss (Korea Institute of Geology, Mining, and Material, 2001) formed in the Paleoproterozoic and belonging to the oldest basement rocks in the Korean Peninsula (Chough, 2013). The elevation ranges between 320 and 868 m above sea level and the area consists of various steep slopes (over 45°) caused by a tectonic uplift that occurred during the Quaternary Period (Lee, 2004). The area is a headwater catchment with narrow depositional areas and valleys, and plays an important role in the biogeochemical cycle of the downstream hydrological system as a key source of nutrients (Wohl, 2000). Its soils are mainly composed of fine gravelly sandy loam soils, fine sandy loam, and gravelly loam soils (National Academy of Agricultural Science). The area is part of a national forest and the main tree species are Mongolian oak (*Quercus mongolica*; 40-50 years) and Korean pine (*Pinus koraiensis*; 30-35 years), locally vegetated with Japanese red pine (*Pinus densiflora*) and Japanese larch (*Larix kaempferi*) (Fig 5.1).

### 5.2.2 Soil sampling and chemical analyses

Soil samples were collected from the organic layer and the A horizon at 91 sampling sites in 2014. Spatial position information of sampling points was recorded with a Qmini H3 global navigation satellite system (GNSS) GPS (accuracy within 5 m). Field studies were carried out under research permission from the Korea Forest Service of Chuncheon. We confirm that the field studies did not involve endangered or protected species. Conditioned Latin Hypercube Sampling (cLHS) was applied to optimize the density functions of the n-dimensional covariate space for the regression models (Minasny and McBratney, 2006). This is a stratified random sampling approach that divides the empirical density functions of the predictor space into quantiles based on the number of samples. In order to obtain a Latin hypercube of exactly one sample per quantile for each of the predictors, an optimization approach is used. In the R package “clhs” (Roudier *et al.*, 2012), this is achieved by simulated annealing.

The organic layer had an average depth of 5 cm and was sampled using a metal frame of 0.3 × 0.3 m. The A horizon of the mineral soil was sampled using a shovel according to the depth of the A horizon, which differed between 10 and 30 cm. Mineral soil samples were air-dried and sieved (< 2 mm). The organic layer samples were oven-dried. Total P was extracted with HNO<sub>3</sub> and HF and measured according to DIN EN ISO 11885 / 22036 (Deutsche Einheitsverfahren

zu Wasser, 2002) by ICP-OES (Perkin Elmer, 2100 ZL, USA). After grinding to a fine powder, total N was measured by an elemental analyzer NA 1108 (CE Instruments, Milano, Italy). N/P ratios were calculated based on mass.

### 5.2.3 Environmental predictors

LiDAR is a remote sensing technology, which provides structural information on the illuminated surface, including the 3D terrain, vegetation canopy information, and object heights (Franklin, 2010). Point data, including x, y, and z coordinates, can be converted to a digital terrain model and a digital surface model (Hyypä *et al.*, 2008). The laser emits short pulses of light and the sensor records several returns from leaves, branches, and the underlying ground surface (Jones and Vaughan, 2010). Vegetation heights can be derived from the difference between the ground and the non-ground returns (Jones and Vaughan, 2010). LiDAR also generates intensity data, reflecting characteristics of objects, which can provide useful information on forest types and tree species (Ørka *et al.*, 2009). Detailed overviews are provided by Asner *et al.* (2015) and Hyypä *et al.* (2015).

We used LiDAR point data which has a vertical accuracy of below 10 cm and an average of 4.08 points/m<sup>2</sup>, surveyed by the National Geographic Information Institute (NGII) in South Korea (National Geographic Information Institute, 2015). The point data were pre-processed to identify ground returns, classify all returns, and calculate the normalized vegetation heights. Furthermore, we calculated a set of forest structural predictors using the LAStools software which provides a wide variety of methods to process LiDAR data (Isenburg, 2014) (Table 5.1). First, the ground and non-ground points were classified using the lasground module of LAStools.

Table 5.1. Environmental predictors for digital soil mapping.

| Predictor                                       | Method  | Reference                     |
|---|---|-------------------------------|
| 1 Elevation (ELEV)                              | Las2dem LAStools module   | Isenburg (2014)               |
| 2 Slope degree (SLO)                            | Slope, aspect, curvature SAGA module                            | Zevenbergen and Thorne (1987) |
| 3 Catchment area (CA)                           | Catchment area (Parallel) SAGA module (Multiple flow direction) | Freeman (1991)                |
| 4 SAGA topographical wetness index (STWI)       | SAGA wetness index SAGA module                                  | Böhner <i>et al.</i> (2002)   |
| 5 Surface curvature (CUR19)                     | CURV3 program   | Park <i>et al.</i> (2001)     |
| 6 Normalized difference vegetation index (NDVI) | (NIR-Red) / (NIR+Red)   | Tucker and Sellers (1986)     |
| 7 Maximum height (Hmax)                         | Lascanopy LAStools module                                       | Isenburg (2014)               |
| 8 Canopy cover percentage (Hccp)                | Lascanopy LAStools module                                       | Isenburg (2014)               |
| 9 Standard deviation of heights (Hstd)          | Lascanopy LAStools module                                       | Isenburg (2014)               |
| 10 Forest canopy and height (Hch)               | Canopy cover percentage (Hccp) × maximum height (Hmax)          | -                             |
| 11 First return intensity average (Hfiravg)     | Lasgrid LAStools module   | Isenburg (2014)               |

Note: NIR, near-infrared.

Then, the ground points were used to produce a digital elevation model with the las2dem module, and heights of non-ground points were calculated using the lasheight module. Finally, LiDAR vegetation metrics were derived using the lascanopy module. The maximum height (Hmax) was

computed from the maximum point height within a grid cell. Variations of all vegetation point heights within a grid cell were converted to the standard deviation of heights (Hstd), which indicates the structural diversity of the forest. The canopy cover (Hccp) was calculated as the number of LiDAR first returns greater than the cover cutoff (1.37 m by default) divided by the total number of first returns (Isenburg, 2014). NDVI was derived from a 4-m Kompsat-2 image obtained on 11th October 2014 (Jensen, 2015, Thenkabail *et al.*, 2011). We selected the clear-sky image taken at the similar time as the field survey.

Most topographical predictors were calculated with the terrain analysis modules of the open source software SAGA based on the LiDAR DEM (Conrad *et al.*, 2015). In addition, surface curvature, which reflects the degree of bending of the three-dimensional surface morphology, was calculated with the CURV3 program (Park *et al.*, 2001). To consider the variability of surface configuration, surface curvature values were calculated with different search window sizes of  $3 \times 3$  to  $35 \times 35$  cells. The one with the highest Pearson's correlation coefficient with the response variables N and P was finally selected as a predictor:  $19 \times 19$  cells (CUR19). All predictors were converted to 10-m cell size via the nearest neighbor resampling method.

#### 5.2.4 Random forest

Random forest (RF) is an ensemble learning method that operates by building a set of regression trees and averaging the results (Breiman, 2001). Each tree is built using bootstrap samples of the data and a subset of predictors. Providing the number of trees is large, the overall accuracy (out-of-bag error) of the RF converges (Breiman, 2001). Accordingly, the number of trees was set to 1000. The size of the predictor subset (mtry) was tuned by the R package “caret” (Kuhn and Johnson, 2013). The R package “randomForest” (Breiman, 2001) was employed as a dependency.

RF is able to model complex nonlinear relationships between soil properties and environmental predictors. It is easier to apply than other supervised learning methods (e.g., neural networks and support vector regression) and does not require much tuning (Kuhn and Johnson, 2013, Strobl *et al.*, 2009, Kampichler *et al.*, 2010). It also has a better interpretability due to the provision of a predictor importance measure. For this measure, the predictor values are permuted. The importance is then determined by the difference in mean square error before and after permutation (Strobl *et al.*, 2009). Overall, RF has demonstrated good performance in DSM applications (Kim *et al.*, 2014, Grimm *et al.*, 2008, Wiesmeier *et al.*, 2011, Tesfa *et al.*, 2009, Ließ *et al.*, 2011).

Predictor selection is reported to influence model performance (Brungard *et al.*, 2015, Miller *et al.*, 2015, Poggio *et al.*, 2013). Recursive feature elimination (RFE), a backward predictor selection method, begins with all predictors and iteratively eliminates the least important predictors one by one based on an initial measure of RF predictor importance until the best predictor remains (Kuhn and Johnson, 2013). At the end, the optimal number of predictors and the final list of selected predictors are returned. The package “caret” provides the functions for RFE (Kuhn and Johnson, 2013).

To assess model performance,  $R^2$  and root mean square error (RMSE) were calculated. For model validation, we used k-fold cross-validation (CV) where the dataset is randomly partitioned into k subsets; one subset is left out for model validation while the remaining subsets are used for model training. The process is repeated k times (once for each fold) and the k estimates of performance are summarized. In k-fold CV, the choice of k determines the size of the test and training dataset. For example, in the case of 10-fold CV, 10% of the data are used for validation and the remaining 90% are used for calibration. The choice of k is usually 5 or 10; however there is no formal rule (Kuhn and Johnson, 2013). Although the subsets are generated randomly, the subdivision still affects model validation results. This can be acknowledged by repetitions of the k-fold CV. Still, the number of repetitions (n) might also affect the estimated model performance; for example, more repetitions lead to better results (Molinaro *et al.*, 2005). We explored 2-, 5-, 10-, 20-fold, and leave-one-out (LOO) CV in n repetitions to account for a total of 100 validation measures:  $n \times k = 100$ . Ultimately, 100 Rsquares and RMSEs were returned for each soil property. Finally, the cell-wise standard deviation of the corresponding 100 predictions provides an estimate of spatial uncertainty.

## 5.3 Results

### 5.3.1 Descriptive statistics of soil nutrients

Summary statistics for the N and P data are shown in Table 5.2. The mean N value of the organic layer ( $N_o$ ) was higher than that of the A horizon ( $N_a$ ).  $N_o$  had the lowest coefficient of variation (CoV), while total P in the organic layer ( $P_o$ ) showed a relatively higher variance based on the standard deviation and CoV. This indicates that the variability in the N/P ratios in the organic layer ( $N_o/P_o$ ) was dependent on  $P_o$  content, and that there was major P input from the litter fall. The N/P ratio in the A horizon ( $N_a/P_a$ ) showed a higher relative variability than did those in the organic layer, as indicated by the CoV. The mean  $N_o/P_o$  was  $20.83 \pm$

4.82 and the mean  $N_a/P_a$  was  $7.91 \pm 2.42$ .

Table 5.2. Statistical summary of N and P content ( $\text{mg kg}^{-1}$ ) and ratios.

|           | Mean  | SD   | MIN   | Median | MAX   | CoV (%) | Skew | Kurt |
|-----------|-------|------|-------|--------|-------|---------|------|------|
| $N_o$     | 12245 | 1986 | 8000  | 12200  | 17800 | 16.22   | 0.35 | 2.92 |
| $P_o$     | 624   | 190  | 310   | 610    | 1240  | 30.39   | 0.44 | 2.97 |
| $N_a$     | 2990  | 1348 | 700   | 2600   | 7300  | 45.07   | 0.81 | 3.52 |
| $P_a$     | 389   | 171  | 160   | 330    | 920   | 43.96   | 1.40 | 4.52 |
| $N_o/P_o$ | 20.83 | 4.82 | 12.16 | 20.17  | 38.06 | 23.12   | 0.76 | 3.77 |
| $N_a/P_a$ | 7.91  | 2.42 | 1.89  | 7.78   | 13.85 | 30.55   | 0.21 | 3.06 |

Notes:SD, standard deviation; MIN, minimum; MAX, maximum; CoV, coefficient of variation; Skew, skewness; Kurt, kurtosis; N, nitrogen; P, phosphorus;  $_o$ , organic layer; and  $_a$ , A horizon.

### 5.3.2 Model validation

Fig 5.2 and Fig 5.S1 show that with increasing  $k$  in repeated  $k$ -fold CV, mean R-square and RMSE values indicate a better model performance, while R-square and RMSE variance increases as well. Based on mean R-square, the LOO CV results were inferior to the repeated 10-fold and 20-fold, but superior to the repeated 2-fold results. Concerning repeated 5-fold CV, LOO CV was superior for the predictions of the organic layer nutrients, but inferior for the predictions of the mineral soil nutrients. Altogether, mean R-square values were higher for  $P_o$  and  $P_a$  compared to  $N_o$  and  $N_a$  respectively. The results for  $N_o/P_o$  and  $N_a/P_a$  were the worst, but showed the highest increase in model performance (mean R-square) with increasing  $k$ . Fig 5.3 shows the standard deviations of all raster cells according to the 100 spatial predictions resulting from the 100 models from the various CV schemes. The mean standard deviation and the variance of the standard deviations decrease with increasing  $k$  for all models.

As an example, spatial prediction patterns of  $P_o$  including mean values and the standard deviations from the 100 predictions according to the various CV schemes are displayed in Fig 5.4. In particular, spatial patterns of mean  $P_o$  of the repeated 5-, 10-, and 20-fold CV are optically very similar (Fig 5.4C, 5.4E, and 5.4G). Only the results from repeated 2-fold CV (Fig 5.4A) show a comparatively smaller range of mean  $P_o$  values with lower values in the valleys and higher values along ridges. Furthermore, the increase of mean  $P_o$  values with elevation, which was particularly observable in the concave valley for repeated 5-, 10- and 20-fold CV, is less pronounced for repeated 2-fold CV. As already indicated by Fig 5.3, standard deviation values decrease with increasing  $k$  and a correspondingly bigger calibration dataset. The spatial patterns of the standard deviations show an abrupt increase in the concave valley in the lower part of

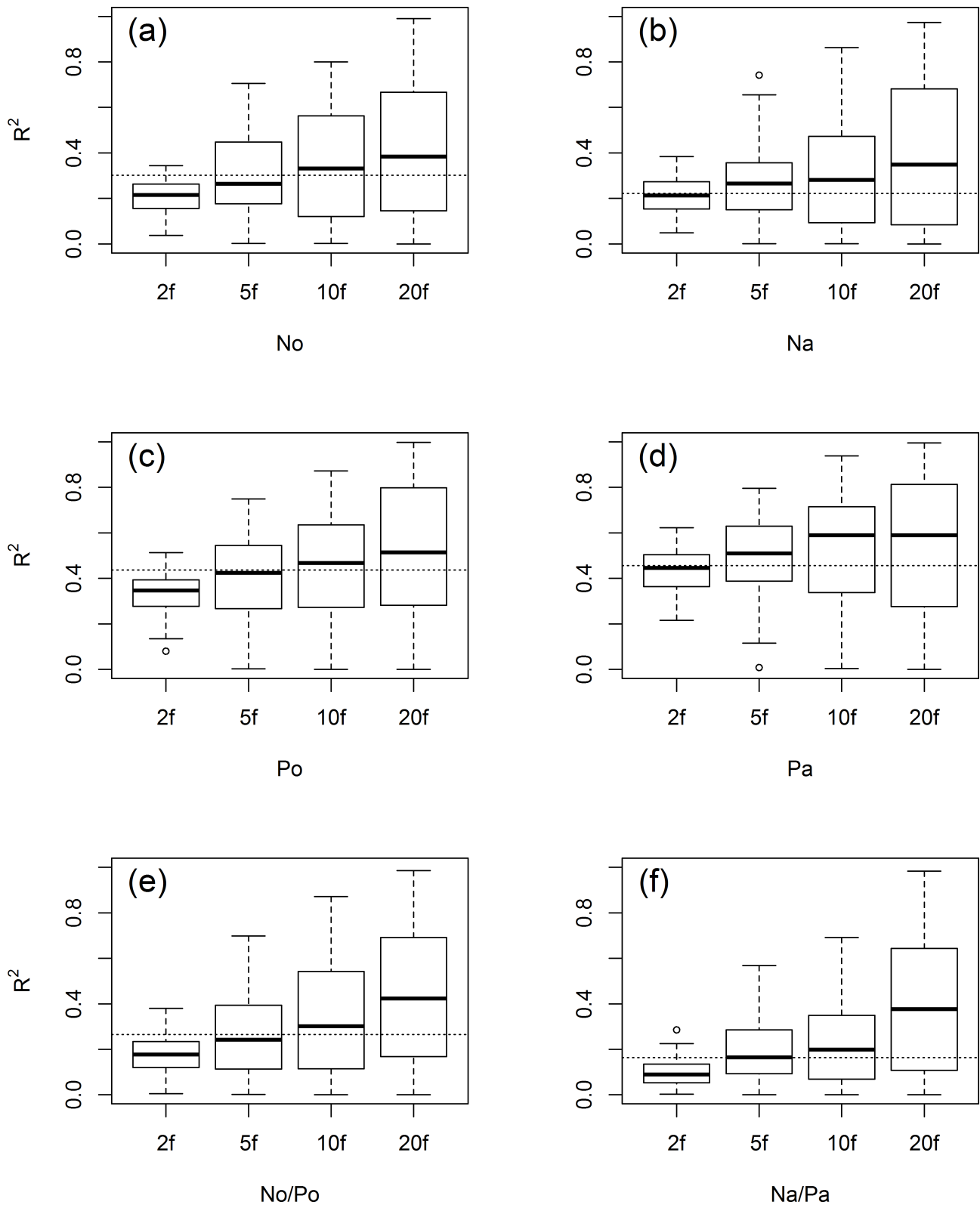


Fig. 5.2. **Model validation based on R-square with cross validation methods.** The dotted lines indicate the leave-one-out cross-validated result. 2f, 2-fold 50 repetitions; 5f, 5-fold 20 repetitions; 10f, 10-fold 10 repetitions; 20f, 20-fold 5 repetitions; N, nitrogen; P, phosphorus; o, organic layer; and a, A horizon.

the study area Fig 5.4B, 5.4D, 5.4F, and 5.4H).

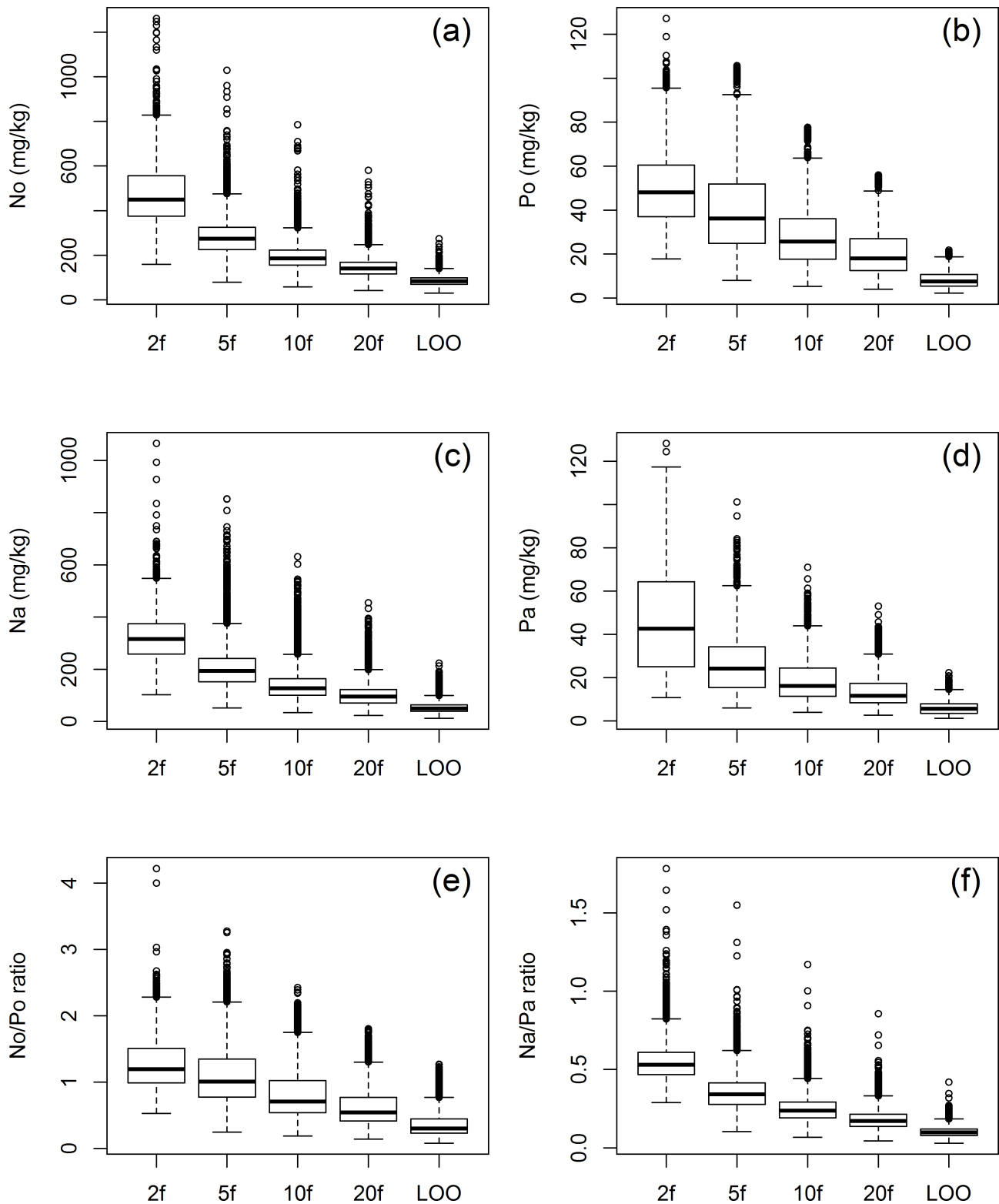


Fig. 5.3. Boxplots showing standard deviations of 100 predicted values for each raster cell with cross validation methods. 2f, 2-fold 50 repetitions; 5f, 5-fold 20 repetitions; 10f, 10-fold 10 repetitions; 20f, 20-fold 5 repetitions; LOO, leave-one-out; N, nitrogen; P, phosphorus; o, organic layer; and a, A horizon.

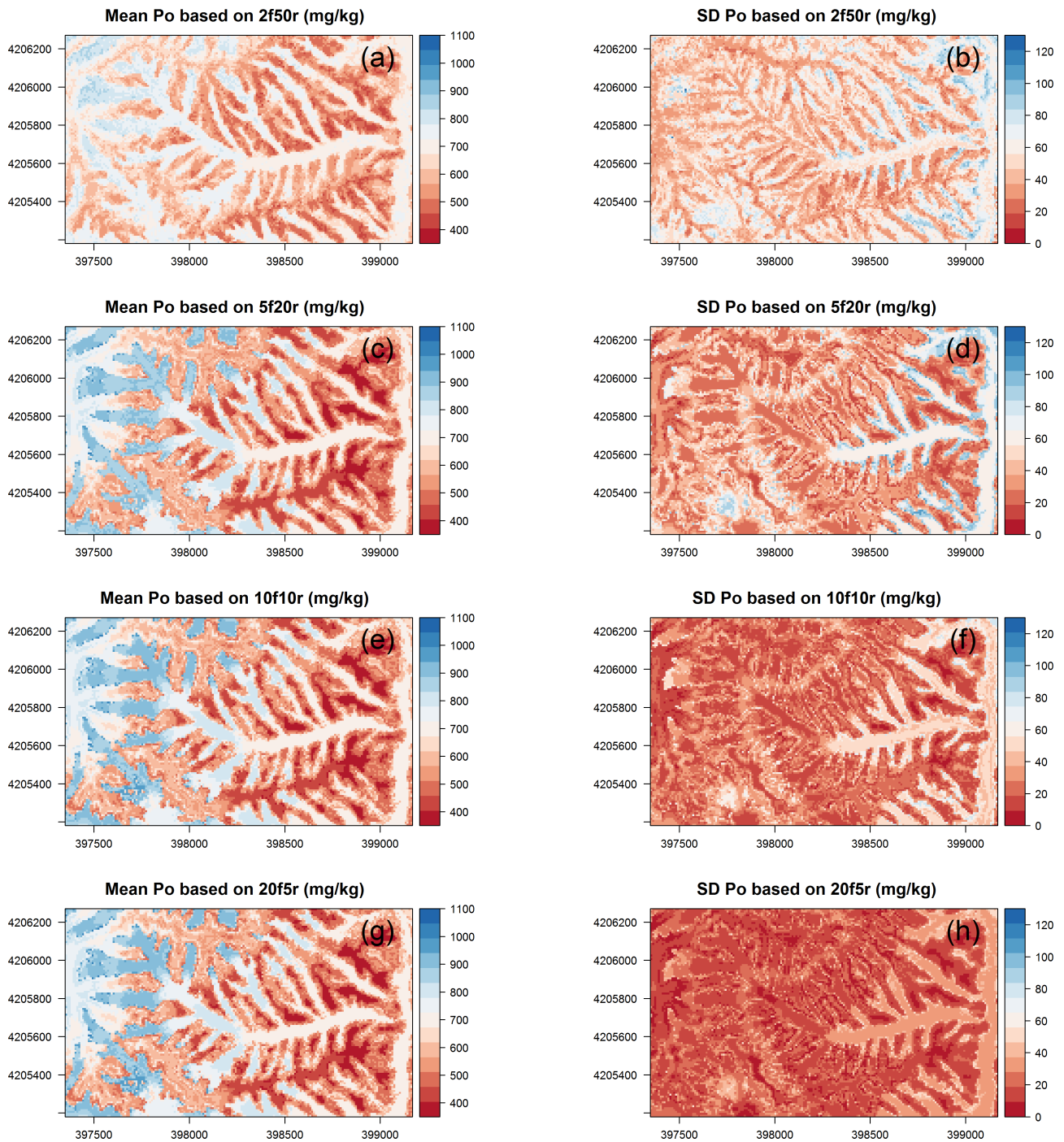


Fig. 5.4. Maps of mean and coefficient of variation (CoV) of 100 models of phosphorus in the organic layer ( $P_o$ ) with cross validation methods. 2f50r, 2-fold 50 repetitions; 5f20r, 5-fold 20 repetitions; 10f10r, 10-fold 10 repetitions; 20f5r, 20-fold 5 repetitions.

### 5.3.3 Environmental drivers of spatial nutrient patterns

To analyze the influence of topography and vegetation on soil nutrients, the results from repeated 10-fold CV are displayed. These correspond to a comparatively good performance for all soil nutrients based on mean R-square, while R-square variance is not as high as for repeated 20-fold CV (Fig 5.2). The predictors selected with RFE are shown in Table 5.3. Surface curvature

and elevation were selected for all soil nutrients. For  $P_o$  and  $P_a$ , they were the only selected predictors. NDVI and LiDAR vegetation predictors (Hfiravg, Hstd, and Hmax) were additionally selected for  $N_o$ . For the N/P ratios parameters corresponding to water flow were additionally selected. While the models for  $N_o/P_o$  in correspondence to  $N_o$  also included vegetation metrics as predictors (Hst, Hmax, and Hch), the model for  $N_a/P_a$  included the NDVI instead. We expected that the tree species influenced the spatial pattern of N/P ratios (Fig 5.1). Tree species were initially also tested as predictors; however, these were not considered important predictors based on previous results. Accordingly, they were excluded due to the simplicity of the model.

Table 5.3. Statistical summary of N and P content ( $\text{mg kg}^{-1}$ ) and ratios.

| Soil properties | Predictors                                   |
|-----------------|--|
| $N_o$           | ELEV, NDVI, Hfiravg, CUR19, STWI, Hstd, Hmax |
| $P_o$           | CUR19, ELEV                                  |
| $N_a$           | ELEV, CUR19                                  |
| $P_a$           | CUR19, ELEV                                  |
| $N_o/P_o$       | CUR19, CA, Hstd, ELEV, Hmax, Hch             |
| $N_a/P_a$       | CUR19, CA, NDVI, ELEV, STWI                  |

Notes: ELEV, elevation; CUR19, surface curvature ( $19 \times 19$  local window); STWI, SAGA topographical wetness index; CA, Catchment area; SLO, slope degree; NDVI, normalized difference vegetation index; Hfiravg, first return intensity average; Hstd, standard deviations of heights; Hmax, maximum height; Hccp, canopy cover percentage; Hch, forest canopy and height ( $\text{Hmax} \times \text{Hccp}$ ); N, nitrogen; P, phosphorus;  $_o$ , organic layer;  $_a$ , A horizon.

Our RF model revealed good performance for all soil nutrients based on  $R^2$  (Fig 5.2). Mean R-square values ranged from 0.23 to 0.52.  $P_a$  showed the best result of the validation, while that of the R-square for  $N_a/P_a$  was lowest. Models for P showed better results than did models for N.

Fig 5.5 shows the mean relative predictor importance of the RF models created by repeated 10-fold CV. Terrain predictors exhibited 5.37-53.07% of the reduction in the mean square error (MSE). Surface curvature was the best or second best predictor for all soil nutrients, with the exception of  $N_o$  (Fig 5.5); contributed 6.50-53.07% of the MSE. Elevation exhibited a similarly high predictor importance: 9.55-39.22%. NDVI and LiDAR derived vegetation metrics (Hstd, Hmax, Hpd, and Hfiravg) were also important predictors for the nutrients. The results showing the RF predictor importance were not consistent with the RFE results; however, the two results were similar and there was no difference in the most important predictors (Table 5.3).

The map of each nutrient displays the mean of the 100 predictions from repeated 10-fold CV (Fig 5.6).  $N_o$  and  $N_a$  content increased with elevation. We found that P content differed

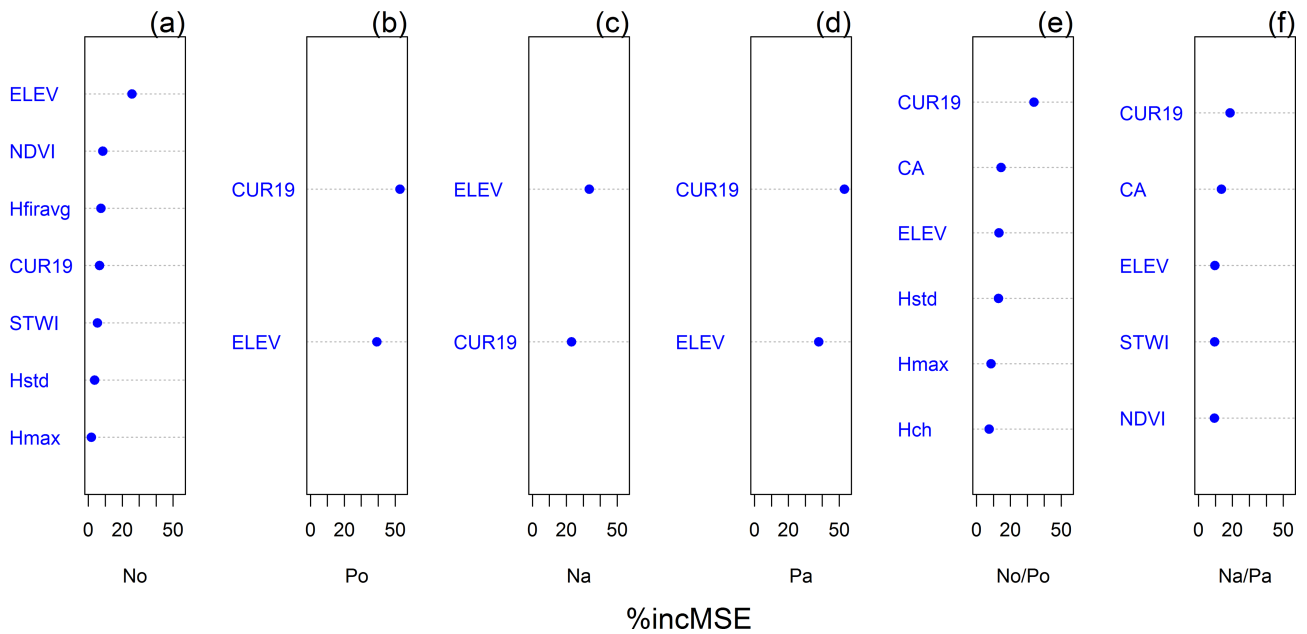


Fig. 5.5. Mean relative importance of predictors for nitrogen and phosphorus based on the increased mean square error (%incMSE) from random forest. N, nitrogen; P, phosphorus; o, organic layer; and a, A horizon.

markedly between the upper and lower slopes.  $N_o/P_o$  and  $N_a/P_a$  were higher on the convex upper slope.

Higher standard deviations of  $P_o$  and  $N_o/P_o$  were found at lower elevations and on the valley floor (Fig 5.S2). The spatial uncertainties of  $P_a$  were higher at the upper part of the catchment. Uncertainties of  $N_o$  (Fig 5.S2) were similarly complex like the spatial pattern of the mean values (Fig 5.6A).

## 5.4 Discussion

### 5.4.1 Predictors of soil N and P

In this study,  $N_o$  ( $r=0.58$ ,  $p<0.001$ ) and  $N_a$  ( $r=0.49$ ,  $p<0.001$ ) were correlated with elevation. Likewise, Bedison and Johnson (2009) also found a strong relationship between  $N_o$  and elevation ( $R^2=0.41$ ,  $P<0.001$ ) in mountainous forested areas in the USA. Additionally, positive relationships between  $N_a$  and elevation were reported by Kunkel *et al.* (2011), Wang *et al.* (2013) and Peng *et al.* (2013). The catchment area (CA) and topographical wetness index (TWI) were important predictors of  $N_o$  in other studies (Johnson *et al.*, 2000, Seibert *et al.*, 2007). In our study, CA and TWI were not significant for  $N_o$ , whereas  $N_a$  was correlated with TWI ( $r=0.26$ ,  $p<0.05$ ). According to Aandahl (1948), higher nitrogen content is found on the lower slope. Higher  $N_a$  was found in areas with high elevation and on the lower slope (Fig 5.6C), which

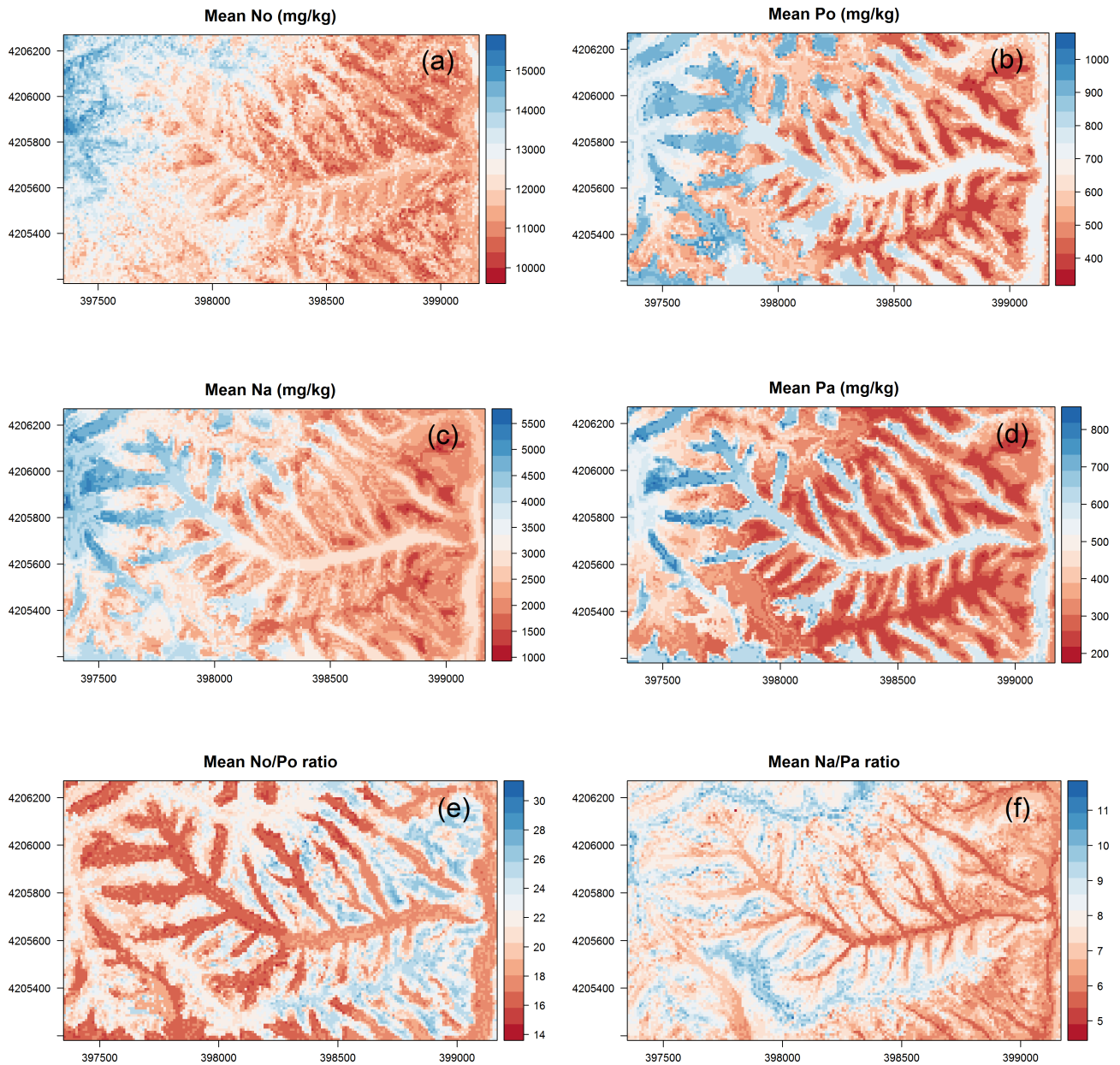


Fig. 5.6. Predicted mean soil N and P content and ratios. N, nitrogen; P, phosphorus; o, organic layer; and a, A horizon.

might have higher productivity (plants and microbes) and therefore, higher nitrogen fixation.

Vegetation can determine the spatial distribution of N in forest ecosystems (Bedison and Johnson, 2009, Zhang *et al.*, 2010). For  $N_o$ , NDVI ranked as the second most important predictor and the LiDAR intensity of first returns (Hfiravg), which is often used as an indicator of forest type (Ørka *et al.*, 2009), was also an important predictor. Although NDVI and LiDAR predictors were not selected as predictors of the  $N_a$  model,  $N_a$  was weakly correlated with maximum height ( $r=0.24$ ,  $p<0.05$ ) and standard deviations of heights ( $r=0.23$ ,  $p<0.05$ ). Other studies have found significant relationships between  $N_a$  and NDVI which can measure vegetation density and aboveground biomass (Kunkel *et al.*, 2011, Kim *et al.*, 2014, Sumfleth and Duttmann, 2008). This implies that the density of forest cover and forest types affects the  $N_o$  content and  $N_o/P_o$

ratios. Vesterdal *et al.* (2008) reported significant differences for  $N_o$  but not for  $N_a$  based on tree species and forest types. However, no relationship was found between P and LiDAR predictors.

As noted, LiDAR-derived predictors are promising for spatial soil predictions. In future studies, vegetation predictors should be applied to forest areas where there is difference in the variation of forest cover. Forest structure (LiDAR metrics) can have an effect on erosion and deposition of materials, which in turn, might alter the soil nutrient content. Hahm *et al.* (2014) confirmed that differences in erosion rates are affected by tree canopy cover. However, to our knowledge, no studies have investigated the relationship between soil erosion, forest structures, and nutrient status using LiDAR data so far.

### 5.4.2 Spatial patterns of N/P ratios

We found that N/P ratios increased with surface curvature and were higher on the upper slope compared to the lower slope. This was due to P enrichment of the soil on the lower slope and a more even distribution of N (Fig 5.6).  $N_o/P_o$  and  $N_a/P_a$  were strongly related to surface curvature (Fig 5.6), which implies that P dynamics are affected strongly by topography. This is likely because P was carried from the upper slope by surface and subsurface flows and accumulated on the lower slope, as observed previously in other areas (Smeck, 1985). Soil erosion in the watershed under study is strong due to storm events and steep slopes (Jeong *et al.*, 2012, Jung *et al.*, 2012). Consequently, higher soil P content on the lower slope than on the upper slope can lead to higher plant P uptake and higher plant litter P content, leading to a lower  $N_o/P_o$ . This implies that spatial patterns of  $N_o/P_o$  might be generated by the interconnected relationships between soil, topography, and vegetation. Similarly, Uriarte *et al.* (2015) found that soil N/P was correlated with leaf litter N/P, and was determined by topography in a tropical mountainous forest with heavy rainfall and steep slopes.

### 5.4.3 Model performance based on different cross validation schemes

We observed the typical bias-variance tradeoff when comparing the various CV schemes as was discussed at length in Hastie *et al.* (2009). With a higher k, the mean test error decreases, while test error variance increases (Fig 5.2, Fig 5.S1). In general, the performance of the learning method varies with the size of the training set. A higher k results in a higher amount of training data, which can be crucial with small datasets. This pattern was consistent with the findings of previous studies. Park and Vlek (2002) tested the change in prediction error with different numbers of training soil data sets, and confirmed that the prediction accuracy increases when

increasing numbers of soil samples are used for the tuning dataset. A similar decrease in the prediction error was found using various methods for soil prediction according to Ballabio (2009). Generally, 10-fold CV is recommended in most studies (Remesan and Mathew, 2015, James *et al.*, 2013, Cichosz, 2015, Feigelson and Babu, 2012, Malley *et al.*, 2011, Ambroise and McLachlan, 2002). Remesan and Mathew (2015) noted that the use of very few datasets might result in poorly calibrated models, while high amounts of data for calibration might lead to overfitting. For small sample sizes, model calibration requires all possible datasets to improve the model performance, while validation results can differ markedly depending on which samples are included in the validation (Kuhn and Johnson, 2013). Therefore, Kuhn and Johnson (2013) suggested repeated 10-fold CV for small sample sizes because the bias and variance are somewhat balanced and the computational efficiency is good.

The size of the standard deviations of the spatial predictions, corresponds to the applied CV scheme (Fig 5.3). Naturally, a low model bias goes along with low standard deviations. With a high amount of samples included in the training dataset, the training datasets and hence the 100 models are very similar to one another and will, therefore, make similar predictions. That this ensemble of RF models (e.g., from repeated 20-fold or LOO CV) comes along with a high error variance indicates that it is not a good choice, as the corresponding model might be overfitting the data and perform poorly on other data.

## 5.5 Conclusions

Here, we created the first digital soil maps, showing the spatial pattern of N/P ratios using LiDAR-derived vegetation and topographic predictors. These maps help to identify areas with low nutrient availability. In our study, repeated 10-fold CV was recommended for model validation with small sample sizes. While surface curvature and elevation were mostly sufficient to explain the overall spatial pattern, particularly N contents as well as nutrient rations in the organic layer benefited from the inclusion of the LiDAR derived vegetation metrics. N/P ratios on the upper slope were higher than those on the lower slope and therefore, productivity on the upper slope might be limited by P in mountainous ecosystems under monsoon conditions. Finally, our analyses show that topographic and vegetation characteristics may help to predict the spatial distribution of nutrients and hence, nutrient limitation in mountainous regions.

## Author contributions

Conceptualization: Gwanyong Jeong, Kwanghun Choi, Marie Spohn, Soo Jin Park, Bernd Huwe, Mareike Ließ; Data curation: Gwanyong Jeong; Formal analysis: Gwanyong Jeong, Kwanghun Choi; Funding acquisition: Bernd Huwe; Investigation: Gwanyong Jeong; Methodology: Gwanyong Jeong, Kwanghun Choi, Bernd Huwe; Project administration: Bernd Huwe; Resources: Gwanyong Jeong; Software: Gwanyong Jeong, Kwanghun Choi; Supervision: Marie Spohn, Soo Jin Park, Bernd Huwe, Mareike Ließ; Validation: Gwanyong Jeong; Visualization: Gwanyong Jeong; Writing – original draft: Gwanyong Jeong; Writing – review & editing: Gwanyong Jeong, Marie Spohn, Bernd Huwe, Mareike Ließ.

## Funding

This study was carried out as part of the International Research Training Group TERRECO (GRK 1565/ 1) at the University of Bayreuth. It was funded by the German Research Foundation (DFG). This publication was funded by the German Research Foundation (DFG) and the University of Bayreuth in the funding programme Open Access Publishing. The funders had no role in study design, data collection and analysis, decision to publish, or preparation of the manuscript.

## Acknowledgments

The authors would like to thank Bomchul Kim, Youngsoon Choi, and Jaesung Eum from Kangwon National University, South Korea for providing a laboratory for the pretreatment of soil samples.

## Competing interests

The authors have declared that no competing interests exist.

## References

- Vitousek, P.M.; Hättenschwiler, S.; Olander, L.; Allison, S. Nitrogen and Nature. *AMBIO* **2002**, *31*, 97–101. doi:10.1579/0044-7447-31.2.97.
- Vitousek, P.M.; Porder, S.; Houlton, B.Z.; Chadwick, O.A. Terrestrial phosphorus limitation: mechanisms, implications, and nitrogen–phosphorus interactions. *Ecol. Appl.* **2010**, *20*, 5–15. doi:10.1890/08-0127.1.
- Laliberté, E.; Grace, J.B.; Huston, M.A.; Lambers, H.; Teste, F.P.; Turner, B.L.; Wardle, D.A.

- How does pedogenesis drive plant diversity? *Trends in Ecology and Evolution* **2013**, *28*, 331–340. doi:10.1016/j.tree.2013.02.008.
- Braun, S.; Thomas, V.F.D.; Quiring, R.; Flückiger, W. Does nitrogen deposition increase forest production? The role of phosphorus. *Environ. Pollut.* **2010**, *158*, 2043–2052. doi:10.1016/j.envpol.2009.11.030.
- Manning, P. The Impact of Nitrogen Enrichment on Ecosystems and Their Services. In *Soil Ecology and Ecosystem Services*; Oxford University Press, 2012; pp. 256–269. doi:10.1093/acprof:oso/9780199575923.003.0022.
- Jang, S.K.; Sung, M.Y.; Shin, A.Y.; Choi, J.S.; Son, J.S.; Ahn, J.Y.; Kim, J.C.; Shin, E.S. A Study for Long-term Trend of Acid Deposition in Korea. *J. Korea Society of Environmental Administration* **2011**, *17*, 183–192.
- Kim, I.N.; Lee, K.; Gruber, N.; Karl, D.M.; Bullister, J.L.; Yang, S.; Kim, T.W. Increasing anthropogenic nitrogen in the North Pacific Ocean. *Science* **2014**, *346*, 1102–1106. doi:10.1126/science.1258396.
- Kim, T.W.; Lee, K.; Najjar, R.G.; Jeong, H.D.; Jeong, H.J. Increasing N Abundance in the Northwestern Pacific Ocean Due to Atmospheric Nitrogen Deposition. *Science* **2011**, *334*, 505–509. doi:10.1126/science.1206583.
- Turner, B.L. Resource partitioning for soil phosphorus: a hypothesis. *J. Ecol.* **2008**, *96*, 698–702. doi:10.1111/j.1365-2745.2008.01384.x.
- Osman, K.T. *Soils: Principles, Properties and Management*; Springer Netherlands, 2013. doi:10.1007/978-94-007-5663-2.
- Huang, W.; Spohn, M. Effects of long-term litter manipulation on soil carbon, nitrogen, and phosphorus in a temperate deciduous forest. *Soil Biol. Biochem.* **2015**, *83*, 12–18. doi:10.1016/j.soilbio.2015.01.011.
- Cleveland, C.C.; Liptzin, D. C:N:P stoichiometry in soil: Is there a “Redfield ratio” for the microbial biomass? *Biogeochemistry* **2007**, *85*, 235–252. doi:10.1007/s10533-007-9132-0.
- Peng, G.; Bing, W.; Guangpo, G.; Guangcan, Z. Spatial Distribution of Soil Organic Carbon and Total Nitrogen Based on GIS and Geostatistics in a Small Watershed in a Hilly Area of Northern China. *PLOS ONE* **2013**, *8*, e83592. doi:10.1371/journal.pone.0083592.

- Liu, Z.P.; Shao, M.A.; Wang, Y.Q. Spatial patterns of soil total nitrogen and soil total phosphorus across the entire Loess Plateau region of China. *Geoderma* **2013**, *197-198*, 67–78. doi:10.1016/j.geoderma.2012.12.011.
- Kunkel, M.L.; Flores, A.N.; Smith, T.J.; McNamara, J.P.; Benner, S.G. A simplified approach for estimating soil carbon and nitrogen stocks in semi-arid complex terrain. *Geoderma* **2011**, *165*, 1–11. doi:10.1016/j.geoderma.2011.06.011.
- Kim, J.; Grunwald, S.; Rivero, R.G. Soil Phosphorus and Nitrogen Predictions Across Spatial Escalating Scales in an Aquatic Ecosystem Using Remote Sensing Images. *IEEE Trans. Geosci. Remote Sens.* **2014**, *52*, 6724–6737. doi:10.1109/tgrs.2014.2301443.
- Roger, A.; Libohova, Z.; Rossier, N.; Joost, S.; Maltas, A.; Frossard, E.; Sinaj, S. Spatial variability of soil phosphorus in the Fribourg canton, Switzerland. *Geoderma* **2014**, *217-218*, 26–36. doi:10.1016/j.geoderma.2013.11.001.
- McKenzie, N.J.; Ryan, P.J. Spatial prediction of soil properties using environmental correlation. *Geoderma* **1999**, *89*, 67–94. doi:10.1016/s0016-7061(98)00137-2.
- Johnson, C.E.; Ruiz-Méndez, J.J.; Lawrence, G.B. Forest Soil Chemistry and Terrain Attributes in a Catskills Watershed. *Soil Sci. Soc. Am. J.* **2000**, *64*, 1804. doi:10.2136/sssaj2000.6451804x.
- Seibert, J.; Stendahl, J.; Sørensen, R. Topographical influences on soil properties in boreal forests. *Geoderma* **2007**, *141*, 139–148. doi:10.1016/j.geoderma.2007.05.013.
- Wilcke, W.; Oelmann, Y.; Schmitt, A.; Valarezo, C.; Zech, W.; Homeier, J. Soil properties and tree growth along an altitudinal transect in Ecuadorian tropical montane forest. *J. Plant Nutr. Soil Sci.* **2008**, *171*, 220–230. doi:10.1002/jpln.200625210.
- Soethe, N.; Lehmann, J.; Engels, C. Nutrient availability at different altitudes in a tropical montane forest in Ecuador. *J. Trop. Ecology* **2008**, *24*, 397–406. doi:10.1017/s026646740800504x.
- McBratney, A.B.; Santos, M.L.M.; Minasny, B. On digital soil mapping. *Geoderma* **2003**, *117*, 3–52. doi:10.1016/s0016-7061(03)00223-4.
- Grunwald, S., Ed. *Environmental Soil-Landscape Modeling*; CRC Press: Boca Raton, 2005. doi:10.1201/9781420028188.

- Ballabio, C. Spatial prediction of soil properties in temperate mountain regions using support vector regression. *Geoderma* **2009**, *151*, 338–350. doi:10.1016/j.geoderma.2009.04.022.
- Dan Binkley, R.F.F. *Ecology and Management of Forest Soils*; John Wiley & Sons, 2012.
- Grunwald, S.; Vasques, G.M.; Rivero, R.G. Fusion of Soil and Remote Sensing Data to Model Soil Properties. In *Advances in Agronomy*; Elsevier, 2015; pp. 1–109. doi:10.1016/bs.agron.2014.12.004.
- Mulder, V.L.; de Bruin, S.; Schaepman, M.E.; Mayr, T.R. The use of remote sensing in soil and terrain mapping — A review. *Geoderma* **2011**, *162*, 1–19. doi:10.1016/j.geoderma.2010.12.018.
- Jones, H.G.; Vaughan, R.A. *Remote Sensing of Vegetation: Principles, Techniques, and Applications*; Oxford University Press, 2010.
- Zellweger, F.; Braunisch, V.; Morsdorf, F.; Baltensweiler, A.; Abegg, M.; Roth, T.; Bugmann, H.; Bollmann, K. Disentangling the effects of climate, topography, soil and vegetation on stand-scale species richness in temperate forests. *For. Ecol. Manage.* **2015**, *349*, 36–44. doi:10.1016/j.foreco.2015.04.008.
- Ørka, H.O.; Næsset, E.; Bollandsås, O.M. Classifying species of individual trees by intensity and structure features derived from airborne laser scanner data. *Remote Sens. Environ.* **2009**, *113*, 1163–1174. doi:10.1016/j.rse.2009.02.002.
- Walker, T.W.; Syers, J.K. The fate of phosphorus during pedogenesis. *Geoderma* **1976**, *15*, 1–19. doi:10.1016/0016-7061(76)90066-5.
- Smeck, N.E. Phosphorus dynamics in soils and landscapes. *Geoderma* **1985**, *36*, 185–199. doi:10.1016/0016-7061(85)90001-1.
- Korea meteorological administration. Korea weather service. Available: <http://www.kma.go.kr/>, 2015. Korea meteorological administration.
- Korea Institute of Geology, Mining, and Material. *Explanatory note of the Gangreung Sokcho sheet 1:250,000*; Korea Institute of Geology, Mining, and Material: Daejeon, 2001.
- Chough, S.K. *Geology and Sedimentology of the Korean Peninsula*; Elsevier, 2013. doi:10.1016/c2012-0-02847-5.
- Lee, G.R. Characteristics of geomorphological surface and analysis of deposits in fluvial terraces at upperreach of Soyang river. *J. Korean Geogr. Soc.* **2004**, *39*, 27–44.

- Wohl, E. *Mountain rivers*; American Geophysical Union: Washington, D.C, 2000.
- National Academy of Agricultural Science. Korean Soil Information System. Available: <http://soil.rda.go.kr/soil/index.jsp>.
- Minasny, B.; McBratney, A.B. A conditioned Latin hypercube method for sampling in the presence of ancillary information. *Comput. Geosci.* **2006**, *32*, 1378–1388. doi:10.1016/j.cageo.2005.12.009.
- Roudier, P.; Hewitt, A.E.; Beaudette, D.E., *Digital Soil Assessments and Beyond*; CRC Press: Boca Raton, 2012; chapter A conditioned Latin hypercube sampling algorithm incorporating operational constraints, pp. 227–231. doi:10.1201/b12728.
- Deutsche Einheitsverfahren zu Wasser. German Standard Methods for the Examination of Water, Wastewater, and Sludge, 2002.
- Franklin, S.E. *Remote sensing for biodiversity and wildlife management*; McGraw-Hill: New York, 2010.
- Hyyppä, J.; Hyyppä, H.; Leckie, D.; Gougeon, F.; Yu, X.; Maltamo, M. Review of methods of small-footprint airborne laser scanning for extracting forest inventory data in boreal forests. *Int. J. Remote Sens.* **2008**, *29*, 1339–1366. doi:10.1080/01431160701736489.
- Asner, G.P.; Ustin, S.L.; Townsend, P.A.; Martin, R.E.; Chadwick, K.D., *Land Resources Monitoring, Modeling, and Mapping with Remote Sensing*; CRC Press: Boca Raton, 2015; chapter Forest biophysical and biochemical properties from hyperspectral and LiDAR remote sensing, pp. 429–448. doi:10.1201/b19322.
- Hyyppä, J.; Karjalainen, M.; Liang, X.; Jaakkola, A.; Yu, X.; Wulder, M.; Hollaus, M.; White, J.C.; Vastaranta, M.; Karila, K.; Kaartinen, H.; Vaaja, M.; Kankare, V.V.; Kukko, A.; Holopainen, M.; Hyyppä, H.; Katoh, M., *Land Resources Monitoring, Modeling, and Mapping with Remote Sensing*; CRC Press: Boca Raton, 2015; Vol. 2, *Remote Sensing Handbook*, chapter Remote Sensing of Forests from Lidar and Radar, pp. 397–427.
- National Geographic Information Institute. National Spatial Data Information Portal. Available online: <https://www.nsic.go.kr>, 2015.
- Isenburg, M. LAStools—efficient tools for LiDAR processing, version 2.1. Available: <http://lastools.org>, 2014.

- Zevenbergen, L.W.; Thorne, C.R. Quantitative analysis of land surface topography. *Earth Surf. Processes Landforms* **1987**, *12*, 47–56. doi:10.1002/esp.3290120107.
- Freeman, T.G. Calculating catchment area with divergent flow based on a regular grid. *Comput. Geosci.* **1991**, *17*, 413–422. doi:10.1016/0098-3004(91)90048-i.
- Böhner, J.; Köthe, R.; Conrad, O.; Gross, J.; Ringeler, A.; Selige, T., Soil Classification 2001; The European Soil Bureau, Joint Research Centre, 2002; chapter Soil Regionalisation by Means of Terrain Analysis and Process Parameterisation, pp. 213–222.
- Park, S.J.; McSweeney, K.; Lowery, B. Identification of the spatial distribution of soils using a process-based terrain characterization. *Geoderma* **2001**, *103*, 249–272. doi:10.1016/s0016-7061(01)00042-8.
- Tucker, C.J.; Sellers, P.J. Satellite remote sensing of primary production. *Int. J. Remote Sens.* **1986**, *7*, 1395–1416. doi:10.1080/01431168608948944.
- Jensen, J.R. *Introductory Digital Image Processing: A Remote Sensing Perspective*, 4th ed.; Prentice Hall Press: Upper Saddle River, NJ, USA, 2015.
- Thenkabail, P.; Lyon, J.; Huete, A. Advances in Hyperspectral Remote Sensing of Vegetation and Agricultural Croplands. In *Hyperspectral Remote Sensing of Vegetation*; CRC Press, 2011; pp. 3–36. doi:10.1201/b11222-3.
- Conrad, O.; Bechtel, B.; Bock, M.; Dietrich, H.; Fischer, E.; Gerlitz, L.; Wehberg, J.; Wichmann, V.; Böhner, J. System for Automated Geoscientific Analyses (SAGA) v. 2.1.4. *Geosci. Model Dev.* **2015**, *8*, 1991–2007. doi:10.5194/gmd-8-1991-2015.
- Breiman, L. Random Forests. *Mach. Learn.* **2001**, *45*, 5–32. doi:10.1023/A:1010933404324.
- Kuhn, M.; Johnson, K. *Applied predictive modeling*; Springer New York: New York, 2013. doi:10.1007/978-1-4614-6849-3.
- Strobl, C.; Malley, J.; Tutz, G. An introduction to recursive partitioning: Rationale, application, and characteristics of classification and regression trees, bagging, and random forests. *Psychol. Methods* **2009**, *14*, 323–348. doi:10.1037/a0016973.
- Kampichler, C.; Wieland, R.; Calmé, S.; Weissenberger, H.; Arriaga-Weiss, S. Classification in conservation biology: A comparison of five machine-learning methods. *Ecol. Inf.* **2010**, *5*, 441–450. doi:10.1016/j.ecoinf.2010.06.003.

- Grimm, R.; Behrens, T.; Märker, M.; Elsenbeer, H. Soil organic carbon concentrations and stocks on Barro Colorado Island — Digital soil mapping using Random Forests analysis. *Geoderma* **2008**, *146*, 102–113. doi:10.1016/j.geoderma.2008.05.008.
- Wiesmeier, M.; Barthold, F.; Blank, B.; Kögel-Knabner, I. Digital mapping of soil organic matter stocks using Random Forest modeling in a semi-arid steppe ecosystem. *Plant Soil* **2011**, *340*, 7–24. doi:10.1007/s11104-010-0425-z.
- Tesfa, T.K.; Tarboton, D.G.; Chandler, D.G.; McNamara, J.P. Modeling soil depth from topographic and land cover attributes. *Water Resour. Res.* **2009**, *45*. doi:10.1029/2008wr007474.
- Ließ, M.; Glaser, B.; Huwe, B. Functional soil-landscape modelling to estimate slope stability in a steep Andean mountain forest region. *Geomorphology* **2011**, *132*, 287–299. doi:10.1016/j.geomorph.2011.05.015.
- Brungard, C.W.; Boettinger, J.L.; Duniway, M.C.; Wills, S.A.; Edwards, T.C. Machine learning for predicting soil classes in three semi-arid landscapes. *Geoderma* **2015**, *239-240*, 68–83. doi:10.1016/j.geoderma.2014.09.019.
- Miller, B.A.; Koszinski, S.; Wehrhan, M.; Sommer, M. Impact of multi-scale predictor selection for modeling soil properties. *Geoderma* **2015**, *239-240*, 97–106. doi:10.1016/j.geoderma.2014.09.018.
- Poggio, L.; Gimona, A.; Brewer, M.J. Regional scale mapping of soil properties and their uncertainty with a large number of satellite-derived covariates. *Geoderma* **2013**, *209-210*, 1–14. doi:10.1016/j.geoderma.2013.05.029.
- Molinaro, A.M.; Simon, R.; Pfeiffer, R.M. Prediction error estimation: a comparison of resampling methods. *Bioinformatics* **2005**, *21*, 3301–3307. doi:10.1093/bioinformatics/bti499.
- Bedison, J.E.; Johnson, A.H. Controls on the Spatial Patterns of Carbon and Nitrogen in Adirondack Forest Soils along a Gradient of Nitrogen Deposition. *Soil Sci. Soc. Am. J.* **2009**, *73*, 2105. doi:10.2136/sssaj2008.0336.
- Wang, K.; Zhang, C.; Li, W. Predictive mapping of soil total nitrogen at a regional scale: A comparison between geographically weighted regression and cokriging. *Appl. Geogr.* **2013**, *42*, 73–85. doi:10.1016/j.apgeog.2013.04.002.
- Aandahl, A.R. The characterization of slope positions and their influence on total nitrogen content of a few virgin soils of Western Iowa. *Soil Sci. Soc. Am. J.* **1948**, *13*, 449–454.

- Zhang, Z.; Yu, X.; Qian, S.; Li, J. Spatial variability of soil nitrogen and phosphorus of a mixed forest ecosystem in Beijing, China. *Environ. Earth Sci.* **2010**, *60*, 1783–1792. doi:10.1007/s12665-009-0314-z.
- Sumfleth, K.; Duttmann, R. Prediction of soil property distribution in paddy soil landscapes using terrain data and satellite information as indicators. *Ecol. Indic.* **2008**, *8*, 485–501. doi:10.1016/j.ecolind.2007.05.005.
- Vesterdal, L.; Schmidt, I.K.; Callesen, I.; Nilsson, L.O.; Gundersen, P. Carbon and nitrogen in forest floor and mineral soil under six common European tree species. *For. Ecol. Manage.* **2008**, *255*, 35–48. doi:10.1016/j.foreco.2007.08.015.
- Hahm, W.J.; Riebe, C.S.; Lukens, C.E.; Araki, S. Bedrock composition regulates mountain ecosystems and landscape evolution. *Proc. Natl. Acad. Sci. U.S.A* **2014**, *111*, 3338–3343. doi:10.1073/pnas.1315667111.
- Jeong, J.J.; Bartsch, S.; Fleckenstein, J.H.; Matzner, E.; Tenhunen, J.D.; Lee, S.D.; Park, S.K.; Park, J.H. Differential storm responses of dissolved and particulate organic carbon in a mountainous headwater stream, investigated by high-frequency, in situ optical measurements. *J. Geophys. Res. Biogeosci.* **2012**, *117*, n/a–n/a. doi:10.1029/2012jg001999.
- Jung, B.J.; Lee, H.J.; Jeong, J.J.; Owen, J.; Kim, B.; Meusburger, K.; Alewell, C.; Gebauer, G.; Shope, C.; Park, J.H. Storm pulses and varying sources of hydrologic carbon export from a mountainous watershed. *J. Hydrol.* **2012**, *440-441*, 90–101. doi:10.1016/j.jhydrol.2012.03.030.
- Uriarte, M.; Turner, B.L.; Thompson, J.; Zimmerman, J.K. Linking spatial patterns of leaf litterfall and soil nutrients in a tropical forest: a neighborhood approach. *Ecol. Appl.* **2015**, *25*, 2022–2034. doi:10.1890/15-0112.1.
- Hastie, T.; Tibshirani, R.; Friedman, J. *The Elements of Statistical Learning*; Springer New York, 2009. doi:10.1007/978-0-387-84858-7.
- Park, S.J.; Vlek, P.L.G. Environmental correlation of three-dimensional soil spatial variability: a comparison of three adaptive techniques. *Geoderma* **2002**, *109*, 117–140. doi:10.1016/s0016-7061(02)00146-5.
- Remesan, R.; Mathew, J. *Hydrological Data Driven Modelling: A Case Study Approach*; Springer International Publishing, 2015. doi:10.1007/978-3-319-09235-5.

- James, G.; Witten, D.; Hastie, T.; Tibshirani, R. *An Introduction to Statistical Learning with Applications in R*; Springer New York, 2013. doi:10.1007/978-1-4614-7138-7.
- Cichosz, P. *Data Mining Algorithms: Explained Using R*; John Wiley & Sons, Ltd: Chichester, West Sussex ; Malden, MA, 2015. doi:10.1002/9781118950951.
- Feigelson, E.D.; Babu, G.J. *Modern Statistical Methods for Astronomy: With R Applications*; Cambridge University Press, 2012. doi:10.1017/cbo9781139015653.
- Malley, J.D.; Malley, K.G.; Pajevic, S. *Statistical Learning for Biomedical Data*; Cambridge University Press, 2011. doi:10.1017/cbo9780511975820.
- Ambroise, C.; McLachlan, G.J. Selection bias in gene extraction on the basis of microarray gene-expression data. *Proc. Natl. Acad. Sci. U.S.A* **2002**, *99*, 6562–6566. doi:10.1073/pnas.102102699.

## Supplementary material

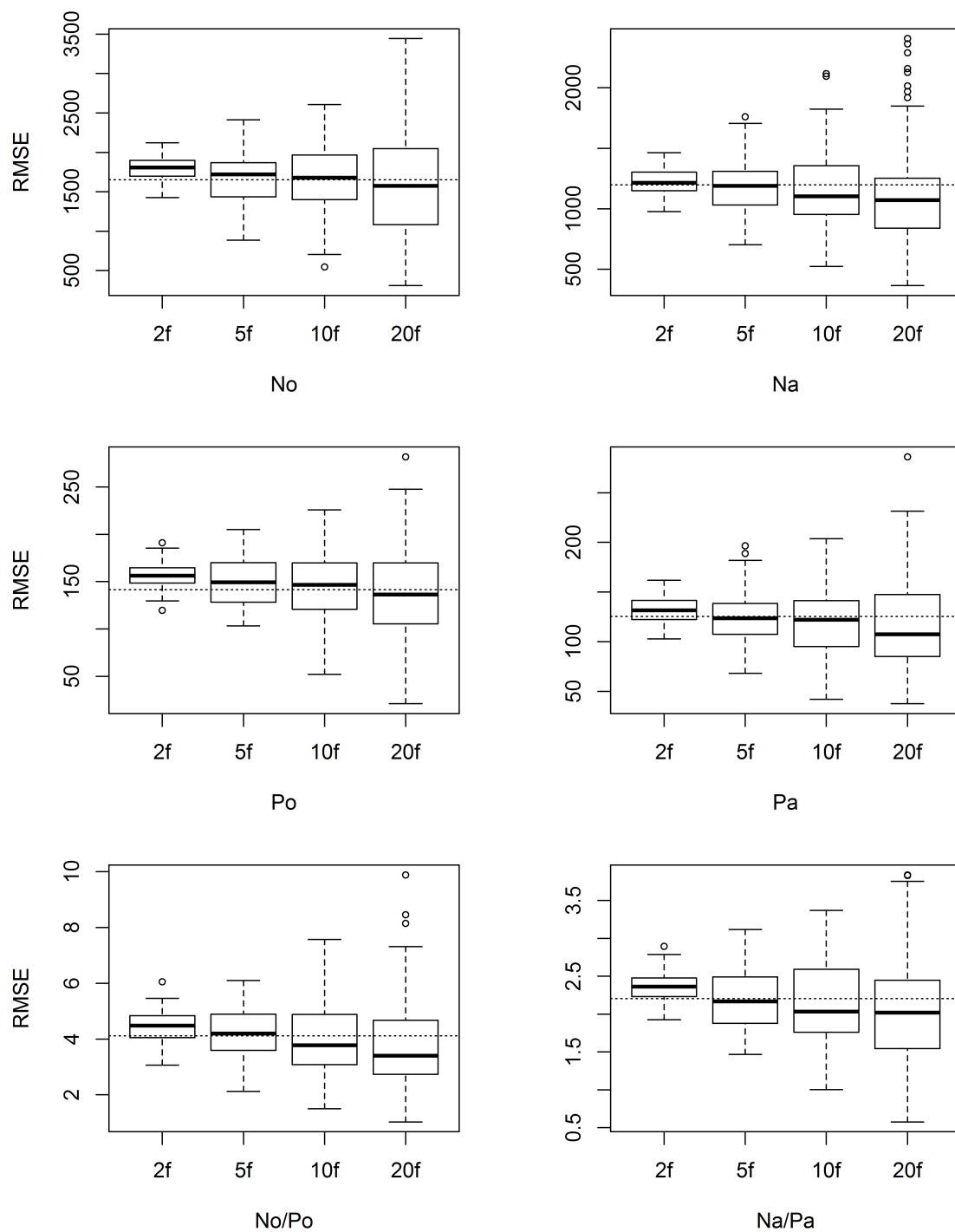


Fig. 5.S1. Model validation based on root mean square error (RMSE) with cross validation methods. The dotted lines refer to the leave-one-out cross-validated result. 2f, 2-fold 50 repetitions; 5f, 5-fold 20 repetitions; 10f, 10-fold 10 repetitions; 20f, 20-fold 5 repetitions; N, nitrogen; P, phosphorus; o, organic layer; and a, A horizon.

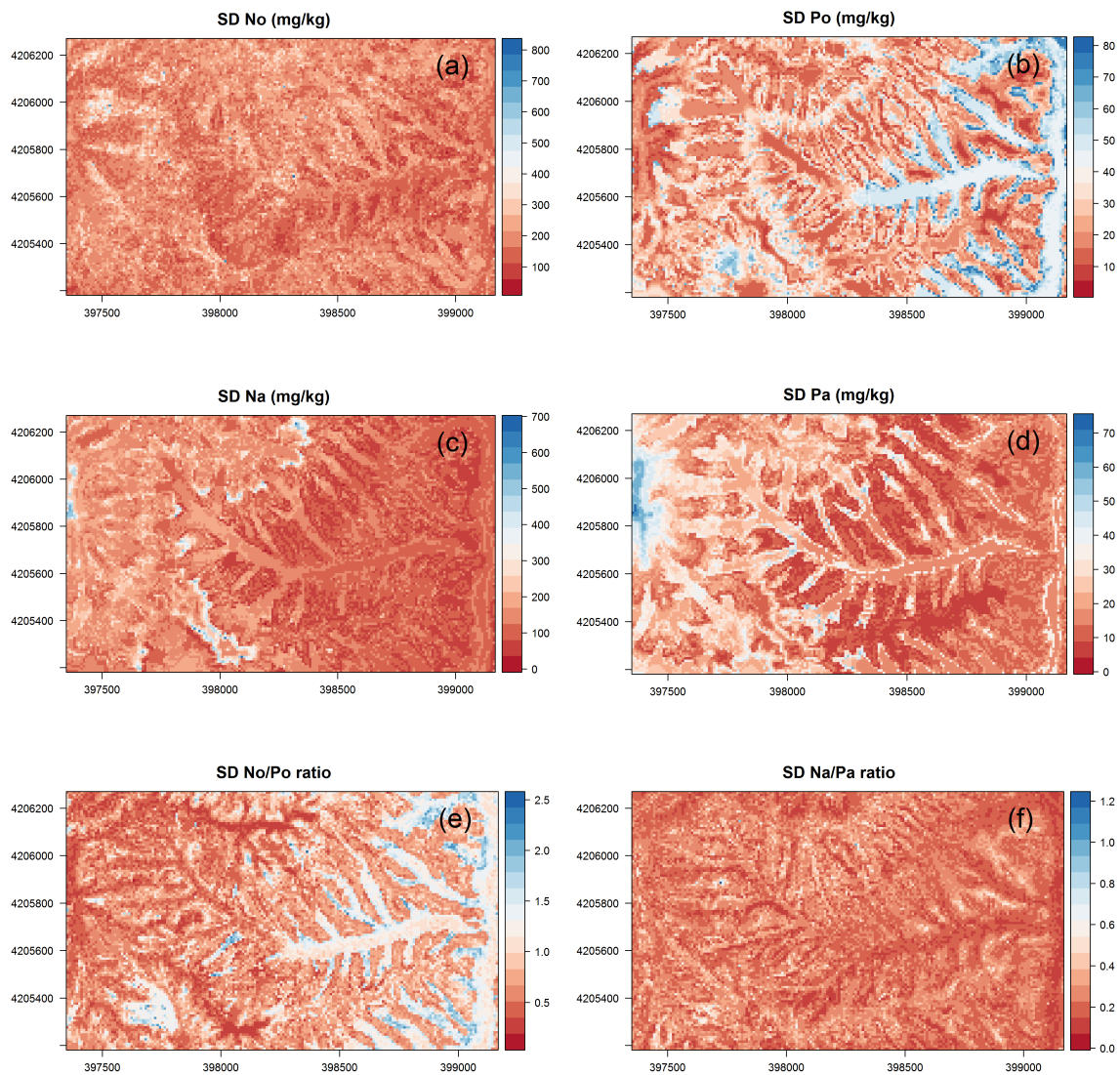


Fig. 5.S2. Predicted SD nitrogen and phosphorus content and ratios. SD, standard deviation; N, nitrogen; P, phosphorus; o, organic layer; and a, A horizon.





## **(Eidesstattliche) Versicherungen und Erklärungen**

(§ 9 Satz 2 Nr. 3 PromO BayNAT)

*Hiermit versichere ich eidesstattlich, dass ich die Arbeit selbstständig verfasst und keine anderen als die von mir angegebenen Quellen und Hilfsmittel benutzt habe (vgl. Art. 64 Abs. 1 Satz 6 BayHSchG).*

(§ 9 Satz 2 Nr. 3 PromO BayNAT)

*Hiermit erkläre ich, dass ich die Dissertation nicht bereits zur Erlangung eines akademischen Grades eingereicht habe und dass ich nicht bereits diese oder eine gleichartige Doktorprüfung endgültig nicht bestanden habe.*

(§ 9 Satz 2 Nr. 4 PromO BayNAT)

*Hiermit erkläre ich, dass ich Hilfe von gewerblichen Promotionsberatern bzw. -vermittlern oder ähnlichen Dienstleistern weder bisher in Anspruch genommen habe noch künftig in Anspruch nehmen werde.*

(§ 9 Satz 2 Nr. 7 PromO BayNAT)

*Hiermit erkläre ich mein Einverständnis, dass die elektronische Fassung meiner Dissertation unter Wahrung meiner Urheberrechte und des Datenschutzes einer gesonderten Überprüfung unterzogen werden kann.*

(§ 9 Satz 2 Nr. 8 PromO BayNAT)

*Hiermit erkläre ich mein Einverständnis, dass bei Verdacht wissenschaftlichen Fehlverhaltens Ermittlungen durch universitätsinterne Organe der wissenschaftlichen Selbstkontrolle stattfinden können.*

.....  
Ort, Datum, Unterschrift